Bone Morphogenetic Protein 7 Regulates Nasal Cartilage Properties Under Physiological And Pathological Conditions

by

Pranidhi Baddam

A thesis submitted in partial fulfillment of the requirements for the degree of

Doctor of Philosophy

Medical Sciences – Oral Biology

University of Alberta

Abstract

Background: The nasal septum is a cartilaginous structure that provides critical structural and growth support for the midface. Nasal septum deviation (NSD) is a relatively frequent abnormality, which can be associated with nasal airway obstruction and disordered breathing in children. Although many children present with NSD, not everyone presents with secondary co-morbidities such as difficulty breathing. Additionally, it has been established that the incidence of NSD increases during midfacial growth spurt in children. However, the cellular and molecular mechanisms contributing to midfacial growth and NSD are poorly understood due to limited access to pediatric clinical samples. As a result, there is a need to understand the biological underpinning of midfacial growth and nasal septum development. Since the nasal septum cartilage is a hyaline cartilage similar to the knee cartilage and the nasal cartilage contributes to the growth of the midface, we hypothesize that nasal septum deviation is a consequence of underlying cartilage differentiation and growth defects. Bone Morphogenetic Proteins (BMP) are signalling molecules important for proliferation and differentiation of chondrocytes to make cartilage. BMPs are thought to regulate extracellular matrix. However, how they do this is yet to be identified. BMP7, in particular, has been extensively investigated in articular cartilage repair models. Articular cartilage is a form of hyaline cartilage. Literature suggests that BMP7, an anabolic growth factor, can repair and maintain articular cartilage both *in vivo* and *in vitro*. However, no studies have demonstrated the role BMP7 plays in craniofacial cartilages such as the nasal septum. Here we assess changes to chondrocyte properties underlying NSD in a mouse model for midfacial hypoplasia to better understand the etiology of NSD as a consequence of growth defects in the face.

Methods: To understand the relationship between severity of NSD and onset of comorbidities, a retrospective study assessing nasal cavity abnormalities was quantified subjectively and objectively and then correlated with their risk for developing sleep-disordered breathing. To understand molecular and cellular changes contributing to normal development of nasal septum and midfacial growth, histological and molecular properties of wild-type nasal septum were characterized in mice. To identify changes to chondrocyte properties in a pathological setting, mice carrying a conditional deletion of Bmp7 in neural crest ($Bmp7^{ncko}$) present with midfacial hypoplasia and NSD were used. Firstly, a timeline of when NSD and its associated co-morbidity (difficulty breathing) were established. This was followed by morphometric, histological, immunohistochemical, genomic and proteomic analyses of the nasal septum to correlate molecular differences to physiological structural changes.

Results: The retrospective study revealed that assessing severity of NSD and onset of associated co-morbidities is not possible using cone-beam computed tomography scans. Nasal cartilage assessment of wild-type mice revealed that nasal septum grows asynchronous across its length with phases of rapid growth interrupted by more stationary growth. Growth appears to be driven predominantly by acquisition of chondrocyte hypertrophy. Morphometric, physiological and metabolomic analysis of $Bmp7^{ncko}$ mice revealed that NSD develops during midfacial growth and precedes the development of an upper-airway obstruction as observed by reduced breathing frequency, apneas and overall reduced oxygen consumption. The nasal cartilage was histologically inconspicuous at 2 weeks; however, structural changes were evident at 4 weeks. The normally hyaline cartilage showed expression of proteins characteristic of hypertrophic chondrocytes, acquisition of elastic cartilage properties, a switch to glucose metabolism, and acquisition of molecular characteristics commonly associated with early-stage osteoarthritis (OA). We also

found that genetic reduction of Bmp2 in these $Bmp7^{ncko}$ mice prevented the deviation. 3D *in vitro* pellet cultures using $Bmp7^{ctrl}$ and $Bmp7^{ncko}$ nasal septum chondrocytes stimulated with/without recombinant BMP7 (rhBMP7) and induced to differentiate using Insulin-Transferrin-Selenium (ITS) demonstrated that pellets treated with both rhBMP7 and ITS completely suppressed induction of Elastin.

Conclusion: Loss of BMP7 resulted in cellular changes in chondrocytes, which altered nasal cartilage properties and compromised its growth, placing BMP7 as a critical factor regulating chondrocyte differentiation. Additionally, there is strong evidence that absence of BMP7 might lead to formation of elastic cartilage in place of hyaline cartilage. Our findings suggest that NSD can occur because of underlying nasal septum cartilage growth and differentiation defects. Overall, NSD, in connection with midfacial growth reduction, might indicate altered chondrocyte biology in affected children.

Preface

This thesis is an original work by Pranidhi Baddam. The research project, of which this thesis is a part of, received ethical research approval from the University of Alberta Animal Policy and Welfare Committee. The protocols were approved by the University of Alberta's Animal Care and Use Committee (AUP 00001149). These studies have been supported by Natural Sciences and Engineering Research Council of Canada, Women and Children's Health Research Institute, Geoffrey. H. Sperber Fund, Gilbert K Winter Fund, American Association of Orthodontists Fund.

A version of Chapter 1 is submitted to the *Federation of American Societies for Experimental Biology*:

Baddam, P., Bayona, F.*, Campbell, S., El-Hakim, H., Graf, D. (2021).* Properties Of The Nasal Cartilage, From Development To Adulthood: A Scoping Review.

**Shared co-authors.*

Pranidhi Baddam screened abstracts and full-length articles and wrote the main body of the manuscript with Francy Bayona. Francy Bayona drew the illustration for Figure 1.1. Pranidhi prepared the rest of figures and tables for this manuscript. Sandra Campbell assisted with the literature search strategy. Hamdy El-Hakim edited the manuscript. Daniel Graf was the supervisory author and edited the manuscript

A version of Chapter 2 is in press at *American Journal of Orthodontics and Dentofacial Orthopedics*:

Baddam, P., Bussolaro, C.-T., Flores-Mir, C. and Graf, D. (2021). Nasal cavity structural anomalies among children at high risk of sleep-disordered breathing: an exploratory cone-beam computed tomography study. *Am. J. Orthodont. Dentofacial Orthop. (In press).*

Pranidhi Baddam and Claudine Bussolaro together collected measurements from cone beam computed tomography (CBCT) scans of children. Pranidhi Baddam prepared figures and wrote and edited the main body of the manuscript while Claudine Bussolaro performed statistical analysis for the measurements obtained. Carlos Flores-Mir edited the manuscript. Daniel Graf was the supervisory author and edited the manuscript.

A version of Chapter 3 was published at *Journal of Anatomy*:

Baddam, P., Kung, T., Adesida, A. B., & Graf, D. (2021). Histological and molecular characterization of the growing nasal septum in mice. *Journal of anatomy, 238(3), 751–764. https://doi.org/10.1111/joa.13332*

Pranidhi Baddam designed the study. Both Tiffany Kung and Pranidhi Baddam conducted experiments, prepared figures and wrote and edited the main body of the manuscript. Tiffany Kung created the illustration in Figure 3.9. Adetola Adesida edited the manuscript. Daniel Graf was the supervisory author and edited the manuscript.

A version of Chapter 4 was published at *Disease Models and Mechanisms*:

Baddam, P., Biancardi, V., Roth, D. M., Eaton, F., Thereza-Bussolaro, C., Mandal, R., Wishart, D. S., Barr, A., MacLean, J., Flores-Mir, C., Pagliardini, S., & Graf, D. (2021). Neural crest-specific deletion of Bmp7 leads to midfacial hypoplasia, nasal airway obstruction, and disordered breathing modelling Obstructive Sleep Apnea. *Disease models & mechanisms, 14(2), dmm047738. Advance online publication. https://doi.org/10.1242/dmm.047738*

Pranidhi Baddam performed initial MicroCT scanning and analysis. She also assisted with preparation of graphs in Figures 4.1 and 4.2 and measurements for Figures 4.3-4.5. Additionally, data analysis and figure preparation for Figures 4.3 and 4.6 were also done by Pranidhi Baddam.

Vivian Biancardi conducted Plethysmography experiments, analyzed the data presented in Figures 4.4 and 4.5. Daniela Roth completed the MicroCT analysis and prepared illustrations and graphs for Figure 4.1, 4.2 and Table 4.1. Farah Eaton assisted with mice maintenance. CLAMS metabolic cage assessment was performed by Amy Barr, and Metabolomics was conducted by Rupasri Mandal. Analysis of both these assessments was conducted by Pranidhi Baddam. Pranidhi Baddam, Daniela Roth and Vivian Biancardi wrote and edited the main body of the manuscript. Claudine Thereza-Bussolaro, Carlos Flores-Mir and Joanna MacLean edited the manuscript. Silvia Pagliardini provided the equipment used for Plethysmography assessments and edited the manuscript. Daniel Graf was the supervisory author and edited the manuscript.

A version of Chapter 5 was published at *Frontiers in Cell and Developmental Biology*:

Baddam, P., Young, D., Dunsmore, G., Nie, C., Eaton, F., Elahi, S., Jovel, J., Adesida AB., Dufour, A., Graf, D. (2021) Nasal septum deviation as the consequence of BMP-controlled changes to cartilage properties. *Frontiers in Cell and Developmental Biology.*

Pranidhi Baddam conducted experiments, analyzed data, prepared figures, wrote and edited the manuscript for submission and revisions. Daniel Young conducted protein isolation and Mass Spectrometry analysis. RNA sequencing was performed by Dr. Juan Jovel. Garrett Dunsmore conducted RNA sequencing analysis. Chunpeng Nie assisted Pranidhi Baddam with the STRING analysis. Farah Eaton helped with mice maintenance. Shokrollah Elahi and Adetola Adesida edited the manuscript. Antoine Dufour provided materials for protein isolation and Mass Spectrometry as well as edited the manuscript. Daniel Graf was the supervisory author and edited the manuscript.

Unless otherwise specified, the data presented in this thesis is Pranidhi Baddam's original work.

This thesis is dedicated to two people who have guided me during the short time I got to spend with them. They would have been really proud to see “Dr.” before my name.

Baddam Bal Reddy, 1939 – 1999

Laxmannagari Narayana Reddy, 1940 – 2014

Acknowledgments

I would like to acknowledge my supervisor Dr. Daniel Graf for inspiring me, motivating me, and providing me with countless opportunities to grow as a scientist. If it weren't for him and his guidance, I don't think I would have been as productive and successful on this journey. Thank you for having confidence in me even during times I, myself, didn't have. My ability to think critically and understand science is primarily due to your mentorship and training. For this, I am very grateful.

Thank you to my committee members, Dr. Adetola Adesida, Dr. Benedikt Hallgrimsson and Dr. Andrew Waskiewicz, for your constant support, guidance, and feedback over the years. I truly appreciate all the discussions we have had, and I am grateful for your advice which has significantly helped me advance my projects and research career.

To my various collaborators, Dr. Antoine Dufour, Dr. Silvia Pagliardini, Dr. Maria Alexiou and Dr. Carlos Flores-Mir – thank you for supporting our work. It wouldn't have been what it is today without all your assistance. Special thanks to Dr. Maria Alexiou for constantly checking up on me and pushing me to achieve greater heights. To all the faculty, staff, and fellow students of the Department of Dentistry – thank you for all the support and guidance you have provided during my time here. I would like to especially thank Dr. Patrick Flood, Dr. Maria Febbraio, Ms. Heather Good and Ms. Dalyce Barss for always supporting me through my award applications and lending an ear whenever I had things to talk about.

To my funding sources, School of Dentistry, Faculty of Medicine and Dentistry, Faculty of Graduate Studies and Research, Graduate Students Association, Natural Sciences and Engineering Research Council of Canada – thank you for believing in my work and financially supporting me such that I focus on doing research.

Thank you also to my lab mates, both past and present, Peter Sabiri, Daniela Roth, Wasif Qayyum, Haiming Lin, Vivian Biancardi, Claudine Bussolaro and Priyanka Maripuri. You have all been such great friends motivating me to do my best. I would like to especially thank Farah Eaton, my lab mom, who has always been so patient, kind, and supportive since the time I joined the lab. To the HSLAS staff, especially Jennifer Kruger, thank you for all your help with mouse colony maintenance. I will cherish all the memories we have created together as a lab over the years.

To all the undergraduate summer students that I got to train in the lab (Tiffany Kung, Ruocun Liu, Arleen Schmidt, Chunpeng Nie, Sarah-Thea D'Souza, Devyn Godziuk and Samiya Rehman) – thank you for being fantastic and patient with me while I learned how to train students in the lab. You all have taught me a lot, and I hope that I have provided a memorable research experience for you.

Thank you to my friends, old and new, who motivated me to keep going and helped me persevere when times were difficult. For many of you, especially Alexandra Joseph, who would keep asking when I would be defending, well, the day has finally arrived. I hope to see you all in person once the pandemic is over. To my family in India – thank you for being supportive and understanding of me not visiting all of you that often. To my parents (Raghu and Pallavi), my brother (Preetham) and my partner (Anudeep) – although at times you didn't know what my research was about, this journey wouldn't have been possible without your love, patience, constant support, and belief in my abilities. I am thankful to the four of you for always standing beside me during my lows and highs.

Overall, I am grateful for this community of individuals that I got to share these last several years with, and I will forever cherish these memories.

Table of Contents

List of Tables

Chapter 1

Chapter 2

Chapter 3

Chapter 4

Chapter 5

List of Figures

Chapter 1

Chapter 2

Chapter 3

Chapter 4

Chapter 5

Chapter 6

List of Common Symbols, Nomenclatures, and Abbreviations

Abbreviation	Definition
ACAN	Aggrecan
ACI	Autologous chondrocyte implantation
AHI	Apnea hypopnea index
ALDH1A2	Aldehyde dehydrogenase 1 family member A2
ALDOA	Aldolase A
ALK2	Activin A receptor type 1
ALK6	Bone morphogenetic protein receptor type 1B
ANOVA	Analysis of variance
AUP	Animal use protocol
BAT	Brown adipose tissue
BIOSIS	BioSciences information service of biological abstracts
BMI	Body mass index
BMP	Bone morphogenetic proteins
BMP2	Bone morphogenetic protein 2
BMP7	Bone morphogenetic protein 7
BS	Basisphenoid
C57BL/6	Mice strain
CASP3	Cleaved caspase 3
CBCT	Cone beam computed tomography
cDNA	Complementary deoxyribonucleic acid
CDSR	Cochrane database of systematic reviews
CHTOP	Chromatin target of PRMT1
CHUK	Component of inhibitor of nuclear factor kappa B kinase
CI	Confidence interval
CLAMS	Comprehensive lab animal monitoring system
CO2	Carbon dioxide
COL I	Collagen 1
COL II	Collagen 2
COL III	Collagen 3
COL IX	Collagen 9
COL VI	Collagen 6
COL X	Collagen 10
CT	Computed tomography
CYP1A2	Cytochrome P450 1A2
DAPI	4′,6-diamidino-2-phenylindole
DCHS2	Dachsous cadherin-related 2

DCN	Decorin
DI	Direct injection
DKK1	Dickkopf WNT signaling pathway inhibitor 1
DMEM	Dulbecco's modified eagle medium
DNA	Deoxyribonucleic acid
DNS	Deviated nasal septum
DTT	Dithiothreitol
ECM	Extracellular matrix
EDAR	Ectodysplasin A receptor
EDTA	Ethylenediaminetetraacetic acid
EIF5A	Eukaryotic translation initiation factor 5A
ELN	Elastin
FB	Francy Bayona
FDR	False discovery rate
fR	Breathing frequency
FRZB	Frizzled related protein
GAG	Glycosaminoglycan
GAPDH	Glyceraldehyde 3-phosphate dehydrogenase
GLI1	GLI family zinc finger 1
GLI3	GLI family zinc finger 3
GO	Gene ontology
GP	Glycoproteins
GPD2	Mitochondrial glycerol 3 phosphate dehydrogenase
GREM1	Gremlin 1
HEPES	4-(2-hydroxyethyl)-1-piperazineethanesulfonic acid
HIF1α	Hypoxia inducing factor 1 alpha
HK1	Hexokinase 1
HNRPU	Heterogenous nuclear ribonucleoprotein U
HSLAS	Health sciences laboratory animal services
HSP47	Heat shock protein 47
IBM	International business machines
ICAT	Imaging science international
ICC	Intraclass correlation
IH	Intermittent hypoxia
IHC	Immunohistochemistry
IHH	Indian hedgehog
ITS	Insulin - transferrin - selenium
JASP	Jeffreys’s amazing statistics program
LC-MS/MS	Liquid chromatography with tandem mass spectrometry
LDHB	Lactate dehydrogenase B

LIPE	Lipase E
MACI	Matrix-assisted chondrocyte implantation
MFAP5	Microfibril associated protein 5
Mmp13	Matrix metallopeptidase 13
MRI	Magnetic resonance imaging
MRM	Multiple reaction monitoring
MSX1	Msh Homeobox 1
mTOR	Mechanistic target of rapamycin
NCC	Neural crest cells
NPBC	Non-phosphorylated beta catenin
nPSG	Nocturnal polysomnography
NS	Nasal septum
NSC	Nasal septum cartilage
NSD	Nasal septum deviation
O2	oxygen
OA	Osteoarthritis
OCN	Osteocalcin
OSA	Obstructive sleep apnea
P_a	Barometric pressure
PAX1	Paired box 1
PB	Pranidhi Baddam
PBS	Phosphate-buffered saline
P_c	Water vapor pressure in the chamber
PCNA	Proliferating cell nuclear antigen
PCR	Polymerase chain reaction
PFA	Paraformaldehyde
PG	Proteoglycans
PI3K-AKT	Phosphoinositide 3-kinases - protein kinase B
P_k	Pressure deflection associated with V_k
PN	Postnatal
PPE	Perpendicular plate of ethmoid
P_r	Water vapor pressure at T_b
PRDX1	Periredoxin 1
PRISMA-S	Preferred reporting items for systematic review and meta analyses statement
PRMT1	Protein arginine methyltransferase 1
PROSPERO	International prospective register of systematic reviews
PRS	Pierre robin sequence
PSA	Post sigh apnea
PSG	Polysomnography
PSQ	Post sleep questionnaire

P_t	Pressure deflection associated with V_t
PTBP1	Polypyrimidine tract binding protein 1
qRT PCR	Quantitative real time polymerase chain reaction
RALY	Heterogeneous nuclear ribonucleoprotein
RER	Respiratory exchange ratio
rhBMP7	Recombinant Bone morphogenetic protein 7
RNA	Ribonucleic acid
ROS	Reactive oxygen species
RT	Room temperature
Runx2	RUNX family transcription factor 2
SA	Spontaneous apnea
SAF O	Safranin O
SC	Sandra Campbell - Health Librarian
SD	Standard deviation
SDB	Sleep disordered breathing
SDS	Sodium dodecyl sulfate
Sox9	SRY-Box transcription factor 9
Sp7	Osterix
SPP1	Osteopontin
SPSS	Statistical software
SRBD	Sleep-related breathing disorder
STRING	Search tool for the retrieval of interacting genes/proteins
T_a	Air temperature
TBK1	TANK binding protein 1
TH	Turbinate hypertrophy
T_i	Inspiratory time
Ttot	Total breath duration
uCT	Micro computed tomography
USF1	Upstream transcription factor 1
V_k	Calibration volume
V_t	Tidal volume
WAT	White adipose tissue
WNT	Wingless and Int
WNT3A	Wnt family member 3A
WNT6	Wnt family member 6
WNT7A	Wnt family member 7
WOS	Web of science

Chapter 1: Properties Of The Nasal Cartilage, From Development To Adulthood: A Scoping Review

This scoping review paints a landscape of the existing knowledge on the nasal septum cartilage. Extensive research has been conducted since the 19th century on nasal septum cartilage; however, various gaps of knowledge still exist, as outlined in this chapter. Chapters 2 – 6 of this thesis demonstrate research addressing the gaps of knowledge identified in this chapter.

Chapter 1 is derived from the article submitted to the *Federation of American Societies for Experimental Biology*:

Baddam, P., Bayona, F.*, Campbell, S., El-Hakim, H., Graf, D. (2021).* Properties Of The Nasal Cartilage, From Development To Adulthood: A Scoping Review.

**Shared co-authors.*

1.1 Abstract

Background: Despite significant advances over the last decades to regenerate functionally stable nasal cartilage, the ability to regenerate cartilage with properties similar to native nasal cartilage remains poor. A contributing factor could be that information on nasal cartilage properties required to rationally engineer functional cartilage is currently widely dispersed. The objectives of this scoping review are to 1) consolidate existing knowledge on nasal cartilage properties, 2) identify gaps of knowledge and generate research questions that require further investigation, and 3) reiterate the need to integrate multiple properties of the nasal cartilage while developing tissue engineering approaches.

Methods: This scoping review incorporated articles identified using PROSPERO, Cochrane Library (CDSR and Central), WOS BIOSIS, WOS Core Collection, and ProQuest Dissertations and Theses Global databases. The following research questions were identified using Arksey and O'Malley's five-step framework: 1) What properties of the nasal cartilage do authors characterize? 2) What techniques are used to identify these properties? And 3) Is there agreement on the identified properties of the nasal cartilage?

Results: Following the screening process, 84 articles were included in the review. The articles were categorized into three groups: growth, extracellular matrix, and mechanical properties. Most articles investigated growth properties followed by extracellular matrix and mechanical properties. Methodologies ranging from MRI, CT, histology, immunohistochemistry were used to investigate nasal cartilage properties in human and animal models. Nasal cartilage growth was demonstrated to be very dynamic with location-specific extracellular matrix composition and mechanical capabilities. Despite the extensive research on cartilage properties, several questions such as the role of nasal septum cartilage in midfacial growth remain

controversial. Moreover, most articles included in the review investigate these properties in isolation, and only very few articles demonstrate the interrelationship between multiple cartilage properties.

Conclusions: This scoping review highlights the need to understand nasal septum cartilage properties in parallel using interdisciplinary approaches, to effectively engineer functional nasal cartilage. It additionally identifies gaps of knowledge, such as the need to understand how cartilage properties intersect. Thus, requiring further investigation relevant to individuals engaged in studies involving nasal septum cartilage.

Keywords: nasal septum, nasal cartilage composition, cartilage growth, extracellular matrix, mechanical properties.

1.2 Introduction

The nasal septum (NS) divides the nasal cavity into two, lending central support to the nasal cavity. The main components of the NS are the nasal septum cartilage (NSC), the perpendicular plate of the ethmoids (PPE), and the vomer bone (Figure 1.1) [1]. The thickest part of the NSC connected to the vomer and PPE, which has clinical implications during reconstructive surgery and tissue engineering[1]. NSC is avascular, aneural, alymphatic, and is surrounded by perichondrium and respiratory epithelium. According to its location, it articulates with the frontal bone, nasal bone, cribriform plate, sphenoid bone, maxillary crest, vomer, and palatine bone, and plays an essential role during breathing and mastication, as well as on the cosmetics and growth of the face[2-3]. Chondrocytes are the exclusive residents of the NSC. They are organized as units called chondrons, and their immediate environment is referred to as the territorial area, while the area in between those areas is named interterritorial area (Figure 1.1)[4]. In addition to the chondrocytes, the extracellular matrix (ECM) of the NSC is composed mainly of Collagen II, Aggrecan and Hyaluronic acid, among other proteins[5]. Interestingly, the origin of the NSC and PPE are the same, a cartilage that at the most posterior aspect undergoes endochondral ossification becoming the PPE, while the most anterior remains cartilaginous and is known as the NSC[1]. The complex composition and organization provide NSC with specific properties, some of them common to other hyaline cartilages, but others exclusive of it, that have been studied over the last decades.

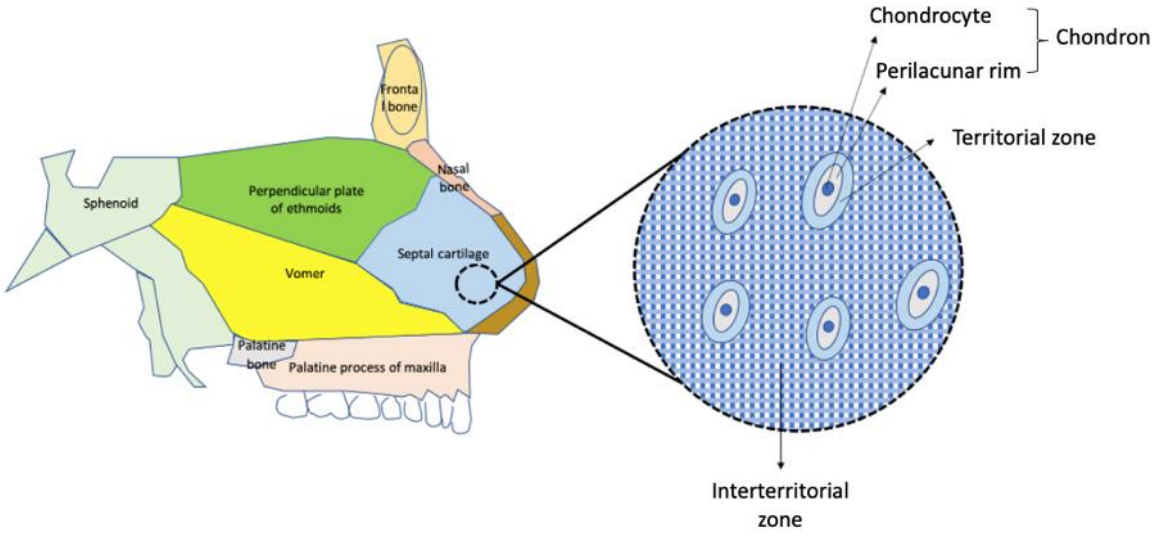

Figure 1. 1 Anatomy of the nasal septum cartilage.

There is interest from several disciplines in understanding NSC (Figure 1.2). For instance, knowledge on NSC significantly aids tissue engineering efforts in generating a functionally stable hyaline cartilage (2). Clinically, NS deviation is one of the most frequent deformations resulting in cosmetic and respiratory alterations. Severe cases require surgical intervention to alleviate breathing obstructions and often require implantation of new cartilage. NSC is furthermore one of the primary and commonly used donor sites for autologous cartilage graft in nasal reconstructive and cosmetic surgery [6]. It is also used for autologous grafting to other locations such as the knee, as it is a relatively easy to harvest hyaline cartilage and shows superior tissue stability compared to auricular or costal cartilages[6]. However, its small size and limited tissue availability pose significant limitations, particularly when previous surgical intervention/trauma to the nose has occurred[6]. Thus, there is interest from tissue engineering, as there is an unmet clinical need to engineer functional hyaline cartilage *in vitro*. A current major challenge is to create cartilage that maintains hyaline NSC properties and does not transform to fibrocartilage over time. An in-depth understanding of NSC properties should enable better engineering of new cartilage suitable for

long-term maintenance. On the other hand, several branches of Biology are interested in understanding NSC development and its contribution to facial growth as well as its structural properties (Figure 1.2).

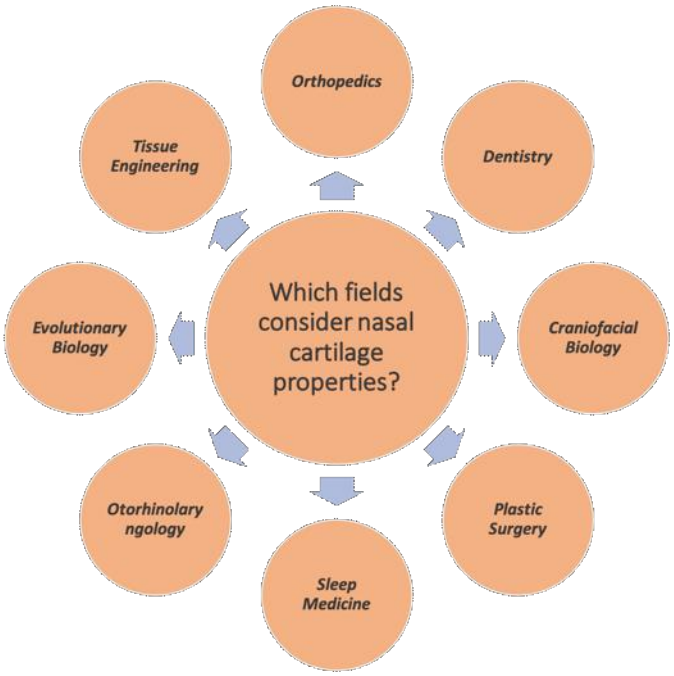

Figure 1. 2 Understanding nasal cartilage properties will benefit an interdisciplinary team of individuals.

NSC has been a focus of investigations since the 19th century. A breadth of knowledge has accumulated over time, conducted in a variety of species using diverse methodological approaches. As a result, much of this knowledge remains singular, and there has not been much unification. Hence, this scoping review aims to unify knowledge, potentially resolving controversies and challenges associated with NSC development and function. This review synthesizes published studies on NSC properties to (1) consolidate the current state of knowledge on extracellular, mechanical, and growth properties, (2) identify the areas that need further investigation and (3) highlight the need to analyze multiple properties while developing NSC tissue engineering approaches.

1.3 Methods

1.3.1 Overview

A considerable amount of research has been conducted in understanding NSC properties. The majority of studies focus primarily on a single property. Studies are often invested in identifying novel capabilities of nasal chondrocytes for cartilage regeneration but very rarely consider in-depth the underlying biological properties that contribute to these capabilities. There appears to be an overall lack of understanding of how these properties collectively contribute to form the mature NSC. By conducting a scoping review, we aim to consolidate existing knowledge on various NSC properties and provide a rationale demonstrating the importance of assessing more than one property while engineering neocartilage. A Preferred Reporting Items for Systematic Reviews and Meta-Analyses (PRISMA-R) checklist was used to provide the reader with a review outline (Table 1.1) and demonstrate methodological transparency and reproducibility.

Table 1. 1 Preferred Reporting Items for Systematic Review and Meta Analyses Statement (PRISMA-S) checklist.

Section/topic	#	Checklist item	Location(s) Reported
INFORMATION SOURCES AND METHODS			
Database name	1	Name each individual database searched, stating the platform for each.	Methods
Multi-database searching	2	If databases were searched simultaneously on a single platform, state the name of the platform, listing all of the databases searched. (Cochrane Library (Reviews and Trials)	Methods
Study registries	3	List any study registries searched.	Methods
Online resources and browsing	4	Describe any online or print source purposefully searched or browsed (e.g., tables of contents, print conference proceedings, web sites), and how this was done.	N/A
Citation searching	5	Indicate whether cited references or citing references were examined, and describe any methods used for locating cited/citing references (e.g., browsing reference lists, using a citation index, setting up email alerts for references citing included studies).	N/A
Contacts	6	Indicate whether additional studies or data were sought by contacting authors, experts, manufacturers, or others.	N/A
Other methods	7	Describe any additional information sources or search methods used.	N/A
SEARCH STRATEGIES			
Full search strategies	8	Include the search strategies for each database and information source, copied and pasted exactly as run.	Appendix 1
Limits and restrictions	9	Specify that no limits were used, or describe any limits or restrictions applied to a search (e.g., date or time period, language, study design) and provide justification for their use.	Methods
Search filters	10	Indicate whether published search filters were used (as originally designed or modified), and if so, cite the filter(s) used.	N/A
Prior work	11	Indicate when search strategies from other literature reviews were adapted or reused for a substantive part or all of the search, citing the previous review(s).	N/A
Updates	12	Report the methods used to update the search(es) (e.g., rerunning searches, email alerts).	Methods
Dates of searches	13	For each search strategy, provide the date when the last search occurred.	Appendix 1
PEER REVIEW			
Peer review	14	Describe any search peer review process.	N/A
MANAGING RECORDS			
Total Records	15	Document the total number of records identified from each database and other information sources.	Appendix 1
Deduplication	16	Describe the processes and any software used to deduplicate records from multiple database searches and other information sources.	Methods
PRISMA-S: An Extension to the PRISMA Statement for Reporting Literature Searches in Systematic Reviews			
Rethlefsen ML, Kirtley S, Waffenschmidt S, Ayala AP, Moher D, Page MJ, Koffel JB, PRISMA-S Group. Last updated February 27, 2020.			

1.3.2 Study Design

A scoping review rather than a systematic or narrative review was used since it is designed to allow unbiased exploration and reporting on a broader research topic. Arksey and O'Malley's [7] five-stage methodological framework was used to conduct this scoping review.

1.3.2.1 Stage 1: Identifying the research questions

This study reviewed published literature from various databases as outlined in appendix 1 to demonstrate the existing knowledge and subsequently identify approaches to integrate this

information into our ongoing cartilage tissue regeneration efforts. The main research question that guided the search was:

1. What NSC properties do authors characterize?
    a. What techniques are used to identify these properties?
    b. Is there agreement on the identified properties of the NSC?

The overarching research question was the objective of this scoping review, with the sub-questions serving as aims of the study. This research question guided the search strategy, organization, and analysis of the scoping review findings. The NSC properties identified from the extracted data were categorized into three groups, and the sub-questions were used to critically assess the state of research conducted on each property (Figure 1.3).

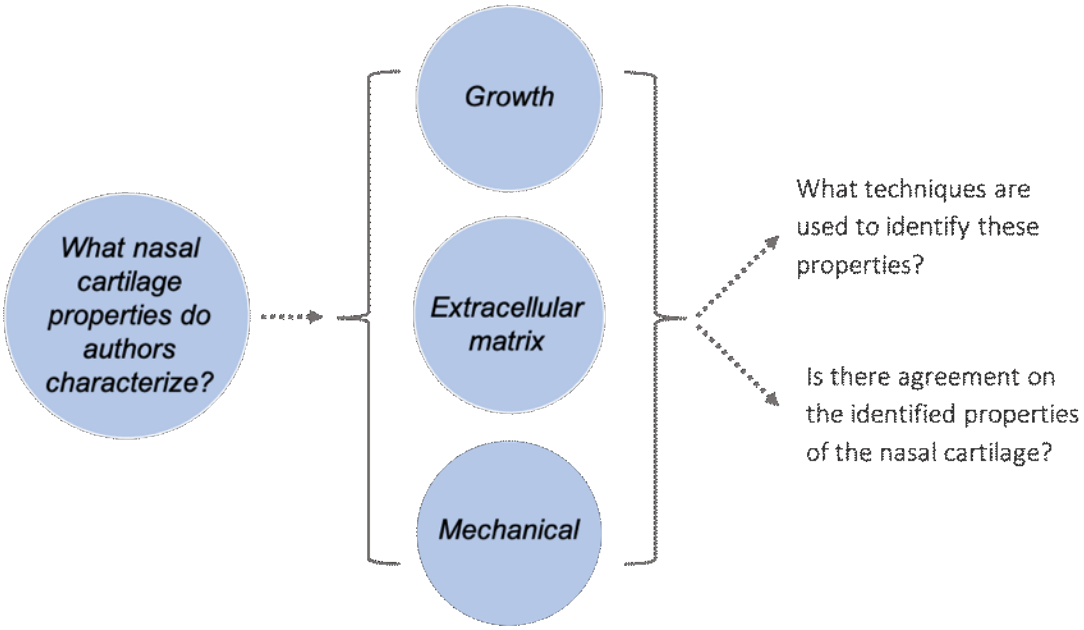

Figure 1. 3 Conceptual framework of the scoping review.

1.3.2.2 Stage 2: Identifying relevant studies – search strategy

A search was executed by an expert searcher/health librarian (SC) on the following databases: PROSPERO, Cochrane Library (CDSR and Central), WOS BIOSIS, WOS Core Collection, and ProQuest Dissertations and Theses Global using controlled vocabulary and text words representing the concepts “nasal cartilage" and “biological or physical properties”. No limits or search filters were applied. Databases were searched from inception to April 2021. Detailed search strategies are available in Appendix 1.

1.3.2.3 Stage 3: Study Selection

An extended PRISMA-R approach was used to report on the findings (Figure 1.4). Articles from the databases mentioned above and search terms identified 3707 articles that were exported to COVIDENCE review management software, where 222 duplicates were removed. A moderate interrater agreement was established using Cohen’s kappa. The inclusion and exclusion criteria outlined in Figure 1.4 and Table 1.2 yielded 84 articles which were thus assessed in this review.

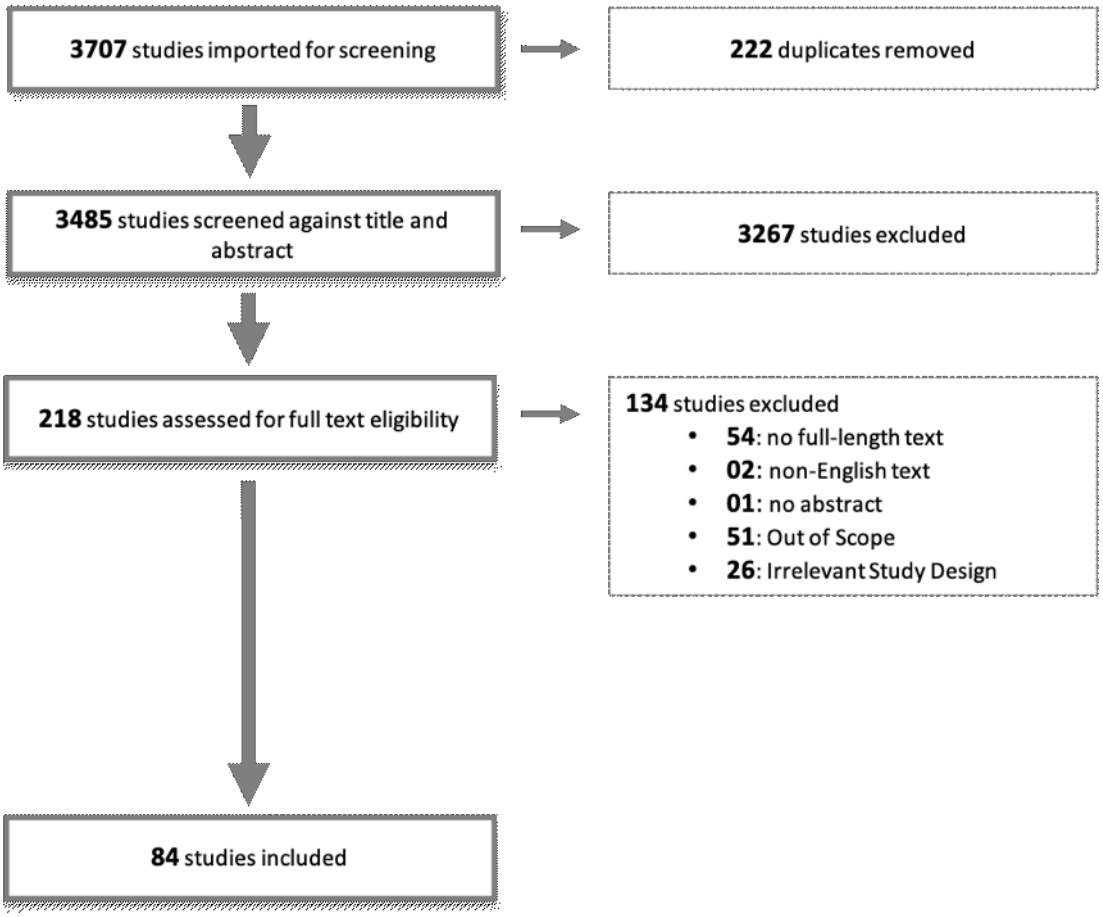

Figure 1. 4 Preferred Reporting Items for Systematic Review and Meta Analyses (PRISMA) flow chart outlining the scoping review process.

Table 1. 2 Inclusion and exclusion criteria used in the review.

Criteria	Inclusion Criteria	Exclusion Criteria
Language	English or English translated articles	Non-English articles with no English translation
Year of Publication	All articles published	None
Peer-reviewed	Yes	None
Study Design	• Original Research, • *In vivo* and *In vitro* research, • Literature reviews, • Human, rodent, rabbit and pig studies	• Tissue engineering using nasal chondrocytes • Surgical case studies • Nasal cartilage pathologies

1.3.2.4 Stage 4: Extracting and Charting Results

The identified articles were reviewed and charted by two evaluators using duplicate screening verification (PB and FB). A consensus-based discussion was performed to resolve inconsistencies and disagreements. The articles were organized by author, title, year, country, type of article and central theme of the article. The 84 articles selected for this review were published between 1963 and 2021. The geographic breakdown revealed that 42.86% (36/84) originated from the United States, 5.95% (5/84) from Canada, 5.95% (5/84) from Germany, 4.76% (4/84) from the United Kingdom, 4.76% (4/84) from Turkey, 4.76% (4/84) from South Korea, 4.76% (4/84) from the Netherlands, 3.57% (3/84) from Japan, 3.57% (3/84) from France, 3.57% (3/84) from Switzerland, 2.38 % (2/84) from Greece, 2.38 % (2/84) from Iran, 2.38 % (2/84) from Denmark, and 1.19% (1/84) article each from Australia, Austria, Hong Kong, Hungary, Norway, Portugal and Sweden.

1.3.2.5 Stage 5: Reporting Results

The findings from the 84 articles were classified based on three groups identified in Figure 1.3. The three groups included:

1. Growth
2. ECM and collagen composition
3. Mechanical properties

Each of the common themes was surveyed based on the sub-questions identified in stage 1.

1.3.3 Availability of Data

The data used in the review are available upon request from the corresponding author.

1.4 Results

1.4.1 Overview

The 84 articles in the review were categorized based on the three groups of NSC properties. Most research articles discussed the growth properties of NSC (46.43%, 39/84)[3,8–45], followed by articles on ECM (27.38%, 23/84) [4,5,46–66] and mechanical properties (22.62%, 19/84) (2, 4, 67–83) (Figure 1.5). Only 1.19% of articles (1/84) addressed both cartilage growth and ECM properties[85], while 2.38% (2/84) discussed ECM in connection with mechanical properties of the NSC[86,87]. No articles were identified investigating growth in conjunction with mechanical properties. None of the articles incorporated all three aspects (growth, ECM and mechanical) of the NSC. Table 1.3 lists the articles characterized as studies investigating NSC growth properties, whereas Table 1.4 and 1.5 lists ECM, and mechanical properties, respectively. Table 1.6 lists articles that discussed more than one property.

1.4.2 Nasal cartilage growth

Growth properties have been the most consistently investigated over the past six decades (40/84), with an exponential increase in studies in the last decade. Most studies were conducted in North America (19) and Europe (15), followed by Asia (4), Middle East (1) and Australia (1) (Figure 1.5). 21 articles studied human samples. In contrast, the rest used various animal models such as rats (7), mice (6), pigs (4), rabbit (1), and chicken (1) (Figure 1.6).

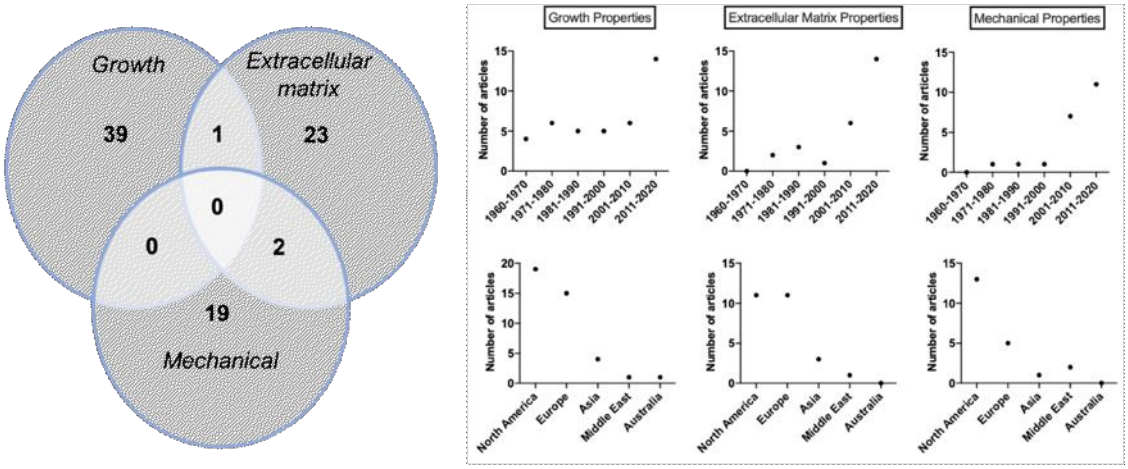

Figure 1. 5 Descriptive information of articles categorized into three nasal cartilage categories.

(Left panel) 39 articles discussed growth properties of the nasal septum cartilage while 23 commented on extracellular matrix properties and 19 articles assessed mechanical properties. (Right panel) Articles categorized based on the three cartilage properties and graphed as a function of time and geographical location. Note articles published in 2021 were added to 2011-2020.

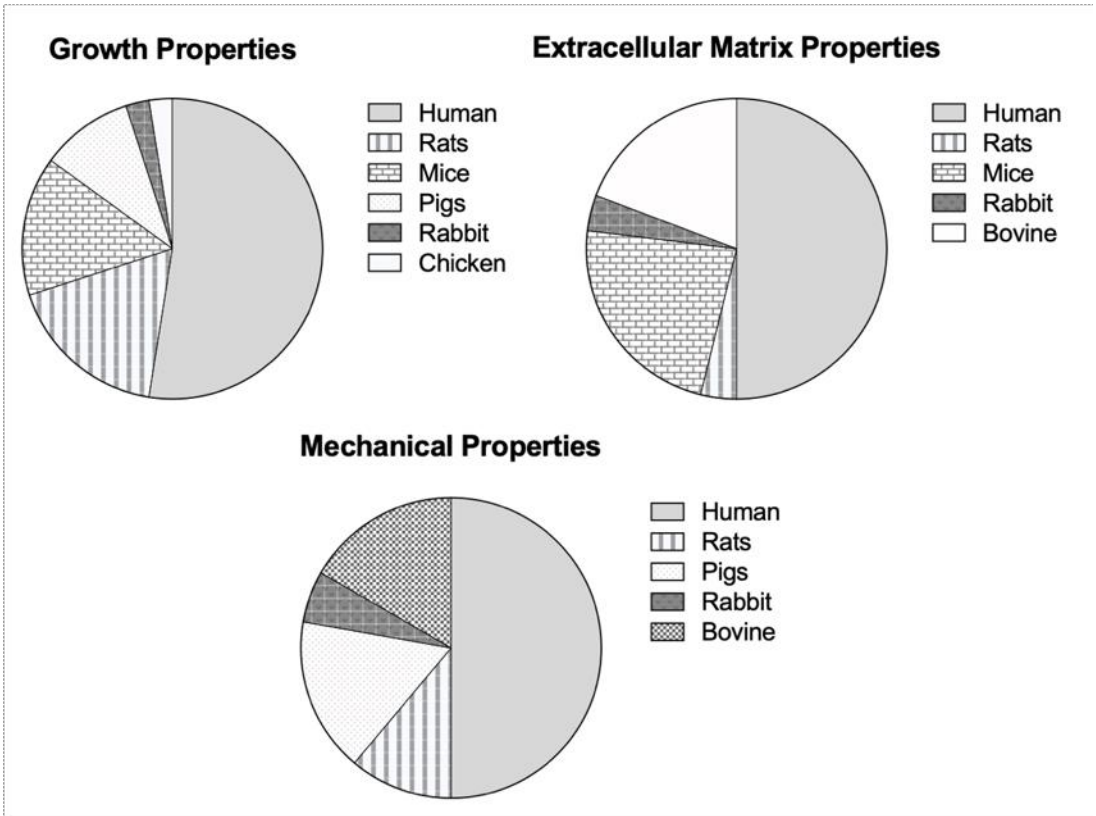

Figure 1. 6 Species used to investigate nasal cartilage properties.

Human studies commented either on NSC development, NSC growth, or the role of NSC in midfacial growth. The majority of the studies investigated NSC growth and its role in midfacial growth. Only a few studies addressed the development of the NSC itself. They established that the NSC originates from the ectomesenchyme (neural crest) and first develops during the third month of embryonic development[40]. Its overall shape is influenced both by the vertical growth and the time the ossifying PPE meets the vomer[20]. Cartilage thickness and appearance vary throughout development. The anterior base of the NS and the posterosuperior area were described as the thickest parts, while the anteroinferior part above the base is thinnest [31,49,80]. The cartilaginous region of the NS decreases with age, while the total area remains constant over time[27,33]. This reduction was attributed to the ossification of the PPE. Sex differences were observed during NSC development, where males have a larger NSC area than females[43,44]. An inverse relationship between NSC and age was observed for both sexes[16,27,45]. One study investigated size differences between different ethnic populations finding that those of European descent have a larger NS than individuals of African descent[29].

NSC growth was assessed using proliferation and cell density measurements. The NS develops both by appositional and interstitial growth, with cell densities decreasing and cell size increasing from birth to adulthood. A rapid increase in cell size was noted during the first two years of life. Much more limited proliferation was noted up to 35 years in the anterior central part of the NS[42,43]. However, it is not clear whether this compensates for cell apoptosis. Studies on minipigs also described a high proliferative capacity of the anterior central cartilage, as well as decreasing cellularity with age[9,10]. Several studies correlated changes to cellularity with episodic growth of the NSC in humans[3,8,27,42,43]. NSC growth is rapid during the first 2 years of life and plateaus by early adulthood (20 years). Data for children and adolescents are largely missing. A

similar episodic growth pattern was also observed in mice, pigs, and rats, although the timing of the bursts and pauses in growth was variable. Because of this growth potential early in development, investigators considered the NSC as a primary growth centre for midfacial growth. Currently unresolved, two contradictory lines of thought persist. One from Scott et al. [30] proposes that the NSC is a growth centre that pushes the midfacial bones downward and forward during prenatal development. Whereas Moss et al. [30] proposed the functional matrix theory where the NS is a strut, and its growth is passive and merely compensatory to the expansion of the nasal cavity and midfacial bones. Due to the inability to directly test these theories in humans, various animal models have been utilized to that effect. Many of those studies were done on rats. For instance, NS was extirpated and the effect on septum height was assessed. Extirpated snouts[30,34] showed reduced nasal height without the overall height of the face being affected. Altering the timing of extirpation led to different growth outcomes. None of the experiments resolved the controversy if NS directly drives or only accompanies midfacial growth.

A variety of techniques were used to assess NSC development. Investigations involving humans commonly used computed tomography (CT), magnetic resonance imaging (MRI) and cephalometric analysis. Access to human cadavers allowed to describe in detail histological appearance and cartilage maturation, adding to the understanding of NSC growth and development. Tissue dissection and histology were predominantly used in studies involving animals. Access to CT imaging was historically limited; however, in the past decade, CT analysis has been more widely used. This disparity in techniques used between human and animal studies has for a considerable time prevented direct data comparison and knowledge translation.

Although NSC growth is one of the most investigated aspects, gaps and controversies related to its development remain. A single time-point analysis and investigations at various ages

resulted in variable, not directly comparable results. The lack of standardized measures for nasal growth is a direct consequence of the use of diverse methodology. Snout resection studies in animals presented contradictory results and furthered the controversy in determining whether NSC is a critical structure for midfacial growth as these studies used animals of varying sizes and ages. Variation in location of resection added to the divide in findings. To overcome poor understanding of developmental timelines and the controversy regarding the role of nasal growth for midfacial growth, investigations need to utilize multiple methodologies to query cartilage thickness, proliferation and growth as the NSC develops. This would provide a strong foundation for developing hypotheses related to the role of NSC in midfacial growth. To illustrate this point, the two opposing theories outlining the role of nasal septum in midfacial growth were in part due to limited methodology and understanding of NS growth when these experiments were performed. Thus, there is a need to conduct age-matched standardized experiments to resolve this controversy.

Table 1. 3 Articles that investigated growth properties of the nasal cartilage.

Author	Year	Title	Country
Al Dayeh and Herring	2014	Cellular proliferation in the nasal septal cartilage of juvenile minipigs	USA
Al Dayeh et al	2013	Real-time monitoring of the growth of the nasal septal cartilage and the nasofrontal suture	USA
Amano et al	2020	Indian hedgehog in craniofacial neural crest cells links to skeletal malocclusion by regulating associated cartilage formation and gene expression	Japan
Ashique et al	2002	Signalling via type IA and type IB bone morphogenetic protein receptors (BMPR) regulates intramembranous bone formation, chondrogenesis and feather formation in the chicken embryo	Canada
Babula et al	1970	Role of cartilaginous nasal septum in midfacial growth	USA
Bruintjes et al	1996	Review of the functional anatomy of the cartilages and muscles of the nose	Netherlands
Burdi	1965	Sagittal growth of the nasomaxillary complex during the second trimester of human prenatal development	USA
Carnevale and Tatum	1996	Chondrocyte volume fraction distribution in porcine septal cartilage: An initial stereoscopic evaluation	USA
Catala and Johnston	1980	Interstitial growth of septal cartilage in the young albino-rat	USA
Copray	1986	Growth of the nasal septal cartilage of the rat in vitro	Netherlands
Daultrey et al	2018	The Caucasian Nasal Septum: An In Vivo Computed Tomography Study	UK
Delaire and Precious	1987	Interaction of the Development of the Nasal Septum the Nasal Pyramid and the Face	France
Diewert	1980	Differential Changes in Cartilage Cell Proliferation and Cell Density in the Rat Cranio Facial Complex during Secondary Palate Development	Canada
Elsaesser et al	2016	Characterization of a migrative subpopulation of adult human nasoseptal chondrocytes with progenitor cell features and their potential for in vivo cartilage regeneration strategies	Germany
Adegani et al	2013	A comparison of pluripotency and differentiation status of four mesenchymal adult stem cells	Iran
Foster and Holton	2016	Variation in the Developmental and Morphological Interaction Between the Nasal Septum and Facial Skeleton	USA
Goergen et al	2017	Morphological interaction between the nasal septum and nasofacial skeleton during human ontogeny	USA
Granstrom and Magnusson	1992	Histochemical analysis of enzymes involved in the formation and metabolism of the nasal septal cartilage	Sweden
Grymer and Bosch	1997	The nasal septum and the development of the midface. A longitudinal study of a pair of monozygotic twins	Denmark
Hall and Precious	2013	Cleft lip, nose, and palate: the nasal septum as the pacemaker for midfacial growth	Canada
Holton et al	2011	Nasal Septal and Premaxillary Developmental Integration: Implications for Facial Reduction in Homo	USA
Holton et al	2012	Nasal septal and craniofacial form in European- and African-derived populations	USA
Howe et al	2004	The growth of the nasal septum in the 6-9 week period of foetal development - Warfarin embryopathy offers a new insight into prenatal facial development	Australia
Hwang et al	2010	Mapping Thickness of Nasal Septal Cartilage	Korea
Kaucka et al	2018	Signals from the brain and olfactory epithelium control shaping of the mammalian nasal capsule cartilage	Austria
Kim et al	2008	Analysis of the Development of the Nasal Septum according to Age and Gender Using MRI	Korea
Kim et al	2010	Anatomical Variation of the Nasal Septum: Correlation Among Septal Components	Korea
Kvinnsland	1974	Partial resection of cartilaginous nasal-septum in rats – its influence on growth	Norway
Long et al	1968	Regional Variations in Chondrocyte Proliferation in the Cartilaginous Nasal Septum of the Growing Rabbit	USA
Marulanda et al	2017	Matrix Gla protein deficiency impairs nasal septum growth, causing midface hypoplasia	Canada
Melsen	1976	Histological Analysis of the Post Natal Development of the Nasal Septum	Denmark
Pavlov et al	2003	Chondrogenic differentiation during midfacial development in the mouse: In vivo and in vitro studies.	France
Searles	1977	A Radioautographic Study of Chondrocytic Proliferation in Nasal Septal Cartilage of the New Born Rat	USA
Seltzer	1963	The problem of the nasal septum	USA
Van Loosen et al	1988	The Nasal Septal Cartilage in the Newborn	Netherlands
Van Loosen et al	1997	Nasal cartilage maturation assessed by automated computer-assisted image analysis	UK
Vetter et al	1983	Growth-activity in human septal cartilage – age dependent incorporation of labeled sulfate in different anatomic locations	Germany
Vetter et al	1984	Postnatal-growth of the human septal cartilage – preliminary report	Germany
Vidic et al	1972	The Structure and Pre Natal Morphogenesis of the Nasal Septum in the Rat	USA

1.4.3 ECM and collagen composition of nasal cartilage

Of the 84 included studies, 26 focused on ECM components of the NSC (Table 1.4). Again, most were carried out in North America (11) and Europe (11), with a few coming from Asia (3) and the Middle East (1) (Figure 1.5). Almost half of the papers (10) came from the USA alone. Half of the studies were published within the last ten years (13), with 23% published between 2001-2010 (6), 11% in the period from 1981-1990, and 8% in the 1970s (Figure 1.5). Half of the studies used human samples, while the other half used different various animal models, specifically mice (6), bovine (5), rats (1), and rabbits (1) (Figure 1.6).

A variety of methods were employed to study the ECM, in particular basic histological techniques and immunohistochemistry/immunofluorescence. The overarching aim was to describe

ECM components and their relative location throughout the NSC. In the last couple of decades, in-situ hybridization and various biochemical assays were employed to support traditional histology[63,66]. The need for quantitative data analysis has seen the inclusion of micro-CT, qRT-PCR, chromatography, and biochemical assays for proteoglycan and glycosaminoglycan content analysis.

Most studies were descriptive and identified the ECM as an irregularly organized network of fine filaments and granules formed of collagen and non-collagen components[5,49]. In particular, collagen fibers fill the interstitial space of the network[49,55,66]. Its composition depends on the site of origin within the cartilage, likely reflecting local functional and physiological demands on the cartilage[85]. The predominant collagen is Collagen II (85-90%) which provides tensile strength and, in a lesser proportion, other types of collagen (I, VI, IX, X and XI)[4,47,64]. There is controversy on the presence of Collagen V[4,61,62,87]. Collagen II is found throughout the entire cartilage, while collagens I and III are restricted around chondrocytes (territorial zone)[4,87]. The variety of collagens, their different localization within the matrix, with some of them difficult to recognize due to masking by proteoglycans (PG). Hyaluronic acid digest is commonly used to expose the minor protein components located in the center of the cartilage[5]. Their specific distribution has been described from embryonic development onwards. Collagen I is found predominantly within the precursor blastema of the NSC[57] at early stages. Following a transition phase with the expression of both Collagen I and II, Collagen II becomes dominant throughout the cartilage, while Collagen I is predominantly found on the periphery[57].

The non-collagenous protein fraction consists mainly of proteins such as Laminin, glycoproteins (GP) such as Fibronectin, and proteoglycans (PG) such as aggrecan[46,61,62]. There is a high content of glycosaminoglycans (GAG; Hyaluronic acid, chondroitin sulfate, heparan

sulfate, and keratan sulfate), essential for maintaining an adequate level of water in the structure[62]. PG seem to be arranged in two groups: a PG-aggregate and a PG-collagen. PG-aggregate connects the core protein and link proteins (glycoproteins), while the PG-collagen binds the core proteins to the surrounding collagen. In the same way, there is an interaction between link proteins and collagen fibers [5,50]. Only one study was identified that compared PG content from human and bovine cartilage[54]. Although the study identified some differences, such as the chondroitin sulfate/keratan sulfate content, PG properties, and link protein distribution, it did not discuss their functional relevance to the development/function of the NSC. The most abundant PG is Aggrecan, which is entrapped within Collagen II, providing resistance against compressive forces[61]. A decrease in the amount of PGs with age was reported. It is thought that this does not compromise adult NSC as a source of cells for tissue engineering[50].

Fibronectin, an essential link protein, is distributed through the interterritorial matrix (in between territorial areas that surround chondrocytes), but it was also found within the territorial area as well as connecting units formed by a single chondrocyte (chondron) and its immediate surrounding (Figure 1.1). These macromolecules are thought to play an essential role in both cell-matrix adhesion and matrix-matrix cohesion in the territorial area [50].

Regarding GAG content, chondroitin sulfate is predominant, followed by hyaluronic acid, keratan sulfate, and in minor proportion dermatan sulfate. A unique role has been attributed to hyaluronic acid, which binds Aggrecan and link proteins. Interestingly, the GAG composition of healthy human NSC differs from scoliotic NSC, lending support to the idea that NSC composition and organization are connected to the ability to withstand functional stresses[61,62].

Several reports refer to a differential and specific distribution of collagen and non-collagen components from the center of the cartilage to the periphery, and in the anteroposterior

direction[46,57]. This specific pattern could hold the clue for the particular mechanical properties that differentiate the NSC from other hyaline cartilage, such as the knee articular cartilage.

The detailed description of ECM characteristics is technically challenging. As in any other field, results are technique sensitive, and this might be the origin of some of the discrepancies noted. For example, separating collagens from the non-collagen portion is difficult, and this likely affects the visualization of the cartilage composition. Few studies compare cartilages from different species, making it difficult to translate findings from non-human studies to humans, particularly since the shape and size of the NSC determine functional abilities. Although there is a high agreement between studies concerning cartilage composition, most studies are qualitative and merely descriptive. Samples are from different locations and ages, making direct comparison difficult. More detailed and comprehensive studies are required to fully understand the functional importance of the ECM organization and disposition in the NSC.

Table 1. 4 Articles that investigated extracellular matrix properties of the nasal cartilage.

Author	Year	Title	Country
Aksoy et al	2011	Structural characteristics of septal cartilage and mucoperichondrium	Turkey
Ayad and Weiss	1984	A New Look at Vitreous Humor Collagen	UK
Boukla	1990	Purification and Properties of Bovine Nasal Hyaline Cartilage Collagenase	Greece
Evans et al	1983	Localization of Collagen Types and Fibronectin in Cartilage by Immuno Fluorescence	UK
Glant et al	1977	The Localization of Proteo Glycans and Glyco Proteins in the Hyaline Cartilage	Hungary
Holden et al	2008	Human Nasal Cartilage Ultrastructure: Characteristics and Comparison Using Scanning Electron Microscopy	USA
Kim et al	2018	Characteristics of Nasal Septal Cartilage-Derived Progenitor Cells during Prolonged Cultivation	Korea
Lee et al	2013	Age-Related Histologic Changes in Human Nasal Cartilage	USA
Neuman et al	2013	A compositional analysis of cadaveric human nasal septal cartilage	USA
Pelttari et al	2017	Nasal chondrocytes as a neural crest-derived cell source for regenerative medicine	Switzerland
Perin et al	1978	Comparative Studies on Human and Bovine Nasal Cartilage Proteo Glycan Complex Components	France
Riedler et al	2017	Age-Related Histologic and Biochemical Changes in Auricular and Septal Cartilage	USA
Rotter et al	2001	Age dependence of cellular properties of human septal cartilage - Implications for tissue engineering	USA
Sasano et al	1992	Distribution of type I collagen, type II collagen and PNA binding glycoconjugates during chondrogenesis of three distinct embryonic cartilages	USA
Sasano et al	2001	Gene and protein expressions of type I collagen are regulated tissue-specifically in rat hyaline cartilages in vivo	Japan
Shafiee et al	2011	Nasal Septum-Derived Multipotent Progenitors: A Potent Source for Stem Cell-Based Regenerative Medicine	Iran
Takahashi et al	2012	Histological study of the nasal septal cartilage in BALB/c-bm/bm mouse which spontaneously induces malocclusion	Japan
Theocharis et al	2002	Isolation and characterization of matrix proteoglycans from human nasal cartilage - Compositional and structural comparison between normal and scoliotic tissues	Greece
Ustunel et al	2003	Immunohistochemical distribution patterns of collagen type II, chondroitin 4-sulfate, laminin and fibronectin in human nasal septal cartilage	Turkey
Wan et al	2018	A six-gene expression toolbox for the glands, epithelium and chondrocytes in the mouse nasal cavity	USA
Wiggenhauser et al	2018	The distribution patterns of COMP and matrilin-3 in septal, alar and triangular cartilages of the human nose	Germany
Yu et al	2017	Expression of Noggin and Gremlin1 and its implications in fine-tuning BMP activities in mouse cartilage tissues	USA
Zhang et al	2012	Expression of dentine sialophosphoprotein in mouse nasal cartilage	USA

1.4.4 Mechanical properties of the nasal cartilage

19 of the 84 studies included in the review investigated mechanical properties of the NSC (Table 1.5). Most of the investigations were conducted in North America (13), followed by Europe (5), Middle East (2) and Asia (1) (Figure 1.5). Most of the studies (85%) were published in the two last decades. An equal number of human (9/19) and animal (9/19) studies were conducted (Figure 1.6). Equilibrium modulus, elastic modulus, compression, hydraulic permeability, stress, strain, and tensile strength were measured in the NSC.

Studies measuring the equilibrium modulus [78,79,88] observed a decrease in modulus with increasing donor age. The most prominent decrease in equilibrium occurred around 25-35 years of age[78,79]. This decrease in equilibrium was accompanied by a reduction in glycosaminoglycan content[79]. No differences between the sexes were observed. Hydraulic permeability measurements assessing flow resistance and collagen content based on hydroxyproline levels demonstrated a decrease in flow resistance and collagen content with age[79]. Studies comparing nasal cartilage to various articular (knee) and elastic (ear) cartilages revealed that NSC is more permeable than those other cartilages[70]. Similarly, a decrease in elastic modulus was noted with age, which was attributed to NSC remodeling becoming more fibrous with age[72,73,79,82]. One study calculated the contribution of the perichondrium that lines the NSC to elastic modulus and deflection strength[80]. NSC with undisturbed perichondrium is 18% more effective in preserving the shape. However, these results might be treated with caution, as they were based on a small sample size, no statistical analysis was performed, and ECM quality might have been compromised due to the use of human cadaver material. Proteoglycans expected to be important for those measurements have a short half-life after isolation.

Between several studies, stress, strain, compression, and tensile measurements on the NSC displayed contradictory results. One study reported that mechanical properties of the NSC were comparable to other load-bearing cartilages. Compression studies revealed that the septo-ethmoidal junction rather than the septum itself was under anteroposterior compression caused by occlusal loading[2]. The NS was found to absorb energy and forces transmitted through the skull. One study commented that the NS is overall stiff, capable to move only at the vomer[2]. Variable stiffness based on orientation was described. A higher stiffness was observed in the caudal-cephalic and vertical orientation than in the horizontal plane[83,88]. Stress relaxation post compression measurements aligned with the heterogeneity of stiffness observed along the NS. In general, the medial plane demonstrated greater tissue relaxation potentially due to reduced stiffness in that region[72,83]. Studies on tensile strength of the NSC were limited, with one study comparing nasal and articular cartilages concluding that NSC has weaker tensile strength than articular cartilage[78]. Another study compared compression and tensile properties and concluded that the NSC was more under the influence of compression rather than tension[69].

The methodologies used to investigate mechanical properties of the NS are diverse, making it challenging to compare different studies involving assessments of the same properties directly. There is a need to develop more universally applicable measurement systems that ideally can be used irrespective of species tested. The use of small sample sizes, performing measurements on isolated tissues rather than on intact tissues, and age differences all could contribute to the incongruence in findings. This makes translation of findings across species challenging. In particular, it remains unclear to what degree mechanical properties of the NSC are heterogeneous and depend on location within the NS.

Table 1. 5 Articles that investigated mechanical properties of the nasal cartilage.

Author	Year	Title	Country
Al Dayeh et al	2009	Deformation of Nasal Septal Cartilage During Mastication	USA
Alkan et al	2011	Tensile Characteristics of Costal and Septal Cartilages Used as Graft Materials	Turkey
Al Dayeh and Herring	2014	Compressive and tensile mechanical properties of the porcine nasal septum	USA
Bos et al	2018	Structural and Mechanical Comparison of Human Ear, Alar, and Septal Cartilage	Netherlands
Caffrey et al	2013	Flexural Properties of Native and Tissue-Engineered Human Septal Cartilage	USA
Colombo et al	2013	Mechanical behavior of bovine nasal cartilage under static and dynamic loading	Switzerland
Correro-Shahgaldian et al	2016	Properties and Mechanobiological Behavior of Bovine Nasal Septum Cartilage	Switzerland
Flam	1974	The Tensile and Flexural Properties of Bovine Nasal Cartilage	USA
Grellmann et al	2006	Determination of strength and deformation behavior of human cartilage for the definition of significant parameters	Germany
Iwanaga et al	2018	Distribution of the internal nasal branch of the infraorbital nerve to the nasal septum: Application to rhinoplasty	USA
Reuther et al	2012	In vivo oxygen tension in human septal cartilage increases with age	USA
Richmon et al	2006	Compressive biomechanical properties of human nasal septal cartilage	USA
Richmon et al	2005	Tensile biomechanical properties of human nasal septal cartilage	USA
Rotter et al	2002	Age-related changes in the composition and mechanical properties of human nasal cartilage	USA
Tekke et al	2014	Importance of nasal septal cartilage perichondrium for septum strength mechanics: a cadaveric study	Turkey
Tsao and Chuah	1988	Development of Bone-Like Substance in Cartilaginous Rat Nasal Septum Under Experimental Conditions	Hong Kong
Westreich et al	2007	Defining nasal cartilage elasticity - Biomechanical testing of the tripod theory based on a cantilevered model	USA
Xia et al	2012	Anisotropic properties of bovine nasal cartilage	USA
Youn et al	2000	Optical and thermal properties of nasal septal cartilage	USA

Only 3/84 papers reported on more than one property of the NSC (Table 1.6). Two of these papers reported on ECM and mechanical properties, while the third study reported on growth and ECM properties. The studies on ECM and mechanical properties demonstrated that NSC expressing collagen V and collagen X is stiffer than epiglottal and articular cartilage[87]. In contrast, collagen VI was only found in elastic and articular cartilage and not the NSC. Thus, expression of various collagens appears to be associated with various cartilage properties. The distribution of collagens might also be important because, for instance, expression of collagen X in the NSC is pericellular, whereas in articular cartilage, it is distributed throughout the matrix surrounding hypertrophic chondrocytes [87]. Another study integrating growth and ECM properties reiterates that NS is a heterogeneous structure with a dynamic growth rate that involves bursts and pauses of growth during development [85]. This investigation, although in mice, confirms that cell density decreases and cell size increases over time as previously described in other rodent and human

samples. Moreover, this study also demonstrates that the NS matures through chondrocyte hypertrophy in an anterior-posterior and dorsal-ventral direction over time. It is one of the very few studies to investigate ECM and growth properties of the NSC throughout postnatal development.

Table 1. 6 Articles that investigated more than one nasal cartilage property.

Author	Year	Title	Country	Cartilage Property
Fertuzinhos et al	2020	Thermo-Mechanical Behaviour of Human Nasal Cartilage	Portugal	Extracellular Matrix and Mechanical Properties
Baddam et al	2021	Histological and molecular characterization of the growing nasal septum in mice	Canada	Growth and Extracellular Matrix Properties
Naumann et al	2002	Immunochemical and mechanical characterization of cartilage subtypes in rabbit	USA	Extracellular Matrix and Mechanical Properties

In conclusion, although attempts have been made to integrate multiple cartilage properties and delineate the functional relationship between them, they ultimately still describe the properties in isolation. They fail to demonstrate how differences in these properties functionally act together and contribute to the development of the NS.

1.5 Discussion

Investigations to define NSC properties have been performed for many decades. Here we present the first scoping review summarizing accumulated knowledge on these properties. The most prominent aspects investigated are growth, ECM, and mechanical properties; hence this review is structured to reflect this.

Studies assessing growth properties revealed that the timeline of growth is variable. Existing data suggest trajectories of growth bursts and pauses during development in several species. Variability in the timeline of growth stems from diverse ages of human and animal samples used. Investigations across different species also demonstrated that cell density decreases and cell size increases with age in the NSC. If and to what degree the NSC directly contributes to midfacial growth remains controversial. Follow-up studies to validate or diffuse Scott et al.'s

functional matrix theory [30] using rats [34] remained inconclusive. The influence of genetics on NSC growth and differentiation has not been widely explored. We identified only one study on twins that assessed how nasal trauma affects septum growth[26(p1)]. Extrapolating from these results, it appears that NSC growth is governed by significant genetic predisposition.

Understanding how ECM properties contribute to or define NSC properties has been a long-standing interest of the research field. ECM properties have consistently been characterized using classic histological methods and more recently from advanced quantitative methodologies such as proteomics. Comparing expression patterns of ECM markers across species is relatively easier. Studies have demonstrated that the NSC shows a dynamic expression of collagens and proteoglycans during development. Collagens I and II are most extensively studied, showing that both collagens I and II are present at early stages of NSC development, with collagen I expression subsiding as the NSC matures. Conversely, collagen II expression increases as the NSC differentiates. Differential staining of proteoglycans like Aggrecans was also observed during the development of NSC. Despite the detailed qualitative description, functional significance of differences in these ECM markers remains unclear. Furthermore, description of expression patterns of ECM components is often limited to one specific location and point in time or comparison to other cartilage types. This makes it challenging to appreciate how changes in ECM components contribute to NSC development and maturation. There are age- and region-specific changes to chondrocyte density and size. It is fair to assume that similar differences also exist in relation to ECM components. Surprisingly, only 2/84 studies have investigated age-specific changes to ECM, while only 1/84 studies explored both age and region-specific changes to expression of ECM markers. Understanding age and region-specific expression patterns of ECM

components become important when comparing native nasal cartilage against tissue-engineered cartilage.

Mechanical properties of the NSC were only relatively recently investigated. To date, in-depth studies considering age and location of the NSC are lacking. Most studies were conducted at a single time point and location. Given the heterogeneous structure of NSC, it is fair to assume that location-dependent mechanical properties may exist. Moving forward, investigations considering age and location when assessing mechanical properties should clarify if and how local variations in properties contribute to the physiological function of the NSC.

1.5.1 Gaps of knowledge

NSC properties are not only defined by growth/maturation, ECM, and mechanical properties. Little is known about the roles nerves, vasculature, and perichondrium play in forming and maintaining healthy NSC. If and how the cartilage remodels throughout life is also unknown. While compiling articles for this review, it became apparent that significant literature exists for each of the three selected aspects of NSC. However, information on how the three properties intersect remains comparatively scarce. Most studies addressed a single property in isolation, contributing to the data heterogeneity.

Although there is sufficient evidence showing that NSC grows rapidly during early stages of development, the time point when this growth stabilizes remains poorly defined. The mechanisms underlying growth stabilization similarly remain unexplored. Several articles have demonstrated that cell density and cell size are inversely related during NSC development. What regulates the switch between a decrease in cell density and an increase in cell size and how this contributes to NSC growth remains unclear. Understanding better the growth mechanism would

help clinicians with treatment planning for growth-dependent pathologies like cleft palate or midfacial hypoplasia.

The expression patterns of ECM components in the mature NSC are mostly well established. Detailed information on age and location-specific differences are, however, lacking. Little is known about the ability of the NSC to remodel and adapt. We found only one report investigating cartilage proteinases (Collagenase 1 and 2) in NSC[48]. Outlining expression of collagenases, proteinases and their inhibitors becomes important when correlating cartilage remodelling to NSC growth. A few articles commented on collagen fibril organization, but no interpretation of how collagen fibril organization would contribute to cartilage maturation and properties was provided. Several studies referred to a similar GAG content in NSC as found in various other hyaline cartilages, although they differ in their properties[73]. Why this may be is still unclear. Understanding these nuances will clearly be important for tissue engineering when deciding on the origin of cell source and transplantation site.

To date, mechanical properties of the NSC have been least explored, and various gaps of knowledge persist. Firstly, there is no standardized methodology to test different parameters such as tension, compression of NSC. The existing methodologies are rather specific to species, size, and location of the sample. While this is to some degree necessary, developing methodological approaches that have broader applicability is important. Secondly, some articles have tested equilibrium and elastic modulus of the NSC. It is currently unclear to what degree the elastic modulus varies within given groups (e.g., patient populations). Similarly, NSC from different species depending on biological constraints is expected to differ. Last but not least, understanding if and how mechanical properties vary depending on location within a given cartilage will be clinically significant, especially in cases of corrective surgeries that remove parts of NSC. It might

be expected that some site of the NSC is more tolerant to invasive procedures than others. Thus, a better understanding of the site-specific impact on stiffness and tensile strength would guide clinicians.

In addition to the above-identified specific gaps of knowledge, we identified two more general research needs:

1. There is a frequent and silent assumption that NSC properties between different species or different hyaline cartilage-bearing tissues are comparable. Given the structural and functional heterogeneity, it is fair to assume that this is not necessarily the case. Thus, there is a need to conduct species- and hyaline cartilage type-specific studies.
2. It is currently not known if and to what degree cartilage properties change as part of NSC pathologies such as nasal septum deviation. Thus, comparative studies between healthy and pathological NSCs are needed.

1.5.2 Strengths and Limitations

This review, to our knowledge, provides the first comprehensive description of the state of research on NSC properties. It identifies the need to incorporate already existing knowledge to generate functionally stable cartilage. It underscores the need to establish more granular, standardized assessment protocols to describe NSC. Technological advances will continue to facilitate this.

A limitation of the review is that it was restricted to NSC. It was not the scope of the review to assess all cartilages. Quite likely, a better understanding of cartilage properties exists for other cartilages such as knee articular cartilage, although it would be challenging to translate this directly to the NSC. The heterogeneity of the studies poses a challenge to integrate existing knowledge of NSC properties coherently. Critically evaluating the methodology used in the included articles was

not part of the scope of this review. The need for standardization of experiments and methodologies became evident; however, it was not the scope of this review to critically evaluate the various approaches. Although a broad search strategy was applied, a possibility remains that some of the articles were not considered in this review.

1.6 Appendix 1: Detailed search strategy

Supplemental Table 1. 1 BIOSIS Previews (WOS) Searched April 1, 2021. Timespan=All Years

Line Number	Search For	Results
#1	TS=(evolution* or model* or "biological" or properties))	6,507,970
#2	(TS=(Abnormal* or Analysis or Analytical or Anatom* or Elastic* or Histolog* or Histopatho* or "Cell" or Cellular or Chemistry or Chemical or Composition or Cytolog* or Differentiat* or Growth or Development or Genetic* or Immunolog* or Inflamm* or Mechani* or Ossifi* or Patholog* or Physiolog* or Physiopatholog* or Proteomic* or Structure or Structural or Ultrastructure*))	26,924,977
#3	#1 or #2	26,924,977
#4	TS= (("nasal cartilage" or septal adj3 cartilage* or :septum near/3 cartilage* or (hyaline near/3 (septal or septum or nose or nasal*))) or "nasal septum" or deviat* near/3 sept*)	3,250
#5	#3 and #4	3,193
#6	TI=("case report*" not ("case report" and review)) or TI= (clinical or therapy or therapeutic)	1,162,238
#7	#5 not #6	3051

Web of Science Core Collection (includes Science Citation Index, Social Sciences Citation Index, Arts & Humanities Citation Index, Conference Proceedings Citation Index Book Citation Index, Emerging Sources Citation Index, Index Chemicus ,Current Chemical Reactions) Searched April 27, 2021 Results = 585

((TS=((evolution* or model* or "biological" or properties))) OR TS=(((Abnormal* or Analysis or Analytical or Anatom* or Elastic* or Histolog* or Histopatho* or "Cell" or Cellular or Chemistry or Chemical or Composition or Cytolog* or Growth or Development or Genetic* or Immunolog* or Inflamm* or Mechani* or Ossifi* or Patholog* or Physiolog* or Physiopatholog* or Proteomic* or Structure or Structural or Ultrastructure*)))) AND TI=((("nasal cartilage" or

"sept* cartilage*" or (hyaline near/3 (sept* or nose or nasal*))) or "nasal septum")) Not TI=(clinical or "case report*" or therapy or therapeutic)

Proquest Dissertations and Theses Global Searched April 27, 2021 Result = 75

noft((Abnormal* OR Analysis OR Analytical OR Anatom* OR Elastic* OR Histolog* OR Histopatho* OR "Cell" OR Cellular OR Chemistry OR Chemical OR Composition OR Cytolog* OR Growth OR Development OR Genetic* OR Immunolog* OR Inflamm* OR Mechani* OR Ossifi* OR Patholog* OR Physiolog* OR Physiopatholog* OR Proteomic* OR Structure OR Structural OR Ultrastructure* OR evolution* OR model* OR "biological" OR properties)) AND noft((("nasal cartilage" OR "sept* cartilage*" OR (hyaline NEAR/3 (sept* OR nose OR nasal*))) OR "nasal septum"))) NOT noft(("case report*" NOT ("case report" AND review)) OR (clinical OR therapy OR therapeutic))

Supplemental Table 1. 2 Cochrane Library (CDSR and Cochrane Trials) Searched April 27, 2021

ID	Search	Hits
#1	(((evolution* or model* or "biological" or properties))):ti,ab,kw	184743
#2	(Abnormal* or Analysis or Analytical or Anatom* or Elastic* or Histolog* or Histopatho* or "Cell" or Cellular or Chemistry or Chemical or Composition or Cytolog* or Differentiat* or Growth or Development or Genetic* or Immunolog* or Inflamm* or Mechani* or Ossifi* or Patholog* or Physiolog* or Physiopatholog* or Proteomic* or Structure or Structural or Ultrastructure*)	859946
#3	#1 or #2	906275
#4	((("nasal cartilage" or "sept* cartilage*" or (hyaline near 3 (sept* or nose or nasal*))) or "nasal septum")):kw or ((("nasal cartilage" or "sept* cartilage*" or (hyaline near 3 (sept* or nose or nasal*))) or "nasal septum")):kw)	228
#5	#3 and #4	125
#6	((clinical or "case report*" or therapy or therapeutic)):ti,ab,kw	1101787
#7	#5 not #6	48

Supplemental Table 1. 3 PROSPERO Searched April 27, 2021

Line	Search for	Hits
#1	(evolution* or model* or "biological" or properties)	55265
#2	(Abnormal* or Analysis or Analytical or Anatom* or Elastic* or Histolog* or Histopatho* or "Cell" or Cellular or Chemistry or Chemical or Composition or Cytolog* or Differentiat* or Growth or Development or Genetic* or Immunolog* or Inflamm* or Mechani* or Ossifi* or Pathолog* or Physiolog* or Physiopatholog* or Proteomic* or Structure or Structural or Ultrastructure*)	106168
#3	#1 OR #2	107296
#4	"nasal cartilage" or "septal cartilage*" or "septum cartilage*"	4
#5	(hyaline and (septal or septum or nose or nasal*)) or "nasal septum" or "deviat* sept*"	20
#6	#4 OR #5	22
#7	#3 AND #6	21
#8	(("case report*" not ("case report" and review))):TI,KW	76
#9	((clinical or therapy or therapeutic)):TI,KW	14176
#10	#8 OR #9	14237
#11	#7 not #10	19

Chapter 2: Nasal cavity structural anomalies among individuals at high risk of SDB: an exploratory CBCT study

Chapter 1 established that the nasal septum grows rapidly by age 2 in humans and stabilizes by 25-36 years of age. It also described that nasal septum deviation is a common pathology observed in humans, with only a small proportion of these individuals presenting with secondary morbidities that require further intervention. Correlating secondary morbidities such as airway obstruction to age and severity of nasal septum deviation is a clinical challenge. Thus, in Chapter 2, the nasal cavity of a cohort of children with or without being at risk for Sleep-disordered breathing was assessed using CBCT scans to identify if age, severity of septum deviation, and being at risk for sleep-disordered breathing were correlated.

Chapter 2 is derived from this accepted article:

Baddam, P., Bussolaro, C.-T., Flores-Mir, C. and Graf, D. (2021). Nasal cavity structural anomalies among children at high risk of sleep-disordered breathing: an exploratory cone-beam computed tomography study. *Am. J. Orthodont. Dentofacial Orthop. (In press).*

2.1 Abstract

Introduction: In this study, we investigated the presence of structural anomalies in the nasal cavity (deviated nasal septum - DNS, turbinate hypertrophy - TH) in individuals at high risk or not of sleep-disordered breathing (SDB).

Methods: A retrospective study considering available CBCT scans of 99 individuals was conducted. Dolphin software was used to process the craniofacial scans. The Pediatric Sleep Questionnaire (PSQ) was used to suggest at high risk of SDB. Subjective and objective assessments of DNS and TH were considered.

Results: Good to excellent intra- and inter-reliability was attained. Prevalence of a PSQ score suggestive of at high risk of SDB in this sample was 59%. The prevalence of subjective DNS and TH assessment was 64% and 70%, respectively. In contrast, based on objective assessments, 27% of individuals presented with DNS, and 25% with TH. Cross-tabulation of DNS and TH with PSQ score indicated a statistically significant association between subjective DNS and subjective TH and subjective TH and positive PSQ. A positive correlation between age and subjective and objective DNS assessments was also observed.

Conclusions: Older individuals are more likely to present with DNS. Only presence of subjectively determined TH in individuals is associated with at high risk for SDB. The study reveals that assessment of DNS and TH using CBCT imaging is not likely suitable to strongly suggest individuals at high risk for SDB. DNS subjective assessments were capable of identifying less than 5% of deviation.

Keywords: nasal cavity; nasal septum deviation; turbinate hypertrophy; pediatric sleep questionnaire; sleep-disordered breathing; Cone Beam Computed Tomography; children; adolescents.

2.2 Introduction

The nasal cavity in humans is divided into two sides by the nasal septum. The nasal septum, a cartilaginous tissue, provides structural support for the upper nasal cavity. Abnormalities to the septum could significantly affect the nasomaxillary complex growth and breathing in humans. One such abnormality is a deviated nasal septum (DNS) sometimes associated with nasal airway obstruction. A DNS is defined by an anterior cartilage deformity of the quadrilateral septal cartilage, or by a combined septal deformity that involves all septal components. The deviation varies from a C/S shape to an irregular, angulated, dislocated septum [89]. Consequences of DNS leading to nasal airway obstruction include snoring and increased nasal resistance [90].

The nasal cavity also contains three pairs of turbinates (superior, middle and inferior) thought to contribute to the regulation of nasal airflow and humidification (Hsu & Suh, 2018a). Turbinate hypertrophy (TH) (enlargement of turbinates) is also associated with nasal airway obstruction [91].

DNS and TH are both considered potential contributors to obstructive sleep apnea (OSA), the most common form of sleep-disordered breathing (SDB)[90], although their relative contribution is still being explored. SDB is a disorder that affects around 1-5% of children [92,93]. If untreated, persistence of SDB could be associated with life-threating cardiovascular, metabolic and neurocognitive complications in addition to a considerate economic health burden (Tarasiuk & Reuveni, 2013). Studies investigated adult patients (mean age: 40 years) with DNS and suggested that DNS [95] leading to severe nasal obstruction could lead to breathing abnormalities during sleep. Additionally, research also suggests that to correct for DNS, a septoplasty may be indicated to alleviate patients from snoring [96,97]. A recent meta-analysis indicated that adult patients who underwent isolated nasal surgery for OSA improved an average of -4.15 (95%CI -6.48, -1.82) in

the apnea-hypopnea index (AHI) scores [98]. Whether such a surgical approach could help individuals with DNS that have developed OSA is unclear. Several studies investigated nasal airway abnormalities as predictors of pediatric OSA. However, to what extent DNS or TH contribute to OSA in children/adolescents is still not clear [99–101]. Should such abnormalities significantly contribute to the risk for OSA in children/adolescents, then it would be crucial to better understand the onset and presentation of these abnormalities in children/adolescents.

Currently, a validated pediatric sleep questionnaire (PSQ) is used as a pre-screen assessment to identify children/adolescents at high risk for SDB [102]. This screening approach is used prior to a full sleep assessment to better identify children/adolescents that are more likely to be affected and hence alleviate the current significant wait times for full diagnostic assessment. The PSQ is not specific in determining the etiology of SDB. Thus, we investigated the use of already available Cone Beam Computed Tomography (CBCT) scans as an additional assessment tool to identify potential anatomical deviations that may contribute to facilitating an increase in risk for SDB among children. If there were a strong link, then a multidisciplinary evaluation and management of the structural abnormalities in individuals with SDB would lead to a better overall treatment planning and outcome and may also prevent secondary morphological and developmental complications [103].

Based on the stated discussion, the aim of this study is to assess the potential association between structural anomalies in the nasal cavity (DNS and TH) with at high risk for SDB in a convenient sample of children/adolescents aged 6-17 years. Additionally, this study aims to identify the assessment capability of subjective and objective methodology using (CBCT) scans to assess DNS and TH.

2.3 Materials and Methods

A retrospective cross-sectional clinical study was performed using already available Cone Beam Computed Tomography (CBCT) scans of children/adolescents. This cohort was identical to the PSQ cohort used in Eimar et al [104] with the exception of two participants for whom CBCT scan quality were deemed insufficient for assessment. Ethical approval was obtained from the University of Alberta, Edmonton, Canada (#Pro00081755). Informed consent was already available from patients/guardians that their scans and information may be used for research purposes. The CBCT scans of 99 children/adolescents who visited the Graduate Orthodontic Program Clinic at the University of Alberta were evaluated. CBCT scans were obtained on an ICAT (Imaging Science International) scanner with 0.3-mm voxel size at 120 kVp, 18.54 mA, and exposure time of 8.5 s. The field of view was 16 cm in diameter and 6 cm in height, resulting in an effective radiation dose of approximately 35 microsieverts). Images were reconstructed and stored using Dolphin 3D software (Dolphin Imaging & Management Solutions).

For orientation and reconstruction purposes, the skull was oriented in a sagittal plane whereby the Y-axis line was at the lower edge of the orbit and X-axis was at the palatine bone. In the axial plane, the reconstruction was oriented such that the Y-axis was placed at the midline of the skull and the X-axis was at the most basal point of the nasal cavity. Whereas in the coronal plane, the Y-axis was placed in the midline with the X-axis being placed at the anterior nasal spine.

These patients had also completed a Pediatric Sleep Questionnaire (PSQ) typically on the same day as the CBCT scan. The age of the children/adolescents ranged from 6 – 17 years with a mean age of 10.96 ± 2.61 years. There was no statistical significance in the BMI between children/adolescents that scored PSQ<8 and PSQ>8 [104]. Hence, we did not consider BMI as a confounding factor. Inclusion criteria: All children/adolescents that had CBCT data of adequate

image quality and completed PSQ records during the assessed time period were considered. Exclusion criteria: children/adolescents diagnosed with a craniofacial anomaly/syndrome. Children with prior surgical intervention or trauma to their nasal region were excluded. For simplicity, children/adolescents will be referred to as individuals throughout the manuscript. This specific sample should not be deemed representative of the general population as it involves individuals seeking assessment for craniofacial problems and also individuals that might be referred to a highly specialized sleep clinic assessing upper airway breathing problems.

2.3.1 Pediatric Sleep Questionnaire

The PSQ was developed based on clinical experience [102], with concise and simple questions, with yes/no/don't know answers. PSQ does not diagnose OSA; it is an accessory tool to identify individuals at high risk or not of potentially having it. It can help to prioritize individuals requiring access to polysomnography (PSG), the reference standard for OSA, which does not have easy access and is expensive. PSQ has specific questions related to snoring, sleepiness, inattention/hyperactive behaviour, and SRBD (sleep-related breathing disorder). Moreover, the question–items are grouped into four main domains: breathing, behaviour, sleepiness, and other. Specifically, questions 1 to 8 plus question 14 belong to the breathing factor, questions 10 and 11 addressed sleepiness, questions 17 through question 22 are related to behaviour factor whereas the rest of the questions belonged to the other category. A positive PSQ was considered based on 33% or more positive answers to the 22 validated question-items, i.e. a score of 8 or more. Non-responded questions or don't know questions were excluded from the calculation as suggested by Chervin et al (Chervin et al., 2000b).

2.3.2 Anatomical assessment guidelines

Anatomical features of the nasal cavity were assessed in coronal and axial planes by two evaluators (C.T.B and P.B.). Abnormalities were identified subjectively (s) and objectively (o). The subjective assessment criteria were introduced as a way to represent a traditional clinical assessment of nasal septum deviation or turbinate hypertrophy.

1. DNS:

   Subjective Assessment – A nasal septum was subjectively considered deviated (DNS) when a slight to mild deviation was observed on the frontal view of the medial nasal septum of the CBCT scan (Figure 2.1). The orientation used for the subjective assessment was the same for the objective assessment.

   Objective Assessment – two landmarks were identified in frontal view, (1) junction of perpendicular plate with cribriform plate of ethmoid bone, and (2) junction of vomer bone with palatine bone. Dolphin "digitalize/measure" tool was used to measure the distance between the two landmarks, leading to an objective measure of the extent of septal deviation. The extent of deviation was calculated by the difference between the actual measured length of the deviated septum (2a) seen in Figure 2.2 and the height of a hypothetical straight septum (2b), which was then divided by the height of the hypothetical straight septum. This value was converted into a percent. DNS was found to vary between 0-18%. A NS was arbitrarily considered deviated when the ratio was ≥ 1.05, corresponding to at least a 5% deviation from the hypothetical straight line.

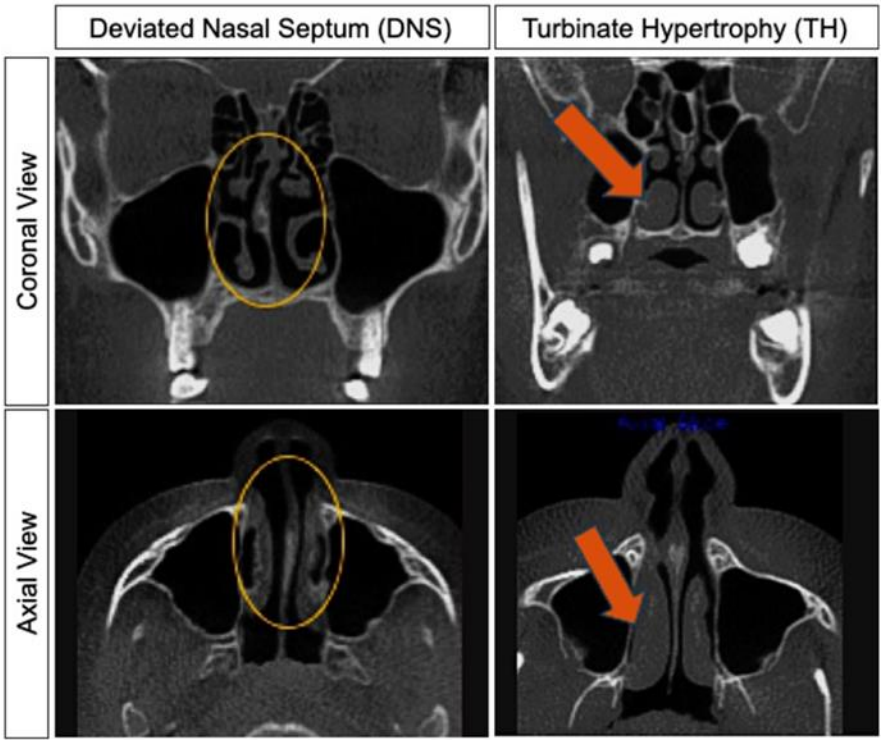

Figure 2. 1 Subjective Assessment of the nasal cavity anomalies.

2-dimensional CBCT scan images in the coronal and axial views were used to characterize a deviated nasal septum (DNS) and turbinate hypertrophy (TH). (Left panels) The nasal septum was considered deviated when a slight to mild deviation was observed (circle). (Right panels) The turbinate was considered hypertrophic when one or both of the turbinates were enlarged (arrow).

2. Turbinate hypertrophy (TH):

   Subjective Assessment – Turbinates were considered hypertrophic when turbinates showed a visible size difference compared to the contralateral turbinate (Figure 2.1). In only 4 of 99 individuals, both-sided enlargement of turbinates was observed. Those cases were marked with 'turbinates fused with septum' and considered hypertrophic.

   Objective Assessment –for the objective assessment, the ratio between the width of space occupied by turbinate soft tissue (Figure 2.2c) and the total width of the nasal cavity (Figure 2.2d) was determined and expressed in % (adapted from [106]). The turbinate was arbitrarily

considered hypertrophic when the ratio was ≥80%, meaning ≥80% of the nasal cavity was obstructed by the turbinate. If both the turbinates were hypertrophic, then the more severe hypertrophic turbinate was selected for the objective assessment.

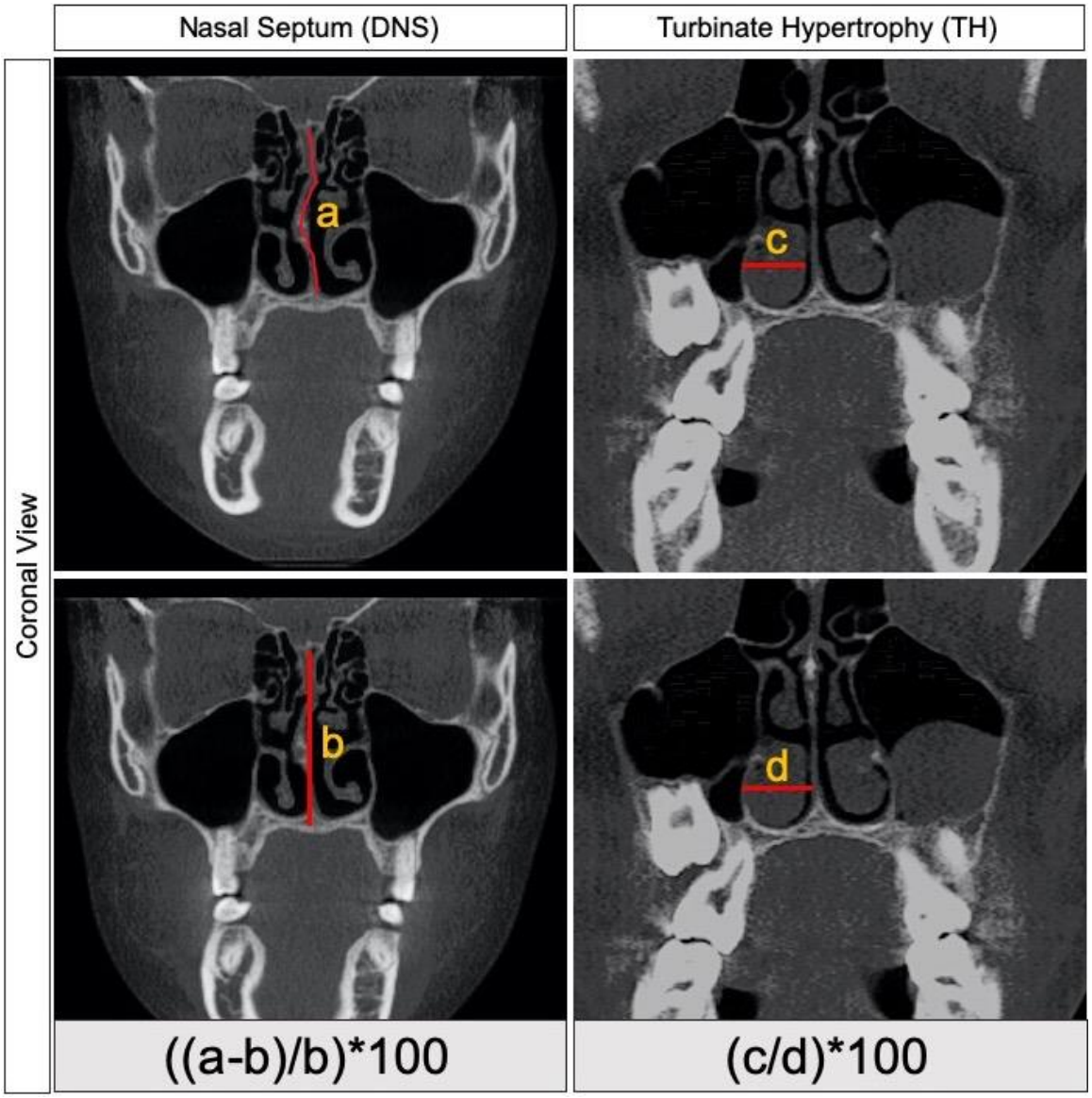

Figure 2. 2 Objective assessment of the nasal cavity anomalies.

(left panels) To calculate the degree of DNS, the length of DNS (a) in addition to the length of a hypothetical straight line (b) was calculated. (right panels) To measure the degree of TH, a ratio using the width of the turbinate itself (c) and the width of the space where the turbinate resides (d) was calculated. Coronal views were used to obtain the measurements.

2.3.3 Reliability

To ensure reliability, all the 99 cases were assessed two times each by two evaluators (C.T.B and P.B.), with each assessment being performed three days apart.

2.3.4 Statistical Analysis

Reliability between two trained raters (C.T-B., and P.B.) was calculated using Kappa for subjective assessments and ICC for objective assessments.

Descriptive, power and effect size (partial eta-squared - η_p^2), correlation between variables was performed using chi-square, and Pearson r correlations. The level of significance was set at 0.05 in all statistical tests. The statistical procedure was carried out by IBM© SPSS© and JASP for Windows software (version 26.0; SPSS Inc., Chicago, IL, USA).

2.4 Results

2.4.1 Summary of Reliability Assessments

Details on reliability assessment are shown in supplemental Table 2.1. Specifically, inter-rater reliability of subjective assessments of DNS was excellent with Kappa measurement of agreement between raters being 0.955. DNS objective assessment showed good intra-reliability of 0.856 (CI 0.55-0.95), and an inter-reliability of 0.788 (CI 0.62-0.89). Inter-rater reliability of subjective assessment of TH was 0.926. Whereas the objective assessment showed intra-rater reliability of 0.89 (CI 0.70-0.96) and inter-reliability of 0.88 (CI 0.74 – 0.96) as shown in supplemental Table 2.1.

2.4.2 Sample Demographics

Of the 99 individuals included in this study, 59 individuals scored positive on the PSQ. Thus, these 59 individuals were considered at high risk of SDB (Table 2.1). Subjective assessment of the nasal septum indicated that 64 of 99 individuals (64.7%) had DNS whereas the objective

assessment indicated that only 27 of 99 individuals (27.3%) had more than 5% septum deviation. We decided on 5% arbitrary cut-off to include most samples that had a visual septum deviation. Anthropometric measurements of the nasal cavity showed that individuals with shorter nasal cavity height (line A 38.89 mm, CI:37.82 – 39.96mm, p<.009), and shorter NS length (line B 40.14 mm, 38.91 – 41.37mm, P<.029) presented significant more risk for SDB (supplemental table 2.2). Overall, individuals with PSQ (+) showed a slightly higher mean for DNS (3.16%, CI 2.13%-4.18%) than individuals with PSQ(-) (2.74%, CI 1.48%-4%), but no statistically significant difference was observed, as seen in supplemental table 2.2. In regard to the subjective assessment of turbinates, 70 individuals had some degree of TH (70.7%). The objective assessment indicated that only 25 individuals (25.3%) had a TH that occupied 80% or more nasal cavity space.

Boys were the majority of participants in this study and presented the highest mean for PSQ score and for TH%. Girls presented the highest mean for DNS%. However, non-significant statistical differences were observed between sexes. Further descriptive statistics on sex, age and objective and subjective nasal cavity assessments are outlined in supplemental tables 2.2 and 2.3.

Power statistics test was performed based on the means and standard deviation. We established power of $\pi = 0.8$ as adequate for our tests, an appropriate power ($\pi = 1.00$) was observed for the nasal septum cluster analysis both subjective and objective, and for TH (Table 2.1).

Table 2. 1 Characterization of Sample Demographics.

	n	Sex	Mean Age (y)	Positive PSQ (> 0.33)
Total Sample	99	57 M & 42 F	10.96 (6-17)	59
	Non-DNS	DNS	Non-TH	TH
Subjective	35	64	29	70
Objective (>5% DNS) (>80% TH)	72	27	74	25
Power	1.00		0.88	

2.4.3 Associations between DNS, TH and PSQ

To identify whether the nasal cavity abnormalities are associated with individuals at high risk of SDB, a cross-tabulation statistical method between DNS, TH and PSQ was used. Considering subjective assessments of DNS and TH, a statistically significant association ($p=0.002$) was identified between individuals who were subjectively categorized to have both DNS and TH (Table 2.2).

With respect to PSQ, no statistically significant association was observed between subjective DNS and PSQ outcomes. However, individuals with subjective TH scored significantly higher on the PSQ ($p=0.017$).

With respect to objective assessments, these associations weren't statistically significant. There was no association between subjective DNS and objective TH, nor were there any significant associations between individuals objectively assessed as having DNS/TH with PSQ (Table 2.2).

Table 2. 2 Clinical Characteristics of Children with DNS and TH.

		Subjective DNS		Significance	Objective DNS		Significance
		Non DNS	DNS	(p-value)	Non DNS	DNS	(p-value)
PSQ Code	Negative PSQ	42.9%	39.1%	0.713	44.4%	29.6%	0.181
	Positive PSQ	57.1%	60.9%		55.6%	70.4%	
Subjective TH	Non TH	48.6%	18.8%	0.002**	33.3%	18.5%	0.149
	TH	51.4%	81.3%		66.7%	81.5%	
Objective TH (>80%)	Non TH	74.3%	25.0%	0.938	75.0%	74.1%	0.925
	TH	25.7%	75.0%		25.0%	25.9%	
		Subjective TH		Significance	Objective TH		Significance
		Non TH	TH	(p-value)	Non TH	TH (>80%)	(p-value)
PSQ Code	Negative PSQ	58.6%	32.9%	0.017*	39.2%	44.0%	0.672
	Positive PSQ	41.4%	67.1%		60.8%	56.0%	
Subjective DNS	Non DNS	58.6%	25.7%	0.002**	35.1%	36.0%	0.938
	DNS	41.4%	74.3%		64.9%	64.0%	
Objective DNS (>5%)	Non DNS	82.8%	68.6%	0.149	73.0%	72.0%	0.925
	DNS	17.2%	31.4%		27.0%	28.0%	

Table 2. 3 Factors associated with DNS

		Pearson's r	p
Age	Subjective DNS	0.354***	< .001
Age	Objective DNS (>5%)	0.209*	0.038
Age	Subjective TH	0.025	0.804
Age	Objective TH (>80%)	0.034	0.740
Age	PSQ	-0.054	0.594
Subjective DNS	Objective DNS (>5%)	0.453***	< .001
Subjective DNS	Subjective TH	0.313**	0.002
Subjective DNS	Objective TH (>80%)	-0.008	0.938
Subjective DNS	PSQ	0.037	0.716
Objective DNS (>5%)	Subjective TH	0.145	0.152
Objective DNS (>5%)	Objective TH (>80%)	0.009	0.926
Objective DNS (>5%)	PSQ	0.134	0.185
Subjective TH	Objective TH (>80%)	-0.086	0.399
Subjective TH	PSQ	0.239*	0.017
Objective TH (>80%)	PSQ	-0.043	0.675

*$p < .05$, **$p < .01$, ***$p < .001$

We next investigated correlations between age and DNS, TH or positive PSQ. Analysis using Person's r correlation coefficient indicated a positive correlation between age and subjective (r=0.354; p value = 0.001) and objective (r=0.209; p value = 0.038) DNS (Table 2.3). Positive correlation was also observed between subjective and objective DNS (r=0.453; p value = 0.001). Additionally, the subjective DNS and subjective TH also were positively correlated (r=0.313; p value = 0.002). No significant correlation was observed between subjective/objective DNS and positive PSQ. In regard to TH, individuals with subjective TH correlated positively with high PSQ score (r=0.239, p=0.017). However, no significant correlation was observed within subjective and

objective TH. A more detailed analysis revealed that there was an equal distribution of individuals with and without DNS/TH who were positive on the PSQ based on subjective assessments (Figure 2.3).

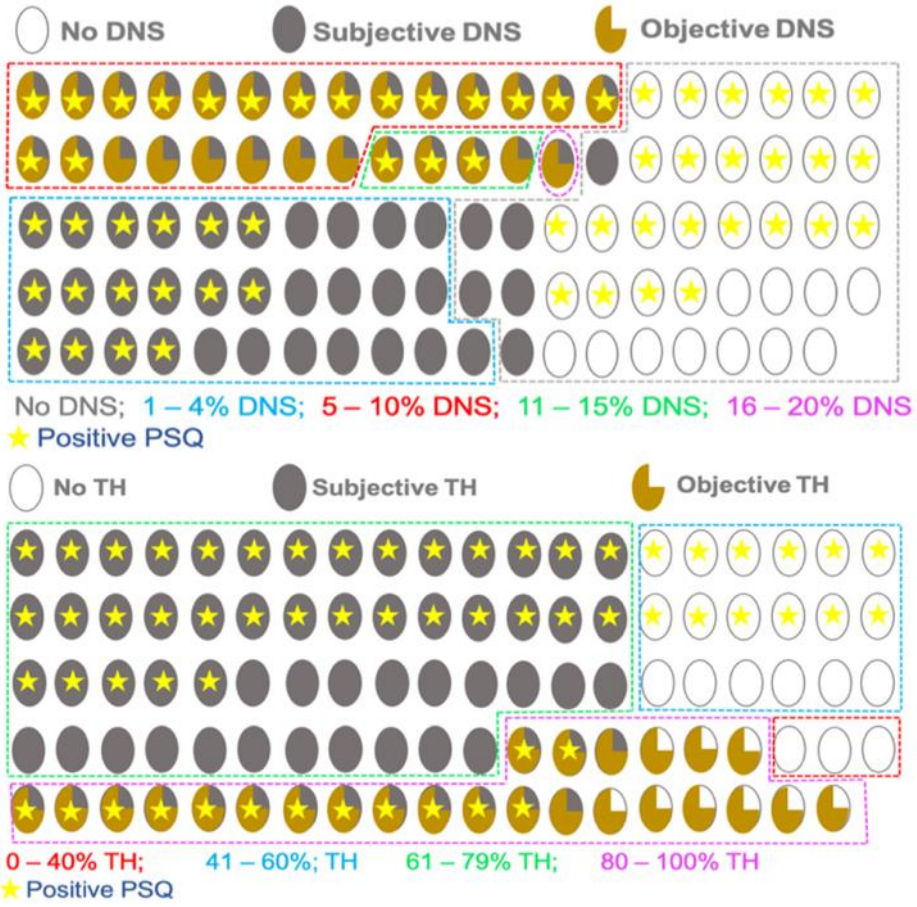

Figure 2. 3 Comparison of subjective and objective classification of DNS and TH with positive PSQ.

(Top panel) Number of individuals categorized with subjective and objective DNS. Individuals with DNS based on objective assessment were part of the overall subjective assessment of DNS thus explains the positive correlation between subjective and objective assessment of DNS. (Bottom panel) Number of individuals categorized with subjective and objective TH. The objective assessment of TH was not stringent enough to capture only individuals who were subjectively assessed to have TH. Rather the objective assessment also included individuals who were previously categorized subjectively to not have TH. Hence, no correlation between subjective and objective assessment of TH was observed.

A statistically significant positive association (r=0.204, p value = 0.043) was observed in individuals with a subjective DNS, TH and a positive PSQ based on the correlation analysis (Figure 2.4). No significant correlations were observed in the objective assessment.

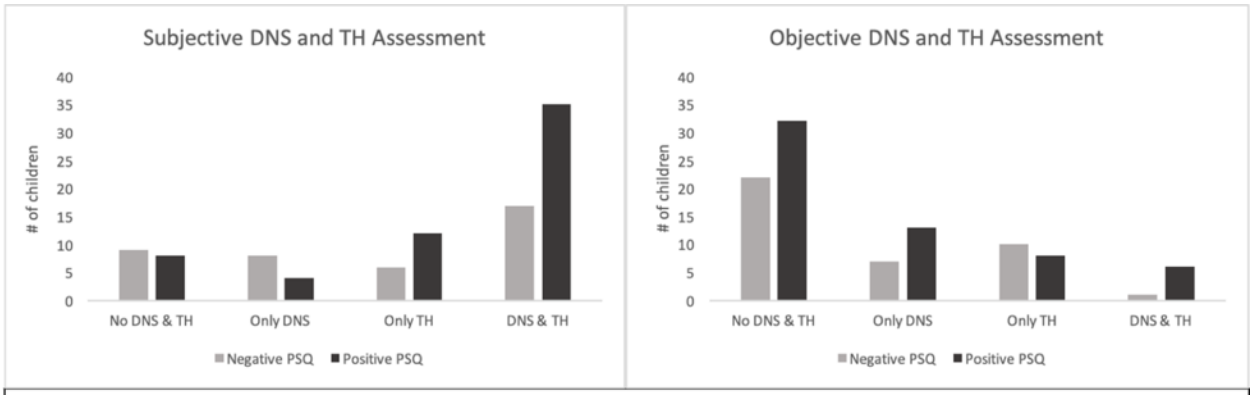

		Pearson's r	p
Subjective NS+TH; 0=none, 1=yes DNS no TH; 2=TH and no DNS; 3=both	PSQ	**0.204***	**< .043**
Objective NS+TH; 0=none, 1=yes DNS no TH; 2=TH and no DNS; 3=both	PSQ	0.023	0.819

Figure 2. 4 Individuals with DNS and TH are more likely at risk for SDB.

A positive correlation was confirmed in individuals with subjective DNS, TH and PSQ but no correlation was observed with objective measurements.

2.5 Discussion

In this study, we retrospectively investigated a cohort of 99 individuals for specific associations between at high risk of SDB as determined by PSQ and the presence of altered nasal features such as DNS and TH. As this sample represents individuals with craniofacial needs and individuals that may be referred to a highly specialized clinic that manages sleep breathing disorders, it might not be representative for the general population. Also, CBCT is not widely available, this could lead to a bias in the study. However, the purpose of this study was to explore whether, in situations where a CBCT is available, features such as nasal septum deviation or turbinate hypertrophy could be used for further diagnostic stratification. Our data suggests that this

is not the case for our cohort. The results may not be openly generalized. At the same time, these individuals are more likely to have upper airway obstructive problems. In this regard, if findings were not conclusive for this sample, it is really unlikely that these or similar categorical trends can be identified in a general population sample.

Overall, only very limited associations were found, supporting the multifactorial etiology of nasal airway obstruction. Our results clearly indicate that identification of altered DNS and/or TH assessed through CBCT imaging alone is not suitable to identify individuals at high risk for OSA and emphasize the importance of a multidisciplinary examination of the anatomical abnormalities associated with airway obstruction leading to SDB. However, we did find a statistically significant association between individuals at high risk of SDB (PSQ based) and subjective TH measurements. The rationale to use objective and subjective measurements derives from discussions with clinicians that are looking for efficient diagnostic criteria. Whereas the objective criterion should be more precise, if it can be reliably replaced by a subjective criterion, this would probably find better adoption to clinical practice. In the absence of guiding literature, the objective criteria were chosen such that approximately 25% of individuals in our cohort would score positive for either DNS or TH. The rationale was that if there was an association between objective score and PSQ, this should have become evident (correlation of DNS or TH with positive PSQ). This was indeed the case for the subjective TH assessment.

This study is novel for several reasons: 1) This is the first Canadian pediatric population-based study that addresses both subjective and objective assessments of anomalies (DNS, TH) in the nasal cavity. 2) This study is the first to associate obstruction due to DNS and TH in the nasal cavity with a higher likelihood of SDB in children/adolescents.

2.5.1 Comparison of our study to other similar studies

The need to correlate age and growth-related changes among anatomical abnormalities such as DNS with SDB for a better treatment outcome has been recognized [107]. Despite this, only a few studies specifically investigated nasal structural abnormalities in pediatric populations [108–110]. Song et al, [109] reported a prevalence of DNS of 13.6% in 6-9 year-old Korean individuals and Subarić et al [110] found a prevalence of 21.2% in Croatian individuals aged 7-14 years. Gray [108] subjectively assessed nasal septum using nasal photographs and reported a prevalence of 58% of DNS in newborns. Our study revealed a variable prevalence of DNS depending on the method of assessment. Whereas the subjective assessment identified 42.5% (ranging from 25 to 62% by age) of individuals between 6-9 years having DNS, the objective assessment put this number to 20.5% (ranging from 15 to 22% by age). Similarly, in the group of 7-14-year-olds the prevalence was 62% (ranging from 25 to 90%) for subjective, and 27% (ranging from 7 to 55% by age) for the objective assessment. Overall, the prevalence of objective DNS in all individuals (6-17 years old) was 26%, ranging from 0%-55% by age, with the highest prevalence observed at 12 years of age.

A study by Goergen et al [3] proposes the use of 3D analysis for more accurate quantification of nasal septum differences. In this study, we specifically decided against 3D analysis. First, within a clinical setting, there is typically not sufficient expertise or time to perform an accurate 3D segmentation and volume analysis. Results might be compromised by inappropriate threshold selection as soft tissues have soft boundaries, potentially skewing the results. Second, 3D volume analysis appears to yield comparable results to linear measurements [3].

As all of these studies used different assessment criteria, therefore comparison between the different studies is difficult. This illustrates the need for the development of standardized assessment criteria as suggested elsewhere [111]. It is currently unclear whether the arbitrary

threshold of 5% DNS is appropriate or even clinically relevant for the development of SDB. It should also be noted the higher prevalence in our study is likely because of a preselected patient population (individuals referred to the Orthodontics clinic). Again, our study is the first that tried to correlate DNS with the risk for SDB.

2.5.2 Correlation between Age with DNS and TH

The primary aim of this retrospective study was to assess the usefulness of CBCT scans as accessory assessing tool to identify children/adolescents at high risk of SDB. The positive correlation between age and DNS may indicate that individuals are more likely to develop DNS as they grow older. The nasal cartilage provides crucial structural support and contributes to the growth of the nasal cavity. The increased incidence of nasal cavity changes with age is compatible with the idea of an underlying cartilage anomaly that becomes evident only later during childhood. This could reflect abnormal nasal septum cartilage development, which itself could also be associated with abnormal midfacial growth such as midfacial hypoplasia. A smaller nasal cavity may result in DNS leading to SDB [112]. The extended period of endochondral ossification of the cartilaginous septum starting after the first 6 months and ending at 36 years [112] could itself also contribute to the greater frequency of DNS in older individuals in our sample. However, the nature of the retrospective study does not allow any further extrapolation in that respect. To address this, longitudinal studies with multiple CBCT scans over time would be required, which are ethically difficult to justify, or larger patient cohorts allowing patient stratification by age.

A similar association between age and TH was not observed. As turbinates are not implicated in midfacial growth so this might have been anticipated. The positive correlation between DNS and turbinate hypertrophy might not be surprising as co-presentation of DNS and turbinate hypertrophy is common in the field of Otolaryngology [113,114]. This correlation is only

seen when subjective assessments are compared. Hypertrophy of the inferior turbinate might develop as a compensatory mechanism to the DNS to protect the more patent nasal side from excess airflow to prevent drying and crusting effects [114]. Alternatively, DNS may be the consequence of unilateral expansion of the turbinate exerting pressure on the nasal septum. Reasons for excessive turbinate growth could be genetic or due to ongoing secondary complications such as early-life trauma, rhinitis medicamentosa, allergic rhinitis, vasomotor rhinitis, dust, tobacco use [114].

2.5.3 Association between PSQ and individuals categorized with DNS or TH

Subjective TH was the only assessment that showed a positive correlation with PSQ. However, this correlation did not extend to individuals objectively positive for DNS/TH as might be expected. The cut-off of 80% for the objective measurement was chosen such that approximately one quarter of the children would score as obstructed, similar to the percentage of the individuals scoring positive for objective nasal septum deviation. Individuals that scored positive in the subjective TH assessment showed objectively 71% TH with a standard deviation of 14%. This might indicate that the 80% cut-off is too stringent. However, for the subjective assessment, in addition to differences in size, we considered direct turbinate apposition to the septum which might not necessarily be reflected by the objective measurement. This indicates that the objective measurement as performed must be overlooking some detail captured by the subjective assessment. Detailed investigations are ongoing whether it is possible to derive objective criteria for individuals with identified subjective TH and a positive PSQ score. Overall, individuals positive for PSQ showed an equal distribution between having or not having DNS based on subjective assessments. Sample size or classification limitations should be considered when attempting to explain these findings.

2.5.4 Association between PSQ and individuals with both DNS and TH

The high proportion of individuals with TH and DNS allowed investigating how many of them present with both DNS and TH. Based on subjective assessments a large proportion (35/52) of individuals with both DNS and TH are at risk for SDB (positive PSQ). This increases with the objective assessment, where 6/7 individuals have both DNS and TH and score positive on the PSQ. Whereas this might indicate that individuals with both DNS and TH are more likely to be at risk for SDB, this also indicates that a significant number of individuals are at risk of SDB that show no structural anomalies in the nasal cavity. It could be that those individuals have abnormalities in their posterior structures (soft palate, pharynx, tongue base), which was not assessed in this study. This underlines our conclusion that CBCT imaging analysis might be an accessory tool to subcategorize individuals at risk for SDB. As it stands, CBCT assessment of the nasal cavity on its own, either using objective or subjective criteria, does not appear to reliably recognize children/adolescents at risk for SDB. These findings need to be validated in larger cohort studies before recommendations with respect to clinical applicability can be made.

Overall, identification of nasal abnormalities does not necessarily translate to an increased risk for SDB. It appears that there are some specific alterations identified by subjective TH or both subjective TH and DNS that correlate with a positive PSQ. The reason why subjective assessments perform better than the objective criteria chosen might be that simple linear measurements do not sufficiently capture the complex geometry of the nasal cavity. Thus, better objective criteria are still required to assess the naval cavity, but clinicians who are currently using CBCT scans might want to subjectively assess children for nasal cavity abnormalities in addition to the PSQ prior to referring them for further sleep assessment.

It should be noted that we focused on PSQ, as this is a tool readily available to orthodontic clinics. PSG assessment would provide more precise data with respect to SDB. However, within a clinical reality, waiting times and logistical constraints for a PSG analysis are considerable. This is the reason why the PSQ was developed as an initial screening tool to refer children for further sleep breathing analysis.

In this regard, there is an urgent need for standardized multidisciplinary assessments (Dentists, Sleep specialists, Ear-Nose-Throat Doctors) for an early and correct diagnosis of SDB and its subsequent optimal treatment.

2.5.5 Limitations

- As a retrospective study, this study was not able to provide longitudinal insights. Furthermore, no detailed clinical/medical histories were available to correlate PSQ with actual clinical SDB.
- The study cohort consisted of individuals referred to the Orthodontics clinic and were prescribed a CBCT scan. As such it might not be representative of the general pediatric population.
- The PSQ adopted shows a limitation due to the fact that the control subjects on the validation study of the PSQ did not have a sleep laboratory exam to confirm the absence of OSA, which may be increasing the number of false-positive in the control sample.
- The objective assessment of the turbinate was done in one specific plane which is different than the subjective assessment scrolling axial and coronal views.

2.6 Conclusions

Assessment of nasal structural features from CBCT imaging does not seem to be well suited to recognize individuals at high risk of OSA.

Only presence of subjectively determined TH in individuals is associated with at high risk for SDB in this specific sample.

Older individuals are more likely to present with DNS.

DNS subjective assessments were capable of identifying less than 5% of deviation.

2.7 Supplementary Information

Supplemental Table 2. 1 Reliability Scores for Subjective and Objective Nasal Septum and Turbinate Assessment.

	Subjective		Objective	
	Intra-rater reliability	Inter-rater reliability	Intra-rater reliability	Inter-rater reliability
Nasal Septum	Kappa: 1.00 SE: 0	Kappa: 0.955 SE: 0.032	ICC: 0.856 *C.I.* [0.553,0.954]	ICC: 0.788 *C.I.* [0.621,0.893]
Turbinate	Kappa: 1.00 SE: 0	Kappa: 0.926 SE: 0.032	ICC: 0.890 *C.I.* [0.695,0.960]	ICC: 0.882 *C.I.* [0.737,0.957]

SE: Standard Error; C.I: Confidence Interval 95%

Supplemental Table 2. 2 Sample demographic descriptive statistics based on PSQ.

PSQ Descriptive (ANOVA)								
		N	Mean	Std. Deviation	Std. Error	95% Confidence Interval for Mean		P=value
						Lower Bound	Upper Bound	
Age	PSQ (-)	40	11.1	2.96	0.468	10.15	12.05	
	PSQ (+)	59	10.81	2.36	0.307	10.2	11.43	
Chervin PSQ Score	PSQ (-)	40	17.0701	9.38332	1.48363	14.0692	20.071	
	PSQ (+)	59	54.7179	15.22467	1.98208	50.7504	58.6855	
NS (Line A)	PSQ (-)	40	41.175	4.325	0.6838	39.792	42.558	0.009
	PSQ (+)	59	38.895	4.1169	0.536	37.822	39.968	
NS (Line B)	PSQ (-)	40	42.317	4.8678	0.7697	40.761	43.874	0.029
	PSQ (+)	59	40.144	4.7224	0.6148	38.913	41.375	
NS Deviation (Line B-A)	PSQ (-)	40	1.1425	1.60654	0.25402	0.6287	1.6563	
	PSQ (+)	59	1.2492	1.58771	0.2067	0.8354	1.6629	
DNS (%)	PSQ (-)	40	2.74%	3.95%	0.62%	1.48%	4.00%	
	PSQ (+)	59	3.16%	3.94%	0.51%	2.13%	4.18%	
Turbinate (turbinate length)	PSQ (-)	40	8.735	2.5049	0.3961	7.934	9.536	
	PSQ (+)	59	9.222	1.7557	0.2286	8.764	9.68	
TH %	PSQ (-)	40	67.15%	18.51%	2.93%	61.23%	73.07%	
	PSQ (+)	59	71.34%	11.99%	1.56%	68.22%	74.47%	
NSD "Degree of Deviation"	PSQ (-)	40	1.0274	0.03946	0.00624	1.0148	1.04	
	PSQ (+)	59	1.0316	0.03936	0.00512	1.0213	1.0418	

Supplemental Table 2. 3 Sample demographic descriptive statistics based on sex.

Sex Descriptive Statistics								
		N	Mean	Std. Deviation	Std. Error	95% Confidence Interval for Mean		
						Lower Bound	Upper Bound	Sig.
Age	Male	59	11.07	2.44	0.319	10.43	11.71	0.524
	Female	40	10.73	2.84	0.45	9.81	11.64	
PSQ Score	Male	59	40.95	24.66	3.21	34.52	47.37	0.446
	Female	40	37.37	19.65	3.1	31.09	43.66	
Chervin PSQ raw score	Male	59	0.4095	0.24668	0.03212	0.3452	0.4738	0.446
	Female	40	0.3738	0.19655	0.03108	0.3109	0.4366	
NS (Line A)	Male	59	40.305	4.2652	0.5553	39.194	41.417	0.174
	Female	40	39.095	4.3749	0.6917	37.696	40.494	
NS (Line B)	Male	59	41.449	4.7735	0.6215	40.205	42.693	0.292
	Female	40	40.392	5.0178	0.7934	38.788	41.997	
NS Deviation (Line B-A)	Male	59	1.1441	1.49831	0.19506	0.7536	1.5345	0.64
	Female	40	1.2975	1.72738	0.27312	0.7451	1.8499	
DNS (%)	Male	59	2.80%	3.68%	0.48%	1.84%	3.76%	0.57
	Female	40	3.26%	4.29%	0.68%	1.89%	4.63%	
Turbinate size	Male	59	9.08	1.9762	0.2573	8.565	9.595	0.755
	Female	40	8.945	2.277	0.36	8.217	9.673	
TH %	Male	59	70.06%	14.92%	1.94%	66.17%	73.95%	0.743
	Female	40	69.05%	15.35%	2.43%	64.14%	73.95%	
NSD "Degree of Deviation"	Male	59	1.028	0.03684	0.0048	1.0184	1.0376	0.57
	Female	40	1.0326	0.0429	0.00678	1.0189	1.0463	

Chapter 3: Histological and Molecular Characterization of the Growing Nasal Septum in Mice

Chapter 2 suggested that older children are more likely to present with nasal septum deviation. It also concluded that nasal cavity abnormalities don't necessarily translate to an increased risk for sleep-disordered breathing, making it difficult to delineate the etiology and consequences of nasal septum deviation. Our inability to appropriately understand and treat nasal cartilage pathologies stems from our lack of understanding of nasal cartilage properties, as identified in Chapter 1. In Chapter 3, growth and extracellular matrix properties of the nasal septum were identified in mice. Mice rather than human samples were used since access to human samples is limited in size and quantity. Moreover, chapter 1 already established that the nasal septum is a heterogeneous structure and that maintaining location and age-specific information while assessing the septum is critical. Hence, we used mice as obtaining this information from human nasal septum samples obtained from surgery would be challenging.

Chapter 3 is derived from this published article:

Baddam, P., Kung, T., Adesida, A. B., & Graf, D. (2021). Histological and molecular characterization of the growing nasal septum in mice. *Journal of anatomy, 238(3), 751–764.* https://doi.org/10.1111/joa.13332

3.1 Abstract

The nasal septum is a cartilaginous structure that serves as a pacemaker for the development of the midface. The septum is a hyaline cartilage which is surrounded by a perichondrium and epithelium. It remains cartilaginous anteriorly, but posteriorly it undergoes endochondral ossification to form the perpendicular plate of the ethmoid. Understanding of hyaline cartilage differentiation stems predominantly from investigations of growth plate cartilage. It is currently unclear if the morphological and molecular properties of the differentiating nasal septum align with growth plate. In this study, we describe growth, molecular and cellular characteristics of the nasal septum with reference to hyaline cartilage differentiation. The nasal septum grows asynchronous across its length with phases of rapid growth interrupted by more stationary growth. Growth appears to be driven predominantly by acquisition of chondrocyte hypertrophy. Similarly, cellular differentiation is asynchronous, and differentiation observed in the anterior part precedes posterior differentiation. Overall, the nasal septum is structurally and molecularly heterogeneous. Early, and extensive chondrocyte hypertrophy but no ossification is observed in the anterior septum. Onset of hypertrophic chondrocyte differentiation coincided with collagen fibre deposition along the perichondrium. Sox9, Col2, Col10, Mmp13, Sp7, and Runx2 expression was heterogeneous and did not always follow the expected pattern established from chondrocyte differentiation in the growth plate. The presence of hypertrophic chondrocytes expressing bone related proteins early on in regions where the nasal septum does not ossify displays incongruities with current understanding of hyaline cartilage differentiation. Runx2, Collagen II, Collagen X, and Sp7 commonly used to mark distinct stages of chondrocyte maturation and early bone formation show wider expression than expected and do not align with expected cellular characteristics. Thus, the hyaline cartilage of the nasal septum is quite distinct from growth plate

hyaline cartilage, and caution should be taken before assigning cartilage properties to less well-defined cartilage structures using these commonly used markers. Beyond the structural description of the nasal cartilage, this study also provides important information for cartilage tissue engineering when using nasal septal cartilage for tissue regeneration.

Key words: Nasal Septum, Hyaline Cartilage Development, Extracellular Matrix, Chondrocyte differentiation markers, mouse

3.2 Introduction

The nasal septum is a cartilaginous structure that divides the nasal cavity and provides structural support to the midface [115]. The septum is a heterogeneous structure with the anterior part remaining cartilaginous throughout life, whereas parts of the posterior septum undergo endochondral ossification to form the perpendicular plate of ethmoid (PPE)[115]. Structurally, the nasal septum is composed of a dense network of chondrocytes, extracellular matrix, and flanked by a perichondrium [116]. Whether the septum also serves a mechanical role besides structural support is controversial. It has been proposed that its stiff cartilage properties serve to absorb stresses resulting from midfacial growth and impact forces from mastication [117]. The stiffness, rigidity, and appearance of the nasal septum cartilage are characteristics of hyaline cartilage.

Hyaline cartilage is the simplest type of cartilage, and due to its relatively uniform structure is also referred to as immature cartilage [118,119]. It is found in different areas in the body, including growth plates of long bones, the knees, as well as the nasal septum. Our detailed molecular and cellular understanding on hyaline cartilage stems predominantly from studies investigating growth plates, articular joints, and pathologies associated with cartilage degeneration such as osteoarthritis of the knee. In the growth plate, hyaline cartilage is temporary and is required to support growth of this initially avascular skeletal structure. It is typically replaced by bone through a process called endochondral ossification. During this process, hypertrophic chondrocytes will either mature and maintain the cartilage, undergo apoptosis to be replaced by bone-forming osteoblasts, or transdifferentiate into osteoblasts to form bone themselves[120]. Hyaline cartilage in articular joints serves a very different, primarily load bearing function and will remain cartilaginous throughout life [121].

There is considerable literature on the contribution of nasal septum for midfacial growth. The nasal septum has been recognized as pacemaker for midfacial development [122]. Its resection interferes with midfacial growth [123–125]. Children with midfacial hypoplasia often present with nasal septum deviation, although the significance of this malformation is not understood [126–128]. Because of its hyaline characteristics, nasal septum cartilage is being explored as source for autologous chondrocytes that can be used for articular cartilage repair [129]. A recent a phase I clinical study explored the use of nasal septum cartilage as source to repair cartilage defects in osteoarthritis patients [129]. Several studies have described the growth pattern of the nasal septum either in the context of growth anomalies in children/adolescents such as midfacial hypoplasia and nasal septum deviation [130] or in large animals mapping proliferation using a histological approach [10,35,117]. A detailed growth analysis at the perpendicular plate of ethmoid (PPE) revealed that nasal septum growth must involve mechanisms other than cell proliferation at the plate itself [131]. A systematic study focusing on the development and maturation combining growth, histological and immunofluorescence analysis of the entire septum has yet to be done. It remains unclear if and how molecular properties of nasal septum chondrocytes change over time, and how they differ from articular chondrocytes. One might expect that the different functional requirements *in vivo* are reflected in differences in cellular and molecular differences.

Gene regulatory networks involving Sox9, Runx2, and Sp7 were identified as core regulators of cartilage and bone differentiation [132]. Sox9 is an early, key transcriptional regulator essential for chondrocyte differentiation. It is required for the formation of all cartilages [132–134]. It is first expressed in the condensing mesenchyme, but can also be found later in mature, hypertrophic chondrocytes co-expressed with Runx2 [132]. Immature cartilage is rich in sulfated proteoglycans, and stains strongly with Safranin O and Alcian Blue [132]. The extracellular matrix

(ECM) of immature cartilage is characterized by high amounts of collagen II (Col2) [132,135]. In contrast, mature cartilage contains comparatively fewer proteoglycans resulting in less intense staining with Safranin O and Alcian Blue. Levels of collagen II are decreased, and the presence of collagen X (Col10) is often observed [136]. The presence of Matrix metallopeptidase 13 (Mmp13) is associated with the degradation of collagen II and the invasion of vasculature to support osteoprogenitor cells [134]. Sp7 (Osterix) is a key transcriptional regulator for bone-depositing osteoblasts [137]. Osteocalcin (Ocn), secreted by osteoblasts and one of the most abundant components of the bone mineral matrix, is a commonly used marker for bone formation [138]. Collagen I (Col1) is the most prevalent collagen in the bone mineral matrix [120,136]. Many of the markers commonly used for mature cartilage overlap with bone [132]. For instance, Sp7 is also expressed in mature cartilage, and Runx2 is not only expressed during endochondral ossification, but also in chondrocyte progenitor cells [135,139]. The ECM of cartilage is very diverse and contains several types of collagen at one time [136]. Despite this complexity, collagen II and Sox9 are commonly used as markers for immature cartilage, Mmp13, collagen X and Runx2 as markers for hypertrophic chondrocyte, and collagen I, Sp7 and Ocn as bone markers in alignment to their expression in the cartilaginous growth zone of long bones. There is increasing realization that classifying cartilages on the basis of expression of those molecular markers is an oversimplification. It does not truly reflect the complexity and molecular requirements for the development of specialized hyaline cartilages in different anatomical locations.

In this study, we investigated the growth and maturation of nasal hyaline cartilage and correlated it to the commonly used molecular properties for growth plate cartilage. Based on previous literature, it wasn't fully resolved when and where nasal cartilage growth occurs [131,140] and how this growth correlates to cellular characteristics described for maturation of other hyaline

cartilages [132,141]. We characterized dynamic changes in the nasal septum cartilage using micro-CT, histological staining, immunofluorescence at several time-points during development. We find that the nasal septum cartilage is a surprisingly dynamic and complex structure displaying significant anterior-posterior differences. It undergoes significant remodeling during and post rapid midfacial growth that contributes to nasal septum growth through the process of chondrocyte hypertrophy.

3.3 Materials and Methods

3.3.1 Mice

Animal experiments were approved by the Research Ethics office of the University of Alberta (Animal Use and Care Committee protocol AUP1149) in compliance with guidelines by the Canadian Council of Animal Care. C57BL/6J mice were euthanized at embryonic day 18.5 (E18.5), postnatal (PN) days 0, 7, 14, 21, 30, and 60 for this study. These time points were chosen to represent different stages in nasal cavity growth development as established by [140]. After euthanasia, mice were perfused and fixed using 4% paraformaldehyde (PFA) for 24 hours prior to further analysis.

3.3.2 Micro-computed Tomography (μCT) analysis

Mice heads (n=3/age) were scanned using MILabs μCT (Milabs, Utrecht, Netherlands) at the School of Dentistry, University of Alberta. The following parameters were applied for scanning: voxel size = 10μm; voltage = 50kV; current = 0.24mA; and exposure time = 75ms. Scans were reconstructed from 3600 individual projections at a voxel size of 25μm and analyzed using AMIRA software (Thermo Scientific). Scans were realigned prior to analysis such that the xz-axis corresponds to vertical line of the nasal septum. The anterior nasal septum was defined as the region anterior to the appearance of the ossified vomer. The articulation of the frontal bones with ethmoid was considered as the posterior nasal septum with the midpoint of the anterior and

posterior nasal septum (a-p midpoint) describing a medial nasal septum (Figure 3.1). The set of landmarks described in [140] was used to quantify growth of the nasal septum and cavity at anterior, a-p midpoint and posterior positions or on a midsagittal region, respectively, as demonstrated in Figure 3.2.

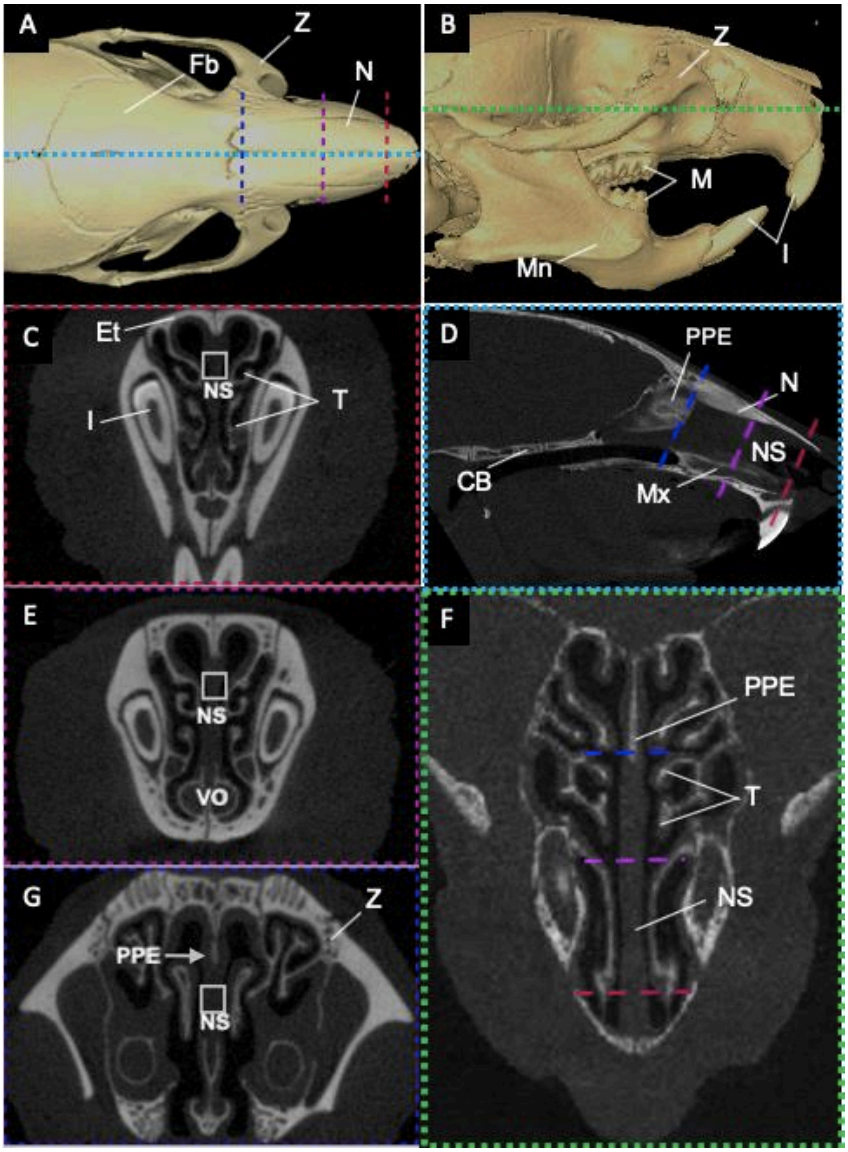

Figure 3. 1 µCT representation indicating the position of vertical planes used for µCT and histological analysis.

(A - B) isosurface representation of a µCT scan of an adult mouse indicating (C) anterior (red), (E) a-p midpoint (purple), and (G) posterior (dark blue) regions of the nasal septum. White boxes indicate the corresponding region where histological stains and immunofluorescence are used for imaging. (D) Mid-sagittal (light blue) and (F) axial (green) representation of the PPE and NS. NS: nasal septum; VO: vomer, PPE: perpendicular plate of ethmoid; Fb: frontal bone; Z: zygomatic bone; N: nasal bone; M: molars; Mn: mandible; I: incisors; Et: ethmoid; T: turbinates; CB: cranial base; Mx: maxilla.

3.3.3 Tissue Preparation and Histology

Mice skulls were decalcified using ethylenediaminetetraacetic acid (EDTA) from 1 day (PN0 heads) to 6 weeks (PN60 heads) before processing for paraffin embedding. Tissues were processed in increasing ethanol gradient washes (75% v/v, 95% v/v, 100%) and xylol prior to being embedding in paraffin. Paraffin blocks were sectioned using a Reichert HistoSTAT rotary microtome. The nasal septum was sectioned at 7µm in a frontal orientation.

3.3.4 Safranin O, Van Gieson and Alcian Blue staining

Safranin O, Van Gieson, and Alcian Blue staining was performed according to publicly available protocols from IHC world [142]. Anterior, a-p midpoint and posterior nasal septum paraffin sections were stained. Only selected ages (PN0, PN7, PN21, PN30, PN60) are shown, with additional ages (E18.5, PN14) provided in the supplemental figures. Safranin O and Alcian blue were used to stain cartilage, and Van Gieson was used to identify collagen fibers in the nasal septum.

3.3.5 Immunofluorescence

For immunofluorescence staining sections were de-paraffinized in xylol and re-hydrated in a decreasing ethanol gradient. Antigens were retrieved by digesting with Hyaluronidase (Sigma-Aldrich H3506) (272µM) for 30 minutes on a heat block at 37ºC in a humidified chamber. Goat/Donkey serum was used to block the sections and primary antibodies were incubated overnight at 4ºC. The details of the primary antibodies are as follows: Collagen II (clone 2b1.5, Abcam, ab185430), Sox9 (clone EPR14335-78, Abcam, ab185966), Matrix Metallopeptidase 13 (Mmp13) (clone C-3, Santa Cruz Biotechnology, sc515284), Runx2 (Novus Biologicals, nbp1-77461), Osterix (Sp7) (Abcam, ab94744), Osteocalcin (Ocn) (Abcam, ab93876), Collagen X (Col X) (clone X-AC9, Santa Cruz Biotechnologies, sc59954), normal mouse IgG1 (Santa Cruz

Biotechnology, sc3877). Secondary antibodies used were donkey anti-rabbit Alexa647 (Life Technologies, a31573), goat anti-mouse IgG1-Alexa647 and IgG2a-Alexa647 (Thermo Fisher Scientific, a21240, a21241). All sections were counterstained with DAPI (1:1500). Slides were imaged using an IXplore Standard Olympus Compound microscope. All staining was done at least three times on different specimens for each antibody and age. Autofluorescence and antibody controls are shown in supplemental figure 3.4.

3.3.6 Data Analysis

Graphs indicate mean ± standard deviation when applicable to demonstrate variability between mice within each age group. Additionally, trendlines with slopes and correlation coefficients are added when demonstrating a relationship between two variables over time using Microsoft Excel.

3.4 Results

3.4.1 The nasal cavity shows dynamic growth phases between birth and adulthood.

To understand if and when regional growth differences occur in the nasal septum, a landmark based [140] nasal septum growth analysis of wildtype mice scans at PN0, 7, 14, 21, 30, 60 was performed. We found that the nasal cavity growth is complex with anterior (Figure 3.1C), a-p midpoint (Figure 3.1E), and posterior (Figure 3.1G) nasal septum regions developing at different rates. Measurements along the anterior-posterior (A-P) (Figure 3.2A-C) axis demonstrated that the nasal bone (a-b in Figure 3.2B) and perpendicular plate of ethmoid (PPE, a-e in Figure 3.2B) grew overall proportionally. This was evident by a linear correlation ($R^2 = 0.949$), although a biphasic growth was apparent (Figure 3.2D). The nasal bone length and PPE demonstrate an almost isometric relationship. Rapid growth was observed between PN0-PN14 and PN21-PN60. The period PN14-PN21 appeared more static. The same dynamic growth pattern was observed along

the A-P axis for nasal cavity height (Figure 3.2E) and nasal septum length. Measurements at anterior, a-p midpoint and posterior positions (Figure 3.2F, landmarks b-c and a-d, respectively, refer to Figure 3.1 for positions) revealed overall linear growth, although again a stalled period was apparent between PN14-PN21. The increased posterior height when compared to anterior was reflected by the larger growth slope of 0.37 compared 0.26. Up to PN14, growth rates between anterior, a-p midpoint and posterior positions were quite similar but became more variable thereafter (Figure 3.2F). After PN14, the growth of the anterior nasal septum was reduced in comparison to the a-p midpoint and posterior nasal septum. The slopes of the anterior, a-p midpoint and posterior nasal septum were 0.33, 0.38, 0.38, respectively. Thus, the growth of the nasal septum is dynamic and undergoes growth spurts with stalled growth in between. Raw data obtained from the measurements demonstrated in Figure 3.2 are outlined in Table S3.1.

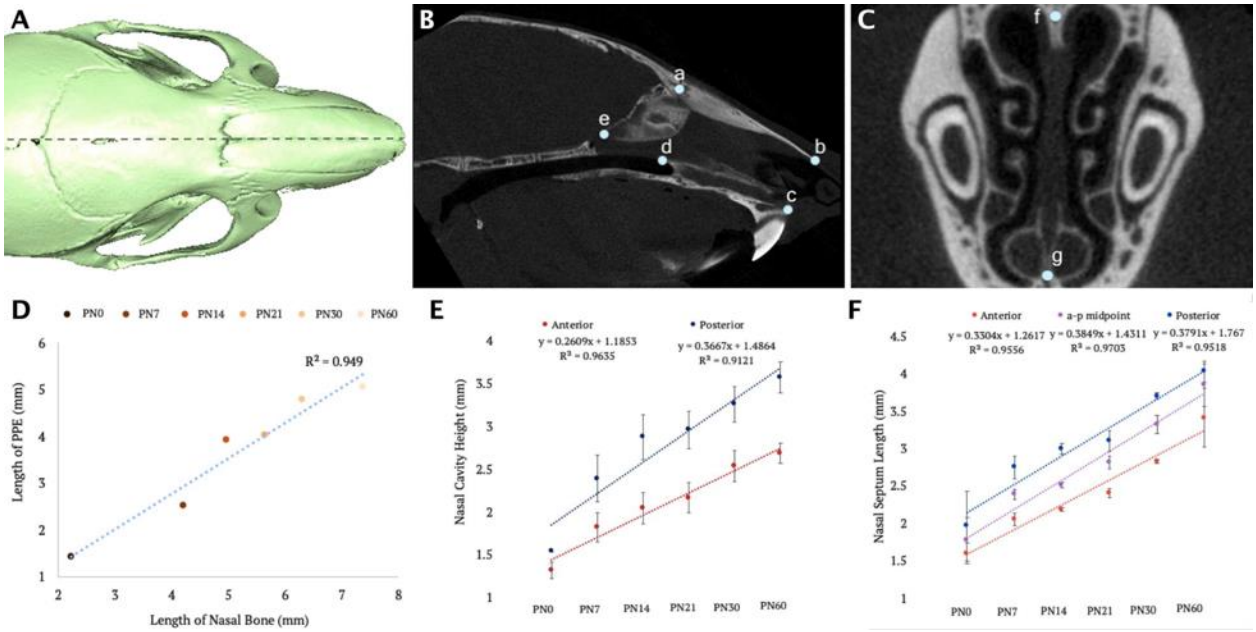

Figure 3. 2 Mapping the dynamic growth of the nasal septum.

Landmark based quantitative analysis was conducted on µCT scans of mice ages PN0, 7, 14, 21, 30, 60 (n=3 for PN0, 7, 60 and n=5 for PN14, 21, 30). For growth analysis of the nasal cavity midsagittal cross-section were used (A) to place the landmarks (B, C). (D) Plotting length of the nasal bone (a-b) against the length of the PPE (a-e) over time demonstrates a linear trend (blue line) indicating concomitant growth of nasal bone and PPE. A growth arrest is evident between PN14-21. (E) Height of nasal cavity at anterior (red, landmarks b-c) and posterior (blue, landmark a-d) positions plotted against the different ages. Trendline and slope show overall linear growth with a faster growth rate posterior. A growth arrest is evident between P14-P21. (F) Septum length (landmarks f-g) at anterior (red), a-p midpoint (purple) and posterior (blue) positions plotted against the different ages. Trendline and slope show overall linear growth with almost comparable growth at all three positions. Note that period of reduced growth occurs at a different time depending on location. Landmarks used are described in Vora, Camci and Cox (2016). Graphs demonstrate means at each timepoint with error bars representing standard deviations when applicable (n=3 for PN0, 7, 60 and n=5 for PN14, 21, 30). Linear trendline, slope and correlation coefficient (R^2) are expressed for D, E and F.

3.4.2 Chondrocytes in the nasal septum undergo a position-dependent maturation process

To identify morphological changes that accompany nasal cartilage growth, we performed histological analysis at each developmental stage on anterior (Figures. 3.3, S3.1), a-p midpoint (Figure S3.1) and posterior sections (Figures. 3.4, S3.1). The central portion of the nasal septum

is shown for representative time points only in Figures 3.3 & 3.4. For the full panel refer to supplemental Figure 3.1. The most obvious change in the septal cartilage was the change in chondrocyte cell size and cellularity starting in the middle of septum. In general, the high number of small chondrocytes was replaced with time by fewer and much larger hypertrophic chondrocytes. In the anterior septum, the presence of hypertrophic-appearing chondrocytes was first noticed at PN7 (Figure 3.3B, white arrows). At PN60, the septum appeared to be entirely composed of large, hypertrophic chondrocytes (Figure 3.3A-E). Apart from this dynamic change in cell size, the width of the cartilage and perichondrium similarly changed. At the same time, the intensity of the Safranin O stain was reduced at PN60 indicative of a change in cartilage properties (Figure 3.3E). Lateral lining of collagen fibres along the presumptive perichondrium became first noticeable at PN7 and persisted through all subsequent stages (Figure 3.3F-J, yellow arrows). At PN60, but not at any earlier time point, an extensive collagen network had formed anterior in between the large hypertrophic chondrocytes (Figure 3.3J). Results for Alcian Blue demonstrated similar morphological observations to those observed in sections stained with Safranin O (Figure S3.1). Results from the a-p midpoint nasal septum demonstrated similar morphological trends to those observed in the anterior nasal septum (Figure S3.2). Overall, it appeared that the chondrocytes in the anterior and a-p midpoint nasal septum undergo dynamic changes resulting in the formation of hypertrophic chondrocytes surrounded by a meshwork of dense collagen fibres.

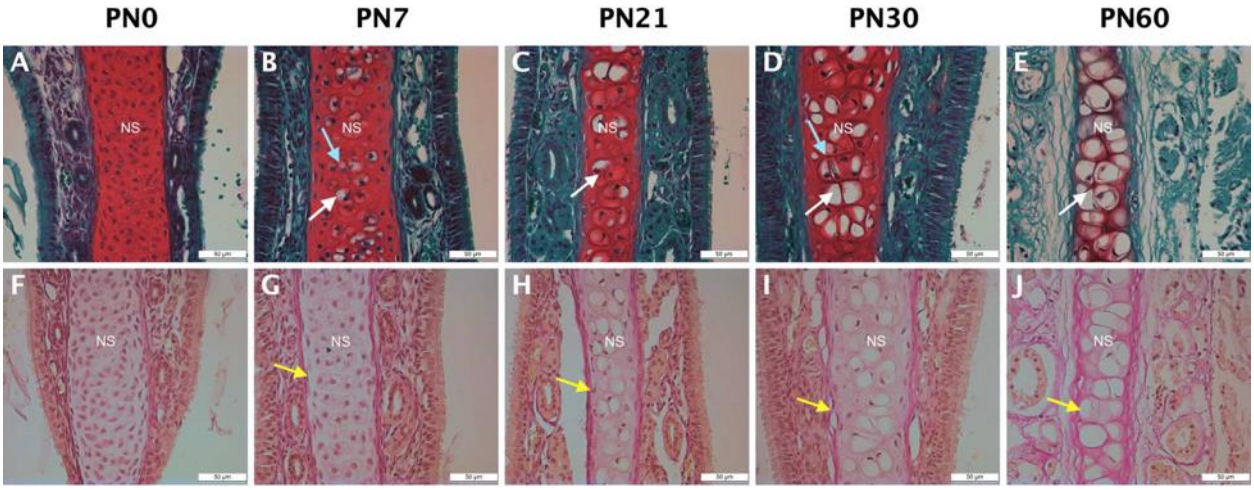

Figure 3. 3 Chondrocytes in the anterior septum mature and develop a strong collagen network.

Safranin O (A-E) and Van Gieson (F-J) staining of the anterior nasal septum on 7µm paraffin sections. Hypertrophic-like chondrocytes become apparent after PN7 (white arrows). Collagen fibril formation (yellow arrow) starts in the perichondrium after PN7 to form a dense collagen network by PN60. Columnar-like chondrocytes were observed at PN7 and PN30 (blue arrows) NS: nasal septum.

In the posterior nasal septum hypertrophic chondrocyte maturation (Figure 3.4, white arrows) started in the central portion of the septum and progressed more slowly. The large hypertrophic chondrocytes observed in the anterior/a-p midpoint septum were not seen (Figure 3.4E). The onset of collagen fibril formation (Figure 3.4H) coincided with the appearance of hypertrophic chondrocytes similar to the anterior septum. The increase in hypertrophic chondrocytes and collagen fibre formation appeared biphasic. The two stages with predominant hypertrophic chondrocytes at PN21 and PN60 was interrupted by the appearance of columnar chondrocytes reminiscent of the columns in the growth plate (Figure 3.4D, blue arrows). Columnar chondrocytes were more prevalent in the posterior septum. Similarly, collagen fibre formation followed a biphasic pattern. Dense collagen fibres were observed at PN21 and PN60 (Figure 3.4H, J, yellow arrows), but appeared reduced at PN30 (Figure 3.4I). Overall, assessing cartilage

development on the basis of cartilage hypertrophy and collagen fiber formation revealed differences between the anterior and posterior septum and over time. Chondrocytes in the posterior nasal septum followed a biphasic pattern of hypertrophy. Anterior, a linear differentiation pattern was observed, and hypertrophic chondrocytes were eventually surrounded by a collagen mesh.

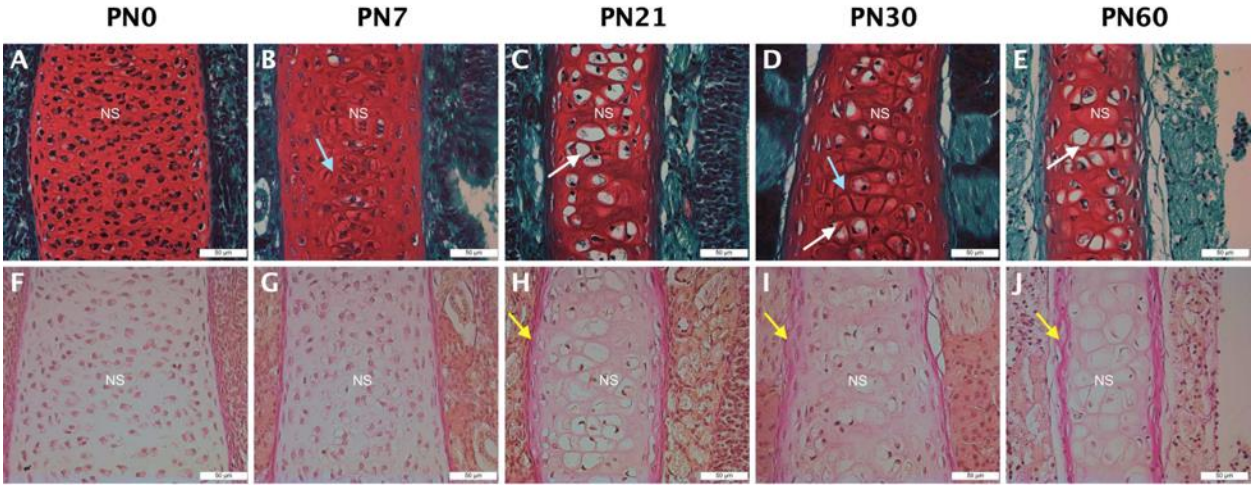

Figure 3. 4 Chondrocytes in the posterior reflect biphasic growth.

Safranin O (A-E) and Van Gieson (F-J) staining of the posterior nasal septum on 7µm paraffin sections. Hypertrophic chondrocytes (C) prevalent from PN21 onwards (white arrows) and a reduction at PN30 reflect the biphasic growth. Columnar-like chondrocytes were observed at PN7 and PN30 (blue arrows). Collagen fibril formation is evident from PN21 (yellow arrow) onwards. Note: absence of dense collagen network at PN60. NS: nasal septum.

3.4.3 Position-dependent differences in chondrocyte maturation is reflected in differences in extracellular matrix composition and cell differentiation.

To correlate molecular changes to the morphological differences in the nasal septum, we stained for proteins commonly used to distinguish the various chondrocyte differentiation stages in the growth plate and articular cartilage [132]. Nuclear expression of Sox9 was only detected at E18.5 (Figure 3.5A-B), whereas expression at PN0 was more cytoplasmic (Figure 3.5C-D). Expression was stronger in anterior sections and no expression was observed at any of the later stages (Figure S3.3). Col II was ubiquitously expressed throughout the septum from E18.5 to P14,

but subsequently steadily decreased showing only weak and more centrally located expression in the posterior cartilage at PN60 (Figure 3.5I-L). Runx2 expression varied by location, time, and subcellular localization. At early stages (E18.5, PN0) expression was predominantly nuclear and more abundant posterior. Around PN7, expression was observed throughout the entire septum but was predominantly cytoplasmic (not shown). At PN30 expression was still abundant, but more restricted to the central part of the septum (Figure 3.6D). Col X was not observed before PN21 posterior and PN30 anterior and was predominantly observed in the lateral aspects of the septum (Figure 3.6G). At PN60, expression became stronger anterior compared to posterior (not shown). Mmp13 was detected first at PN0 in the posterior septum. The expression of Mmp13 appeared nuclear at most time-points. At PN14, its expression became more distinct and was mostly restricted to the centre of the septum (Figure 3.6L). Expression persisted until PN60 in the posterior sections, albeit levels appeared reduced (not shown). Anterior, Mmp13 was observed only in the perichondrium (Figure 3.6I, 3.6K). although staining was difficult to distinguish from background (Supplemental Figure 3.4). Sp7 was first detected in posterior regions at PN0. Expression was observed throughout the septum with both nuclear and cytoplasmic localization. (Figure 3.7B). Expression almost disappeared by PN14 (Figure 3.7C and 3.7D). No or very limited expression was observed within septum cartilage anterior. At PN60 cytoplasmic expression could be observed in areas where the PPE would be expected. Anterior expression was cytoplasmic and restricted to the perichondrium. Ocn was already present at E18.5 (not shown). Expression peaked at PN0 posterior and PN7 anterior (Figure 3.7G), and then steadily decreased to PN60 (Figure 3.7I). At PN60, anterior expression was predominately observed in the perichondrium but not posterior (Figure 3.7J).

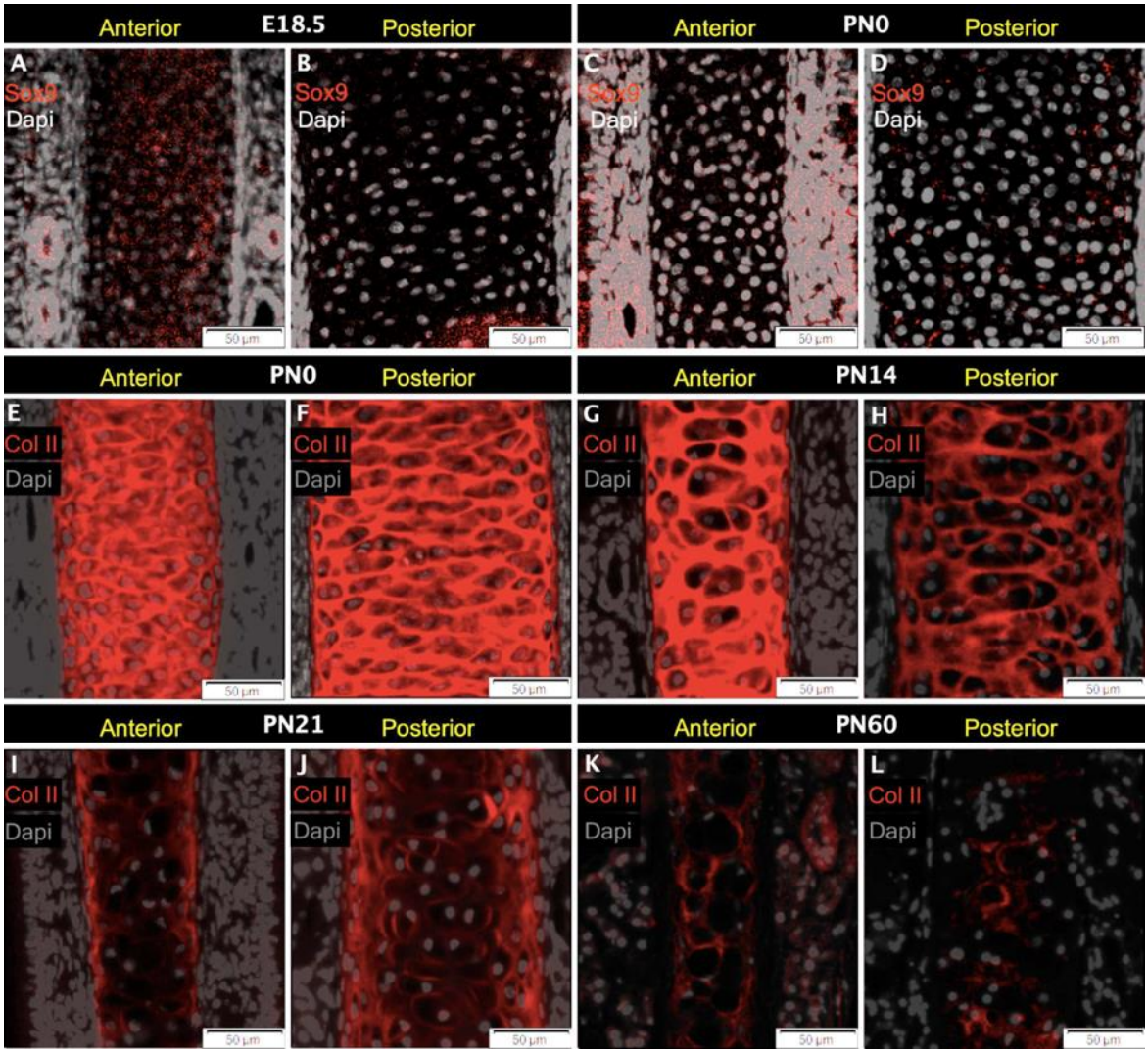

Figure 3. 5 Proteins marking early chondrogenesis show anterior-posterior differences.

Immunofluorescence staining for Sox9 (A-D) and Collagen II (Col II)(E-L) on 7µm paraffin sections. Presence of Sox9 is only noted at E18 and PN0 and is more prominent in the anterior nasal septum. Presence of Col II decreases over time, which is more prominent in the posterior nasal septum at PN60 (L). (A, C, E, G, I, K) anterior sections, (B, D, F, H, J, L) posterior sections.

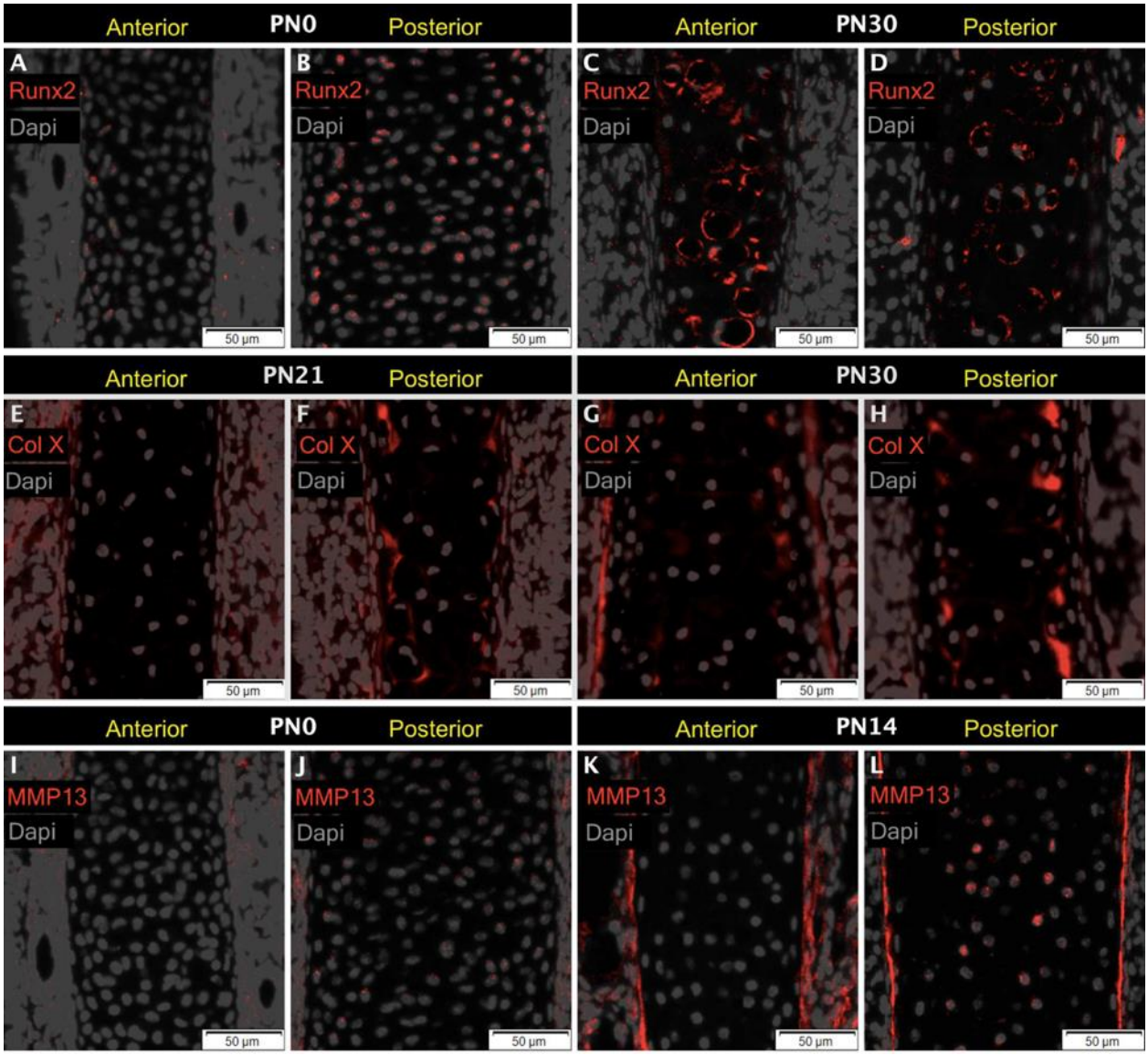

Figure 3. 6 Proteins indicative of hypertrophic chondrocytes are dynamically expressed in anterior and posterior nasal septum.

Immunofluorescence staining on anterior (A, C, E, G, I, K) and posterior (B, D, F, H, J, L) 7µm paraffin sections at different ages. (A-D) Runx2 expression is initially nuclear (DAPI-grey) in both anterior and posterior septum and becomes ubiquitously cytoplasmic by PN30. (E-H) Collagen X (Col X) expression is evident posterior from P21 (F) onwards whereas anterior Col X is not expressed until PN30 (G). (I-L) MMP13 is expressed at low levels posterior starting at PN0 (J) and becomes more apparent at PN14 (L). No expression of MMP13 is observed in the chondrocytes of the anterior nasal septum (I, K) at all ages except for PN7 (not shown).

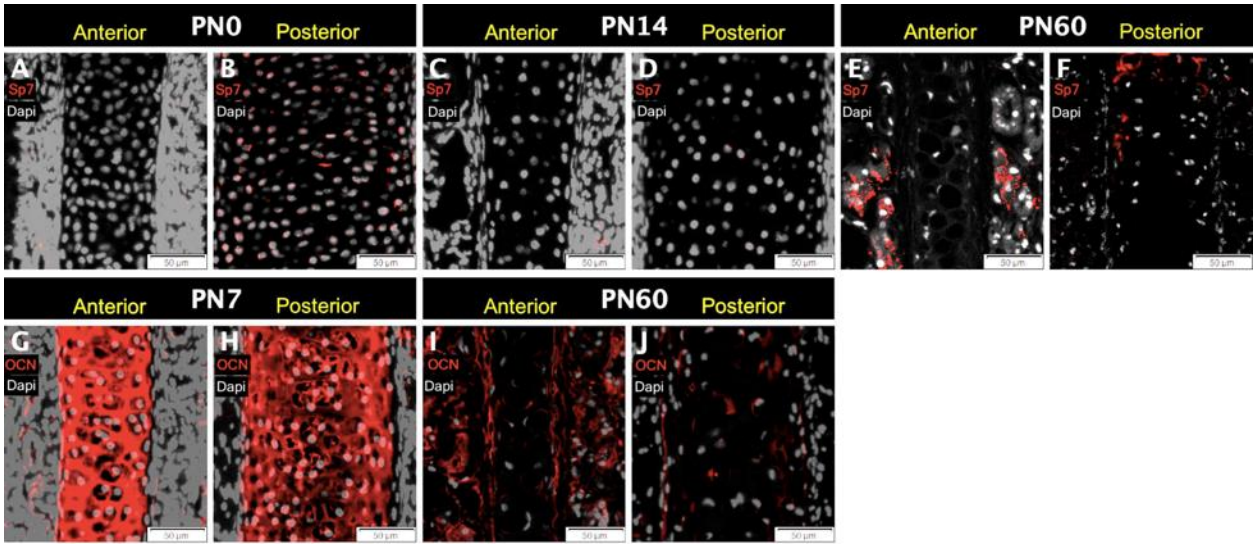

Figure 3. 7 Bone specific proteins are not restricted to the posterior region.

Immunofluorescence staining on anterior (A, C, E, G, I) and posterior (B, D, F, H, J,) 7µm paraffin sections at different ages. (A-F) Sp7 is already restricted to the posterior nasal septum. It is first evident at PN0 (B), then expression is reduced (D) until the formation of bone in the posterior nasal septum at PN60 (F). Osteocalcin (Ocn) is highly expressed in chondrocytes from PN0 to PN7 (G-J) with stronger staining anterior. Expression becomes less over time both anterior and posterior.

3.4.4 Spatiotemporal pattern of PPE ossification in the nasal septum.

We next correlated the expression of hypertrophy (ColX, Mmp13) and ossification (Sp7, Ocn) markers to the spatiotemporal ossification of the PPE. PPE ossification was evident from PN7 onwards (Supplemental Figure 3.5B) and the extent of ossification steadily increased through to PN60 (Supplemental Figure 3.5F). Comparison of midsagittal slices from µCT scans of mice at PN30 and PN60 clearly indicated the increase in mineralization. PPE mineralization followed a superior to inferior trajectory (Figure 3.8A, G). Hypertrophic chondrocytes became successively incorporated into the bony matrix of the PPE (Figure 3.8B, D, H, J). Intensity of Safranin O staining decreased from PN30 to PN60 (Figure 3.8D,J) at sites of presumptive bone formation. A collagen matrix surrounded the PPE both at PN30 and PN60, but was more prominent at the older

age (Figure 3.8C, I). Runx2 and Sp7 could both be observed at the sites of presumptive transformation of cartilage into bone. Whereas Runx2 was predominantly observed in hypertrophic chondrocytes still staining positive for Safranin O, the Sp7 expression domain was primarily associated with the ossified PPE. These findings suggest that nasal septum ossification follows a posterior-anterior and dorsal-ventral direction. Figure 3.9A provides a summary showing that protein expression varies over time and with location and Figure 3.9B demonstrates a proposed model for chondrocyte maturation through hypertrophy, suggesting that nasal septum cartilage is a much more dynamic cartilaginous tissue than previously thought.

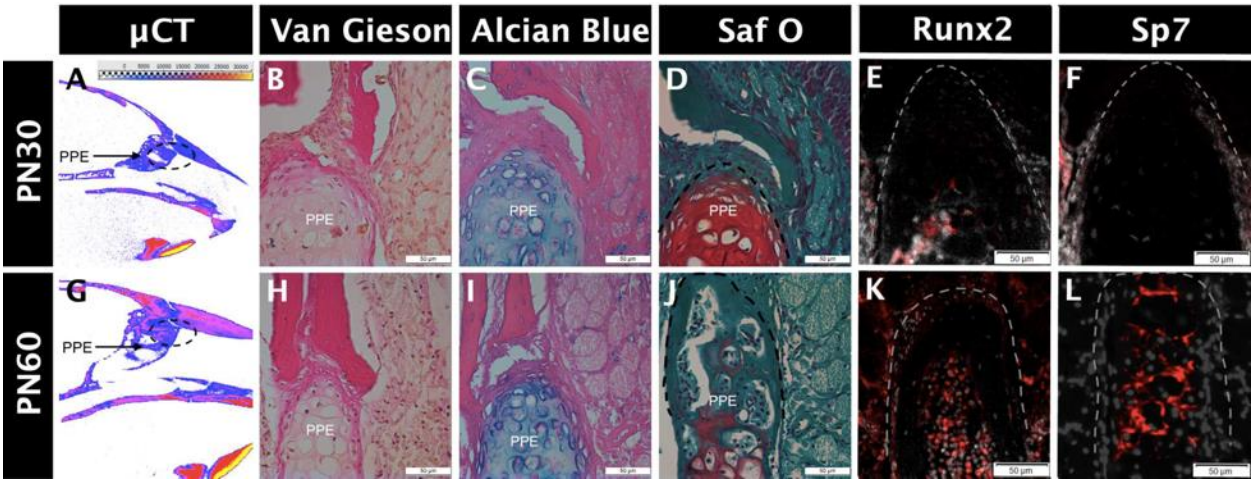

Figure 3. 8 The perpendicular plate of the ethmoid (PPE) ossifies in a superior to inferior direction.

(A, G) midsagittal slice from micro-CT analysis shows highly calcified, mature (pink) and lesser calcified, immature bone at PN30 (A) and PN60 (G). Color map for false-colored mineral density is shown in A. Ossification (dotted oval) descends from dorsal (superior) to ventral (inferior). Van Gieson (B, H), Alcian Blue (C, I), and Safranin O (D, J) stains on posterior 7µm paraffin sections at PN30 (B-D) and PN60 (H-J) indicate loss of Safranin O and increase in collagen fibres indicative of bone formation in PN60 nasal septum. Immunostaining for Runx2 (E, K) shows cytoplasmic staining at PN30 (E) and increased nuclear expression in the marrow space of the newly forming bone at PN60 (K). Sp7 (F, L) is restricted to PN60 (L) to sites of ossification.

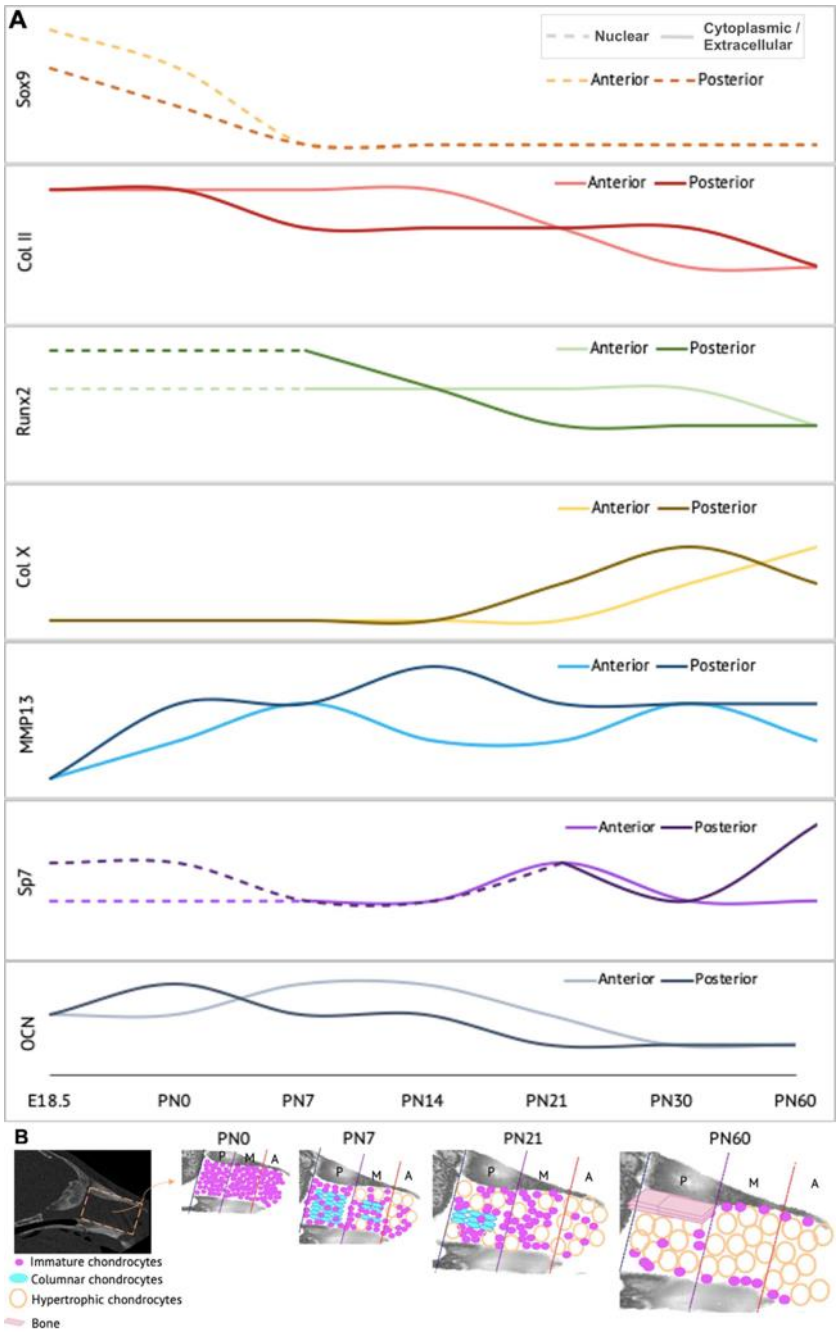

Figure 3. 9 Illustration summarizing the dynamic expression of proteins involved in nasal cartilage development as well as the proposed model for nasal cartilage growth through hypertrophy.

(A) Schematic is based on findings from all immunofluorescence experiments (n=3/protein/age). Solid lines indicate cytoplasmic expression, dotted lines indicate nuclear expression. (B) Overlay on isosurface rendering of a μCT scan of an adult mouse indicating growth of immature chondrocytes, columnar chondrocytes, hypertrophic chondrocytes and bone over time. Schematic is based on findings from all histological analysis (n=3/age). Anterior (A) chondrocytes (red) mature first through the process of hypertrophy followed by a-p midpoint (M) (purple) and posterior (P) (blue) regions.

3.5 Discussion

In this study we correlated growth of the nasal cartilage to cellular properties across its length and over time. Although generally defined as hyaline cartilage, we found that the nasal cartilage is a more complex and dynamic structure than anticipated that could only incompletely be described using commonly used markers for hyaline cartilage.

3.5.1 Asynchronous growth phases in the nasal cavity over time

Previous studies [131,140] described the dynamic growth of the nasal complex in context of overall craniofacial growth. The nasal unit grows continuously and rapidly between PN7 to PN56, with individual aspects, such as nasal bone length or width, displaying different growth rates. Our data indicates that the nasal cartilage similarly grows heterogeneously. In particular, a reduced growth rate for the height of the nasal cartilage was observed between PN14-PN21.

The growth pattern of the nasal septum have been deduced in the context of growth anomalies in children/adolescents such as midfacial hypoplasia and nasal septum deviation using a morphometric approach [130] or in large animals mapping proliferation using a histological approach [10,35,117]. Measuring nasal septum growth at multiple positions along the anterior-posterior axis over time provides thus context for those studies. Growth and ossification of the PPE followed a postero-anterior and superior-inferior direction, in line with and extending previous results using Calcein tracing over a more restricted timeframe in PN0 – PN15 mice [131]. The cartilage followed the endochondral ossification pathway as previously suggested [131]. Correlating mineralization at early and late stages to the expression of ossification markers suggest that a chondrocyte to osteoblast transdifferentiation process takes place at the PPE [143].

3.5.2 Onset of chondrocyte hypertrophy coincides with appearance of collagen fibre network and growth of the nasal septum

Gross morphological analysis using Safranin O and Van Gieson staining demonstrated dynamic changes in cell size and density over time. Small immature chondrocytes were successively replaced by large hypertrophic chondrocytes. This change did not occur in a uniform fashion. These dynamic changes were accompanied by changes in septal cartilage width, which seemed to inversely correlate with the thickness of the perichondrium. In the anterior nasal septum, differentiation into hypertrophic chondrocytes started at PN7 (Figure 3.3B). Posterior, hypertrophic chondrocytes were not detected before PN21. Similarly, remodelling of the extracellular matrix (ECM) coincided with chondrocyte maturation and differentiation. Based on these observations and the fact that no overt apoptosis can be observed (not shown), we propose that acquisition of hypertrophy and concomitant spatial redistribution of chondrocytes constitutes the major mechanism driving the 3-dimensional growth of the septal cartilage (Figure 3.9B). Hypertrophy is first observed anterior, thus this part of the septum matures first, followed by the appearance of a cartilage network surrounding each chondrocyte, while columnar stacks of chondrocytes are observed posterior and a-p midpoint. This is followed by hypertrophic maturation in the a-p midpoint and posterior regions. This form of growth driven by chondrocyte maturation is somewhat reminiscent to the developing synchondrosis in the cranial base, where chondrocyte growth ceases in an anteroposterior manner while ossification occurs in a posteroanterior direction [144]. In the case of the nasal septal cartilage, differentiation towards posterior occurs last and only the posterior portion will ever ossify through the process of chondrocyte to osteoblast transdifferentiation. The anterior portion remains cartilaginous throughout. The early differentiation in the anterior region is in line with previously reported reduction in growth and

proliferation [145]. The appearance of an extensive collagen network surrounding the hypertrophic chondrocytes across the entire anterior region was noted, which could provide stiffness and increased mechanical resistance to the anterior nasal cartilage [146]. The stiffness of collagen fibrils has been shown to promote chondrocyte differentiation [147]. Whether the formation of collagen fibrils triggers the early cell differentiation, or whether cell differentiation is a prerequisite for collagen network formation is not clear. In the posterior nasal septum, the onset of collagen fibre remodelling concurred with the appearance of hypertrophic chondrocytes, albeit at a later stage.

3.5.3 Molecular properties contribute to extracellular matrix composition in the nasal septum

Studies on the growth zone of long bones have led to the identification of a set of molecular markers useful to follow hyaline cartilage differentiation [148]. Using these markers, spatiotemporal changes in the nasal cartilage were mapped in an attempt to describe nasal hyaline cartilage differentiation/maturation. Expression of Sox9 and Col II largely followed the expected pattern. Sox9 was present in the early stages of nasal septum development at E18.5 and PN0 with expression subsiding at later stages. Coll II was ubiquitous throughout the septum with highest expression at early stages from PN0 to PN14, and only faint expression at PN60 remained in the posterior region. In the knee, Col II becomes diminished with age making it a less prominent ECM component of mature hyaline cartilage [134]. Runx2, a key regulator of bone formation, is expressed during most stages of cartilage maturation [134]. In progenitor cells, Runx2 promotes chondrocyte over adipocyte fate [139]. Maybe not unexpected, widespread nuclear expression of Runx2 was observed at PN0, when chondrocytes were still immature. Whether this early expression is associated with a commitment to the chondrocyte lineage or serves some other, not yet recognized function is not clear. At later stages, Runx2 was more sparsely expressed and mostly observed in the cytoplasm. It has been shown that this shift from nuclear to cytoplasmic Runx2 localization is

microtubule-driven and has been associated with chondrocyte maturation in chick growth plate chondrocytes [139,149,150]. The role of cytoplasmic Runx2 in cartilage and bone is not understood. Nuclear Runx2 is seen in hypertrophic chondrocytes during endochondral ossification [151]. Stronger cytoplasmic Runx2 expression was observed in the anterior nasal cartilage, which incidentally never ossifies, compared to posterior where ossification occurs. The shift from cytoplasmic to nuclear Runx2 localization in the PPE coincided with ossification, whereas cytoplasmic localization correlated with an arrest in chondrocyte maturation.

Expression of Mmp13 is normally restricted to hypertrophic chondrocytes [152] and has been associated with collagen remodeling and degradation [153]. In the posterior nasal septum, Mmp13 expression was already detected in immature chondrocytes from PN0 onwards. Expression was maintained until PN60, but expression decreased over time, in line with the association of reduced Mmp13 expression with hypertrophic chondrocyte proliferation in the growth plate [152]. Whereas the role of Mmp13 at later stages of chondrocyte development is well established, its role during early cartilage development is not well understood. In E15.5 Mmp13-deficient embryos, the growth plate was longer and columnar chondrocytes were misaligned [154] indicating a role in the spatial organization and growth of the developing cartilage. Growth plate length and organization of columnar chondrocytes are both dependent on collagen matrix remodelling [147]. Mmp13 might play a similar role in the nasal cartilage.

Expression of Osterix/Sp7 differed from the expected expression pattern. Nuclear Sp7 was observed at PN0 in the posterior nasal septum, significantly earlier than the onset of posterior ossification. This early expression might reflect an early commitment to the bone lineage [155]. Ocn, a frequently used marker for osteoblast differentiation [138], was expressed at all time-points both anterior and posterior. The strong expression in the anterior nasal septum suggests a role for Ocn

other than ossification. The recent identification of an endocrine function for Ocn in the regulation of glucose metabolism [156] might indicate a similar function in cartilage.

Overall, the commonly used molecular markers to describe cartilage differentiation in the growth plate cannot be faithfully applied to the growing nasal septum. Whereas presence of Sox9, Runx2 and Sp7 in the growing nasal cartilage is in line with the gene regulatory networks described for immature cartilage, mature cartilage, and bone based on the fossil record [132], Safranin O and Alcian Blue clearly ascertain chondrocyte properties to these cells. Additional signalling networks must contribute to the subspecification of chondrocytes.

3.5.4 Differences between nasal septum and growth plate cartilage.

The nasal septum cartilage and growth plate cartilage are both hyaline cartilages albeit with different functional requirements. The growth plate is physically organized into subzones such as resting, proliferating, hypertrophic and ossification zone. This clear distinction of these subzones is not observed in the nasal septum [157]. Growth plate properties are present at the septoethmoidal junction at least till P15 [131], although later timepoints weren't analyzed. The same study also proposed that some septum growth must occur by interstitial cartilage expansion. Here, we show that the mechanism for this appears to be chondrocyte hypertrophy. The growth plate contributes primarily to the longitudinal growth of the limb, whereas the nasal septum needs to grow in all dimensions. In the growth plate, organized stacks of columnar chondrocytes are observed allowing for synchronous coordinated growth [145,158]. In the septum, columnar stacks are present, but their stacking is horizontal and appears asynchronous. This interspersed stacking may contribute to the observed heterogeneous growth. Whereas the columnar chondrocytes in the growth plate contribute to the elongation of the bone[159], the horizontal stacking in the nose would be expected to contribute to nasal septum width. Indeed, rod-shaped cartilages like the nasal septum have

transverse clonal arrangements that contribute to the diameter of the cartilaginous rod [160]. The interspersed clonal arrangements could be a reflection of asynchronous differentiation of the cartilage itself. The transverse columns were centrally located and hypertrophic chondrocytes were interspersed between them [161]. In the growth zone, the longitudinal stacking of columnar chondrocytes is regulated by Parathyroid hormone–related protein and Indian Hedgehog [162]. Whether the same signaling networks are also active in the nasal septum is yet to be investigated.

The majority of the nasal septum does not ossify, with the exception of the posterior region. During endochondral ossification, hypertrophic chondrocytes either undergo apoptosis to allow for invasion of osteoprogenitors and vasculature [163,164], or directly transdifferentiate into osteoblasts [165]. It has been speculated that the fate of hypertrophic chondrocytes during endochondral ossification might depend on the type of hyaline cartilage, its stage of development and the cellular location within [120,132,163–165]. In the PPE, expression of Runx2 and SP7 in relation to histological stains suggest that transdifferentiation might be the prominent mechanism [166]. However, formal proof using detailed lineage tracing would be required to ascertain this.

Our study adds to previous literature on nasal septum cartilage. It shows that cartilage differentiation in the nasal septum does not follow a homogenous differentiation path as set out in growth plate cartilage. The observed spatiotemporal variation was unexpected. Whereas the posterior septum appeared to follow the path of endochondral ossification, the anterior septum develops properties atypical for hyaline cartilage, such as extensive collagen networks. It will be of interest to see if and which of those cartilage properties are altered in a deviated septum or a septum with stunted growth. This study also highlights the need to carefully investigate different hyaline cartilages to better understand their functional specialization. Lastly, the current perception of the nasal cartilage as a hyaline cartilage is quite likely is an oversimplification. The dynamic

molecular and cellular heterogeneity observed along the length of the septum will need to be considered when using this cartilage for tissue engineering.

3.6 Supplementary Information

Supplemental Table 3. 1 Raw data points obtained from measurements outline in Figure 3.2.

Age	Nasal Septum Length Anterior					Nasal Septum Length a-p midpoint					Nasal Septum Length Posterior				
PNO	1.51		1.70		1.71	1.56		1.99		1.75	1.64		2.3		1.8
PN7	2.12		2.00		1.9	2.44		2.34		2.31	2.65		2.52		2.86
PN14	2.22	2.19	2.2	2.15	2,2	2.54	2.52	2.45	2.55	2.52	3.03	3.07	2.93	2.91	3.05
PN21	2.39	2.43	2.32	2.46	2.45	2.84	2.78	2.71	2.94	2.81	3.2	3.12	2.85	3.18	3.16
PN30	2.8	2.83	2.85	2.81	2.85	3.4	3.2	3.21	3.32	3.48	3.69	3.7	3.65	3.76	3.72
PN60	3.38		3.82		3.04	3.92		4.09		3.54	4.04		4.17		3.89

	PPE Length			Nasal Bone Length			Nasal Cavity Height									
							Anterior					Posterior				
PNO	1.36	1.53	1.48	2.05	2.39	2.20	1.39	1.25	1.30			1.54	1.55	1.50		
PN7	2.98	2.12	2.08	4.53	4.30	3.88	1.94	1.70	1.50			2.59	2.20	2.15		
PN14	4.58	3.44	3.76	4.85	5.04	5.00	2.26	1.90	1.83	2.08	2.18	2.7	2.98	3.25	2.58	2.88
PN21	4.20	3.86	4.02	5.92	5.69	5.30	2.30	1.97	2.30	2.30	1.98	3.2	3.14	2.76	3.00	2.72
PN30	5.44	4.55	4.40	7.01	5.63	6.27	2.32	2.73	2.39	2.56	2.70	3.16	3.10	3.61	3.31	3.14
PN60	4.86	5.37	4.93	7.5	6.89	7.72	2.61	2.83	2.63			3.72	3.37	3.63		

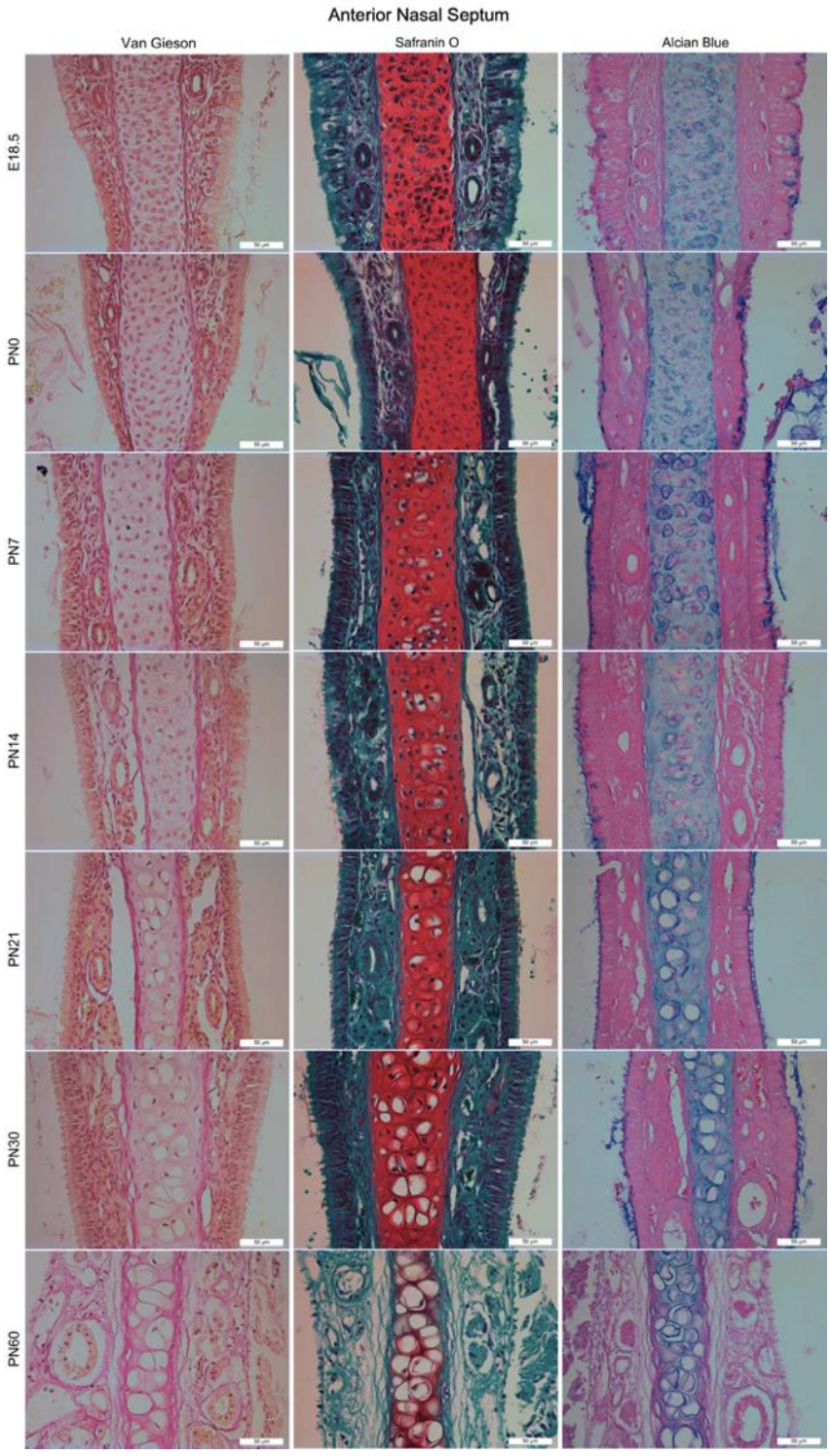

Supplemental Figure 3. 1 Van Gieson (collagen fibers- pink), Safranin O (cartilage- red) and Alcian Blue (glycosaminoglycan- blue) staining of the anterior nasal septum at all ages investigated.

7µm paraffin sections were used for all histological stains.

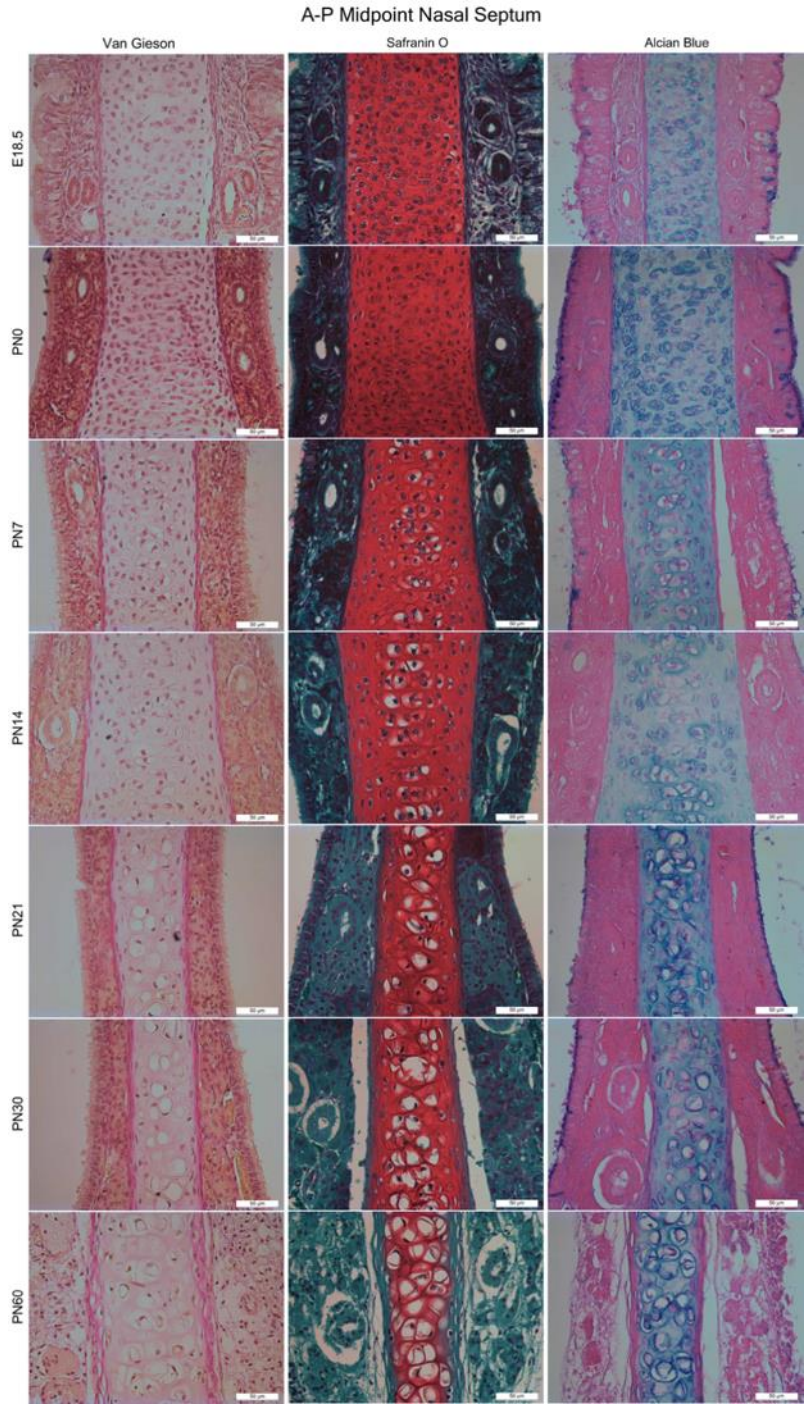

Supplemental Figure 3. 2 Van Gieson (collagen fibers- pink), Safranin O (cartilage- red) and Alcian Blue (glycosaminoglycan- blue) staining of the a-p midpoint nasal septum at all ages investigated.

7µm paraffin sections were used for all histological stains.

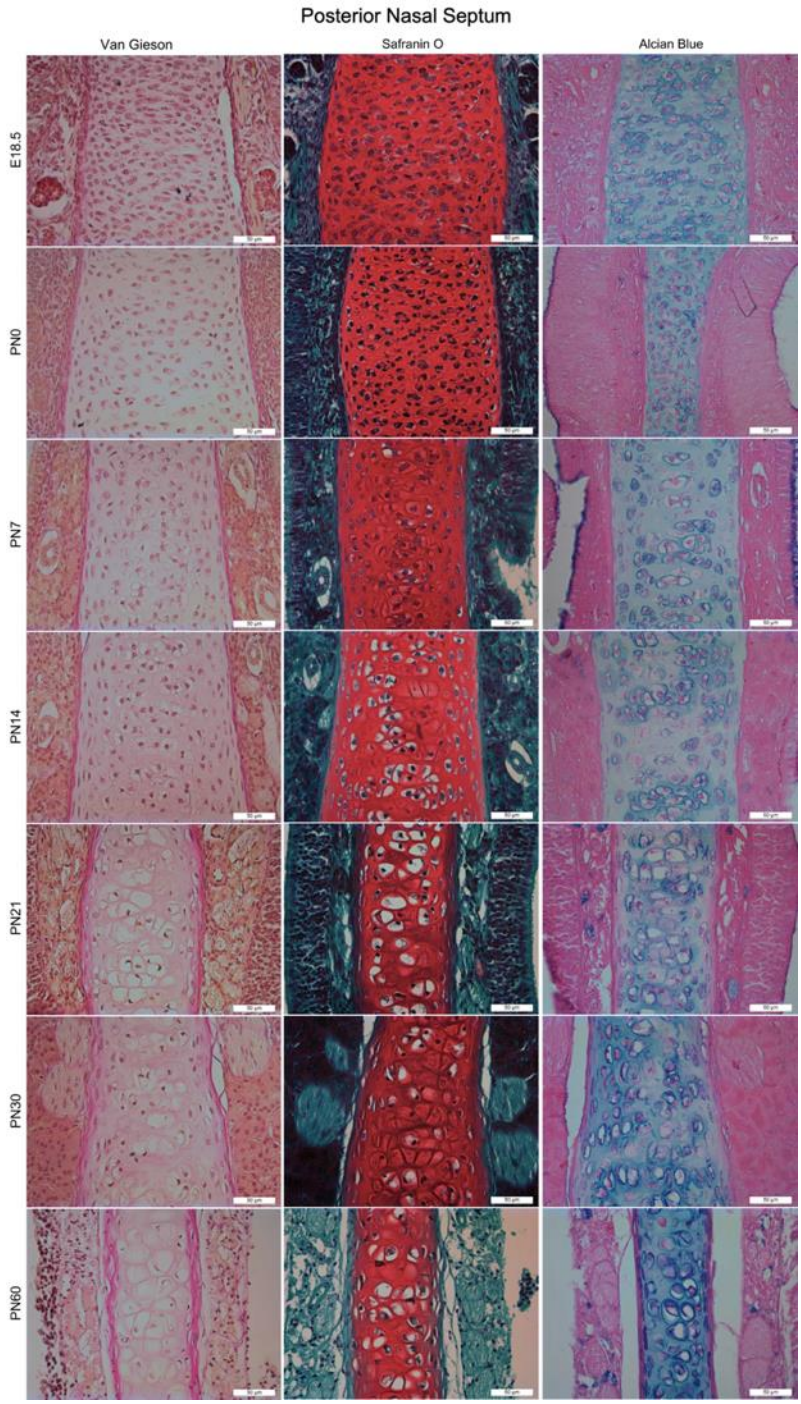

Supplemental Figure 3. 3 Van Gieson (collagen fibers- pink), Safranin O (cartilage- red) and Alcian Blue (glycosaminoglycan- blue) staining of the posterior nasal septum at all ages investigated.

7µm paraffin sections were used for all histological stains.

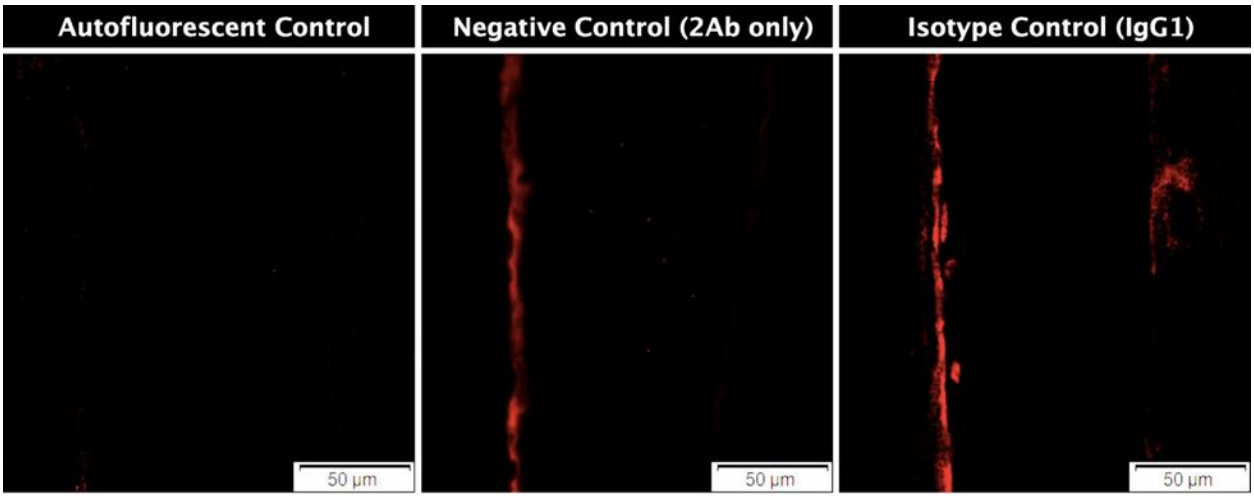

Supplemental Figure 3. 4 Control used to interpret immunofluorescence staining. Controls for autofluorescence, negative (IgG1) and isotype (IgG1) were tested.

No autofluorescence was observed in the nasal septum. However, IgG1 negative control indicated some background staining in the perichondrium. Similar result was observed in the isotype control. 7µm paraffin sections were used for all immunofluorescence staining.

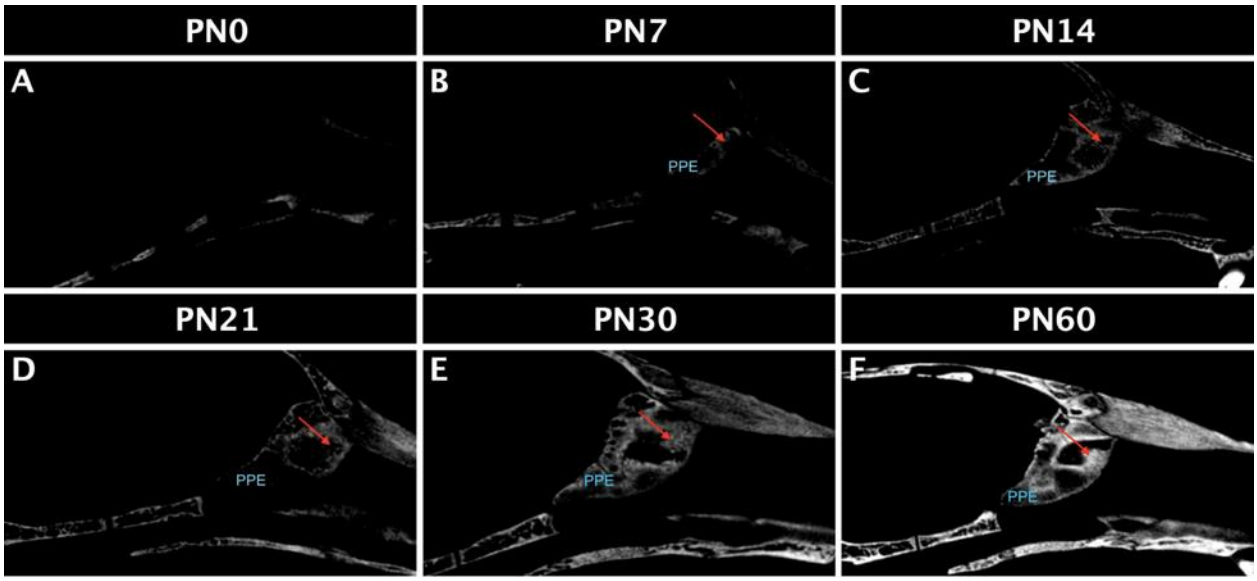

Supplemental Figure 3. 5 Growth and ossification of perpendicular plate of ethmoid (PPE) occurs in a superoinferior and posteroanterior manner.

Midsagittal cross-section of mice skulls at ages PN0(A), PN7(B), PN14(C), PN21(D), PN30(E), PN60(F) demonstrate growth of PPE begins at PN7(B) (arrows) with ossification at its peak (increased gray value) at PN60(F).

Chapter 4: Neural crest-specific loss of Bmp7 leads to midfacial hypoplasia, nasal airway obstruction and disordered breathing, modeling obstructive sleep apnea

Chapter 3 established that the nasal cartilage is a heterogeneous structure that matures through chondrocyte hypertrophy. With this information, we wanted to identify how these properties might be changing when the nasal septum deviates. To do so, we needed to establish a mouse model for nasal septum deviation. Chapter 4 characterizes the Bmp7 neural crest knockout ($Bmp7^{ncko}$) mouse model where deletion of Bmp7 in neural crest presents with nasal septum deviation at a time when the mice are undergoing rapid midfacial growth. We assessed structural and physiological changes associated with the onset of nasal septum deviation.

Chapter 4 is derived from this published article

Baddam, P., Biancardi, V., Roth, D. M., Eaton, F., Thereza-Bussolaro, C., Mandal, R., Wishart, D. S., Barr, A., MacLean, J., Flores-Mir, C., Pagliardini, S., & Graf, D. (2021). Neural crest-specific deletion of Bmp7 leads to midfacial hypoplasia, nasal airway obstruction, and disordered breathing modelling Obstructive Sleep Apnea. *Disease models & mechanisms, 14(2), dmm047738. Advance online publication. https://doi.org/10.1242/dmm.047738*

4.1 Abstract

Pediatric obstructive sleep apnea (OSA), a relatively common sleep-related breathing disorder (SRBD) affecting ~1-5% of children, is often caused by anatomical obstruction and/or collapse of the nasal and/or pharyngeal airways. The resulting sleep disruption and intermittent hypoxia lead to various systemic morbidities. Predicting the development of OSA from craniofacial features alone is currently not possible and a controversy remains as to whether upper-airway obstruction facilitates reduced midfacial growth or vice-versa. Currently, there is no rodent model that recapitulates both the development of craniofacial abnormalities and upper airway obstruction to address these questions. Here, we describe that mice with a neural crest-specific deletion of *Bmp7* ($Bmp7^{ncko}$) present with a shorter, more acute-angled cranial base, midfacial hypoplasia, nasal septum deviation, turbinate swelling and branching defects, and nasal airway obstruction. Interestingly, several of these craniofacial features develop after birth during periods of rapid midfacial growth and precede the development of an upper airway obstruction. We identified that in this rodent model, no single feature appeared to predict upper airway obstruction, but the sum of those features resulted in a reduced breathing frequency, apneas and overall reduced oxygen consumption. Metabolomics analysis of serum from peripheral blood identified increased levels of hydroxyproline, a metabolite upregulated under hypoxic conditions. As this model recapitulates many features observed in OSA, it offers unique opportunities for studying how upper airway obstruction affects breathing physiology and leads to systemic morbidities.

Keywords: Bone Morphogenetic Protein 7, midfacial hypoplasia, airway obstruction, nasal septum deviation, turbinate hypertrophy, apneas, sleep related breathing disorders.

4.2 Introduction

Sleep-related breathing disorders (SRBDs) encompasses a spectrum of problems including obstructive sleep apnea (OSA), central sleep apnea (CSA) and complex sleep apnea [167,168]. In children, pediatric OSA is the most common and widely investigated form of apnea, with a prevalence of 1.2% – 5.7% [168]. It is often caused by physical obstruction of either nasal and/or pharyngeal airways, leading to reduced airflow intake and/or intermittent apneas, resulting in difficulty to breathe. This can lead to intermittent hypoxia (IH) conditions most prominently noticed during sleep, and has been associated with a variety of systemic (including cardiovascular, metabolic and neurocognitive) morbidities as well as behavioral problems at home and school that may continue and progress into adulthood [169,170].

The etiology of pediatric OSA is multifactorial. Craniofacial and neuromuscular factors along with lymphoid tissue hypertrophy and airway soft tissue inflammation are considered critical components contributing to pediatric OSA [171]; however, controversy remains regarding the causes or consequence of these various manifestations. The resulting IH is considered a critical factor in the systemic pathogenesis of OSA [172]. The gold standard for diagnosis of OSA should include nocturnal polysomnography (nPSG). Chronic untreated OSA can result in cardiovascular, neurocognitive and metabolic morbidities [173], whereby the presence of IH is associated with increased severity of these morbidities [174]. Current surgical approaches are primarily aimed at relieving the physical obstruction [175]. Hypertrophy of tonsils and adenoids can contribute to pharyngeal obstruction. Hence, a common paediatric surgical approach is tonsillectomy and adenoidectomy (T&A) to remove enlarged lymphoid tissue [176]. However, upper airway obstruction commonly remains as a post-operative symptom, residual pediatric OSA, suggestive of a more complex, multifactorial aetiology of pediatric OSA/SRBD. The lack of complete resolution with

these interventions also highlights the need to consider various craniofacial components in addition to adenoids [176] for better screening, diagnosis and management outcomes.

Craniofacial abnormalities strongly predispose to upper airway obstruction, as the prevalence of OSA increases to up to 67% in children with craniofacial syndromes [177,178]. Midfacial hypoplasia, nasal septum deviation, micrognathia, craniosynostosis, achondroplasia and cleft palate are all considered contributing factors to upper airway obstruction [179]. A common denominator in all these abnormalities is altered or lack of craniofacial growth. However, it remains unclear if whether altered growth predisposes to physical upper airway obstruction or vice-versa, because most clinical studies are static retrospective rather than long-term prospective [179].

Various animal models have been used to assess the short- and long-term consequences of SRBD, ranging from experimentally induced hypoxia through the use of hypoxia chambers, forced sleep deprivation, or naturally occurring obstruction models like that of the English bulldog [180]. Risk factors for SRBD, such as obesity, have also been examined [181–183]. Whole-body plethysmography was used to assess changes to respiration in rodent models [184]. However, none of those models was able to clearly delineate the causes and consequences of pediatric OSA. As a result, it remains uncertain whether craniofacial abnormalities such as midfacial hypoplasia precede nasal airway obstruction or whether airway obstruction predisposes or enhances craniofacial abnormalities.

Pierre Robin sequence (PRS) is frequently associated with craniofacial abnormalities such as micrognathia, midfacial hypoplasia, and airway obstruction [185]. Deletion of bone morphogenetic protein 7 (*Bmp7*) in mice recapitulates many of those craniofacial features [186]. However, complete loss of *Bmp7* results in cleft palate and perinatal lethality [187] precluding post-natal assessment of

craniofacial growth. Mice with neural crest-specific deletion of *Bmp7* ($Bmp7^{ncko}$) survive postnatally and present with micrognathia and midfacial hypoplasia [186].

Using micro-computed tomography (μCT) and morphometrics we describe here the sequence of when these midfacial abnormalities develop in $Bmp7^{ncko}$ mice. Unrestrained whole-body plethysmography was used to characterize respiratory function under normoxic, hypoxic and hyperoxic conditions. Oxygen consumption and respiratory gas exchange were monitored using a Comprehensive Lab Monitoring System (CLAMS). An unbiased metabolomics analysis on blood serum was conducted to identify changes to metabolites at the onset of upper airway obstruction. We demonstrate that a combination of craniofacial defects leads to nasal airway obstruction, and that craniofacial growth deficiencies precede nasal airway obstruction.

To our knowledge, this is the first genetic rodent model of midfacial hypoplasia in which airway obstruction has been assessed. It thus presents as an important model to the study etiology and systemic consequences of midfacial hypoplasia. Findings from this study will serve as a foundation to better understand the development and management of pediatric airway obstruction in humans.

4.3 Materials and Methods

4.3.1 Animals

All animal experiments were approved by the Research Ethics Office of the University of Alberta (Animal Use and Care Committee; protocol AUP1149), in compliance with guidelines by the Canadian Council of Animal Care. Mouse lines were kept on a C57Bl/6J background at the animal facility of the University of Alberta. $Bmp7^{fl/fl}$ ($Bmp7^{ctrl}$) mice [188] were crossed to Wnt1-Cre mice, Tg(Wnt1-Cre)11Rth, for neural crest–specific deletion of *Bmp7*($Bmp7^{fl/fl}$:Wnt1-Cre)

(Bmp7^{ncko}). Mice were genotyped using polymerase chain reaction (PCR) with DNA obtained from tissue biopsies [188].

4.3.2 Micro-Computed Tomography

For micro-computed tomography (μCT), Bmp7^{ctrl} and Bmp7^{ncko} mice were scanned using MILabs μCT at the School of Dentistry, University of Alberta. The mice were perfused with 4% PFA and mouse heads were subsequently fixed in 4% PFA for another 24 hrs prior to scanning. The following parameters were applied for scanning: voltage = 50kV, current = 0.24mA, and exposure time = 75ms. Scans were reconstructed at a voxel size of 25μm. The μCT- based skull reconstructions were used for anatomical comparison of the heads. Landmarks were placed on the skulls and defined angles/lengths were collected to quantify craniofacial differences (Fig. S3.1). Reconstructed scans were analyzed using AMIRA (Life Technologies) independently by one rater in triplicate, each time placing landmarks anew and collecting measurements.

4.3.3 Whole Body Plethysmography experimental design

Animals were placed individually in the whole-body plethysmography chamber that was initially flushed with room air (21% O_2) for an acclimation period of 30 to 40 min. $\dot{V}_E$ and $\dot{V}O_2$ were then recorded during baseline (normoxic conditions, 21% O_2 and N_2 balance) for 150 min to guarantee that mice would go through the sleep-awake cycle, followed by 20 min exposure to hypoxia (10% O_2 and N_2 balance), allowed to recover to normoxia values for 60 min and then exposed to hyperoxia (40% O_2) for 20 min. Gas mixtures were provided by a gas mixing system (GSM-3 Gas Mixer; CWE Inc., Ardmore, PA, USA). Respiratory and metabolic variables reported represent average values measured during 150 min of normoxia, between 0 to 5 min and 10 to 15 min of hypoxia, the last 10 min of the recovery period and between 10 to 15 min of hyperoxia.

Body temperature was measured before placing the mice into the chamber, 1 min after hypoxia exposure, at 45 min of the recovery period in normoxia, and at the end of hyperoxia.

4.3.4 Measurements of ventilation, O_2 consumption and body temperature

Ventilation was measured using the open flow whole-body plethysmography method [189]. The mice were placed in a 100 mL or 200mL volume chamber, depending on the mouse's body mass, through which gas flow was maintained at rates of 150mL/min and 300 mL/min, respectively [190]. In this system, the heating and humidification of the air that occurs with rhythmic inspiration and expiration of air causes pressure changes in the chamber that were detected with the differential pressure transducer (Validyne Engineering, Northridge, CA, USA). The pressure signal was acquired using PowerLab System (ADInstruments, Sydney, Australia) and sampled at 200 Hz. Data were analyzed using the data analysis software, LabChart (PowerLab System, ADInstruments/ LabChart Software, version 8, Sydney, Australia). The system was calibrated with injections of 0.25 mL into the plethysmography chamber at the same rate as breathing rate. Tidal volume (V_T) was calculated with the appropriate formula [191]: $V_T = V_K \times (P_T/P_K) \times T_C \times (P_B - P_C) / Tb \times (P_B - P_C) - T_A \times (P_B - P_R)$, where P_T is the pressure deflection associated with each V_T, P_K is the pressure deflection associated with the injection of the calibration volume (V_K), T_A is the air temperature in the animal chamber, P_B is the barometric pressure, P_C is the water vapor pressure in the animal chamber, Tb is the body temperature (in Kelvin), and P_R is the water vapor pressure at Tb. Ventilation ($\dot{V}_E$) was calculated as the product of respiratory frequency (fR) and tidal volume (V_T). P_C and P_R were calculated indirectly using appropriate tables [192]. All variables were normalized to body mass. Body temperature was measured using a rectal probe (Physiosuite, Kent Scientific, Torrington, CT, USA). Metabolic rate [O_2 consumption, $\dot{V}O_2$] was measured using pull mode indirect calorimetry [193,194]. An O_2 analyzer pump (ADInstruments, Sydney, Australia) was

connected to the outflow of the chamber, where sub sampled air was dried through a small drying column (Drierite, Sigma Aldrich, St. Louis, MO, USA) before passing to the analyzer. The gas was continuously sampled (1000 Hz) by the O_2 and CO_2 analyzers, and the fraction of O_2 and CO_2 in the inflow and outflow gas was recorded via PowerLab (System, ADInstruments / LabChart Software, version 8, Sydney, Australia). O_2 consumption ($\dot{V}O_2$) was calculated based on the following equation [190,195]: $\dot{V}O_2 = [FR_e (FiO_2 – FeO_2) – FiO_2 (FeCO_2 – FiCO_2)]/1 – FiO_2$ where FR_e is the excurrent flow rate, FiO_2 is the inflow O_2 fraction, and FeO_2 is the outflow O_2 fraction; $FiCO_2$ is the inflow CO_2 fraction; $FeCO_2$ is the outflow CO_2 fraction. $\dot{V}O_2$ was normalized to body mass (in kg) and the values were reported under STPD (standard conditions of temperature, pressure and dry air).

4.3.5 Spontaneous Apnea, Sigh and Post-sigh Apnea analysis

Spontaneous apneas were defined as at least two missing breath cycles which corresponds to pauses of 1 second or longer in the breathing recordings depending on the breathing frequency of each mouse. Sighs were defined as an increased breath at least twice a normal breath volume. Post-sigh apneas were defined as apneas that occurred within 20 seconds from the occurrence of a sigh [196]. Post-sigh apneas were further differentiated as 1) sighs followed by < 2 apneas, i.e., sigh not followed by apnea, or accompanied by one apnea; and 2) sighs followed by ≥ 2 apneas, separated at least by one breath.

4.3.6 Comprehensive Lab Monitoring System (CLAMS)

CLAMS (Oxymax/CLAMS; Columbus Instruments, Columbus, OH, USA) was used to measure delta oxygen (ΔO_2) and respiratory exchange ratio (RER= $\dot{V}CO_2$ / $\dot{V}O_2$) in vivo. A previously described protocol was used to conduct these experiments [197]. One-month old mice

(n=5/genotype) were monitored for 24 hrs to measure under both light (inactive) and dark (active) cycles for 12 hours each.

4.3.7 Metabolomics – combined direct flow injection and liquid chromatography with tandem mass spectrometry (LC-MS/MS) compound identification and quantification

A targeted quantitative metabolomics approach was used to analyze the blood serum samples of $Bmp7^{ctrl}$ and $Bmp7^{ncko}$ mice (n=5 mice/genotype) using a combination of direct injection mass spectrometry (AbsoluteIDQ™ kit) with a reverse-phase liquid chromatography with tandem mass spectrometry (LC-MS/MS) kit (BIOCRATES LifeSciences AG, Austria). This kit, in combination with an ABI 4000 Q-Trap (Applied Biosystems/MDS Sciex) mass spectrometer, combines the derivatization and extraction of analytes, and the selective mass-spectrometric detection using multiple reaction monitoring (MRM) pairs. Isotope-labeled internal standards and other internal standards are integrated in the kit plate filter for metabolite quantification. All the serum samples were analyzed with the AbsoluteIDQ kit using the protocol described in the AbsoluteIDQ user manual. Briefly, serum samples were thawed on ice and were vortexed and centrifuged at 13,000x g. Then 10 µL of each serum sample was loaded onto the center of the filter on the upper 96-well kit plate and dried in a stream of nitrogen. Subsequently, 20 µL of a 5% solution of phenyl-isothiocyanate was added for derivatization. After incubation, the filter spots were dried again using an evaporator. Extraction of the metabolites was then achieved by adding 300 µL methanol containing 5mM ammonium acetate. The extracts were obtained by centrifugation into the lower 96-deep well plate, followed by a dilution step with the kit mass spectrometry running solvent. Mass spectrometric analysis was performed on an API4000 Qtrap® tandem mass spectrometry instrument (Applied Biosystems/MDS Analytical Technologies, Foster City, CA, USA) equipped with a solvent delivery system. The samples were

delivered to the mass spectrometer by a liquid chromatography method followed by a direct injection (DI) method. The Biocrates MetIQ software was used to control the entire assay workflow, from sample registration to automated calculation of metabolite concentrations to the export of data into other data analysis programs. A targeted profiling scheme was used to quantitatively screen for known small molecule metabolites using multiple reaction monitoring, neutral loss and precursor ion scans. Significantly altered metabolites between $Bmp7^{ctrl}$ and $Bmp7^{ncko}$ mice were identified via a unpaired Student's t-test.

4.3.8 Treadmill Endurance Test

Mice were run on the Exer 3/6 treadmill with a variable speed controller (Columbus Instruments) [198]. For endurance, after initial training, mice were familiarized with a speed of 3 meters (m)/minute for 2 minutes(min), increasing every 2 minutes by 1 m/min. Distance recording started at a speed of 6 m/min for 6 minutes, followed by 8 m/min for 10 minutes, subsequent to which the speed was increased by 2 m/min every 3 minutes. The time is recorded when animals tired was recorded and the distance run is calculated. For speed testing, mice were familiarized at 7 m/min for 5 minutes, and then speed was set to 12m/min for up to 5 minutes. Mice were video recorded. For endurance testing, four mice/genotype were recorded. For speed testing, five mice/genotype were recorded.

4.3.9 Statistics

Results are expressed as means ± SD. For the morphometric μCT, CLAMS and metabolomics analyses, significant differences between $Bmp7^{ctrl}$ and $Bmp7^{ncko}$ mice were estimated by a two-tailed independent unpaired Student's t-test and differences were considered statistically significant when $p < 0.05$. Morphometric μCT measurements were conducted by one rater in triplicate. Intra-rater reliability was assessed wherever possible by intraclass correlation

(ICC) calculation based on six mice at the 1-month time point with ICC values greater than 0.9 being considered as excellent reliability (Table S4.4). For findings from whole body plethysmography, a statistical comparison of means was performed to compare respiratory (V_T, fR, $\dot{V}_E$, number of SAs and sighs, % PSA), metabolic ($\dot{V}O_2$, $\dot{V}_E/\dot{V}O_2$) and body temperature (Tb) variables between the experimental groups [$Bmp7^{ctrl}$, $Bmp7^{ncko\ (r)}$ and $Bmp7^{ncko\ (a)}$ mice] and gas exposure (21% O_2, 10% O_2 and 40% O_2). Two-way repeated measures ANOVA and Holm-Sidak post-test were used for each of these comparisons. Comparison of the normoxic breath cycle duration (T_{TOT}), inspiratory (T_i) and expiratory (T_e) times among the experimental groups [$Bmp7^{ctrl}$, $Bmp7^{ncko\ (r)}$ and $Bmp7^{ncko\ (a)}$ mice] was performed using One-way ANOVA. Values of $p < 0.05$ were considered significant. Values were expressed as mean±SD.

4.4 Results

4.4.1 Loss of Bmp7 leads to midfacial hypoplasia and early lethality.

$Bmp7^{ncko}$ mice appeared inconspicuous during the first two weeks of life. From around 2 weeks of age, a midfacial depression was be observed in the mutants to a varying degree (Figure 4.1A, B). Starting at about 3 weeks of age, a failure to thrive with variable onset was observed that ultimately led to death, with only 30% of mutant mice surviving past 8 weeks (Figure 4.1C). To determine whether the midfacial depression/hypoplasia is associated with the mortality, a morphometric assessment of the craniofacial complex was conducted on 2-week-old [postnatal day (P) 14], 3-week-old (P21) and 4-week-old (P30) mice using a landmark-based approach [199]. A detailed description of the landmarks used can be found in Fig. S4.1. The difference in facial length (Figure 4.1F) between $Bmp7^{ncko}$ and control mice only became significant at P21 (Figure 4.1D) (p=2.40E-04) as a consequence of reduced facial growth between the 2- and 3-week time-points. Although craniofacial growth catches up subsequently, the difference still persisted at P30

(p=2.10E-03). Other craniofacial characteristics such as snout angle (Figure 4.1E, F) frontal bossing (Figure 4.1G, I), nasal depression (Figure 4.1H, I), nasal width (Figure 4.1J, L) and length (Figure 4.1K, L) showed no significant differences in this limited cohort of mice. The p values for these measurements are provided in Table S4.1. This morphometric analysis establishes that deletion of *Bmp7* from neural crest cells leads to midfacial hypoplasia that becomes prominent around P21.

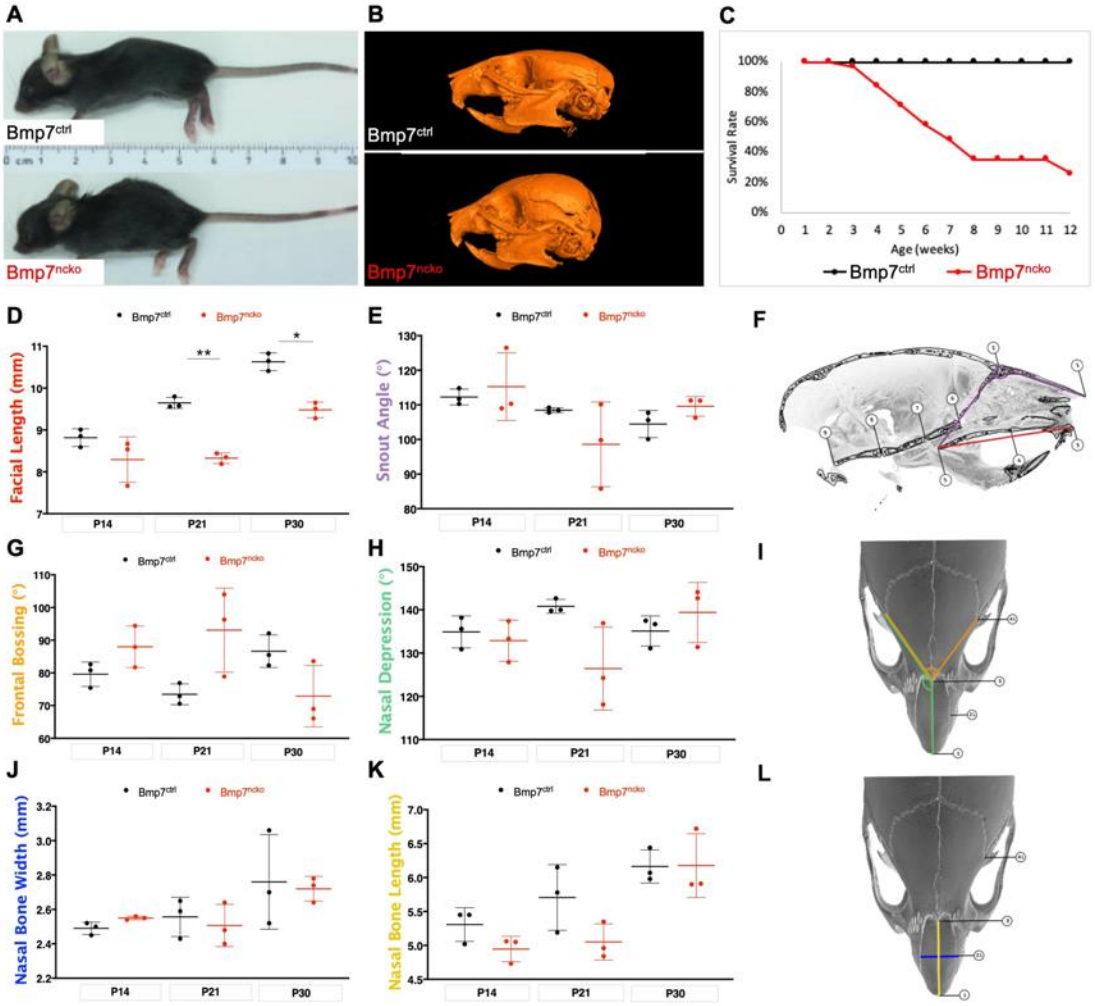

Figure 4. 1 Bmp7^{ncko} mice present with midfacial hypoplasia at 2 weeks which persists with age.

(A) Overview of Bmp7 control (Bmp7^{ctrl}) and Bmp7 mutant (Bmp7^{ncko}) mice. (B) Micro-computed tomography (μCT) reconstruction of 1-month old mouse skulls. Bmp7^{ncko} skull has a distinctive dished midface when compared with that of Bmp7^{ctrl}. (C) Survival rate plotted against nouse age indicating marked decrease in the survival of Bmp7^{ncko} mice beginning at 3 weeks with only 30% of Bmp7^{ncko} mice surviving past 8 weeks (n=30). (D) Cross-sectional longitudinal morphometric measurement of facial length of Bmp7^{ctrl} (black) and Bmp7^{ncko} (red) skull dimensions at 2 weeks of age (P14), 3 weeks (P21), and 1 month (P30) indicating a shorter facial length in the mutant mice. Landmarks used for this measurement are depicted in (F) in red. I Snout angle, depicted in panel (F) in purple. (F) Midsagittal representation of landmarks used for measurements taken in (D) and I. (G) Frontal bossing angle depicted in panel (I) in orange. (H) Average of left and right nasal depression angles, depicted unilaterally in panel (I) in green. (I) Superior view diagram of measurements taken in (G) and (H). (J) Nasal bone width depicted in panel (L) in blue. (K) Nasal bone length depicted in panel (L) in yellow. (L) Diagram of measurements taken in (J) and (K). Superior view of the skull. For all measurements, n=3/genotype/age. * Indicates $p<0.05$. Anatomical description of the landmarks is shown in Supplemental Figure 4.1.

4.4.2 Bmp7^{ncko} develop craniofacial abnormalities commonly observed in children with midfacial hypoplasia

We next performed a detailed morphometric analysis on a larger cohort of 4-week-old control (Bmp7^{ctrl}) and Bmp7^{ncko} mice to test for additional craniofacial alterations commonly observed in children with midfacial hypoplasia and upper airway obstruction [179]. Landmark-based morphometrics (for details see Fig. S4.1) identified a more acutely angled cranial base (p=1.7E-02; Figure 4.2A,B) with a significantly shorter basisphenoid (BS) (p=3.58E-06; Figure 4.2C,D). No significant changes were observed in the length of the basioccipital, presphenoid and ethmoid bones (Table S4.2). Assessment at earlier time-points (P14, P21) showed no significant changes (Table S4.3). Significant length reductions were found both for the posterior (p=2.44E-05) and anterior frontal complex (p=1.18E-06; Figure 4.2E-F). Changes to snout angle (Figure 4.2G-H), frontal bossing angle (Figure 4.2G-H), nasal depression angle (Figure 4.2G-H) along with nasal width (Figure 4.2I-J) and length (Figure 4.2I-J) are a reflection of the significantly more acute angled snout (p=1.43E-05), depressed nasal bones (p=3.21E-07), and increased frontal bossing (p=4.84E-06) in 1-month old Bmp7^{ncko} mice. Additionally, the length (p=3.80E-03), but not the width, of the nasal bones was significantly reduced. Overall, these findings are consistent with features of midfacial hypoplasia and reduced upper airway space.

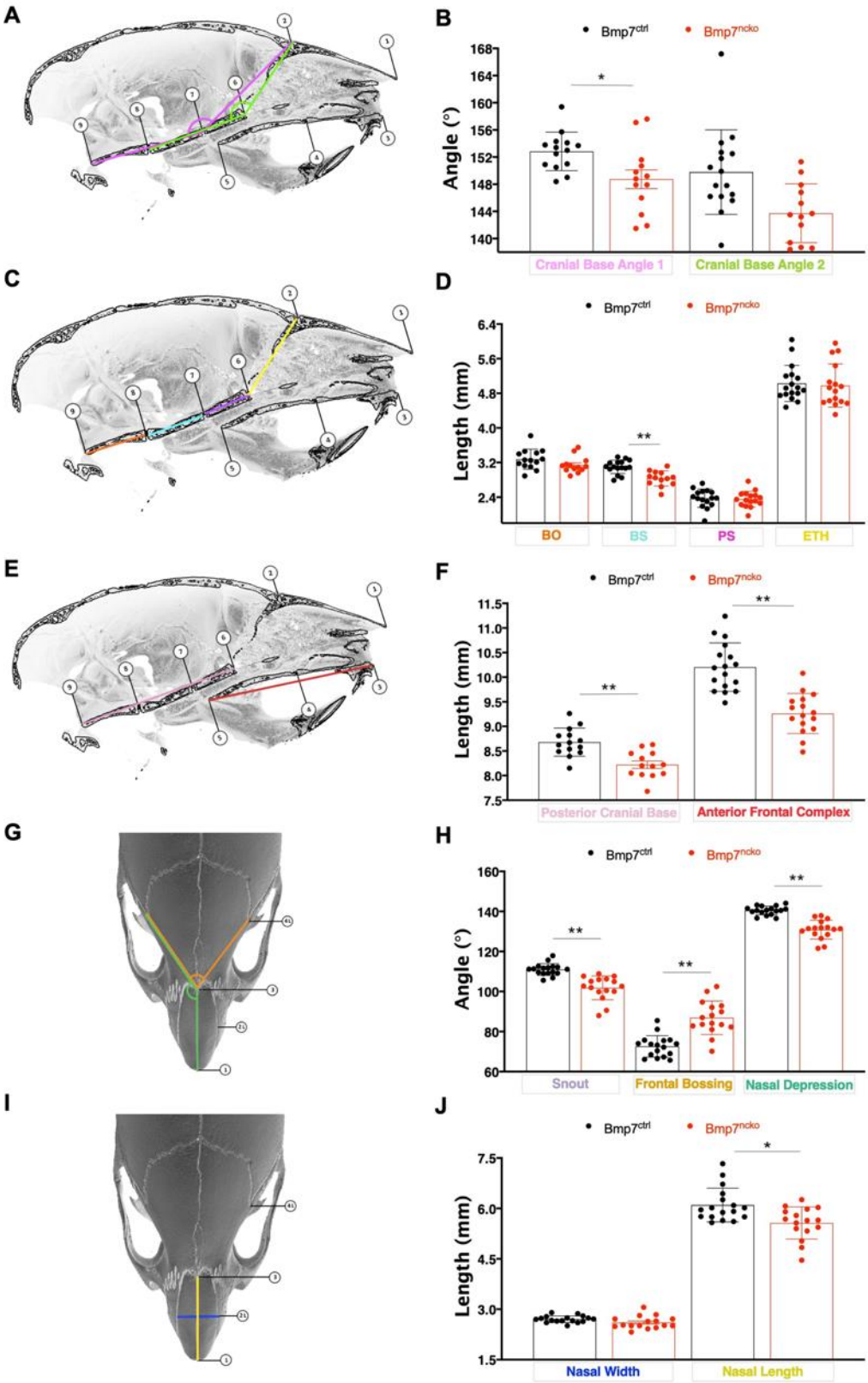
A
B
Bmp7ctrl
Bmp7ncko
Angle (°)
168
164
160
156
152
148
144
140
*
Cranial Base Angle 1
Cranial Base Angle 2
C
D
Bmp7ctrl
Bmp7ncko
Length (mm)
6.4
5.6
4.8
4.0
3.2
2.4
**
BO
BS
PS
ETH
E
F
Bmp7ctrl
Bmp7ncko
Length (mm)
11.5
11.0
10.5
10.0
9.5
9.0
8.5
8.0
7.5
**
**
Posterior Cranial Base
Anterior Frontal Complex
G
H
Bmp7ctrl
Bmp7ncko
Angle (°)
160
140
120
100
80
60
**
**
**
Snout
Frontal Bossing
Nasal Depression
I
J
Bmp7ctrl
Bmp7ncko
Length (mm)
7.5
6.0
4.5
3.0
1.5
*
Nasal Width
Nasal Length

Figure 4. 2 Craniofacial growth defects contributing to midfacial hypoplasia in 1-month $Bmp7^{ncko}$ mice.

The angle (A-B) and lengths (C-D) of the individual components forming the cranial base were measured using landmarks placed on mid-sagittal cross-sections of the mouse skulls. (A) Angles of cranial base 1 (pink) (n=27) and cranial base 2 (green) (n=29) demonstrated an acute angled cranial base in $Bmp7^{ncko}$ mice with p values of 0.05, 0.23, respectively (B). (C) Landmarks used to measure lengths of the BO, BS, PS, ETH depicted in orange, cyan, violet, and yellow, respectively. Measurements indicated a reduction in length of BS in the $Bmp7^{ncko}$ mice (D) (bo: n=27, p=0.11. bs: n=29, $p<0.001$. ps: n=32, p=0.76. eth: n=33, p=0.76). (E) Landmarks of the posterior cranial base and anterior frontal complex, depicted in pink and red, respectively. (F) Measurements demonstrate a significant decrease in both posterior cranial base (n=27, $p<0.001$) and anterior frontal complex (n=33, $p<0.001$). Angles of snout (E), frontal bossing (G, compare to Figure 4.1I), and nasal depression (G), depicted in purple, orange, and green respectively. $Bmp7^{ncko}$ mice demonstrate more acute snout angle, increased frontal bossing and more acute angle of nasal depression (n=33, $p<0.001$) (H). Lengths of nasal bone width and length, depicted in panel (I) in blue and yellow, respectively (compare to Figure 4.1L). Measurements of nasal width and length (J) suggest that the mutant mice have a decreased nasal bone length (n=33, $p<0.05$) with no changes to nasal width (n=33, p=0.07). BO: basioccipital length; BS: basisphenoid length; PS: presphenoid length; ETH: ethmoid length. * indicates $p<0.05$, ** indicates $p<0.001$. Anatomical description of the landmarks is shown in Supplemental Figure 4.1.

In addition to changes to cranial base length and angle, two other craniofacial differences are commonly observed in children with midfacial hypoplasia and upper airway obstruction: nasal septum deviation and turbinate hypertrophy [200]. To characterize potential changes to nasal septum and turbinates, frontal (blue lines, Figure 4.3) and axial (orange dotted lines, Figure 4.3) planes were identified from μCT scans of P14 and P30 mice skulls. The nasal septum (pink arrows, Figure 4.3) in P14 $Bmp7^{ctrl}$ (Figure 4.3A-C) and $Bmp7^{ncko}$ mice (Figure 4.3D-F) showed no obvious differences on both frontal and axial planes. However, $Bmp7^{ncko}$ mice showed reduced turbinate branching (yellow arrows) and their turbinates appeared larger (Figure 4.3F). At P30, all $Bmp7^{ncko}$ mice had developed nasal septum deviation (pink arrows) (Figure 4.3J-O) when compared to controls (Figure 4.3G-I). The extent, shape, direction and location, as well as the degree of deviation was variable (Figure 4.3K, N). Turbinate development appeared disturbed. Reduced branching and ossification as well as slight swelling of turbinate soft tissue were apparent bilaterally at P14. This swelling and reduced turbinate branching was even more noticeable at P30 (Figure 4.3I, L, O). Both nasal septum deviation and turbinate swelling can impede airflow in the nasal cavity, thus potentially exacerbating any other physical airway obstruction.

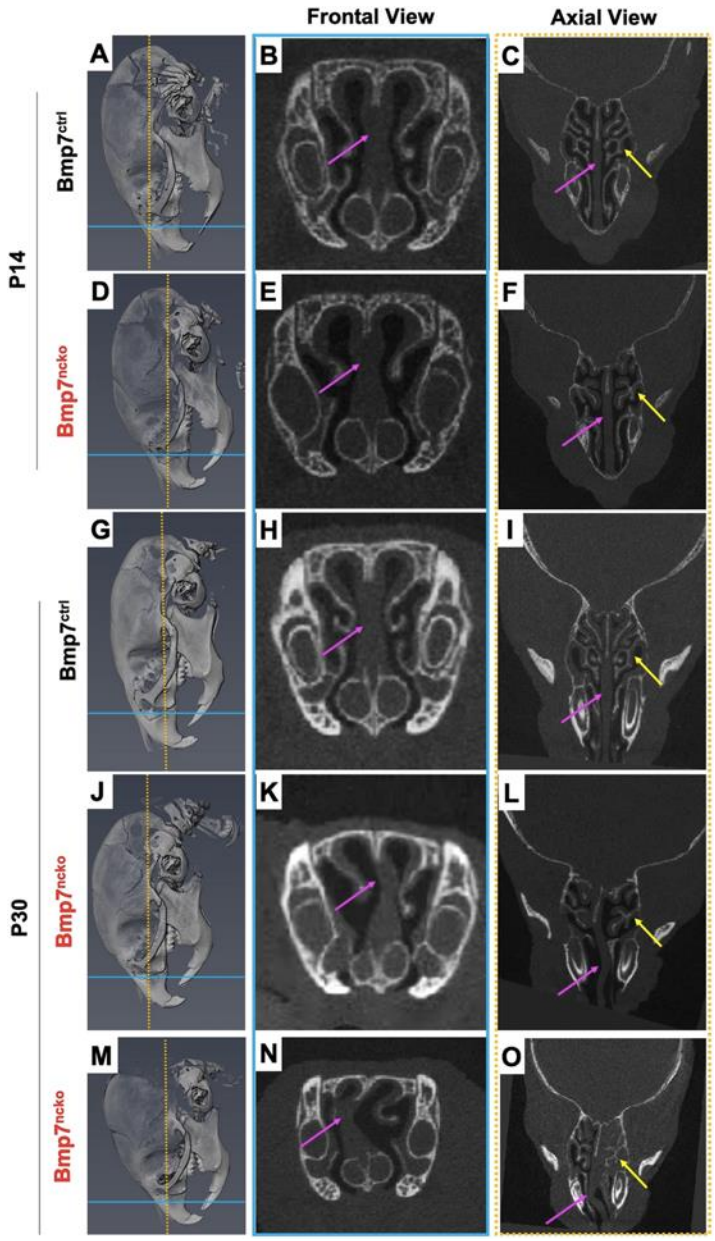

Figure 4. 3 Bmp7^{ncko} mice present with nasal septum deviation and turbinate dysfunction. (A-O)

Micro-computed tomography (μCT) representation of frontal (blue line) and axial (orange dotted line) planes used to characterize nasal septum and turbinate abnormality in 2-week-old (P14) (A,D) and 1-month old mice (P30) (G, J, M). At P14, mice present no structural differences in the nasal septum (pink arrows) between the control (B-C) and mutant (E-F) mice under both views. However, abnormal turbinate branching and swelling of mucosa surrounding the turbinates (yellow arrows) was already observed in the mutant mice at 2 weeks (F). At P30, all mutant mice present with nasal septum deviation in both frontal (K-L) and axial (N-O) views in comparison to the control mice (H-I). However, the degree of nasal septum deviation varies between each mutant (K versus. N). Similarly, turbinate branching dysfunction and swelling of the mucosa persists in the mutant mice (L-O) at P30 as well. Frontal views of the nasal cavity are outlined in blue lines and axial views in orange dotted lines. n=3/age/genotype.

4.4.3 Evidence of spontaneous apneas (SA) and post sigh apneas (PSA) in Bmp7^{ncko} mice

Whole-body plethysmography was used to assess breathing patterns in Bmp7^{ncko} mice. Eight control and ten Bmp7^{ncko} mice were measured at a time when the mutant mice had developed nasal septum deviation (4-6 weeks of age). Of the ten Bmp7^{ncko} mice analyzed in this study, five elicited a greater number of spontaneous apneas (SA) in normoxia compared to Bmp7^{ctrl} mice ($p = 4.00E-03$) and the remaining Bmp7$^{ncko\,(r)}$ mice ($p = 2.00E-02$; Figure 4.4A,B). Consequently, we divided the mutant mice cohort into two groups for all respiratory analysis: Bmp7$^{ncko\,(r)}$ (regular breathing) and Bmp7$^{ncko\,(a)}$ (high frequency SA).

Movie S1 shows recordings of plethysmography traces associated with the behaviour of a Bmp7^{ctrl} mouse during eupneic breathing, and a Bmp7$^{ncko\,(a)}$ mouse experiencing SA. The presence of greater number of SAs in the Bm p7$^{ncko\,(a)}$ mice in comparison to Bmp7^{ctrl} mice persisted during hypoxia ($p = 0.01$) as well as during the first minute of recovery to normoxia ($p = 5.00E-03$; Bmp7^{ctrl}: 0.3±0.5; Bmp7$^{ncko\,(r)}$: 3.0±4.7; Bmp7$^{ncko\,(a)}$: 8.2±5.5). The presence of greater number of SAs in the Bmp7$^{ncko\,(a)}$ group in comparison to the Bmp7^{ctrl} and Bmp7$^{ncko\,(r)}$ disappeared during hyperoxia (40% O_2) ($p = 0.21$ and $p = 0.54$, respectively; Figure 4.4B). However, there was one animal that appeared to be an outlier, so it was excluded from the statistical analysis for all the gas exposures. These results indicate that during normoxic and hypoxic conditions, apneas are more frequent in a subpopulation of Bmp7^{ncko} mice and this difference was eliminated in hyperoxia.

Sigh frequency was comparable between all experimental groups. As expected [201], hypoxia exposure induced an increased number of sighs in all groups ($p < 0.001$) compared to normoxia (Figure 4.4C). Under physiological conditions sighs may be followed by brief apneas (post-sigh apneas - PSA) or respiratory irregularities [202]. Short respiratory disruptions following a sigh (≤ 1 apnea) was reduced in the Bmp7$^{ncko\,(a)}$ group compared to the Bmp7^{ctrl} and Bmp7$^{ncko\,(r)}$ groups (p

< 0.01; Figure 4.4D), whereas prolonged PSA events (≥2 apneas following a sigh, as shown in Fig4.4A) increased ($p < 0.001$; Figure 4.4E).

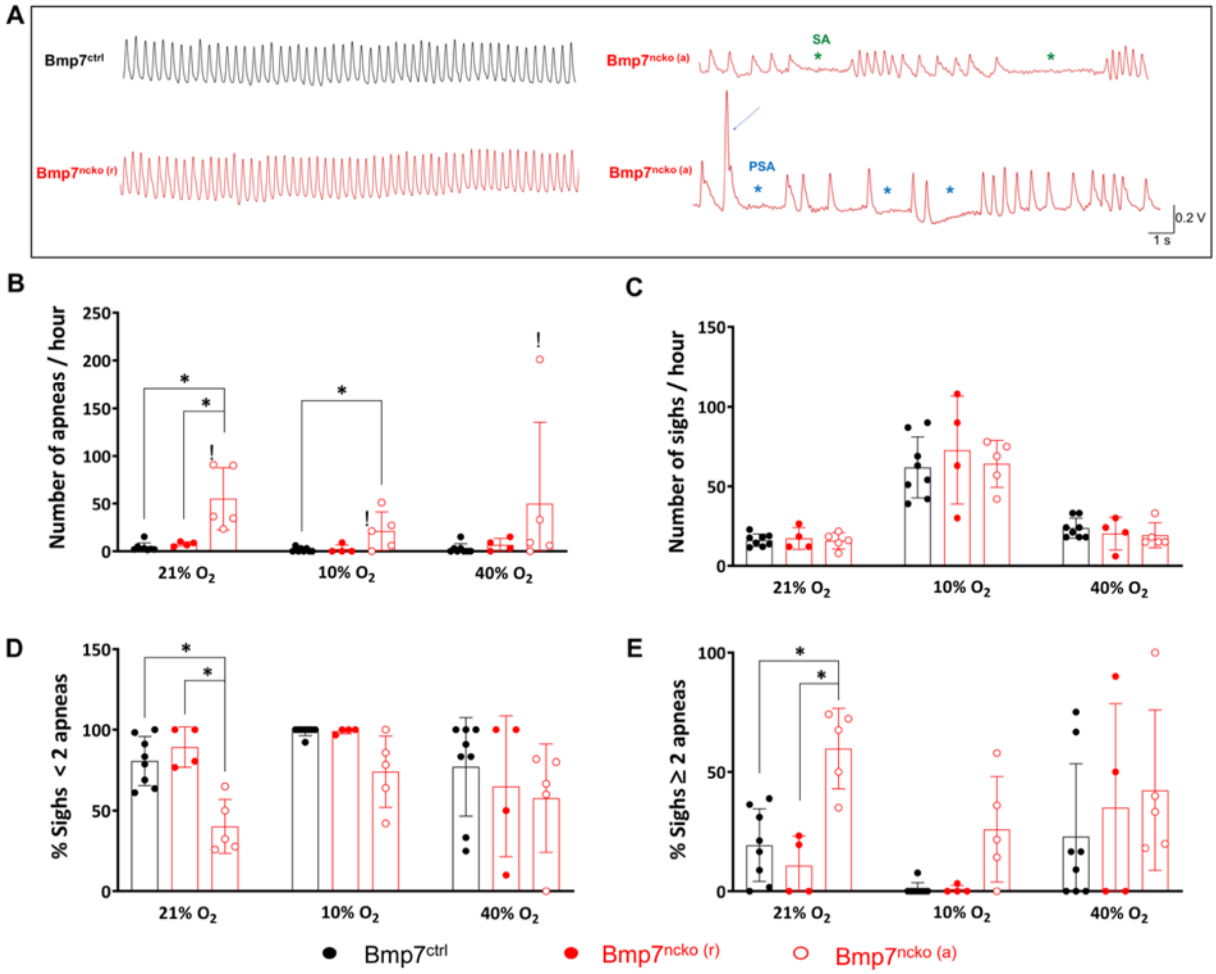

Figure 4. 4 Spontaneous apnea, sigh and post-sigh apnea during normoxia, hypoxia and hyperoxia in Bmp7^{ctrl}, Bmp7$^{ncko\ (r)}$ and Bmp7$^{ncko\ (a)}$ mice.

(A) Representative traces showing normal breathing pattern in Bmp7^{ctrl} (black trace) and Bmp7$^{ncko\ (r)}$ mice (bottom-left red trace); breathing pattern with spontaneous apneas (SA) (green asterisks) in Bmp7$^{ncko\ (a)}$ mice, and sigh (blue arrow) followed by three apneas (PSA; blue asterisks) in Bmp7$^{ncko\ (a)}$ mice. Number of apneas/hour (B) and number of sighs/hour (C) in the three experimental groups during normoxia (21% O_2), hypoxia (10% O_2) and hyperoxia (40% O_2). Percentage (%) of sighs with < 2 apneas (D) and % of sighs with ≥ 2 apneas (E) in the three experimental groups during normoxia (21% O_2), hypoxia (10% O_2) and hyperoxia (40% O_2). *Means statistical difference between groups (*$p < 0.05$). The exclamation mark indicates an outlier. Bmp7$^{ncko\ (r)}$, mutant mice with no changes to regular breathing. Bmp7$^{ncko\ (a)}$ is used to denote Bmp7^{ncko} mice with SA.

4.3.4 $Bmp7^{ncko}$ mice with apneas show altered baseline respiratory, metabolic, and thermoregulatory patterns

Along with a greater number of SAs and longer PSA events, $Bmp7^{ncko\,(a)}$ mice had a lower baseline respiratory frequency (fR) ($p = 1.60E-02$; Figure 4.5A) and an increase in cycle duration of each respiratory event (T_{TOT}) ($p = 4.10E-02$) owing to an increase in the inspiratory time (T_i; $p = 1.90E-02$) with a trend to increase the expiratory time (T_e; $p = 7.90E-02$; Figure 4.5B). Noteworthy, the two $Bmp7^{ncko\,(a)}$ mice with greater SA number showed greater T_{TOT}, T_i and T_e compared to the other mice from the same group. $Bmp7^{ncko\,(r)}$ mice showed a trend towards reduced values for fR compared to control mice, however, the differences were not significant. Despite fR changes, baseline tidal volume (V_T) and minute ventilation ($\dot{V}_E$), a measure of total volume of gas inhaled per minute, did not differ between the groups (Figure 4.5C, D, respectively). Despite the greater number of SAs in the $Bmp7^{ncko\,(a)}$ mice, we did not find changes in variability of respiratory parameters among the groups (Table S4.5) or normoxic O_2 consumption ($\dot{V}O_2$) and air convection requirements ($\dot{V}_E/\dot{V}O_2$) (Figure 4.5E and F), among the groups. Overall baseline body temperature (Tb) was lower in the $Bmp7^{ncko\,(r)}$ mice compared to that in the control group ($p = 1.20E-02$; Figure 4.5G), mainly due to a greater Tb individual variability within the $Bmp7^{ncko\,(r)}$ mice.

To establish the timeline of when $Bmp7^{ncko}$ mice develop respiratory disturbances, a separate plethysmography assessment was conducted at 2 weeks of age, prior to the development of nasal abnormalities. At this time, the number of SAs and PSAs were comparable between the $Bmp7^{ncko}$ and $Bmp7^{ctrl}$ mice (Fig. S4.2). However, the $Bmp7^{ncko}$ mice demonstrated a trend towards lower baseline respiratory frequency (fR) and an increase in duration of each respiratory event (T_{TOT}) as a result of an increase in inspiratory (T_i) and expiratory times (T_e). These results

suggest that the majority of respiratory disturbances develop following the development of craniofacial abnormalities.

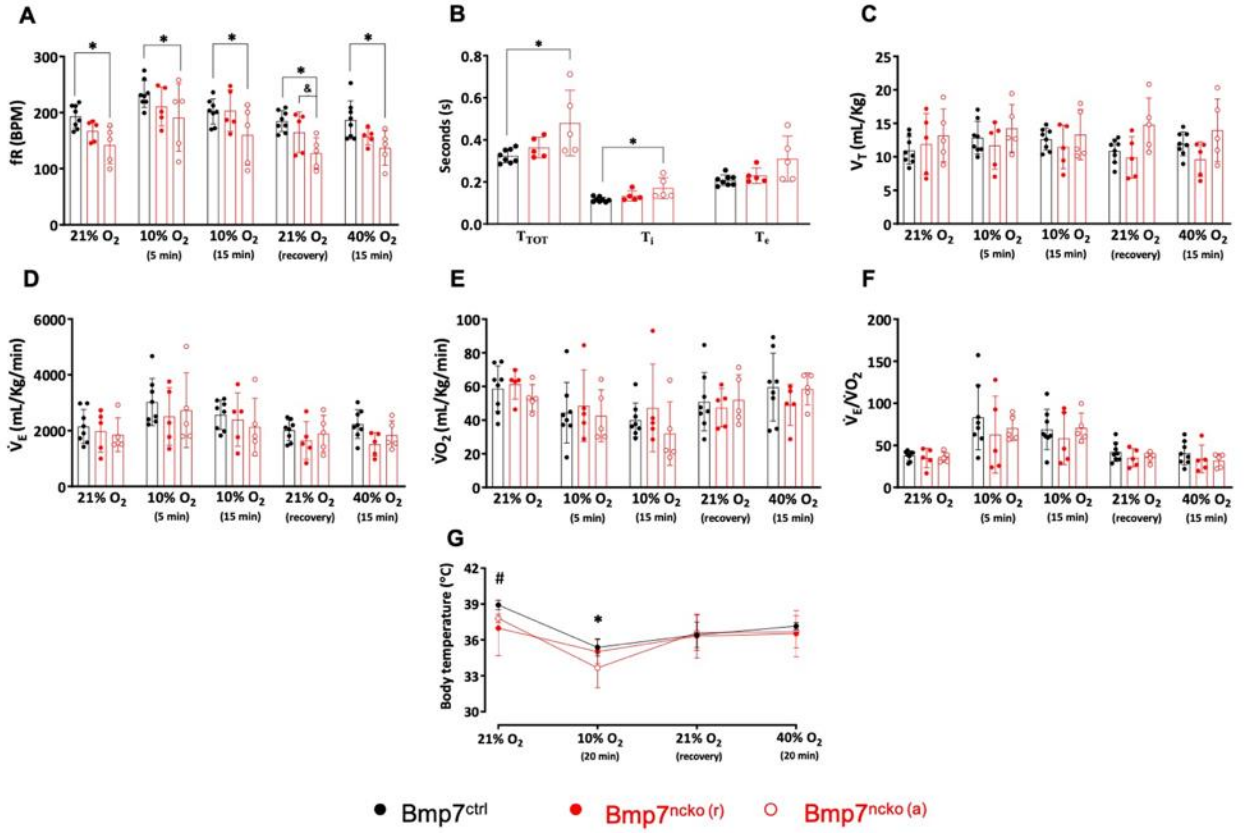

Figure 4. 5 Respiratory and metabolic patterns during normoxia, hypoxia and hyperoxia in Bmp7^{ctrl}, Bmp7$^{ncko\ (r)}$ and Bmp7$^{ncko\ (a)}$ mice.

(A) Respiratory frequency (fR) in the three experimental groups during normoxia (21% O_2), 5 and 15 min of hypoxia (10% O_2), recovery to baseline conditions (21% O_2) and 15 min of hyperoxia (40% O_2). (B) Breath cycle duration (T_{TOT}), Inspiratory time (T_i) and Expiratory time (T_e) during normoxia in the three experimental groups. (C-F) Tidal volume (V_T), Minute Ventilation ($\dot{V}_E$), O_2 consumption ($\dot{V}O_2$), Air convection requirements ($\dot{V}_E$ /$\dot{V}O_2$) in the three experimental groups during normoxia (21% O_2), 5 and 15 min of hypoxia (10% O_2), recovery to baseline conditions (21% O_2) and 15 min of hyperoxia (40% O_2). (G) Body temperature (Tb) in the three experimental groups during normoxia (21% O_2), 20 min of hypoxia (10% O_2), recovery to baseline conditions (21% O_2) and 20 min of hyperoxia (40% O2). *Indicates statistical difference between groups (*$p < 0.05$). In the Tb graph, *Indicates statistical difference between Bmp7^{ctrl} and Bmp7$^{ncko\ (a)}$ mice; #Indicates statistical difference between Bmp7^{ctrl} and Bmp7$^{ncko\ (r)}$ mice. & Indicates statistical difference between Bmp7$^{ncko\ (a)}$ and Bmp7$^{ncko\ (r)}$ mice. Bmp7$^{ncko\ (r)}$ is used for mutant mice with no changes to regular breathing. Bmp7$^{ncko\ (a)}$ is used to denote Bmp7^{ncko} mice with apneas. Eight control mice and 10 Bmp7^{ncko} mice were used in the study.

4.4.4 Ventilatory and metabolic responses to hypoxia (10% O_2) and hyperoxia (40% O_2)

The same mice used for breathing analysis in normoxia were exposed to acute hypoxia (10% O_2) and hyperoxia (40% O_2) to evaluate their respiratory responses to different levels of oxygen. In the control group, we observed the biphasic ventilatory response, in which hypoxia induced hyperventilation as shown by an increase in $\dot{V}_E$ and $\dot{V}_E/\dot{V}O_2$ in the first 5 min of exposure ($p<0.001$; Figure 4.5D and 4.5F, respectively), followed by an attenuation at 15 min, with no significant difference from baseline values. Significant increase in fR was observed both at 5 min ($p < 0.001$) and at 15 min ($p < 0.001$; Figure 4.5A; Fig. S4.2). Hypoxia also caused a decrease in $\dot{V}O_2$ ($p<0.05$; Figure 4.5E) and body temperature ($p<0.001$; Figure 4.5G). A comparable physiological response to hypoxia was observed in both the $Bmp7^{ncko\ (a)}$ and $Bmp7^{ncko\ (r)}$ groups ($p<0.05$). Even though $Bmp7^{ncko(a)}$ had a lower breathing frequency in normoxic conditions, the hypoxic frequency response shown as a percentage of baseline was similar among the three groups (Fig. S4.3). However, mice from the $Bmp7^{ncko(r)}$ group showed a variable hypoxic ventilatory response. Two mice showed hyperventilation as seen by larger values in the $\dot{V}_E/\dot{V}O_2$ data (Figure 4.5F), whereas the other 3 mice showed no change in $\dot{V}_E/\dot{V}O_2$ compared to the values in normoxia. It is noteworthy that the one $Bmp7^{ncko}$ mouse in which $\dot{V}O_2$ did not drop during hypoxia showed a baseline body temperature of 33°C, which is below the normal range, and no further decrease during hypoxia was observed. Therefore, it is legitimate to deduct that thermoregulation in this specific mouse seemed compromised, potentially further affecting ventilation and O_2 consumption modulation. Interestingly, all $Bmp7^{ncko\ (r)}$ mice showed an increased fR induced by hypoxia at 5 min that persisted throughout the hypoxic exposure ($p<0.01$) (Figure 4.5A), although no changes were observed for the other physiological variables ($\dot{V}_E$, V_T, $\dot{V}O_2$ and $\dot{V}_E/\dot{V}O_2$).

Hyperoxia did not evoke any changes in the respiratory, metabolic or thermoregulatory variables within and between experimental groups, with the exception of a lower fR in $Bmp7^{ncko}$ [(a)] mice during 40% O_2 (p=5.00E-03), owing to the lower baseline fR.

4.4.5 Reduced delta oxygen and upregulation of hydroxyproline observed in $Bmp7^{ncko}$ mice.

Four-week-old $Bmp7^{ctrl}$ and $Bmp7^{ncko}$ (n=5/genotype) mice were placed individually in CLAMS chambers for 24 hours to measure oxygen consumption and respiratory exchange. Delta oxygen, the difference in oxygen fraction in the inflow and outflow of the chamber, indicating oxygen consumption, was reduced in $Bmp7^{ncko}$ mice, as shown by representative traces of one control and two $Bmp7^{ncko}$ mice (Figure 4.6A). The trace of the respiratory exchange ratio (RER), which is the rate of carbon dioxide production to the rate of oxygen consumption, showed no clear differences (Figure 4.6B). Quantification of ΔO_2 (Figure 4.6C) and RER (Figure 4.6D) demonstrated a significant reduction in ΔO_2 ($p<0.05$) and no change in RER in the $Bmp7^{ncko}$ mice. To understand systemic consequences, blood serum from P30 $Bmp7^{ctrl}$ and $Bmp7^{ncko}$ mice (n=5/genotype) was collected and screened for changes to metabolite concentrations using an unbiased metabolomics assay. In each sample, 154 metabolites were detected and quantified in each sample. A significant upregulation of hydroxyproline ($p<0.05$), an indicator of collagen synthesis or release, was identified in $Bmp7^{ncko}$ mice (Figure 4.6E). This demonstrated that $Bmp7^{ncko}$ mice consume less oxygen over time and that it is possible to identify metabolite differences between control and mutant mice.

4.4.6 $Bmp7^{ncko}$ mice show decreased exercise capacity at P30

To test whether $Bmp7^{ncko}$ mice develop reduced endurance for physical activity, mice were assessed on a treadmill longitudinally starting at the age of 3 weeks. Physical activity in the mice at 3 weeks was comparable between the groups with an increasing reduction in activity after every

subsequent assessment (Figure 4.6F). The difference in physical ability was confirmed in an acute speed test in which Bmp7 mutant mice tired very quickly and spent more time on the resting plate, indicating that they do not have the same capacity for physical exercise (Movie S2). Thus, craniofacial defects and associated breathing disturbances might lead to a reduced ability for physical activity possibly due to airway obstruction in this rodent model.

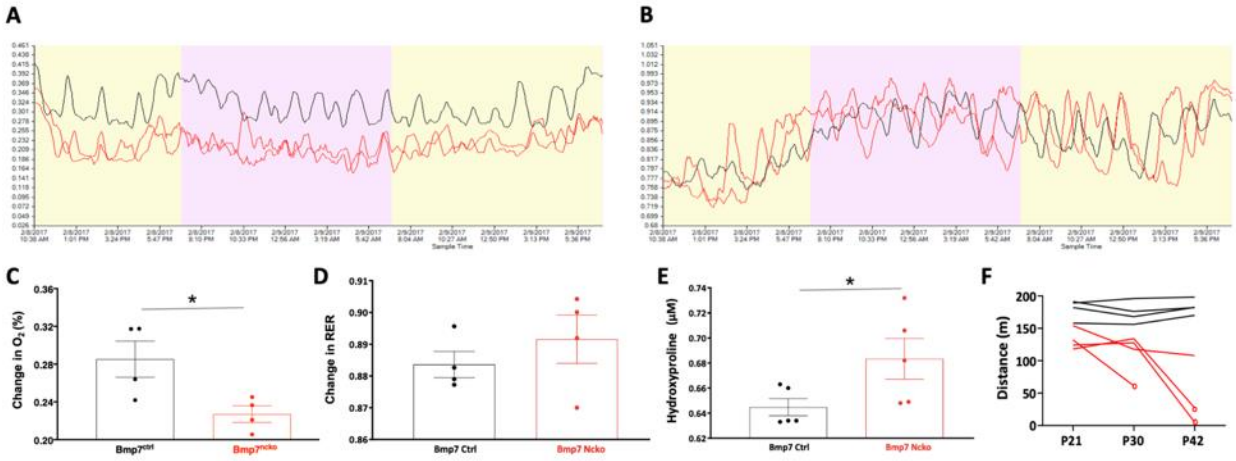

Figure 4. 6 Oxygen consumption is reduced in the Bmp7^{ncko} mice.

One-month old Bmp7^{ctrl} and Bmp7^{ncko} mice were measured in the Comprehensive Lab Monitoring System (CLAMS) chamber for oxygen consumption and respiratory exchange. (A) Representative trace of delta oxygen consumption plotted against time for one control (black) and two Bmp7^{ncko} mice (red) demonstrated a reduction in oxygen consumption (C) (n=4, $p<0.05$). (B) Representative trace of respiratory exchange ratio (RER) plotted against time for one control (black) and two Bmp7^{ncko} mice (red) demonstrated no significant changes (D) (n=4, p=0.39). (E) Metabolite analysis of blood serum collected from Bmp7^{ctrl} and Bmp7^{ncko} mice demonstrated a significant upregulation in Hydroxyproline concentration in the mutant mice (n=5, $p<0.05$) (F) Exhaustion treadmill test on Bmp7^{ctrl} and Bmp7^{ncko} mice revealed a reduction in physical activity in the mutant mice (red) as mice age. P21: post-natal day 21; P30: post-natal day 30; P42: post-natal day 42. Circle denotes mutant mice that became severely fatigued and had to be euthanized. * indicates $p<0.05$.

4.5 Discussion

In this study, Bmp7^{ncko} mice demonstrated structural and growth abnormalities in the craniofacial complex, alteration in breathing pattern, i.e., apnea events and lower breathing frequency, and reduction in the capacity for physical exercise. Thus, the Bmp7^{ncko} mouse model emulates several features often linked to the onset of airway obstruction in pediatric OSA [179], including midfacial hypoplasia, shorter cranial base, and nasal septum deviation. By delineating the sequence of craniofacial changes, we show that they tend to precede the onset of respiratory disturbances. We also show how this model might be used to identify systemic manifestations caused by upper airway obstruction.

Despite the abundance of genetic rodent models of midfacial abnormalities, to our knowledge no rodent model of nasal airway obstruction, SRBD and midfacial deficiency has been described. Such a model could greatly benefit the field of pediatric sleep medicine. Most rodent models of SRBD and/or airway obstruction address only isolated facets of this complex disorder (Table 4.1). Animals exhibiting intermittent hypoxia (IH) have most commonly been used to study the effects of obstruction [203,204]. However, there is controversy in whether the settings used to mimic IH in rodent experiments are clinically translatable to IH experienced in humans [205]. Mechanical obstruction of the airways or oxygen deprivation have also been used [206,207]. The SRBD/OSA rodent models with 'naturally occurring' airway obstruction, such as the Zucker hooded rat [208], exhibit loss of airway patency owing to excessive soft tissue or obesity. Understanding how abnormalities of the craniofacial complex lead to airway obstruction and SRBD has been hampered by the fact that models with severe congenital craniofacial anomalies, which often involves a cleft palate, die at birth, preventing postnatal analysis [209,210]. On the other hand, models that show snout asymmetries, as for instance often observed in *Bmp7*

haploinsufficient mice, have not been assessed for breathing abnormalities or show early lethality as a consequence, thus making the $Bmp7^{ncko}$ model unique. It is the first model to describe how craniofacial abnormalities such as midfacial hypoplasia, short and acute-angled cranial base, and nasal septum deviation predispose mice to nasal airway obstruction postnatally. A shorter cranial base is often associated with premature fusion of cranial base synchondrosis [211]. Careful examination revealed that this was not the case in $Bmp7^{ncko}$ mice. It is therefore possible that the shorter cranial base is a consequence of reduced growth itself. $Bmp7^{ncko}$ mice develop midfacial hypoplasia during the time of rapid midfacial growth (2-3 weeks of age). Midfacial hypoplasia on its own appears to be insufficient to induce upper airway obstruction. Hypoplasia and associated shorter and more acute angled cranial base and reduced nasal bone length (Figure 4.1 and 4.2) are all established prior to nasal airway obstruction. Only once nasal septum deviation and turbinate swelling are observed around 4 weeks, the animals start developing respiratory disturbances. The hypopneas (lower fR), an increase in T_{TOT} and T_i, and increased number of SA and PSA irregularities in a subpopulation of the $Bmp7^{ncko}$ mice are features likely to be associated with nasal airway obstruction owing to the combination of craniofacial abnormalities. Little was known about the sequence, etiology, and consequences of these different craniofacial anomalies. Craniofacial characteristics have been described in detail for several mouse strains with midfacial hypoplasia [36,212,213], see also Table 4.1. None of these models show nasal septum deviation and or nasal airway obstruction, supporting the notion that midfacial hypoplasia on its own does not necessarily lead to nasal airway obstruction [177,214]. The survival plot (Fig. 4.1C) indicates that the majority of $Bmp7^{ncko}$ mice die by the age of 8-12 weeks, which coincides with the plateauing of craniofacial growth [140]. Although challenging to assess in detail, we believe that cumulative

craniofacial changes either fatally affect mice by that age, or will never be sufficiently severe allowing mice to survive long-term.

Table 4. 1 Examples of rodent models of airway obstruction and midfacial abnormalities.

Model name	Midfacial abnormality	Hypoxia	Airway obstruction	Respiratory disturbances	References
Mechanical obstruction models					
Tracheal narrowing			×		(Tarasiuk and Segev, 2018)
Tracheal balloon		×	×	×	(Schoorlemmer et al., 2011)
Tracheostomy		×	×	×	(Farré et al., 2018)
Tracheal cannula			×		(Tarasiuk et al., 1991)
Environmental models					
Nasal mask		×	×	×	(Almendros et al., 2011)
Intermittent hypoxia box		×			(Fletcher et al., 1992; Gozal et al., 2001)
Head/body chamber setup		×	×		(Farré et al., 2003)
Long-term intermittent hypoxia		×		×	(Veasey, 2009)
Craniofacial genetic models					
Crouzon syndrome mouse	×				(Perlyn et al., 2006)
Fetal alcohol syndrome mouse	×				(Hong and Krauss, 2012)
Osterix-*Cre* transgenic mouse	×				(Huang and Olsen, 2015)
Achondroplasia mouse model	×				(Wang et al., 1999)
$Bmp7^{ncko}$ mouse model	×	(×)	×	×	
Sleep-disordered breathing genetic models					
Diet-induced obese (DIO) mouse			×	×	(Berger et al., 2019)
Zucker hooded rat			×		(Iida et al., 1996)
Koletsky rat			×		(Ishizuka et al., 1998; Takaya et al., 1996)
New Zealand obese mouse			×		(Brennick et al., 2009; O'Donnell et al., 2000)
Orexin knockout mouse				×	(Chemelli et al., 1999; Diniz Behn et al., 2010)

'(x)' denotes transient hypoxia.

Similarly, when comparing pediatric OSA cohorts of different ethnicities, differences in the prevalence of craniofacial abnormalities were noted [177,215]. Those ethnicities have distinct craniofacial features with different degrees of sagittal, vertical and transversal maxilla-mandibular interrelations. It was also observed that nasal septum deviation, turbinate hypertrophy and enlarged adenoids greatly increase the prevalence of upper airway obstruction in children with midfacial hypoplasia [177,216,217]. Turbinate hypertrophy and deviated nasal septum frequently occur together [218,219], but again their presence on their own is insufficient to predict upper airway obstruction [218]. In $Bmp7^{ncko}$ mice turbinate swelling precedes nasal septum deviation. Currently, the cause of turbinate swelling is unclear. Although abnormal turbinate development can be

observed, the swelling could also be a consequence of abnormal mucus drainage, cellular changes to turbinates mucosa and/or altered airflow.

Although all Bmp7^{ncko} develop nasal septum deviation at 4 weeks, 50% of these mice developed SA between 4 and 6 weeks. This is suggestive that Bmp7^{ncko} mice experience respiratory distress due to airway obstruction to varying degrees. Here, we showed evidence that morphological changes in the upper airways disrupt regular breathing pattern possibly due to airway obstruction. Increased inspiratory airway resistance may lead to two mechanisms to maintain ventilation: (1) an increase in inspiratory muscle drive; and (2) an increase in the inspiratory time, to achieve a comparable V_T over an expanded inspiratory time (Hernandez et al., 2012; Mann et al., 2017). In the present study, Bmp7$^{ncko\ (a)}$ mice showed an increased in T_{TOT}, mainly due to an increase in the T_i and a tendency for a prolonged T_e compared to control mice resulting in no changes in V_T and $\dot{V}_E$. In patients with OSA, when these adjustments in breath timing do not compensate ventilation, apneas or hypopneas may occur [220–222] as we have observed in a subpopulation of Bmp7^{ncko} mice. Indeed, adaptation to mouth breathing has been observed in children with upper airway obstruction [223]. Although mice are described as obligate nose breathers [224], adaptation to mouth breathing [225,226] or gasping [227] has been observed in the event of nasal obstruction. Assuming that adaptation occurs in Bmp7^{ncko} mice, further experiments will be necessary to distinguish adaptation to mechanical and/or central control of breathing.

Along with a greater SA incidence, Bmp7$^{ncko\ (a)}$ mice also present with a greater frequency of irregular breathing following a sigh. The mechanisms underlying apneas and, particularly, PSA are not completely understood. They may involve inhibition of inspiration through activation of pulmonary stretch receptors, the Breuer-Hering reflex, or decreased drive to breathe due to lower CO_2 levels induced by the sigh [202,228,229]. Bmp7$^{ncko\ (a)}$ mice may have alteration in the vagal reflex,

or compromised central responses to the reflex, leading to more apneic events, which could also explain the lower breathing frequency. Derivatives of neural crest contribute to the carotid body and sensory neurons [230,231], both of which provide important excitatory signals for central breathing control, especially in hypoxic conditions. Bmp7 could affect the development of either structure. Although a role for Bmp7 in neurogenesis is well established [232,233] nothing is known about neural crest-derived Bmp7 contribution to carotid body development and function. It should be noted that the Wnt1-Cre driver used in this study has been shown to affect brain development [234]. For this reason, *Bmp7fx*/+;Wnt1-Cre mice were additionally assessed for craniofacial changes. There was no evident septum deviation or early lethality as seen in $Bmp7^{ncko}$ mice. Therefore, these mice were not subjected to functional plethysmography.

In the present study, both $Bmp7^{ctrl}$ and $Bmp7^{ncko}$ mice showed a biphasic ventilatory response to hypoxia [235,236], with a decrease in $\dot{V}O_2$ and body temperature [237], indicating that peripheral chemosensitivity and centrally regulated breathing control are most likely intact. However, the drop in Tb was greater in the $Bmp7^{ncko\,(a)}$ mice compared to controls, suggesting that the thermoregulatory control to hypoxia may be affected by deletion of *Bmp7* in the neural crest.

Supplemental oxygen therapy has been examined to have effects on the pathophysiology of OSA, in humans, although its benefits are controversial [238–240]. We wanted to test whether, after reducing the ventilatory drive with hyperoxia exposure, $Bmp7^{ncko\,(a)}$ mice would show changes in breathing pattern or irregularities. Hyperoxia did not affect the number of PSAs, or cause any dysfunction in ventilation. However, it reduced the number of SAs in the $Bmp7^{ncko\,(a)}$, except for one mouse in which hyperoxia potentiated the number of SAs. These results suggest that, at least in our mouse model, hyperoxia may help to reduce the occurrence of SAs in $Bmp7^{ncko\,(a)}$ mice. However, the fact that one outlier $Bmp7^{ncko\,(a)}$ mouse showed the opposite effect should not be

ignored. The respiratory variability might be a true reflection of the unpredictable response observed in some children using continuous positive airway pressure [241].

The trend for lower fR and increased T_i and T_e in 2-week-old Bmp7^{ncko} mice (Fig. S4.3), a time prior to structural nasal abnormalities being established, is suggestive that the lack of Bmp7 in the neural crest during embryonic development may affect developmental processes that only later manifest as phenotypic changes. Hence, the structural abnormalities could be a consequence of the inability to repair and recover and grow during the growth spurt (after 3 weeks in mice). Additionally, the understanding that altered cellular and molecular processes in the human body precede structural abnormalities later in life [242] reaffirms the plasticity of the human body as well as the notion that nasal septum deviation and its consequences establish gradually and not overnight. Thus, better understanding of the underlying genetic alterations associated with nasal airway obstruction will assist in effective management and treatment of the obstruction along with its associated co-morbidities.

The Bmp7^{ncko} model could be used to further investigate the origin of mixed apneas in individuals with craniofacial or neural crest abnormalities. The inability to use craniofacial abnormalities and degree of nasal septum deviation as predictors for the severity of upper airway obstruction and relative contribution of the different apneas is an accurate reflection of the challenges clinicians face in determining/diagnosing using CT scans whether children with nasal obstruction will develop SRBD and require further intervention [218].

Several biomarkers such as kallikrein-1, uromodulin, urocortin-3 and orosomucoid-1 have been proposed as diagnostic markers for pediatric OSA in children although their sensitivity and specificity have yet to be fully understood [243]. Using a limited quantitative metabolomics approach, we tested whether this model can be used to identify potential biomarkers for airway obstruction.

From the screening of 154 metabolites, we observed a significant increase in hydroxyproline. This metabolite has been used as an index of total collagen degradation [244] but more recently has been directly associated with hypoxia in hepatocellular carcinoma [245]. In that study, hydroxyproline was part of the metabolic axis promoting cell survival through modulating hypoxia inducing factor 1 alpha (HIF1α). Although arterial partial pressure of O_2 (paO_2) was not directly measured in our study, the increase in hydroxyproline may suggest, in addition to reduced physical activity, that the $Bmp7^{ncko}$ mice experience episodes of hypoxia. $Bmp7^{ncko}$ mice showed a decrease with age in the ability to sustain a physical exercise such as running on a treadmill with age. This may be in indication of their inability to ventilate efficiently. Similarly, a reduced exercise capacity was also observed in children with OSA [246]. In $Bmp7^{ncko}$ mice, the nasal airway obstruction is likely to be present both during active and rest phases. OSA has been shown to have wider systemic consequences including bone remodeling [212]. A reduction in bone mineral density indicative of changes to bone remodelling has previously been identified in children with OSA [104], but it was not clear whether hypoxia affected bone remodelling or vice-versa. Based on our findings, we propose that altered bone metabolism is part of the congenital abnormalities and that hypoxia may be a consequence of altered craniofacial growth.

Our observations on $Bmp7^{ncko}$ mice shed new light on the etiology of nasal airway obstruction as a consequence of insufficient midfacial growth. Midfacial hypoplasia on its own cannot predict nor determine the severity of SRBD highlighting the need to carefully investigate craniofacial abnormalities in children. We find that various anomalies in craniofacial structures synergistically predispose to upper airway obstruction. The primary reason for these malformations appears to be altered cartilage and bone development. Although the nasal septum, cranial base and nasal bones grow as a developmental unit, the relative contribution of individual

components varies even in this genetically defined model. Environmental factors do play a role, although this has not been well studied yet. For this reason, onset and severity of upper airway obstruction remains largely unpredictable. Although hypoxic ventilatory response appears largely intact, an increased number of post-sigh apneas events and alterations in body temperature during normoxia and hypoxia suggest the involvement of the central network for respiratory and thermoregulatory control in the features of the $Bmp7^{ncko}$ mice model. At present it is not possible to distinguish whether this is a systemic consequence of upper airway obstruction or due to neural crest-specific roles of Bmp7 outside of bone/cartilage. The multifactorial etiology and presence of mixed apneas reflects the challenges clinicians face in treating complex cases of pediatric OSA, warranting an appropriate genetic model for further study. We have shown that this model can be used for the identification of potential predictive biomarkers to help identify which children with craniofacial malformations are likely to develop SRBD.

In summary, this study demonstrates that the $Bmp7^{ncko}$ mouse can be used to identify molecular mechanisms underlying craniofacial abnormalities resulting in nasal airway obstruction to better understand the genetic component contributing to obstruction in children with SRBD.

4.6 Supplemental Information

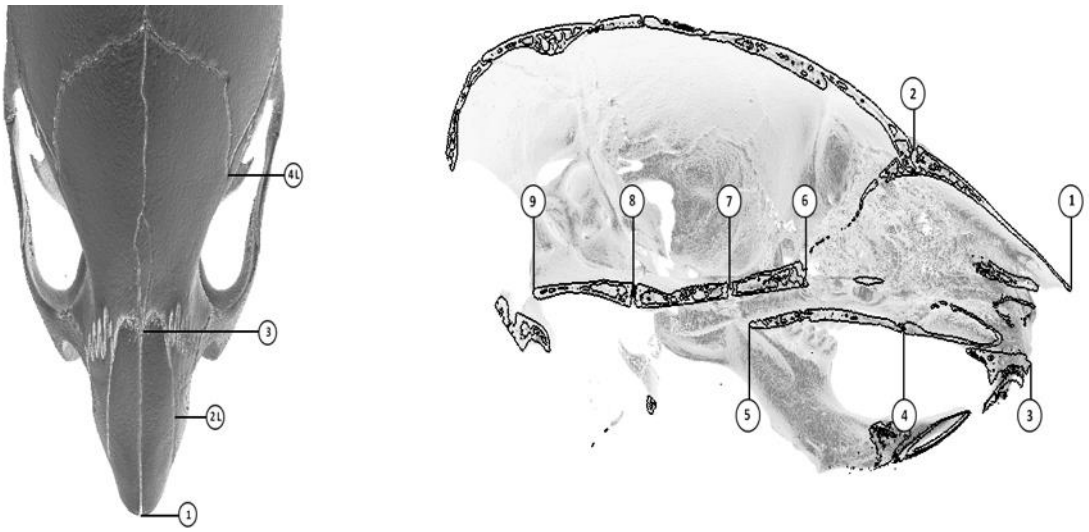

Superior Landmarks

1) Nasale (rostral intersection of nasal bones)
2) Nasion (caudal intersection of nasal bones)
3) External margin of nasal bones (left and right)
4) Frontal-temporal-parietal junction (left and right)

Mid-sagittal Landmarks

1) Nasale (rostral tip of nasal bone)
2) Nasion (intersection of frontal and nasal bone)
3) Anterior-most point of alveolar bone of upper incisor
4) Intersection of maxilla and pre-maxilla
5) Caudal-most point of palatine bone
6) Rostral pre-sphenoid bone
7) Ventral-most point of ISS
8) Ventral-most point of SOS
9) Caudal-most point of basi-occopital bone

Supplemental Figure 4. 1 Diagram of morphometric landmarks and measurements used to characterize craniofacial growth, or lack thereof, in Bmp7^{ctrl} and Bmp7^{ncko} mice.

(left panel): superior view of the skull. (right panel): mid-sagittal view of the skull.

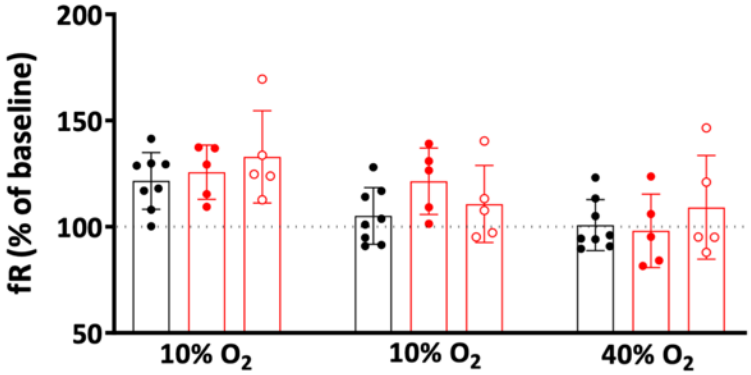

Supplemental Figure 4. 2 Respiratory pattern during normoxia in 2-week-old Bmp7^{ctrl} and Bmp7^{ncko} mice.

(A) Respiratory frequency (fR). (B) Breath cycle duration (TTOT), Inspiratory time (Ti) and Expiratory time (Te). (C) Number of apneas/hour. (D) Number of sighs/hour. (E) Percentage (%) of post sigh apneas (PSA) / total number of sighs with < 2 PSA or ≥ 2 PSA apneas. There was no statistical difference between the groups ($p > 0.05$).

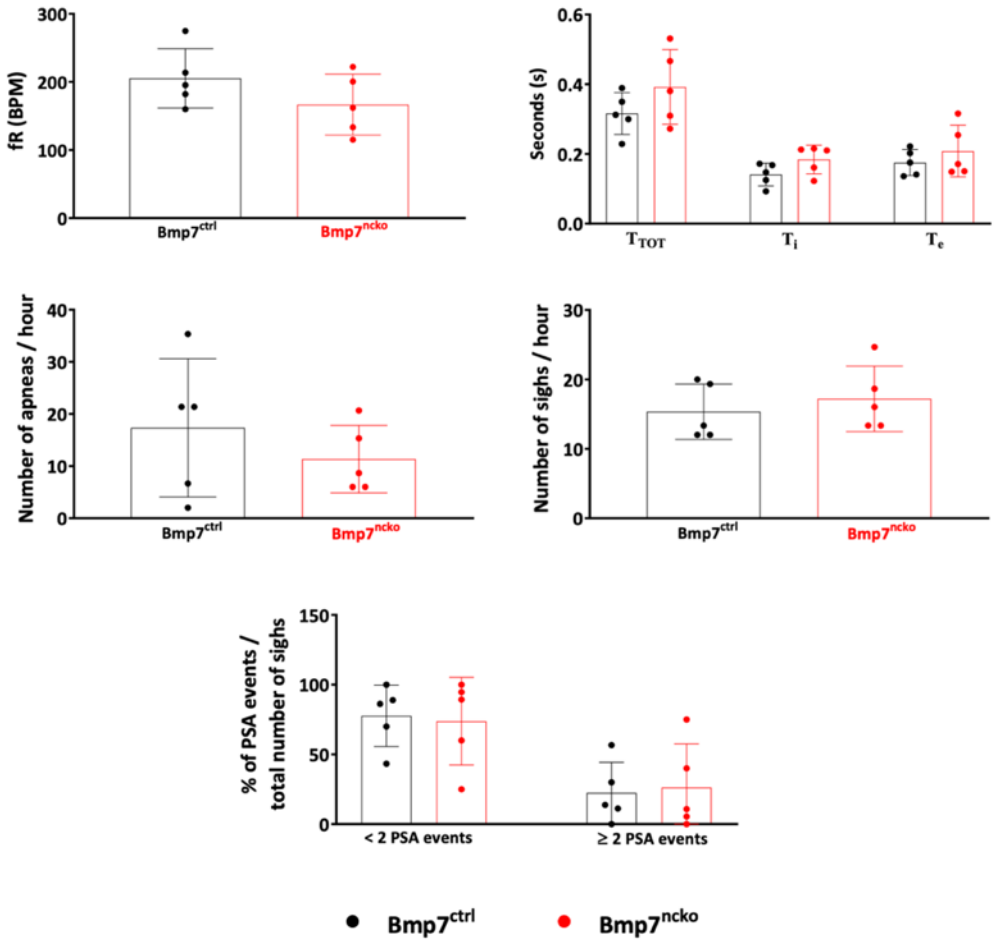

Supplemental Figure 4. 3 Respiratory frequency (fR) during hypoxia and hyperoxia exposures.

Absolute values from figure 4.5A shown as percentage (%) of baseline values during 5 and 15 min of hypoxia (10% O2) and 15 min of hyperoxia (40% O2), in $Bmp7^{ctrl}$, $Bmp7^{ncko\ (r)}$ and $Bmp7^{ncko\ (a)}$ mice.

Supplemental Table 4. 1 Two-tailed independent t-test statistical comparison of control and mutant morphometric data to accompany Figure 4.1.

P14: 2-week-old mice; P21: 3-week-old mice; P30: 1-month-old mice. n=3 for each age group per genotype.

	Age	Degrees of freedom	T statistic	p-value
Facial length				
	P14	3	1.553238	0.218187
**	P21	4	12.44201	0.00024
*	P30	4	7.073297	0.002108
Snout angle				
	P14	2	-0.51867	0.655675
	P21	2	1.393439	0.298145
	P30	4	-1.83126	0.141021
Frontal bossing				
	P14	3	-1.97315	0.143007
	P21	2	-2.56254	0.12448
	P30	3	2.238238	0.111143
Nasal depression				
	P14	4	0.583792	0.590695
	P21	2	2.566908	0.124132
	P30	3	-0.95634	0.409451
Nasal bone width				
	P14	2	-2.77746	0.108867
	P21	4	0.518786	0.631289
	P30	2	0.243733	0.830158
Nasal bone length				
	P14	4	2.003438	0.115662
	P21	3	2.057673	0.13179
	P30	3	-0.04358	0.96798

Supplemental Movie 4. 1 Video representation of $Bmp7^{ncko}$ mice experiencing apneas.

$Bmp7^{ncko}$ mice experience spontaneous apnea events Mice were placed in plethysmography chambers and video of the mutant mouse behaviour during baseline measurements was recorded.

Supplemental Movie 4. 2 Video representation of $Bmp7^{ncko}$ mice demonstrating lethargy.

$Bmp7^{ctrl}$ (top panel) and $Bmp7^{ncko}$ (bottom panel) mice were placed on the treadmill for 5 mins after acclimatization to run. The $Bmp7^{ctrl}$ mice demonstrated no signs of inactivity and rest, however the $Bmp7^{ncko}$ mice demonstrate short period of running followed by long periods of rest.

Supplemental Table 4. 2 Two-tailed independent t-test statistical results to accompany Figure 4.2 morphometric data from 1 month old mice.

* indicates p<0.05; ** indicates p<0.001. n=3 for each age group per genotype.

	Measurement	Degrees of freedom	T statistic	p-value
*	cranial base angle 1	19	2.607641	0.017301
	cranial base angle 2	23	1.225689	0.232719
	basioccipital length	25	1.669665	0.107462
**	basisphenoid length	25	5.914634	3.58E-06
	presphenoid length	29	0.313573	0.75609
	ethmoid length	29	0.311218	0.757861
**	posterior cranial base length	25	4.27551	0.000244
**	facial length	31	6.013647	1.18E-06
**	snout angle	22	5.541883	1.43E-05
	cranium maxilla angle	23	0.610879	0.54727
**	frontal bossing	25	-5.79575	4.84E-06
**	nasal depression	21	7.335938	3.21E-07
	nasal bone width	22	1.879617	0.07347
*	nasal bone length	31	3.12455	0.003847

Supplemental Table 4. 3 $Bmp7^{ncko}$ mice showed no changes to cranial base angles and lengths prior to nasal septum deviation.

P14: 2-week-old-mice; P21: 3-week-old-mice; n=3 for each age group per genotype.

Measurement	P14 $Bmp7^{ctrl}$	P14 $Bmp7^{ncko}$	p-value	P21 $Bmp7^{ctrl}$	P21 $Bmp7^{ncko}$	p-value
cranial base angle 1	154.93±1.42	151.66±5.99	0.40	150.55±2.71	144.46±6.62	0.13
cranial base angle 2	150.64±2.50	148.18±4.44	0.31	146.48±4.46	143.64±5.20	0.42
basioccipital length	2.89±0.33	2.758±0.15	0.44	3.32±0.71	2.93±0.29	0.29
basisphenoid length	2.712±0.20	2.468±0.19	0.086	2.67±0.31	2.69±0.37	0.92
presphenoid length	2.14±0.12	2.04±0.19	0.35	2.21±0.17	2.14±0.13	0.50
ethmoid length	4.36±0.28	4.5±0.37	0.53	4.95±0.27	4.88±0.22	0.72
posterior cranial base length	8.03±0.26	7.75±0.23	0.11	8.09±0.75	7.67±0.23	0.27

Supplemental Table 4. 4 Intraclass correlation (ICC) assessment to address intrarater reliability.

Three P30 mice of each genotype were landmarked and measured in triplicate by a single rater.

		confidence interval	
mouse ID	ICC	lower	upper
C324	0.999524	0.998854	0.999833
C325	0.999798	0.999513	0.999929
C327	0.999274	0.998253	0.999746
C531	0.996789	0.992222	0.998877
C586	0.997853	0.994838	0.999247
C600	0.998306	0.995721	0.999416
K3308	0.998042	0.995252	0.999315
K3309	0.998773	0.997022	0.999571

Supplemental Table 4. 5 The variability of tidal volume (V_T), breathing frequency (fR), breath duration (T_{TOT}) and inspiratory time (Ti) (mean ± S.D.) during normoxia in $Bmp7^{ctrl}$, $Bmp7^{ncko\ (r)}$ and $Bmp7^{ncko\ (a)}$ mice.

*P=0.016 for $Bmp7^{ncko\ (r)}$ versus $Bmp7^{ncko\ (a)}$ mice.

	$Bmp7^{ctrl}$ (n=8)	**$Bmp7^{ncko\ (r)}$ (n=5)**	**$Bmp7^{ncko\ (a)}$ (n=5)**
V_T			
SD1	0.4±0.7	0	0.6±0.8
SD2	1.9±3.4	0	2.7±3.9
fR			
SD1	25.1±13.9	18.1±4.0	25.6±7.0
SD2	50.2±17.1	34.5±6.1	50.0±9.0*
T_{TOT}			
SD1	0.4±0.7	0	0.6±0.8
SD2	1.1±2.4	0.1	2.8±3.9
Ti			
SD1	0.4±0.7	0	0.6±0.8
SD2	1.1±2.4	0	2.7±3.9

Chapter 5: Nasal septum deviation as the consequence of BMP-controlled changes to cartilage properties

Chapter 4 demonstrated that $Bmp7^{ncko}$ mouse model presents with midfacial hypoplasia, nasal septum deviation and disordered breathing. Having established this, Chapter 5 characterizes the cellular and molecular changes underlying nasal septum deviation by using knowledge obtained on growth and extracellular matrix properties identified in a wild-type mouse in Chapter 3.

Chapter 5 is derived from this published article:

Baddam, P., Young, D., Dunsmore, G., Nie, C., Eaton, F., Elahi, S., Jovel, J., Adesida AB., Dufour, A., Graf, D. (2021) Nasal septum deviation as the consequence of BMP-controlled changes to cartilage properties. *Frontiers in Cell and Developmental Biology.*

5.1 Abstract

The nasal septum cartilage is a specialized hyaline cartilage important for normal midfacial growth. Abnormal midfacial growth is associated with midfacial hypoplasia and nasal septum deviation (NSD). However, the underlying genetics and associated functional consequences of these two anomalies are poorly understood. We have previously shown that loss of Bone Morphogenetic Protein 7 (BMP7) from neural crest ($BMP7^{ncko}$) leads to midfacial hypoplasia and subsequent septum deviation. In this study we elucidate the cellular and molecular abnormalities underlying NSD using comparative gene expression, quantitative proteomics, and immunofluorescence analysis. We show that reduced cartilage growth and septum deviation are associated with acquisition of elastic cartilage markers and share similarities with osteoarthritis (OA) of the knee. The genetic reduction of BMP2 in $BMP7^{ncko}$ mice was sufficient to rescue NSD and suppress elastic cartilage markers.

To our knowledge this investigation provides the first genetic example of an *in vivo* cartilage fate switch showing that this is controlled by the relative balance of BMP2 and BMP7. Cellular and molecular changes similar between NSD and knee OA suggests a related aetiology underlying these cartilage abnormalities.

Keywords: Nasal septum deviation, hyaline cartilage, elastic cartilage, BMP7, BMP2, Wnt signaling, glucose metabolism, chondrocyte properties.

5.2 Introduction

Nasal septum cartilage that divides the nasal cavity in two is a hyaline cartilage. It resists deformation, provides structural support to the midface, and is the pacemaker for midfacial growth. Nasal septum deviation (NSD) that describes a non-straight, deformed nasal septum is a common abnormality and can be observed in 80% of the population [247]. NSD might be inconspicuous but frequently is associated with various degrees of nasal airway obstruction resulting in Sleep Disordered Breathing (SDB) [248–250]. Congenitally acquired deviation frequently develops during time of rapid midfacial growth and is associated with reduced midfacial growth and a strong predisposition for SDB [251]. Another common etiology is trauma to the face and nose. Corrective septoplasties often require graft cartilage, which depending on the site of harvest is either limited in amount, associated with donor site morbidity, or both. Despite the ability to model surgical septoplasty outcomes virtually before surgery [252], revision rates remain high and exceed 15% [253]. This high rate may be a consequence of our limited understanding of the etiology of pediatric, congenital acquired NSD and its associated secondary complications [218]. It is currently unknown if NSD has an underlying molecular and cellular etiology, even though this might be implied from congenital cases that are associated with reduced midfacial growth.

Although the nasal septum cartilage is a hyaline cartilage, it differs from other hyaline cartilages in several aspects. First, it is an active center for midfacial growth and much of its growth occurs, at least in the mouse, through chondrocyte hypertrophy [85]. Second, hypertrophic chondrocytes situated in the middle part of the septum do not undergo apoptosis or ossification, except in the posterior part to form the bony perpendicular plate of the ethmoid [131]. Third, it is a mirrored structure with progenitor cells and immature chondrocytes located on either side of the septum, close to the perichondrium [85]. Fourth, hypertrophic chondrocytes are surrounded by a

dense collagen fibril matrix thought to provide rigidity and stiffness. To what degree any of these features are altered in NSD remains unexplored.

Changes to hyaline cartilage in the context of cartilage pathologies are best understood for osteoarthritis (OA) of the knee. There, common accepted features are loss of glycosaminoglycans (GAGs), increase in chondrocyte hypertrophy along with an increase in Collagen X (COL X), Indian Hedgehog (IHH) and Runt-related transcription factor 2 (RUNX2), increase in reactive oxygen species (ROS) production and increase in glucose metabolism [254]. Other changes, such as altered elasticity remain controversial, as some studies report a decrease in elasticity while others propose an increase [255,256]. On a molecular level, perturbations to several signaling networks can be observed in knee OA. Reduction of the WNT antagonists Dickkopf1 (DKK1) and Frizzled Related Protein (FRZB) concomitant with an increase in non-phosphorylated Beta-Catenin (NPBC) as readout for canonical WNT signalling have been described [257,258]. Alterations to Bone Morphogenetic Protein (BMP) signalling are associated with chondrocyte hypertrophy. BMP7 suppresses while BMP2 promotes chondrocyte hypertrophy and matrix degradation [259] and decreased levels of BMP7 have been directly associated with OA [260,261]. If and to what degree similar changes occur in cartilage of a deviated septum is not known.

We recently described that mice with neural crest-specific deletion of BMP7 ($BMP7^{ncko}$) develop midfacial hypoplasia and nasal airway obstruction [262]. A hallmark of this model is the development of a significantly deviated nasal septum at a juvenile age that is associated with progression to abnormal breathing. Deletion of BMP7 from developing limbs leads to articular cartilage degeneration and synovial inflammation [263]. Proteoglycan content and aggrecan expression were reduced, while expression of matrix metalloproteinase-13 (MMP13) was

increased. In this study, we asked whether similar molecular and cellular changes as observed in the knee are associated with the development of NSD in the BMP7^{ncko} mouse.

We demonstrate that BMP7 is expressed in the perichondrium and nasal chondrocytes throughout postnatal development. Loss of BMP7 leads to histomorphological changes by 4-weeks of age, the time the NSD is established. Correlating those changes to molecular changes using gene expression analysis, quantitative shotgun proteomics and immunofluorescence analysis at various developmental time-points, we identified that alterations to chondrocyte properties precede NSD. This included acquisition of elastic cartilage markers, a switch to glucose metabolism, along with increase in molecular markers commonly associated with knee OA. Loss of BMP7 was also associated with a significant increase in canonical WNT signaling in mature chondrocytes. Concomitant reduction of BMP2 in BMP7^{ncko} mice restored the change in WNT signaling, prevented the development of the deviation, and rescued the midfacial hypoplasia, demonstrating that the balance of BMP2 and BMP7 synergistically determines cartilage properties. As many of the cellular and molecular changes in NSD in Bmp7^{ncko} mice share pathophysiological similarities with knee OA, this study sets a precedent for the need to further understand nasal cartilage properties for use in tissue engineering or clinical applications relating to regeneration of damaged cartilage in knee OA.

5.3 Methods

5.3.1 Animal Models

Both male and female mice were used for this study. All mice were maintained on the C57BL/6 background and backcrossed for at least 10 generations. *BMP7* expression was identified using BMP7LacZ reporter mice [264]. BMP7$^{fl/fl}$ mice also referred to as BMP7^{ctrl} mice, were crossed to WNT1-cre mice to delete BMP7 from neural crest cells (subsequently referred to BMP7^{ncko}

mice) [264]. To rescue the nasal septum deviation, BMP7^{ncko} mice were crossed with BMP2$^{wt/fl}$ [265] to obtain BMP2$^{wt/fl}$BMP7^{ncko}, also referred to as BMP2^{het}BMP7^{ncko} subsequently. Lineage tracing was done using mT/mG mice (*Gt(ROSA)26Sor$^{tm4(ACTB-tdTomato,-EGFP)Luo}$*/J) [266]. BMP7 expression and identification of neural crest cells in the nasal septum was conducted at birth (postnatal day 0, P0), 2 weeks (postnatal day 14, P14) and 4 weeks (postnatal day 30, P30). Additionally, nasal septum of BMP7^{ctrl} and BMP7^{ncko} mice were also assessed at the abovementioned time-points. BMP2^{het}BMP7^{ncko} mice were assessed only at P30.

5.3.2 Micro-computed tomography (μCT) analysis

Morphological changes to nasal septum of BMP7^{ctrl} and BMP7^{ncko} (n=3/genotype) were assessed at P14 and P30 using μCT. Acquisition and reconstruction of nasal septum using MILabs μCT at the School of Dentistry, was conducted as previously described [85]. The degree and severity of nasal septum deviation were quantified on coronal representations of the nasal septum using Amira software. Two landmarks were placed at the abutment where the perpendicular plate meets the cribriform plate of ethmoid bone and where the vomer articulates with the palatine bone, respectively. A straight line was drawn between these two points indicating a hypothetical straight septum, and its length was considered as its height (a). Next, the actual length of the septum was determined by tracing the actual length of the septum (b). The degree of deviation was determined as (b – a)/a and expressed as percentage. Longitudinal experiments to determine whether nasal septum deviation becomes severe overtime were assessed by calculating the degree of nasal septum deviation on the same mice twice at two different ages (4 weeks (P30) and 10 weeks (P74)).

5.3.3 RNA Sequencing

Total RNA from isolated nasal septum of P0 BMP7^{ctrl} and BMP7^{ncko} mice (n=4/genotype) was extracted with TRIzol reagent (Invitrogen). RNAseq libraries were constructed from 500 ng

of total RNA using the NEBNext Ultra II Directional RNA Library Prep Kit for Illumina (NEB). Polyadenylated mRNAs were enriched with oligo dTs conjugated to paramagnetic beads. Enriched mRNAs were fragmented chemically and used for cDNA synthesis. cDNA was end-repaired and A-tailed, ligated to linkers and finally indexed by PCR, to enable multiplexing during sequencing. Sequencing was done on a MiSeq instrument, following a paired-end 75 cycles protocol. Raw sequencing data is publicly available from the NCBI SRA portal under accession number PRJNA622501. The Bioinformatic analysis was conducted where fragments were mapped to the human cDNA database (GRCh38) using Kallisto [267], with 100 permutations during pseudo-alignments. Differential expression analysis of RNAseq data was conducted using negative binomial generalized linear models with the edgeR R package [268]. Gene abundance differences with a corrected p-value < 0.05 and a log fold change of ≤-2 or ≤2 were considered differentially expressed. Mean-differential plots were generated with edgeR and heatmaps were generated using the R package pheatmap. Gene ontologies were identified using PANTHER gene ontology consortium [269]. Only significant ontologies were selected for representation (FDR<0.05).

5.3.4 Shotgun Proteomics

Nasal septum of P14 and P30 $BMP7^{ctrl}$ and $BMP7^{ncko}$ mice (n=4/genotype) were isolated and frozen until processing for proteomics experiments. Protein lysates were obtained by tissue lysis in buffer containing 1% SDS, in 200 mM HEPES (pH 8.0) and cOmplete™ Protease Inhibitor Cocktail (MilliporeSigma, Oakville, ON, Canada). Samples were reduced with 10 mM dithiothreitol (DTT) for 30 mins at 37 °C. Once cooled at room temperature (RT), cysteine alkylation was achieved by incubation with a final concentration of 15 mM iodoacetamide for 25 min in the dark at RT. Next, samples were precipitated in acetone/methanol, washed three times in methanol, and trypsinized (Trypsin Gold from Promega, Madison, WI, USA). The pH was

adjusted to 6.0 with HCl. To label peptide α- and ε-amines, samples were incubated for 18 h at 37 °C with isotopically heavy [40 mM 13CD2O + 20 mM NaBH3CN (sodium cyanoborohydride)] or light labels [40 mM light formaldehyde (CH2O) + 20 mM NaBH3CN]. Next, samples were combined and subjected to C18 chromatography before being run on liquid chromatography and tandem mass spectrometry.

5.3.4.1 High-Performance Liquid Chromatography (HPLC) and Mass Spectrometry (MS)

The liquid chromatography and mass spectrometry experiments were carried out by the Southern Alberta Mass Spectrometry (SAMS) core facility at the University of Calgary, Canada. The analysis was performed on an Orbitrap Fusion Lumos Tribrid mass spectrometer (Thermo Scientific) operated with Xcalibur (version 4.0.21.10) and coupled to a Thermo Scientific Easy-nLC (nanoflow liquid chromatography) 1200 system. Tryptic peptides (2 µg) were loaded onto a C18 column (75 µm × 2 cm; Acclaim PepMap 100, P/N 164946; Thermo Scientific) at a flow rate of 2 µL/min of solvent A (0.1% formic acid and 3% acetonitrile in LC-MS grade water). Peptides were then electrosprayed using 2.3 kV voltage into the ion transfer tube (300 °C) of the Orbitrap Lumos operating in the positive mode. The Orbitrap first performed a full MS scan at a resolution of 120,000 fwhm to detect the precursor ion having a m/z between 375 and 1,575 and a +2 to +7 charge. The Orbitrap AGC (Auto Gain Control) and the maximum injection time were set at 4×10^5 and 50 ms, respectively. The Orbitrap was operated using the top speed mode with a 3 s cycle time for precursor selection. The most intense precursor ions presenting a peptidic isotopic profile and having an intensity threshold of at least 5,000 were isolated using the quadrupole and fragmented with HCD (30% collision energy) in the ion routing multipole. The fragment ions (MS2) were analyzed in the ion trap at a rapid scan rate. The AGC and the maximum injection

time were set at 1×10^4 and 35 ms, respectively, for the ion trap. Dynamic exclusion was enabled for 45 s to avoid the acquisition of the same precursor ion having a similar m/z (±10 ppm).

5.3.4.2 Proteomic Data and Bioinformatics Analysis

Spectral data were matched to peptide sequences in the murine UniProt protein database using the Andromeda algorithm [270] as implemented in the MaxQuant software [271] package v.1.6.0.1, at a peptide-spectrum match false discovery rate (FDR) of <0.01. Search parameters included a mass tolerance of 20 ppm for the parent ion, 0.5 Da for the fragment ion, carbamidomethylation of cysteine residues (+57.021464 Da), variable N-terminal modification by acetylation (+42.010565 Da), and variable methionine oxidation (+15.994915 Da). N-terminal and lysine heavy (+34.063116 Da) and light (+28.031300 Da) dimethylation were defined as labels for relative quantification. The cleavage site specificity was set to Trypsin/P, with up to two missed cleavages allowed. Significant outlier cut-off values were determined after log(2) transformation by box-and-whisker analysis using the BoxPlotR tool ([272]). A minimum of two distinct peptides per protein for the quantification was used. Following an interquartile boxplot analysis, proteins with a quantification ratio of under 0.65 and above 1.5 were considered for the analysis. The proteomic data has been deposited to the ProteomeXchange Consortium via the PRIDE partner repository with the data set identifier px-submission #488429. A list of all differentially regulated proteins is provided in the Supplemental Tables 5.1&5.2.

5.3.5 RNA extraction Quantitative Real-Time Polymerase Chain Reaction (qRT-PCR)

Nasal septum from P0, P14 and P30 $BMP7^{ctrl}$ and $BMP7^{ncko}$ mice (n=3/genotype) were dissected and processed for RNA extraction. RNA extraction and qRT-PCR were conducted as previously described [264]. Fold difference was determined in relation to the housekeeping gene 36B4 using ΔΔCt method [264]. Analysis was conducted on biological and technical triplicates. Data

shown are representatives from three biological samples per genotype. A list of primer pairs used for gene expression analysis is outlined in Supplemental Table 5.3.

5.3.6 Tissue Processing and Histology

BMP7^{ctrl} and BMP7^{ncko} mice (n=3/genotype/age) were fixed using 4% paraformaldehyde (PFA). Mice skulls were dissected and decalcified in 0.5M Ethylenediaminetetraacetic acid (EDTA) as previously described [264]. Mouse skulls were frontally embedded in paraffin and sectioned using 820 Spencer microtome at 7 microns. For histological staining, sections were deparaffinized as previously described [85].

5.3.7 Histological stains

Medial nasal septum sections were used for histological and immunofluorescence analysis [85]. Hematoxylin and Eosin (H&E) and Safranin O staining on nasal septum of P14 and P30 BMP7^{ctrl} and BMP7^{ncko} mice (n=3/genotype/age) were performed as previously described [85,264]. Picrosirius staining was performed using Sirius Red staining protocol from IHC world [273]. H&E was performed to assess gross morphology. Safranin O staining was used to stain cartilage and Picrosirius Red staining was used to stain collagen fibers. Images were acquired on an Olympus IX73 microscope using 20X and 40X objectives.

5.3.8 Immunofluorescence

Immunofluorescent staining was performed on medial nasal septum paraffin sections of P0, P14, P30 BMP7^{ctrl} and BMP7^{ncko} and P30 BMP2^{het}BMP7^{ncko} mice as previously described [85]. Specifications of primary and secondary antibodies are provided in Supplemental Table 5.4. Images were acquired on an Olympus IX73 microscope using 20x objectives. Analysis was performed on three biological replicates. Negative controls demonstrating background staining were previously demonstrated [85].

5.3.9 LacZ Staining

P0, P14 and P30 BMP7LacZ reporter mice (n=3/genotype/age) were stained using previously described staining procedure [264]. Mouse skulls were fixed, decalcified, processed as described above. The paraffin sections were counterstained using Safranin O staining protocol.

5.3.10 Statistics

Graphs indicate individual measurements as well as mean ± standard deviation when applicable. A two-tailed independent t-test was conducted to test for statistical significance between $BMP7^{ctrl}$ and $BMP7^{ncko}$ mice. Microsoft Excel was used to display graphs and an independent unpaired t-test was conducted using online statistical software [274]. * $P<0.05$; **$P<0.01$; ***$P<0.001$; ns: not significant $P>0.05$.

5.3.11 Study Approval

This study was approved by the Health Sciences Animal Care and Use Committee at the University of Alberta (protocol #: AUP1149). All experiments in this study were conducted in accordance with the Canadian Council on Animal Care guidelines.

5.4 Results

5.4.1 BMP7 is expressed in nasal cartilage and its deletion results in nasal septum deviation.

Anterior and medial nasal septum sections were used for histological assessment of the nasal septum [85]. Images were acquired at the abutment of nasal septum with internasal suture as well as the middle of the nasal septum (Figure 5.1A). To identify when and where BMP7 is expressed in the nasal septum, we used BMP7LacZ reporter mice (n=3/age). Expression was observed at the abutment at all ages investigated (Figure 5.1A'-C; Post-natal day 0 (P0), Post-natal day 14 (P14), Post-natal day 30 (P30)). In the middle region of the septum, BMP7 was clearly expressed in chondrocytes as well as the perichondral lining from P0 onwards (Figure 5.1D-F).

The expression was variable over time, with least expression observed in chondrocytes at P14 (Figure 5.1E). Lineage tracing confirmed neural crest origin of septum chondrocytes and perichondrium (n=3/age) (Figure 5.1G-I). As previously shown [262], the nasal septum in BMP7^{ncko} mice becomes severely deviated by P30 (Figure 5.1J-O) (n=3/age/genotype) with the degree of deviation reaching between 10-35% (Figure 5.1L; $p<0.001$) and variable in severity over time (Figure 5.1O). The nasal septum in the mouse grows rapidly between P7-P14 and P21-P30 but shows a significant reduction between P14-P21 [140]. As BMP7^{ncko} mice develop midfacial hypoplasia in addition to NSD, we suspected that changes to cartilage appearance and properties are associated with the development of these two pathologies.

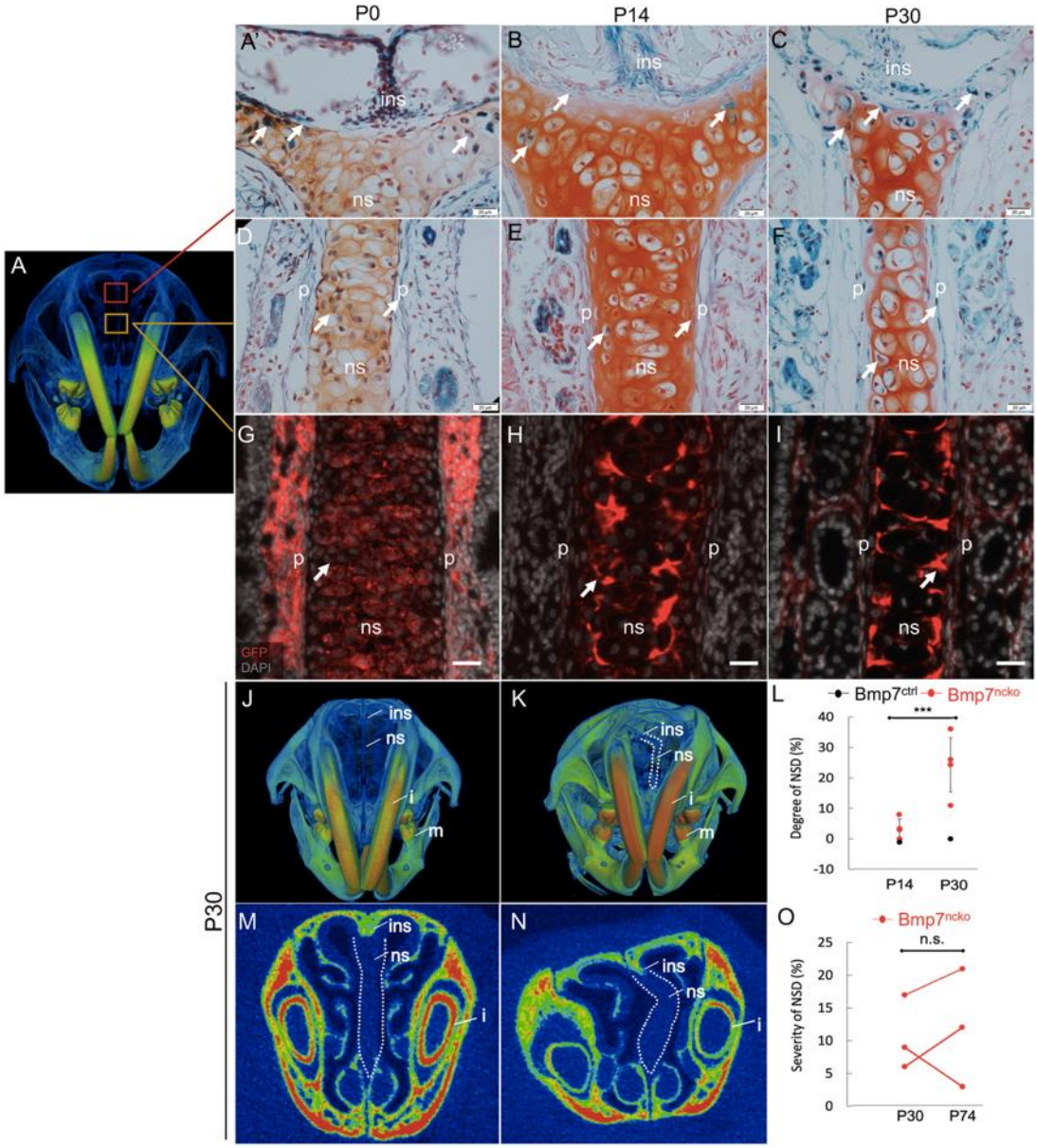

Figure 5. 1 Deletion of BMP7 in neural crest cells results in nasal septum deviation (NSD).
(A) µCT reconstruction of P30 mouse skull demonstrating the location of nasal septum where images were acquired from. LacZ stained (blue) nasal septum paraffin sections demonstrating BMP7 expression in P0 (A', D), P14 (B, E), and P30 (C, F) Bmp7LacZ reporter mice. Neural crest cells in the nasal septum of P0 (G), P14 (H), and P30 (I) identified by Green Fluorescent Protein (GFP) (red) antibody. DAPI used to stain nuclei (gray). Scale bar=50µm. 3D frontal view of P30 $Bmp7^{ctrl}$ (J) and $Bmp7^{ncko}$ (K) mice demonstrating nasal septum deviation as outlined in white. (L) Quantification of NSD in P14 and P30 mice (n=4/genotype/age). 2D frontal crossection of nasal septum in $Bmp7^{ctrl}$ (M) and $Bmp7^{ncko}$ (N) mice. (O) Quantification of nasal septum deviation in $Bmp7^{ncko}$ mice over time (n=3/age). Data points represent individual mice with error bars demonstrating biological variation. ins: internasal suture; ns: nasal septum; p: perichondrium; i: incisor; m: mandible. P14: postnatal day 14; P30: postnatal day 30; P74: postnatal day 74. ***: $p<0.001$, 2-tailed independent t-test. n.s.: not significant. Scale bar (Figure 5.1A-F): 20µm and (Figure 5.1G-H): 50µm.

5.4.2 Apoptosis precedes nasal septum deviation and reduced GAGs observed in the deviated septum.

At P14, histological analysis of the nasal septum using H&E, Safranin O and Picrosirius Red showed a comparable cellular organization with round (mature/hypertrophic) cells restricted to the middle and flat (immature/chondrocyte progenitors) cells located at the periphery (Figure 5.2A; n=3/genotype). At P30, $BMP7^{ncko}$ cartilage had lost this clear organization. The degree of hypertrophy was reduced, fewer flat cells were evident at the periphery. Safranin O staining was reduced indicative of a reduction in GAGs. Deposition of collagen fibers was asymmetric with increased deposition on the outer side of the deviation and a reduction on the contralateral side (Figure 5.2B, n=3/genotype). Cellular proliferation (PCNA) was unaffected. Apoptosis, measured by cleaved Caspase 3 staining, was increased at P14 only with no apparent differences at P30. Thus, a burst of cell apoptosis precedes cellular disorganization and reduction in GAGs, indicating that changes to chondrocyte properties might predispose to the development of NSD.

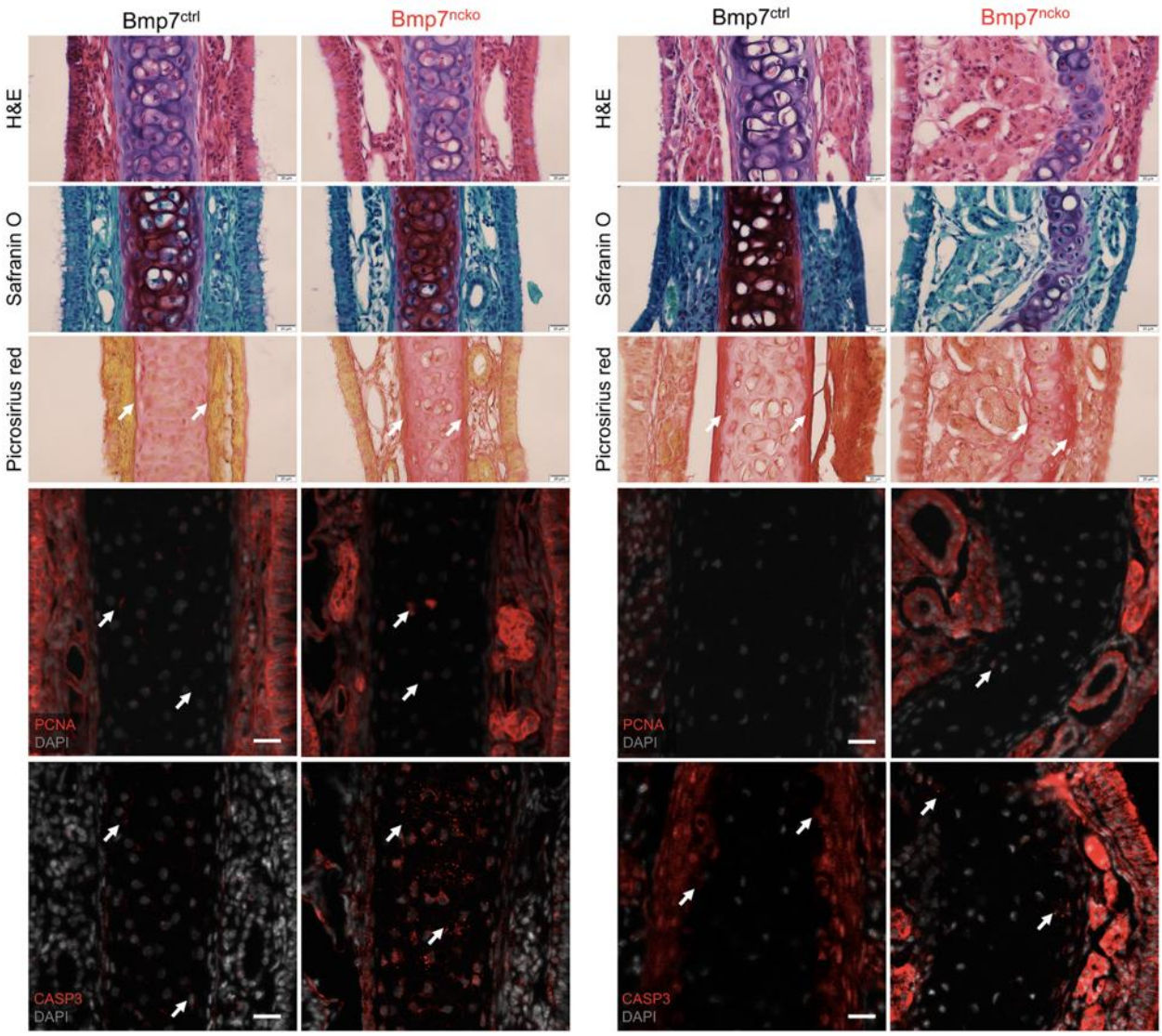

Figure 5. 2 Cell death altered glycosaminoglycan and collagen fibril organization observed in Bmp7^{ncko} mice.

Histological staining on nasal septum paraffin sections at P14 (A) and P30 (B) timepoints (n=3/genotype/age). Hematoxylin (purple) and Eosin (pink) (H&E) staining for gross morphology of the nasal septum. Representative Safranin O(red) staining for cartilage and Picrosirius Red (pinkish-red) staining for collagen fibres. Reduction in Safranin O staining was observed only in P30 Bmp7^{ncko} mice. To identify proliferation in the nasal septum, immunofluorescence staining using PCNA antibody (red) was performed with sections counterstained with DAPI for nuclei (gray). No changes to proliferation were observed. Apoptosis was characterized using CASP3 antibody (red) and counterstained with DAPI for nuclei (gray). Apoptosis precedes nasal septum deviation in Bmp7^{ncko} mice. PCNA: proliferating cell nuclear antigen; CASP3: cleaved caspase 3. Arrows denoting positive stain/signal. Scale bar (histological stains) = 20µm and (Immunos) = 50µm.

5.4.3 Proteins involved in extracellular matrix organization and cell metabolism deregulated before nasal septum deviation.

We performed shotgun proteomics (Figure 5.3A) on isolated P14 and P30 $BMP7^{ctrl}$ and $BMP7^{ncko}$ nasal septum (n=4/genotype/age) to identify potential proteome changes in the mutant septum before and following septum deviation. STRING database (https://string-db.org) was used to assign ontology and map protein-protein interactions. At P14, several clusters reflecting a decrease in proteins involved in extracellular structure organization, cell adhesion, and degradation of extracellular matrix were identified (Figure 5.3B), exemplified by Elastin (ELN), Collagen I (COL 1), Collagen II (COL 2), Osteopontin (SPP1), and Aggrecan (ACAN). Several of those proteins as well as reduced mTOR associate with the PI3K-AKT signalling pathway, indicating a reduction of this important pathway regulating cell proliferation, survival, and metabolism [275]. At the same time, a cluster of proteins involved in retinoic acid signaling and lipid metabolism, such as CYP1A2, and ALDH1A2, was upregulated. Together this suggested that loss of BMP7 is associated with a change in cell metabolism at P14.

At P30, when NSD is established, a rather different picture of proteome changes was observed (Figure 5.3C). An increase in proteins involved in the response to oxygen-containing compounds, catalytic activity, and cytoskeletal organization such as Decorin (DCN) was observed in $BMP7^{ncko}$ mice. In addition, changes in mRNA processing and nucleotide metabolic processes were observed. Of interest, the increase in Hexokinase 1 (HK1), Aldolase A (ALDOA) and Glyceraldehyde 3-phosphate dehydrogenase (GAPDH) indicated an increase in glycolysis and proteins involved in RNA metabolism, such as Heterogeneous nuclear ribonucleoprotein U (HNRPU), were also upregulated. In summary, we identified global dynamic changes to several cellular processes in BMP7-mutant nasal cartilage, most prominently extracellular matrix and cell

metabolism both prior to and once NSD is established. However, spatial information on the expression of these proteins in the septum is not known.

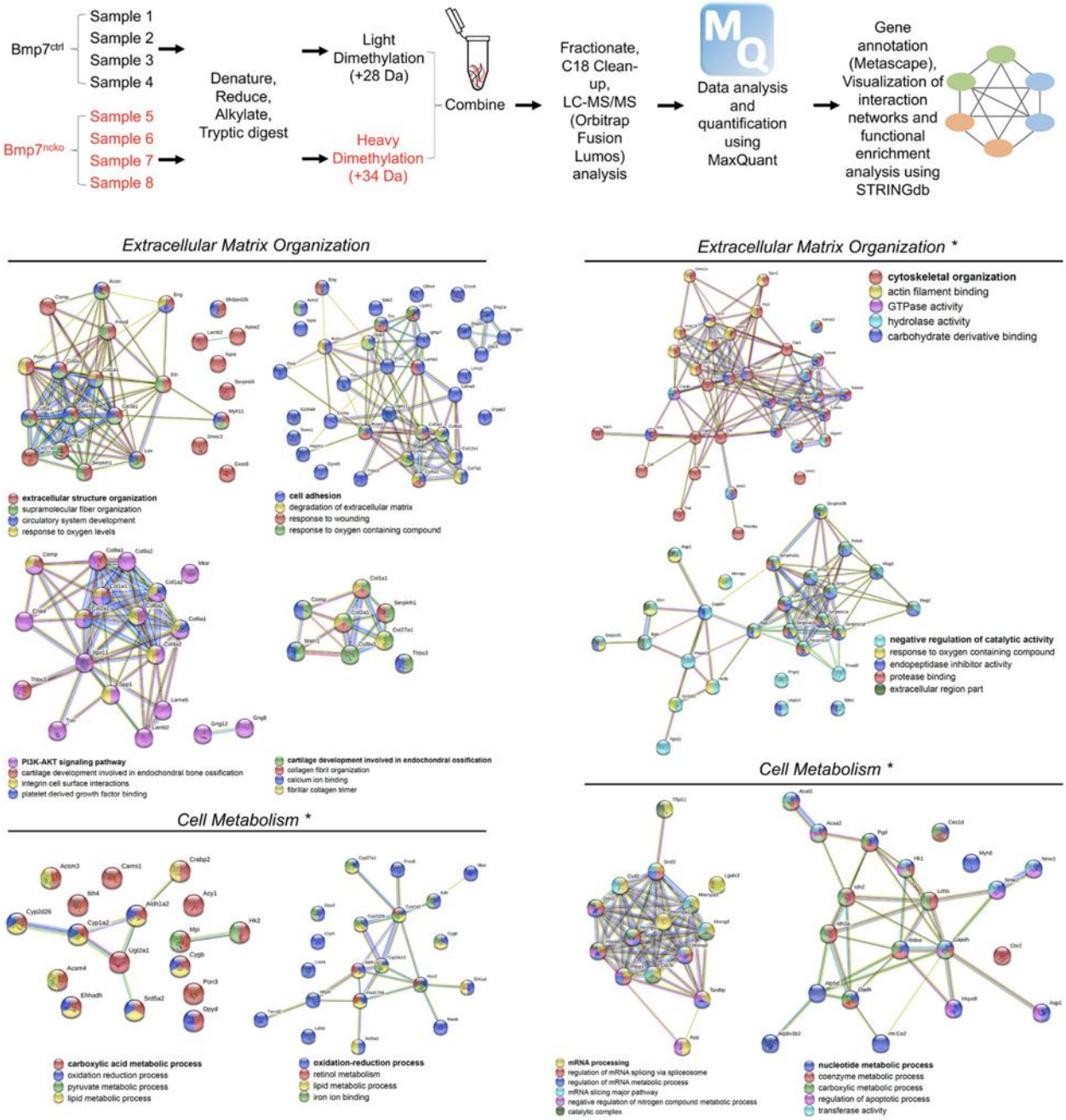

Figure 5. 3 Altered extracellular matrix (ECM) organization and cell metabolism precede nasal septum deviation in Bmp7^{ncko} mice.

(A) Workflow of Proteomics experiment and analysis (n=4/age/genotype). STRINGdb software was used to identify protein-protein interactions. (B) Differentially expressed proteins and their associated biological processes altered in P14 Bmp7^{ncko} mice in comparison to Bmp7^{ctrl}. (C) Differentially expressed proteins and their associated biological processes altered in P30 Bmp7^{ncko} mice in comparison to Bmp7^{ctrl}. *denotes proteins upregulated in Bmp7^{ncko} mice. Proteins involved in retinoic acid signaling and lipid metabolism were upregulated at 2 weeks whereas proteins involved in glucose metabolism were upregulated at 4 weeks. A list of all differentially regulated proteins is provided in the Supplemental Table 5.1&5.2.

5.4.4 Increase in markers abundantly expressed in hypertrophic chondrocytes and acquisition of elastic cartilage markers in deviated nasal septum of BMP7^{ncko} mice.

Gene expression analysis and immunofluorescence staining (n=3/age/genotype) was performed using antibodies against proteins identified in the proteomics data. We assessed expression of extracellular matrix components associated with hyaline cartilage, cartilage hypertrophy, and OA at P0, P14, P30 to capture the timing of any changes. We additionally compared these protein changes to changes in gene expression (Figure 5.4A). COL II was significantly increased at P0 BMP7^{ncko} mice ($p<0.05$) but became comparable by P30. Expression of COL VI, a pericellular matrix gene [276], was initially comparable but showed a significant reduction at P30 ($p<0.05$). However, protein expression was increased at the site of deviation. OPN, a gene involved in early chondrogenesis [85,277], was significantly reduced in P14 mutant nasal septum. Additionally, at P30, OPN protein expression was lost in a subset of cells that appear to extend from the perichondrium at the site of deviation. Thus, loss of BMP7 alters expression of several extracellular matrix components associated with chondrogenesis.

RUNX2 [259], COL X, IHH, CRTAC1 [278], Osteocalcin, and BAPX [279] have all been associated with hypertrophic differentiation of chondrocytes, with RUNX2, COL X and IHH being the most commonly assessed proteins for chondrocyte hypertrophy. Although RUNX2 gene expression (Figure 5.4B) was slightly increased at P0 ($p<0.01$), it did not show the increase seen in control mice at P14 ($p<0.01$). BMP7^{ncko} mice indicate early induction of genes typically expressed in hypertrophic chondrocytes. Antibody staining for RUNX2 at P0 confirmed increased expression. While expression of COL X was comparable at all stages, expression of IHH was significantly increased ($p<0.05$) in the mutant septum at P30. Antibody staining showed increased COL X and IHH in the deviated septum. Expression of both CRTAC1, a gene involved in

chondrocyte differentiation [278], and BAPX, an inhibitor of chondrocyte hypertrophy [279], was significantly upregulated at P14 and P30 (*=$p<0.05$, ***=$p<0.001$). Osteocalcin previously described to accumulate at the onset of hypertrophy [280] was significantly decreased at P14 ($p<0.001$) but increased at P30 ($p<0.05$) in $BMP7^{ncko}$ mice. These observations indicate that the development of NSD appears to be associated with altered regulation of markers commonly associated with hypertrophic chondrocytes.

A key function of hyaline cartilage is to provide stiffness and rigidity to the nasal cavity. Given the significant molecular changes that precede the development of the deviation, we wondered whether the structural deformation might be the associated with the acquisition of elastic cartilage markers that are not normally seen in hyaline cartilage. Immunofluorescence staining for Elastin (ELN), a protein abundant in elastic cartilage, revealed that loss of BMP7 resulted in Elastin expression at the abutment and the middle region of the septum, suggesting that at least parts of the nasal septum indeed might have acquired elastic cartilage properties (Figure 5.4C). This potential switch to elastic cartilage markers in P30 $BMP7^{ncko}$ mice was supported by an increase in Emilin3 expression ($p<0.01$), another characteristic elastic cartilage gene [281]. Additional evidence for structural changes and alterations to collagen fibrils (Figure 5.2B) came from the altered distribution of Decorin (DCN) and HSP47 [282] in P30 $BMP7^{ncko}$ mice.

Collectively, our data suggest that NSD is associated with altered cartilage properties, in particular a gain in expression of elastic cartilage markers.

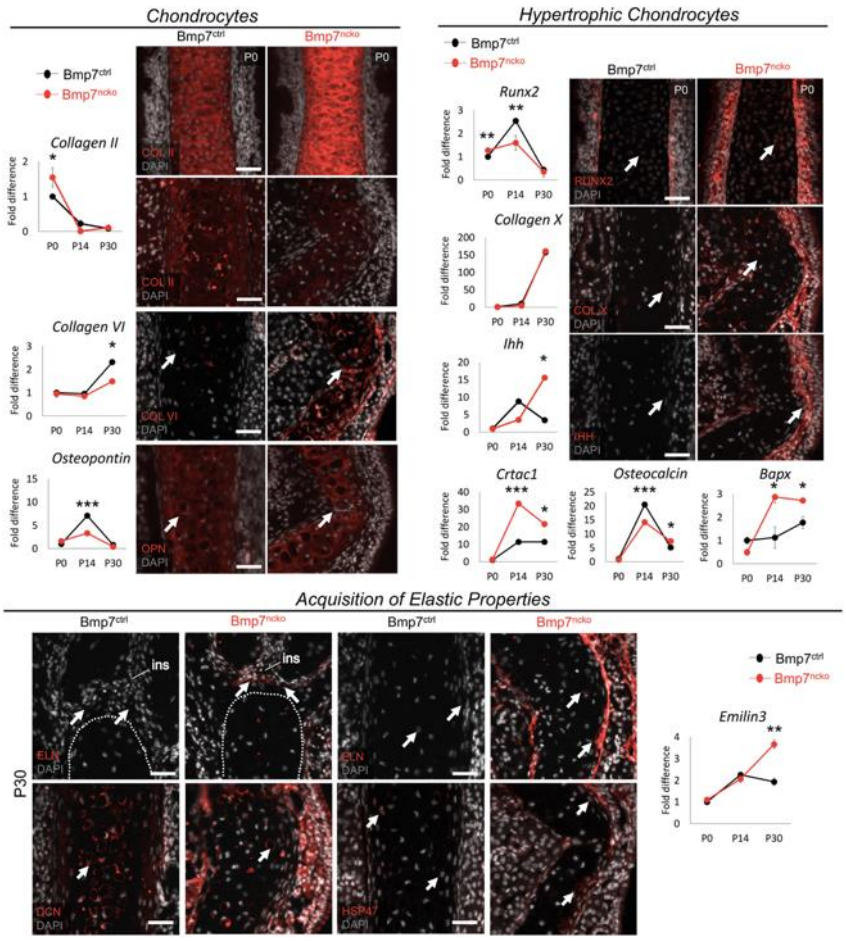

Figure 5. 4 Bmp7^{ncko} mice demonstrate an increase in expression of chondrocyte hypertrophy markers and acquire elastic cartilage markers.

(A) qRT-PCR of dissected nasal septum demonstrating differential gene expression of Collagen II (COL II), Collagen VI (COL VI) and Osteopontin (OPN) at P0, P14 and P30 timepoints. Immunofluorescence staining of COL II revealed an increase at P0 (top panel) and a decrease at P30 (bottom panel). Expression of COL VI was increased in the Bmp7^{ncko} mice while reduced expression of OPN was observed in P30 mutant mice via immunofluorescence. (B) Differential gene expression of genes involved in chondrocyte hypertrophy RUNX2, Collagen X (COL X), Indian hedgehog (IHH), Cartilage acidic protein 1 (CRTAC1), Osteocalcin, and Bapx) indicating that Bmp7^{ncko} mice demonstrate an increase in markers expressed in hypertrophic chondrocytes.. Immunofluorescence staining of P0 nasal septum demonstrates an increase in RUNX2 expression in addition to an increase in expression of COL X and IHH in P30 Bmp7^{ncko} mice. (C) Expression of Elastin (ELN) was observed in the abutment of the nasal septum and internasal suture (ins) as well as in the middle of the nasal septum in P30 Bmp7^{ncko} mice. EMILIN3 expression was also significantly increased at P30 in the mutant mice. Expression of Decorin (DCN) and SERPINH1 (HSP47) were also identified to be increased in the mutant nasal septum. Independent two-tailed t-test was performed with significance denoted as *: $p<0.05$, **: $p<0.01$, ***: $p<0.001$. (n=3/genotype/age). Antibody expression demonstrated in red and DAPI stained nuclei in gray for all immunofluorescence images. Arrows denoting positive antibody signal. Scale bar = 50μm.

5.4.5 Increase in glycolytic activity may be a consequence of altered WNT and BMP signalling.

Proteome analysis at P30 revealed an increase in several key enzymes in the glycolysis pathway (HK1, ALDOA, GAPDH and Lactate Dehydrogenase B (LDHB) [283] in the mutant septum (Figure 5.3C). Immunofluorescence analysis of HK1 confirmed the increased expression in the deviated nasal septum (Figure 5.5A). Proteins involved in RNA metabolism like HNRPU were also identified (Figure 5.3C), and its increased expression was confirmed in P30 $BMP7^{ncko}$ mice. The glycolysis pathway is under control of WNT and BMP signaling pathways [283]. Probing for changes in these two pathways, we identified altered expression of various WNT ligands (WNT3A, WNT6, WNT7A), WNT antagonists (FRZB, DKK1) culminating in increased WNT signalling (NPBC) in mature chondrocytes of the P30 mutant septum (Figure 5.5B). In general, the changes were largest at P14. WNT3A involved in canonical WNT signaling was decreased at P14 ($p<0.001$). The two other canonical WNT ligands WNT6 and WNT7A were upregulated at P14 ($p<0.05$) and P30 ($p<0.01$) [260]. The WNT-antagonists FRZB and DKK1 were upregulated and downregulated, respectively, in P14 mutant mice ($p<0.001$) and to a lesser degree at P30 ($p<0.05$). Overall, canonical WNT signalling apparent by nuclear NPBC staining was increased in the mutant septum, particularly at the site of deviation, whereas cytoplasmic NPBC staining was observed in $BMP7^{ctrl}$ mice. Loss of BMP7 was associated with a reduction in MSX1, a gene downstream of BMP signalling that promotes chondrogenic differentiation of NCC [284], at both P14 ($p<0.05$) and P30 ($p<0.001$) timepoints (Figure 5.5C). Gremlin 1 (GREM1), a BMP antagonist and inhibitor of chondrocyte hypertrophy [285], was significantly decreased once septum deviation was established. The BMP receptors ALK2 and ALK6, previously described to regulate chondrogenic differentiation [259], were decreased at P14 (ALK2; $p<0.001$) and P30 (ALK6; $p<0.01$), respectively.

Thus, the development of nasal septum deviation in BMP7^{ncko} mice is accompanied by a switch towards glycolysis along with dynamic changes in WNT and BMP signaling pathways.

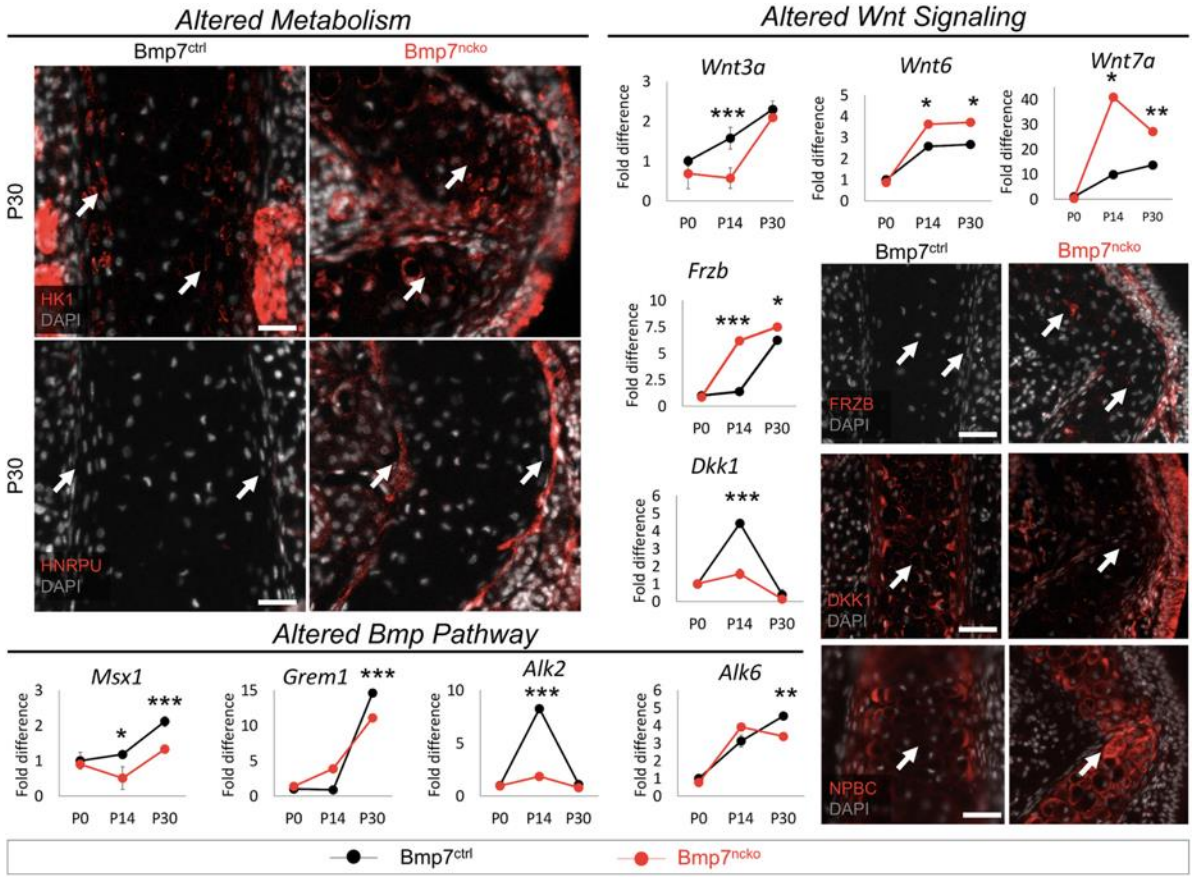

Figure 5. 5 Altered metabolism and Wnt signalling in P30 Bmp7^{ncko} mice.
(A) Immunofluorescence staining of Hexokinase (HK1) and Heterogeneous nuclear ribonucleoprotein U (HNRPU) in P30 Bmp7^{ctrl} and Bmp7^{ncko} mice revealed an increase in expression of both proteins in the mutant mice. (B) qRT-PCR of dissected nasal septum at P0, P14 and P30 timepoints demonstrating differential gene expression of Wnt ligands (WNT3A, WNT6, WNT7A) and Wnt antagonists (FRZB, DKK1). Immunostaining of Wnt antagonists (FRZB, DKK1) in P30 Bmp7^{ctrl} and Bmp7^{ncko} mice demonstrate an increase in expression of FRZB and decrease in DKK1 expression in the mutant mice. Immunofluorescence staining using Non-phosphorylated Beta-Catenin (NPBC) in P30 mice demonstrates nuclear expression in Bmp7^{ncko} and cytoplasmic expression in Bmp7^{ctrl} mice. (C) qRT-PCR of nasal septum at P0, P14 and P30 ages revealed alterations to genes in the Bmp pathway (MSX1, GREM1, ALK2, ALK6). Independent two-tailed t-test was performed with significance denoted as *: $p<0.05$, **: $p<0.01$, ***: $p<0.001$. (n=3/genotype/age). Antibody expression demonstrated in red and DAPI stained nuclei in gray for all immunofluorescence images. Arrows denoting positive antibody signal. Scale bar = 50µm.

5.4.6 Loss of BMP7 affects cell differentiation and cell metabolism processes already in P0 nasal septum.

Above experiments revealed that the most significant changes to gene expression could be observed at P14. However, some changes were already evident at birth. To systematically identify gene expression changes at P0, RNA-sequencing was performed on dissected P0 $BMP7^{ctrl}$ and $BMP7^{ncko}$ nasal septa (n=3/genotype). A Volcano plot identified both upregulated and downregulated genes, while the biological coefficient of variation within samples was between 0.4-0.5, within an acceptable range variation (Figure 5.6A). A heat map following unsupervised, hierarchical clustering was created (Figure 5.6B), and gene ontology (GO) was used to map differentially expressed genes to cellular processes, such as cell metabolism, cell differentiation, and cell and structure morphogenesis (Figure 5.6C). Validation of differentially expressed genes identified from RNA-Seq analysis demonstrated alterations to proliferation, apoptosis, cell metabolism, production of ROS, and BMP signalling. Individual genes validated by RT-qPCR mapped to significantly altered gene ontologies are shown in Figure 5.6D.

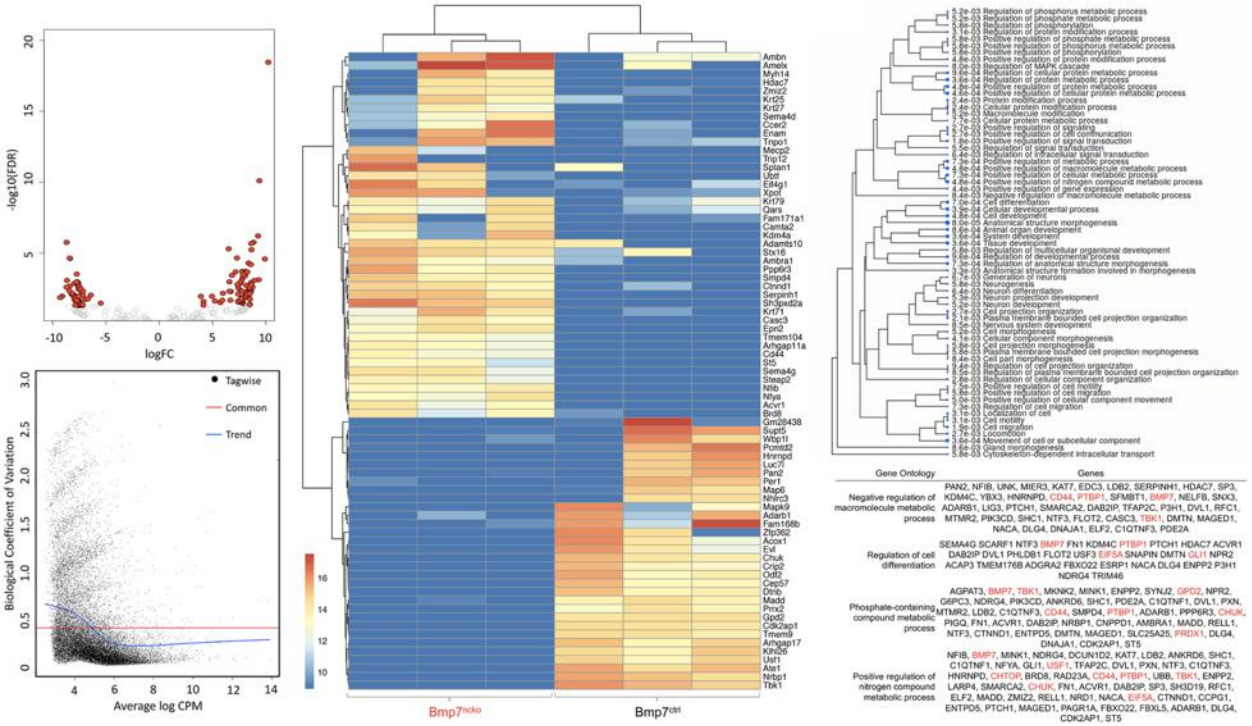

Figure 5. 6 RNA Sequencing analysis of P0 Bmp7^{ctrl} and Bmp7^{ncko} mice demonstrating differentially expressed genes (n=3/genotype).

(A) Volcano plot demonstrating genes differentially upregulated and downregulated. Additionally, the biological coefficient of variation plot indicating biological variation within the samples to be between 0.4-0.5. (B) Heat-map outlining differentially expressed genes between Bmp7^{ctrl} and Bmp7^{ncko} mice. (C) Gene ontology (GO) terms of genes identified to be differentially expressed. (D) Specific GO terms and their associated genes. Altered metabolic was a prominent GO term identified in the RNASeq analysis. Genes in red have been validated using qRT-PCR (Figure 5.7).

5.4.7 Early signs of altered cell proliferation, apoptosis, and metabolism in BMP7^{ncko} mice.

We first confirmed changes to proliferation and apoptosis in P0 septa from BMP7^{ctrl} and BMP7^{ncko} mice (n=3/genotype). Polypyrimidine Tract Binding Protein 1 (PTBP1) [286], RALY Heterogeneous Nuclear Ribonucleoprotein (RALY) [287] and Eukaryotic Translation Initiation Factor 5A (EIF5A) [288] known to promote cell proliferation were all significantly reduced in BMP7^{ncko} mice ($p<0.01$, $p<0.001$, $p<0.05$) (Figure 5.7A). Staining for PCNA confirmed the reduction in chondrocyte proliferation. In parallel, expression of genes promoting cell survival, such as Component Of Inhibitor Of Nuclear Factor Kappa B Kinase (CHUK) [289], TANK Binding

Kinase 1 (TBK1) [290] and Upstream Transcription Factor 1 (USF1) [291], was also significantly reduced ($p<0.05$) except for CHUK (Figure 5.7B). This was mirrored by increased levels of cleaved Caspase-3 (CASP3) and a reduction in mTOR [291].

Protein Arginine Methyltransferase 1 (PRMT1), Chromatin Target Of PRMT1 (CHTOP) and GLI Family Zinc Finger 1 (GLI1) impact glucose metabolism [292,293]. Both PRMT1 and CHTOP were significantly reduced ($p<0.001$) suggestive of impaired glucose metabolism already at P0. Conversely, genes involved in lipid metabolism and production of triglycerides and cholesterol (CD44 [294], Lipase E (LIPE) [295], mitochondrial Glycerol 3 Phosphate Dehydrogenase (GPD2) [296] were also altered. While CD44 was significantly increased ($p<0.001$), LIPE and GPD2 were significantly reduced ($p<0.01$) in the mutant septa (Figure 5.7C). Altered cell metabolism in chondrocytes has been associated with the production of ROS and stress response [297]. Indeed, Peroxiredoxin-1 (PRDX1), a ROS scavenger [298], was significantly reduced ($p<0.001$). Heat shock protein 47 (HSP47), an endoplasmic collagen-binding stress protein, was increased in $BMP7^{ncko}$ septa (Figure 5.7D). ROS can induce chondrocyte hypertrophy [299] in a BMP-dependant manner [298]. Several genes associated with hypertrophic chondrocytes and bone were indeed increased [Matrix metalloproteinase-13 (MMP13) ($p<0.001$), RUNX2 ($p<0.01$), Collagen I (COL 1) ($p<0.001$)] (Figure 5.7E), while phosphorylated SMAD1/5/8 (pSMAD1/5/8) was overall reduced (Figure 5.7F). Collectively, this establishes that loss of BMP7 changes the developmental trajectory of nasal chondrocytes already at birth long before septum deviation is manifested.

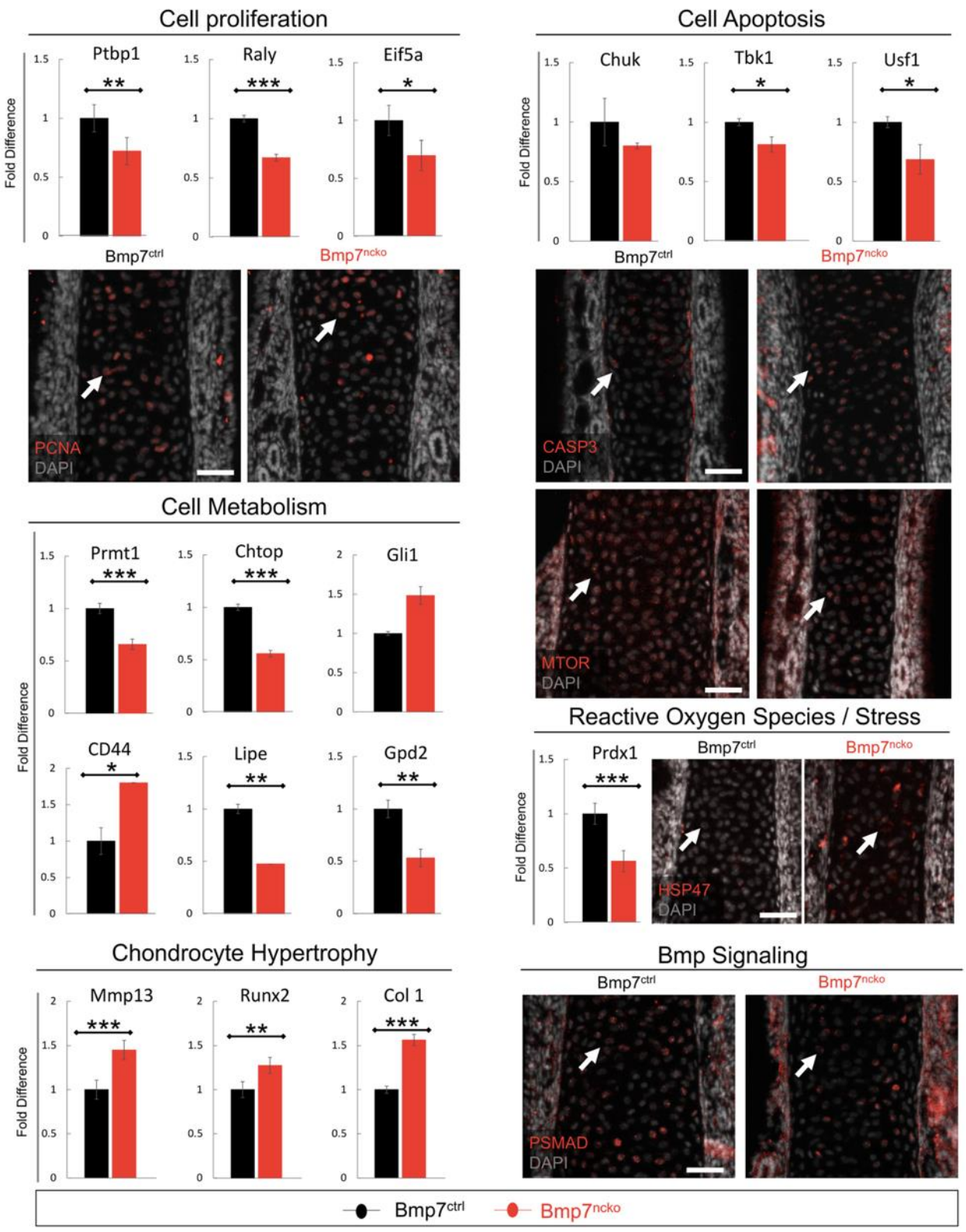
Cell proliferation
Ptbp1
Raly
Eif5a
Fold Difference
Bmp7ctrl
Bmp7ncko
PCNA
DAPI
Cell Apoptosis
Chuk
Tbk1
Usf1
CASP3
DAPI
Cell Metabolism
Prmt1
Chtop
Gli1
CD44
Lipe
Gpd2
MTOR
DAPI
Reactive Oxygen Species / Stress
Prdx1
HSP47
DAPI
Chondrocyte Hypertrophy
Mmp13
Runx2
Col 1
Bmp Signaling
PSMAD
DAPI
Bmp7ctrl
Bmp7ncko

Figure 5. 7 Altered cell proliferation, apoptosis and Bmp signalling precede nasal septum deviation.

qRT-PCR validation on P0 dissected nasal septum of genes identified in RNASeq analysis and immunofluorescence staining revealed alteration to (A) cell proliferation as evident by reduced PTBP1, RALY and EIF5a as well as PCNA expression in $Bmp7^{ncko}$ mice. (B) Increased cell apoptosis was observed as demonstrated by reduced expression of CHUK, TBK1, USF1, increased CASP3 expression and reduced mTOR expression. (C) Alterations to lipid metabolism were observed by a significant reduction in PRMT1, CHTOP, LIPE and GPD2 with an increase in CD44 expression. (D) A reduction in expression of PRDX1 and an increase in expression of stress protein HSP47 was observed. (E) An increase in MMP13, RUNX2 and COL 1 was observed in $Bmp7^{ncko}$ mice. (F) Bmp signalling assessed using immunofluorescence staining of PSMAD revealed a decrease in pSMAD in P0 $Bmp7^{ncko}$ mice. PTBP1: Polypyrimidine tract-binding protein 1, RALY: Heterogeneous Nuclear Ribonucleoprotein, EIF5A: Eukaryotic Translation Initiation Factor 5A, CHUK: Component Of Inhibitor Of Nuclear Factor Kappa B Kinase Complex, TBK1: TANK Binding Kinase 1, USF1: Upstream Transcription Factor 1, PRMT1: Protein Arginine Methyltransferase 1, CHTOP: Chromatin Target Of PRMT1, GLI1: GLI Family Zinc Finger 1, LIPE: Lipase E, GPD2: Glycerol-3-Phosphate Dehydrogenase 2, PRDX1: Peroxiredoxin 1, MMP13: matrix metalloproteinase 13, RUNX2: RUNX Family Transcription Factor 2, COL 1: Collagen I, PCNA: Proliferating Cell Nuclear Antigen, CASP3: Cleaved Caspase 3, MTOR: Mammalian Target of Rapamycin, HSP47: SERPINH1, pSMAD: Phosphorylated Smad. Independent two-tailed t-test was performed with significance denoted as *: $p<0.05$, **: $p<0.01$, ***: $p<0.001$. (n=3/genotype/age). Antibody expression demonstrated in red and DAPI stained nuclei in gray for all immunofluorescence images. Arrows denoting positive antibody signal. Scale bar = 50μm.

5.4.8 Reduction of BMP2 in $BMP7^{ncko}$ mice rescues nasal septum deviation.

While assessing changes to the BMP signaling pathway (Fig. 5.5C), we also tested for changes in BMP2 expression, another BMP involved in cartilage development [300]. Indeed, BMP2 was increased at P0 ($p<0.01$), failed to be induced at P14 but remained significantly increased at P30 ($p<0.05$) (n=3/age/genotype) (Figure 5.8A). BMP2 and BMP7 have been shown to exert opposite effects on chondrocyte hypertrophy induction [259]. To assess if the increase in BMP2 directly contributes to the development of NSD, we genetically reduced BMP2 in $BMP7^{ncko}$ mice (subsequently $BMP2^{het}BMP7^{ncko}$). To our surprise, the nasal septum in P30 $BMP2^{het}BMP7^{ncko}$ mice remained straight (Figure 5.8B-C), the deviation observed in $BMP7^{ncko}$ appeared to be

completely rescued ($p<0.01$) (Figure 5.8D). Some key changes identified in the deviated septum were also fully or partially rescued (Fig. 5.8E-G). ELN was not induced anymore (Figure 5.8E), HNRPU and HK1 demonstrated a partial reversal (Figure 5.8F), while FRZB and NPBC were comparable to $BMP7^{ctrl}$ mice (Figure 5.8G). These findings indicate that the net balance of BMP signaling is critical for chondrocyte differentiation and that this balance also affects canonical WNT signaling, a key regulator of energy metabolism, including glycolysis.

Together, our data establish an unexpected complex etiology for the development of NSD involving both BMP and WNT signaling. Changes to these pathways are associated with changes to chondrocyte specification, subsequent differentiation involving many cellular pathways including cell metabolism as summarized in Figure 5.9. Thus, a detailed assessment of extracellular matrix, cell metabolism and signalling properties are required when developing effective treatments and tissue engineering approaches for septoplasties.

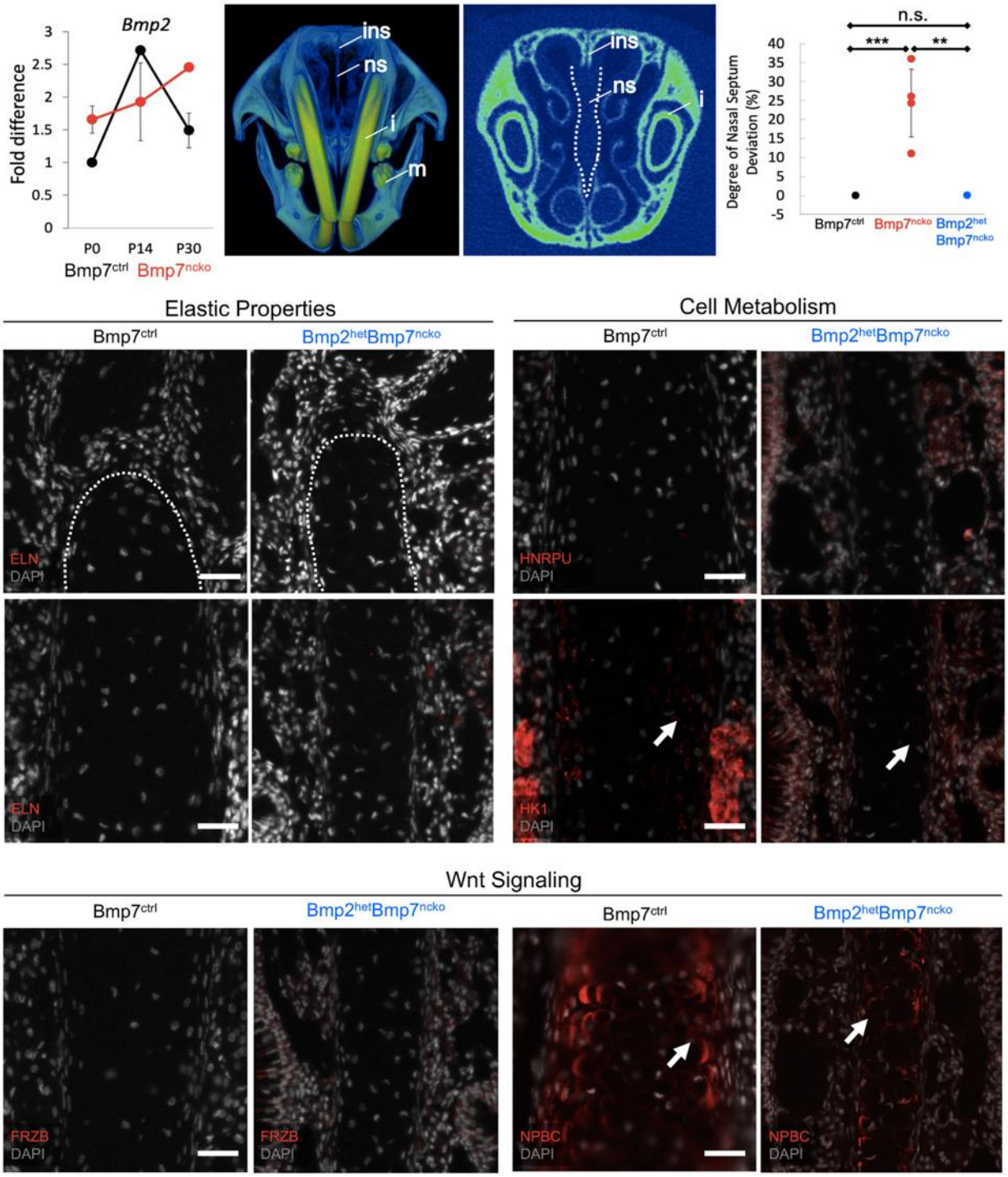
Bmp2
Fold difference
3
2.5
2
1.5
1
0.5
0
P0
P14
P30
Bmp7ctrl
Bmp7ncko
ins
ns
i
m
ins
ns
i
n.s.
***
**
Degree of Nasal Septum Deviation (%)
40
35
30
25
20
15
10
5
0
-5
Bmp7ctrl
Bmp7ncko
Bmp2het Bmp7ncko
Elastic Properties
Bmp7ctrl
Bmp2hetBmp7ncko
ELN
DAPI
ELN
DAPI
Cell Metabolism
Bmp7ctrl
Bmp2hetBmp7ncko
HNRPU
DAPI
HK1
DAPI
Wnt Signaling
Bmp7ctrl
Bmp2hetBmp7ncko
FRZB
DAPI
FRZB
DAPI
Bmp7ctrl
Bmp2hetBmp7ncko
NPBC
DAPI
NPBC
DAPI

Figure 5. 8 Reduction of BMP2 in $Bmp7^{ncko}$ mice rescues the nasal septum deviation.
qRT-PCR of P0, P14, P30 dissected nasal septum revealed an increase in BMP2 expression at P30 in $Bmp7^{ncko}$ mice. (B) 3D frontal view of P30 $Bmp2^{het}Bmp7^{ncko}$ mouse demonstrating a straight nasal septum. (C) 2D overview of nasal septum (outlined in white). (D) Quantification of nasal septum deviation in $Bmp2^{het}Bmp7^{ncko}$ mice revealed no significant difference between $Bmp7^{ctrl}$ and $Bmp2^{het}Bmp7^{ncko}$. Note that the data for $Bmp7^{ctrl}$ and $Bmp7^{ncko}$ is repeated from Figure 5.1L. (E) No expression of Elastin (ELN) was observed in P30 $Bmp2^{het}Bmp7^{ncko}$ mouse. (F) Immunofluorescence staining of Heterogeneous nuclear ribonucleoprotein U (HNRPU) in P30 $Bmp7^{ctrl}$ and $Bmp2^{het}Bmp7^{ncko}$ mice was comparable, however, staining with Hexokinase (HK1) showed a reduction in expression of HK1 in the $Bmp2^{het}Bmp7^{ncko}$ mouse. (G) Expression of FRZB between P30 $Bmp7^{ctrl}$ and $Bmp2^{het}Bmp7^{ncko}$ mice was comparable but a slight reduction in Non-Phosphorylated Beta-Catenin (NPBC) was observed in $Bmp2^{het}Bmp7^{ncko}$ mice. However, both $Bmp7^{ctrl}$ and $Bmp2^{het}Bmp7^{ncko}$ mice demonstrated cytoplasmic expression of NPBC. Ins: internasal suture; ns: nasal septum; i: incisor; m: mandible. Independent two-tailed t-test was performed with significance denoted as *: $p<0.05$, **: $p<0.01$, ***: $p<0.001$. (n=3/genotype/age). Antibody expression demonstrated in red and DAPI stained nuclei in gray for all immunofluorescence images. Arrows denoting positive antibody signal. Scale bar = 50μm.

Figure 5. 9 Cartilage changes observed in Bmp7^{ncko} mice.
(A) Altered cartilage properties, signalling and cellular processes observe over-time in Bmp7^{ncko} mice. Proteomics analysis revealed proteins involved in retinoic acid signaling at 2 weeks (B) and glucose metabolic process at 4 weeks (C).

5.5 Discussion

This study provides the first detailed characterization of the molecular and cellular etiology of NSD in a well-characterized model of midfacial hypoplasia associated with nasal airway obstruction [262]. We uncovered that the deviated cartilage expressed several markers

abundant in elastic cartilage and showed hallmarks commonly associated with osteoarthritic cartilage. This suggests a fundamental change in cartilage properties and highlights the complex etiology of nasal septum deviation and likely has ramifications for other hyaline cartilage-related pathologies.

NSD is classified based on the type of shape changes [301,302]. Some forms of NSD result from uncoordinated growth of the septum and its articulating structures (vomer, ethmoid, nasal bones) resulting frequently in facial asymmetries. While in those cases underlying cartilage defects are unlikely, cartilage defects have been proposed in other situations [301]. Why in some cases the septal hyaline cartilage would catastrophically fail has remained unclear. In the BMP7^{ncko} mouse, the initially straight septum gives way to a C-shaped kink, which is additionally associated with a growth defect resulting in midfacial hypoplasia [262]. C or S-shaped deviations are commonly observed in neonates. It is unclear to what degree cartilage growth abnormalities are already pre-existing *in utero* or can be attributed to trauma to the face during birth [303].

Nasal cartilage growth in mice occurs in two phases. Rapid growth between P0-P14 and from P21 onwards [27,85] is interrupted by a period of limited to no growth in between. A similar bimodal nasal growth occurs also in humans with significant growth occurring between 3-4 years and 11-12 years [304]. The onset of septum deviation in BMP7^{ncko} mice prior to the second growth phase coincides with the increased prevalence of NSD in adolescents [218]. While the first phase of septum growth is governed by cell proliferation, growth during the second phase occurs predominantly through cell hypertrophy [85]. BMP7 is expressed in and around the nasal cartilage at all stages, with the lowest expression observed at the P14 time-point. Given this cellular and molecular heterogeneity, we investigated three time-points (P0, P14, P30) to understand if and when changes to the nasal cartilage manifest. Discrete changes were already observed at birth

when chondrocytes were still immature [85,305] suggesting that BMP7 controls aspects of early chondrocyte differentiation, although the forming cartilage is histologically inconspicuous until at least P14. The largest proteome and gene expression differences were observed at P14. Substantial apoptosis was accompanied by reduced protein levels for markers expressed in hypertrophic chondrocytes (RUNX2 and IHH) and increased presence of proteins inhibiting hypertrophy (BAPX, FRZB, GREM1) in BMP7^{ncko} mice. This picture was changed at P30, where an increase in proteins associated with hypertrophic chondrocytes (COLX and IHH) was observed. Thus, the earliest changes identified already suggest a change in chondrocyte properties towards an elastic cartilage phenotype. Around P14, when septum growth switches from proliferation to hypertrophic growth, this change leads to catastrophic apoptosis, midfacial hypoplasia, and because of altered chondrocyte properties, septum deviation. Our data is compatible with a transformation of hyaline cartilage to elastic cartilage and a subsequent loss of mechanical resistance. The reduction of collagen fibril network at the deviated side is suggestive of reduced stiffness [306]. The contralateral increase in collagen fibrils might indicate an attempt to stabilize the septum. Interestingly, both BMP7 and GREM1 [307] are expressed at sites of Elastin expression, suggesting that these genes may contribute to chondrocyte remodelling and cartilage specification. Most of the changes were initially observed in the perichondrium rather than mature chondrocytes, the site where cartilage progenitor cells reside [308]. Cell death within the cartilage may activate these chondrocyte progenitor cells to replace dying cells [309]. These perichondrial cells express MFAP5, another gene found in elastic cartilage [310]. We propose that these MFAP5 expressing cells in the perichondrium precipitate the proposed switch from hyaline to elastic cartilage. More detailed lineage tracing of perichondrial-derived cells will be required to shed further insights into the mechanism underlying the cartilage switch.

We used quantitative shotgun proteomics to characterize cellular consequences of this change in cartilage properties and understand why chondrocytes might undergo apoptosis. Focusing on cellular metabolism, we found that mTOR, an established suppressor of autophagy [311], was decreased at P14. Several members of the cytochrome P450 (CYP) family [312,313], which are involved in the maintenance of white adipose-tissue, and other proteins involved in retinoic acid signaling and lipid metabolism were increased. BMP7 has an established role in adipocyte lineage determination, promoting brown adipogenesis at the expense of white adipocytes [314]. These two adipocyte lineages are characterized by very different cell metabolism, with brown adipocytes specialized in thermogenesis through uncoupling mitochondrial energy production. It is thus possible that BMP7 in nasal chondrocytes similarly controls specification of different cartilage-types.

An increase in autophagy and metabolic changes have been described to delay the progression of OA [315]. Thus, these two changes might reflect protective mechanisms to delay cartilage degradation in the septum. It is not clear whether all or only a subset of chondrocytes shows these changes, whether these changes occur within the same chondrocyte, and whether these changes are directly associated with the observed cell death. A clue might come from the P30 data where an increase in classical chondrocyte hypertrophy markers (IHH, COLX), as well as an upregulation of proteins involved in glycolysis, was observed. Hollander et al [316] demonstrated that hypertrophic chondrocytes express higher levels of glyceraldehyde-3-phosphate dehydrogenase (GAPDH) and lactate dehydrogenase (LDH), two proteins upregulated in P30 $BMP7^{ncko}$ mice. It is possible that the cells surviving at P14 might be those that switched to glycolysis, and the cells with increased lipid metabolism are destined to die. While further studies are required to resolve these possibilities, our data strongly suggest that BMP7 controls early

chondrocyte differentiation along different developmental trajectories (hyaline versus elastic cartilage). Whether these trajectories correspond to truly different cell lineages as described for brown/white adipocytes needs to be shown.

It has been shown that BMP7 is not the only BMP controlling adipocyte differentiation. BMP2 is an inducer of white adipose tissue [317]. BMP2 and BMP7 belong to different BMP subgroups. Whereas the former is the orthologue of *Drosophila Melanogaster* Decapentaplegic, latter is the orthologue of glass-bottom-boat and belongs to the 60A group [264]. In BMP7 control septum, BMP2 was dynamically expressed during nasal septum maturation, with peak expression seen at P14, and expression was low at P30. In the $BMP7^{ncko}$ mouse, BMP2 induction at P14 was stunted, but expression was substantially increased at P30. The increase in BMP2 at P30 in BMP7-deficient cartilage might suggest an attempt of molecular compensation. If so, the reduction of BMP2 in $BMP7^{ncko}$ mice would be expected to lead to more severe NSD. BMP2/BMP7 double neural crest-knockout mice die at birth. We thus created BMP2 heterozygous/$BMP7^{ncko}$ mice. The reduction in BMP2 prevented acquisition of elastic markers and partially restored cell metabolism. In primary chondrocytes, BMP2 has been shown to increase glucose metabolism during endochondral ossification [283], hypertrophy in chondroprogenitor cells [259] and has been associated with cartilage degradation in OA cartilage [318]. We thus propose that the balance between BMP2 and BMP7 rather than the individual signals controls chondrocyte metabolism and differentiation. Our findings not only illustrate how metabolic requirements change during chondrocyte maturation, but that metabolic differences themselves appear to be associated with different cartilage properties. Whether altered metabolism drives the change in chondrocyte properties or is a consequence of altered chondrocyte properties remains to be established. Increase in proteins expressed in hypertrophic chondrocytes (COLX, IHH) and change to glucose metabolism

observed in the deviated septum are hallmarks of knee OA [319]. In addition, several other similarities were observed. COL2 and OPN are reduced in both knee OA [320,321] and NSD. COL VI, a pericellular matrix protein upregulated in OA [322] was also increased in NSD. Alterations in the extracellular matrix may affect mechanosensation leading to cellular stress [320] and might directly contribute to an increase in apoptosis.

WNT signalling controls cell growth, differentiation, motility, and cell metabolism. In cartilage, canonical WNT signalling has been shown to promote chondrocyte hypertrophy [258,318,323]. As BMP and WNT signaling often cross-talk [233,264], we probed for changes in WNT pathway genes. Loss of BMP7 led to a changed expression of several WNT ligands (increase in WNT6 and WNT7A, decrease in WNT3A), WNT antagonists (increase in FRZB, decrease in DKK1), and overall activation of canonical WNT signaling evidenced by nuclear localization of non-phosphorylated β-catenin [233]. The reduction in BMP2, in addition to preventing Elastin expression and metabolic changes, also readjusted canonical WNT signalling. Which of these effects is a direct consequence of restored WNT signaling or is the direct result of rebalanced BMP signaling is currently unclear. For instance, septum deviation is associated with increased mechanical strain [151], which itself is linked to an increase in canonical WNT signalling [324]. However, the rescue of NSD highlights the need to understand how this balanced signaling controls normal nasal and possibly wider midfacial growth. Identifying commonalities and differences between BMP and WNT signaling will be critical to get a better handle on this molecular complexity. Nevertheless, this study clearly establishes the critical involvement of BMP and WNT signaling in the etiology of NSD. The magnitude and timing of alterations in these signaling pathways might determine onset and severity of NSD and its associated symptoms.

In summary, our findings demonstrate that a multifactorial etiology underlies midfacial hypoplasia-associated NSD. At present, it is not clear which of these changes are a direct consequence of lack of BMP7, and which changes develop as consequence. It is also not clear whether cellular changes (e.g. cell metabolism, hypertrophy) or associated tissue level changes (e.g. thinner septum) predispose or lead to septum deviation. The $BMP7^{ncko}$ mouse model presents a genetic basis relevant for cartilage development and pathologies pertaining to not just the nasal septum but hyaline cartilage in general. It also points to the possibility that cartilage type is specified at an early developmental stage and that BMP7 might be a contributing factor. Our data further suggest that cartilage from different origins may share similarities but are differently programmed to meet the requirements of the location the cartilage resides in. The similarities observed in NSD to OA validate to some extent the beneficial outcomes observed when nasal cartilage is transplanted in place of articular cartilage to treat OA. Henceforth, the changes described in $BMP7^{ncko}$ mouse model pre- and post- establishment of septum deviation could be relevant for better understanding of OA and other cartilage pathologies. Significant advances in understanding endochondral ossification and cartilage transdifferentiation into bone have been made; however, it is still not clear how different types of cartilages are specified from chondrocyte progenitors. Understanding cartilage lineage specification will alleviate the clinical challenge of fibrocartilage being formed despite efforts to regenerate hyaline cartilage to treat OA [325]. Additionally, cell-based tissue engineering strategies such as autologous chondrocyte implantation (ACI) [129,326] or its more recent variant, matrix-assisted chondrocyte implantation (MACI) [327–329], to repair focal articular cartilage lesions will benefit strongly from understanding the cellular processes that simultaneously promote hyaline cartilage and mitigate fibrocartilage formation.

5.6 Supplemental Information

Supplemental Table 5. 1 Shotgun proteomics proteins from $Bmp7^{ncko}$ and $Bmp7^{ctrl}$ Nasal septum tissues at 2 weeks identified without constraint by enzyme specificity rules during spectrum-to-sequence matching.

Supplemental Table 5. 2 Shotgun proteomics proteins from $Bmp7^{ncko}$ and $Bmp7^{ctrl}$ Nasal septum tissues at 4 weeks identified without constraint by enzyme specificity rules during spectrum-to-sequence matching.

Supplemental Table 5. 3 List of All primer pairs used for qRT-PCR.

Gene Name	Primer Pair	Gene Name	Primer Pair
36B4	GTG TGT CTG CAG ATC GGG TA CAG ATG GAT CAG CCA GGA AG	COL II	TGGAAAAGACGGTGAGACGG GCTCCAGCTTCACCAGGAAT
COL VI	AAGGCCCCATTGGATTCCC CTCCCTTCCGACCATCCGAT	Osteopontin	AATCTCCTTGCGCCACAGAA GCAGTGACGGTCTCATCAGA
RUNX2	GCTCACGTCGCTCATCTTG ACACCGTGTCAGCAAAGC	COL X	TTCTGCTGCTAATGTTCTTGACC GGGATGAAGTATTGTGTCTTGGG
Indian Hedgehog (IHH)	CTCTTGCCTACAAGCAGTTCA CCGTGTTCTCCTCGTCCTT	CRTAC1	CAGTCACCAACTCAGTCCTGC CACAACGATCTCGAAGTCCCC
Osteocalcin	ATAGCTCGTCACAAGCAGGG TGACAAAGCCTTCATGTCCA	BAPX	CAGGCGTAACGCTGTCATC CAAGGACCTGGAGGAGGAA
Emilin3	GAGGTGAGCAACACATTACAGA TCCACGTATTCCTCTAGGAGC	WNT3A	TCACTGCGAAAGCTACTCCA CACCACCGTCAGCAACAG
WNT6	CTCCTACAGTGTGGTTGTCAGG GCGCATCCATAAAGAGTCTTGA	WNT7A	GGCTTCTCTTCGGTGGTAGC TGAAACTGACACTCGTCCAGG
FRZB	AGCCCGGATGACATAGTTGT AGTACTGGACACTGCAGAGGG	DKK1	GTCAGTGTGGTTCTTCTGGGA CCGGGAACTACTGCAAAAAT
MSX1	TCTCGGCCATTTCTCAGTCG AGCTGAGCTGTGGTGAAAGG	GREM1	CAGCTGTTGGCAGTAGGGTC ACAGCGAAGAACCTGAGGAC
ALK2	CCT TCA CAG TGG TCC TCG TT TGC TAA TGA TGA TGG CTT TCC	ALK6	TCC AGA GCT TCG TAA GAG CA ATT TGG CGC TGA GCT ATG AC
PTBP1	ATAAGAAGGAGAACGCACTTGTG TGATGCTTGGACAGTGTAATGC	RALY	ACTCTCGGGTCTTCATCGGAA GCGCTCATTGGCATACTGGA
EIF5A	CCATGTAAGATCGTCGAGATGTC ATTCCGTTTGATGTTGGGGAC	CHUK	GTCAGGACCGTGTTCTCAAGG GCTTCTTTGATGTTACTGAGGGC
TBK1	GGAGCCGTCCAATGCGTAT GCCGTTCTCTCGGAGATGATTC	USF1	CTGAAACCGAAGAGGGAACAG GTTGGGGTCAGGAAAAGTGG
PRMT1	CTTGGCTAATGGGATGAGCCT GCGTTGGGCTTCTCACTACTT	CHTOP	TAGGGCGTGGAGCTATGGG CCCTCTTCCCCGACCTATCA
GLI1	CCAAGCCAACTTTATGTCAGGG AGCCCGCTTCTTTGTTAATTTGA	CD44	TCGATTTGAATGTAACCTGCCG CAGTCCGGGAGATACTGTAGC
LIPE	CCAGCCTGAGGGCTTACTG CTCCATTGACTGTGACATCTCG	GPD2	GACTCTCTCCGTTTGCTCATTAC GGATGTCAAATTCGGGTGTGT
PRDX1	AGTCCAGGCCTTCCAGTTCACT GGCTTGATGGTATCACTGCCAG	MMP13	CTTCTGGCACACGCTTTTCC CTTCTGGCACACGCTTTTCC
COL I	TGTCCCAACCCCCAAAGAC CCCTCGACTCCTACATCTTCTGA	BMP2	GGAAGACGTCCTCAGCGAAT ACGGCTTCTTCGTGATGGAA

Supplemental Table 5. 4 Specification of antibodies used.

Antibody	Catalogue #	Antibody	Catalogue #
Green Fluorescent Protein (GFP)	Ab6556	Proliferating Cell Nuclear Antigen (PCNA)	sc-56
Cleaved Caspase 3 (CASP3)	Cell Signalling 9664s	Collagen II (COL II)	ab185430
Collagen VI (COL VI)	sc-377143	Osteopontin (OPN)	Ab8448
RUNX2	sc-390351	Collagen X (COL X)	sc-59954
Indian Hedgehog (IHH)	sc-271101	Elastin (ELN)	sc-166453
Decorin (DCN)	ab175404	Heat Shock Protein 47 (HSP47)	sc5293
Hexokinase I (HK1)	sc-46695	Heterogeneous Nuclear Ribonucleoprotein U (HNRPU)	sc-32315
Frizzled Related Protein (FRZB)	sc-514350	Dickkopf-Related Protein 1 (DKK1)	ab61034
Non-Phosphorylated Beta-Catenin (NPBC)	Cell Signalling 19807	Mammalian Target Of Rapamycin (MTOR)	Cell signalling 2971
Phosphorylated-Smad (PSMAD)	Cell Signalling 13820s	Alexa Flour 647 goat anti-mouse IgG2a	A21241
Alexa Flour 647 goat anti-mouse IgG1	A21240	Alexa Flour 647 donkey anti-rabbit IgG (H+L)	A31573
Alexa Flour 647 goat anti-mouse IgG2b	A21242	DAPI (Molecular Probes)	D-1306

Chapter 6: Bmp7 regulates elastin expression

Chapter 5 demonstrated that nasal septum deviation was associated with acquisition of markers abundant in elastic cartilage. We wanted to further identify how the transition from hyaline to elastic cartilage characteristics is regulated. Thus, in Chapter 6, we suggest a role for Bmp7 in regulating elastin expression using *in vitro* primary chondrocyte pellet cultures.

6.1 Abstract

Nasal septum is a hyaline cartilage that undergoes changes to cartilage properties, including increase in proteins expressed in hypertrophic chondrocytes when the septum deviates. The molecular regulation underlying these cartilage changes is not well understood. Delineating this is imperative to better understand cartilage changes associated with nasal septum deviation (NSD) and are expected to directly benefit tissue engineering efforts in regenerating functionally stable nasal septum cartilage or even growing cartilage implants to repair damaged cartilage in knee osteoarthritis (OA). We previously described that neural crest deletion of Bmp7 ($Bmp7^{ncko}$) in mice results in the increase of proteins abundantly expressed in hypertrophic chondrocytes and acquisition of elastic cartilage characteristics. Hence, using the $Bmp7^{ncko}$ model, we assessed 1) when cartilage differentiation is specified and 2) whether Bmp7 directly regulates this differentiation. A three-dimensional (3D) chondrocyte pellet culture system using nasal chondrocytes from P7 and P30 $Bmp7^{ctrl}$ and $Bmp7^{ncko}$ mice identified that P7 nasal cartilage pellets demonstrate more plasticity when compared with P30 cartilage pellets. In P7 $Bmp7^{ctrl}$ and $Bmp7^{ncko}$ pellets, Insulin-Transferrin-Selenium (ITS) suppressed collagen II (COL II) expression and increased expression of elastin (ELN), a protein abundantly found in elastic cartilage. We also observed that concomitant treatment of recombinant Bmp7 and ITS suppressed expression of ELN. Together, this data suggests that cartilage types are determined at an early progenitor state and that chondrocytes have the capability to switch cartilage type. These findings challenge the current dogma surrounding cartilage differentiation and specification.

Key words: Nasal septum deviation, chondrocyte pellets, BMP7, ELN, COL II, ITS, chondrocyte properties.

6.2 Introduction

Nasal septum is a hyaline cartilage that divides the nasal cavity and provides structural support to the midface. In some cases, damage to the septum results in nasal septum deviation (NSD), which affects the functioning of the nasal cavity and predisposes individuals to breathing disorders such as obstructive sleep apnea[90]. Previous studies investigating nasal septum deviation using mice models[330,331] indicated that alterations to chondrocyte differentiation, such as an increase in proteins normally found in hypertrophic chondrocytes, contribute to the deformation of the septal cartilage. Additionally, we described in our previous work that mice with neural crest-specific deletion of Bone Morphogenetic Protein 7 (BMP7; $Bmp7^{ncko}$) present with molecular and cellular changes to their nasal septal cartilage that precede the pathological septum deviation. This includes acquisition of elastic cartilage properties, a switch to glucose metabolism, and acquisition of molecular characteristics commonly associated with early-stage osteoarthritis (OA). Instead of hyaline cartilage, a firm, resilient cartilage, the $Bmp7^{ncko}$ cartilage appears more elastic, responding to tension or compression with shape changes (septum deviation). Both studies were conducted *in vivo*, making it challenging to identify how these changes are directly regulated on a molecular level. Determining the molecular regulation underlying hyaline versus apparently elastic cartilage differentiation would significantly contribute to our understanding of how chondrocytes differentiate into different types of cartilages.

The current understanding of cartilage development suggests that cartilage differentiation occurs along a linear differentiation pathway. Starting with the condensation of mesenchymal progenitor cells, these progenitor cells differentiate into chondrocytes which can form hyaline cartilage, followed by further differentiation into hypertrophic chondrocytes as required for the formation of other cartilage types (elastic/fibrocartilage)[332]. This linear differentiation stems from

the evo-devo concept of cartilage development, for which the underlying basis is the fossil record and comparative biology studies. Evolutionarily, cartilage was thought to exist as two types: immature vs mature cartilage, where the immature cartilage exists during early stages of cartilage development, whereas the mature cartilage undergoes further differentiation to become hypertrophic[305]. However, this model doesn't explain when and how differentiation into the various cartilage types is regulated since not all cartilage types undergo hypertrophy. It might be early during cartilage development (immature cartilage) or at a late stage (mature cartilage)[85,305]. Hence, a three-dimensional (3D) chondrocyte pellet culture system using nasal chondrocytes from P7 and P30 $Bmp7^{ctrl}$ and $Bmp7^{ncko}$ mice was assessed to address this gap of when cartilage differentiation is specified.

We demonstrate that young nasal cartilage presents with plasticity regarding cartilage differentiation, whereas this plasticity is lost in the nasal cartilage from older mice. Addition of recombinant Bmp7 *in vitro* suppresses Elastin (ELN) expression, a protein abundantly found in the elastic cartilage. Collectively, our data suggest that cartilage types are determined at an early progenitor state, with immature chondrocytes having the ability to switch cartilage properties based on functional requirements.

6.3 Methods

6.3.1 Animal Model

Nasal septum of $Bmp7^{ctrl}$ (control) and $Bmp7^{ncko}$ (mutant) mice as previously described [264] were used in this investigation. Both male and female mice were used, and all the mice were maintained on the C57BL/6 background and backcrossed for at least 10 generations. Two time points were assessed, one before the significant changes to the nasal septum was observed (postnatal day 7; P7) and one when the septum was deviated (postnatal day 30; P30). All

experiments were conducted following the Canadian Council on Animal Care guidelines. Ethical approval for this study was given by the Health Sciences Animal Care and Use Committee at the University of Alberta (protocol #: AUP1149).

6.3.2 Tissue Dissection and Cell Isolation

Nasal septum cartilage was dissected from P7 and P30 $Bmp7^{ctrl}$ and $Bmp7^{ncko}$ mice, as demonstrated in Figure 6.1. Nasal cartilage samples were enzymatically digested as outlined by Anderson-Baron et al.[333]. The digested samples were passed through a 100μm nylon strainer. The nasal chondrocytes released from the digested cartilage were washed with sterile phosphate-buffered saline (PBS), resuspended in DMEM (D6429, Sigma) standard media, and plated in culture flasks. The flasks were incubated for 48 hours under normal atmospheric conditions.

6.3.3 Cell culture and Pellets

After 48 hours, media of the nasal chondrocytes was changed from standard media to expansion media as outlined in Anderson-Baron et al.[333]. Chondrocytes were expanded under normal atmospheric conditions (21% O_2, 5% CO_2) at 37°C, with culture media being changed every three days. Chondrocytes were expanded until they reached 90% confluency, at which point adherent cells were trypsinized, viable – trypan blue negative cells were counted using a hemocytometer. $2.5x10^5$ cells per pellet were distributed and centrifuged at 1500rpm for 7 minutes. The 3D pellets cultures rather than monolayer cultures were used since it has been previously reported that 3D cultures promote better chondrogenesis in addition to recapitulating a similar *in vivo* environment [334,335].

The pellets were then cultured in four different treatment conditions: chondrogenic media, chondrogenic media + Bmp7, Chondrogenic media + Insulin-Transferrin-Selenium (ITS) and chondrogenic media + ITS + Bmp7. The chondrogenic media condition evaluates the chondrocytes

response in the absence of a growth factor (Bmp7) and growth supplement (ITS). Whereas the chondrogenic media + ITS + Bmp7 tests the chondrocyte's response to the presence of growth factor and supplement. The chondrogenic media is a serum-free media composed of DMEM supplemented with 100 U/mL of penicillin and streptomycin (Gibco 15240-062), 2mM L-glutamine (Gibco 25030-081), 100mM of HEPES (Gibco 15630-080), 0.1µM of dexamethasone (Sigma, D2915), 0.1mM of ascorbic acid (Sigma, A8960), 0.1mM L-proline (Sigma, P5607-256). For treatment with Bmp7, 2.5ng/mL of Bmp7 (Peprotech, 120-03P) was used. For conditions requiring Insulin-Transferrin-Selenium (ITS, Sigma I2521), 1% ITS was used. Unlike several other studies [333,335,336], we didn't add ITS to the chondrogenic media and assessed its function in nasal chondrocytes separately as its function has not been clearly outlined other than a couple of studies stating that ITS prevents dedifferentiation and hypertrophy [336,337]. The pellets were in treatment conditions for 21 days, and media was changed every three days. After three weeks, histological and immunohistochemical analyses on the pellets were conducted.

6.3.4 Histology and Staining

After 21 days, the pellets were fixed in 4% paraformaldehyde (PFA) for 4 hours at room temperature and then washed with PBS, processed in increasing ethanol gradients and xylene and embedded in paraffin wax. Pellets were cut at 4 microns using an 820 Spencer microtome. The sectioned pellets were then deparaffinized using Xylene and decreasing ethanol gradients to be stained with Safranin O (SAF O) as previously described[85].

6.3.5 Immunofluorescence

The chondrocyte pellet sections were stained using Collagen II (COL II, ab185430) and ELN (sc-166453) following previously described immunofluorescence staining protocol[85]. Images were acquired on an Olympus IX73 microscope using 20X objectives for both safranin O and immunofluorescence staining.

6.4 Results

$Bmp7^{ctrl}$ and $Bmp7^{ncko}$ mice at P7 and P30 were dissected and cultured as per the workflow demonstrated in Figure 6.1A. The chondrocytes, after digest and expansion, maintain a flat spindle-like shape (Figure 6.1B). The chondrocyte pellets were treated using four conditions (Figure 6.1C). We specifically assessed expression of Collagen II (COL II) and Elastin (ELN) to address if, when and how Bmp7 regulates hyaline vs elastic cartilage characteristics. Additionally, we wanted to identify whether addition of recombinant Bmp7 to the cultures would revert elastic cartilage characteristics observed in $Bmp7^{ncko}$ mice to hyaline cartilage. Thus, we first assessed P30 nasal septa to investigate whether characteristics can be reverted once the cartilage has matured and septum deviation is established.

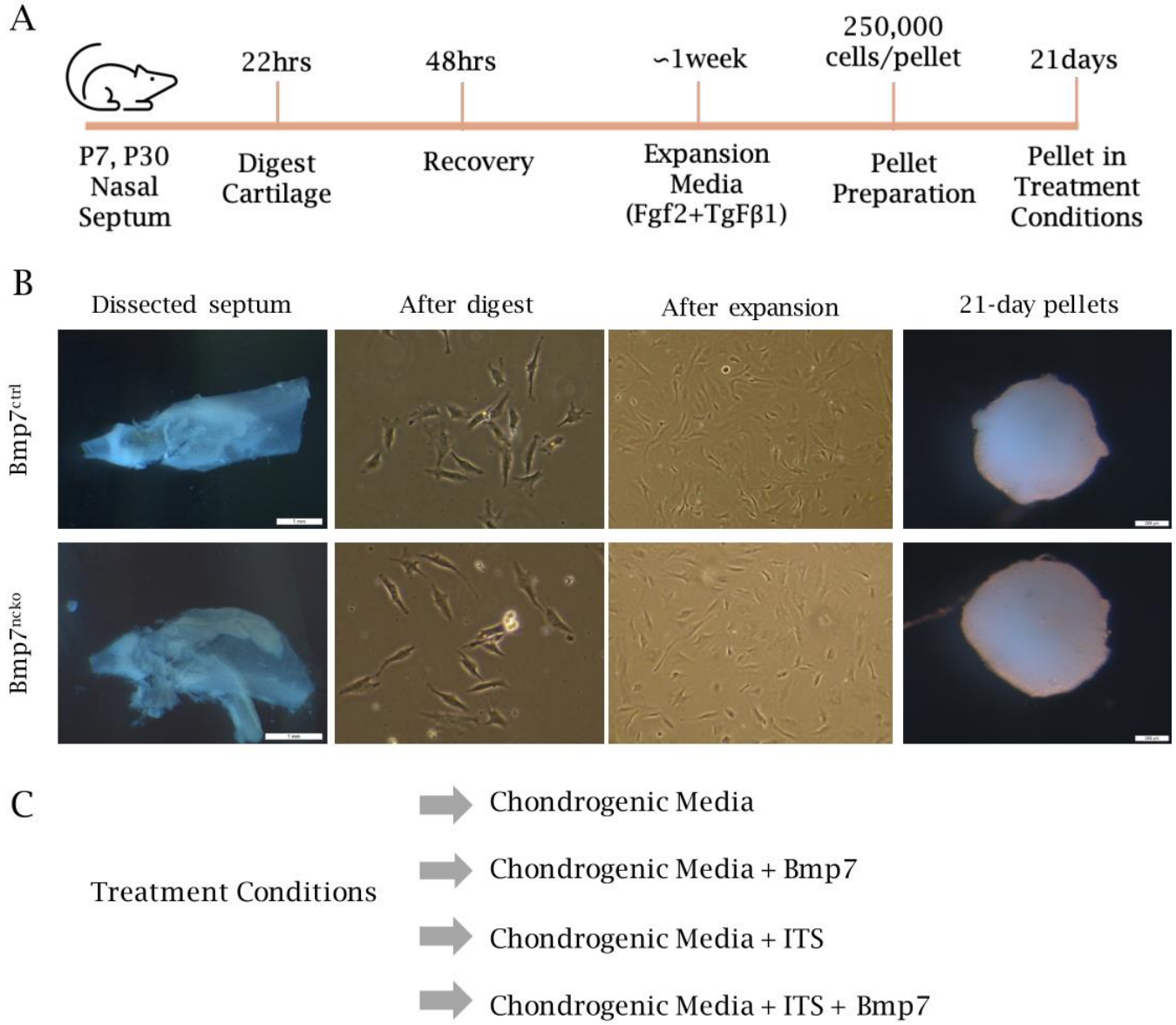

Figure 6. 1 Workflow of nasal chondrocyte pellet cultures.

(A) Nasal septum from P7 and P30 Bmp7^{ctrl} and Bmp7^{ncko} were used to set up nasal chondrocyte pellet cultures. (B) Images representing morphology of cartilage and chondrocytes during the process of making pellets. (C) Conditions that the pellets were treated with. P: postnatal, Bmp7: Bone Morphogenetic Protein 7; ITS: Insulin, Transferring, Selenium.

6.4.1 Addition of Bmp7 doesn't alter ELN expression in P30 Bmp7^{ctrl} nasal chondrocytes

Pellets from P30 Bmp7^{ctrl} nasal chondrocytes in chondrogenic media didn't show any SAF O staining (Figure 6.2). However, the addition of Bmp7 induces SAF O staining in the control pellets. The staining was even stronger under ITS and remained comparable when pellets were treated with ITS + Bmp7. Pellets stained with COL II, a protein abundantly present in nasal septum cartilage, were analogous with SAF O staining. Low expression of COL II was observed in pellets in chondrogenic media. However, addition of Bmp7 increases COL II expression, which then further intensifies under the presence of ITS + Bmp7. Pellets treated with ITS + Bmp7 expressed COL II in the centre as well as periphery, whereas expression was restricted to the periphery in the other treatment conditions. To our surprise, ELN expression was observed in the Bmp7^{ctrl} nasal chondrocytes before the addition of Bmp7 and/or ITS. However, neither addition of Bmp7 or ITS altered expression of ELN.

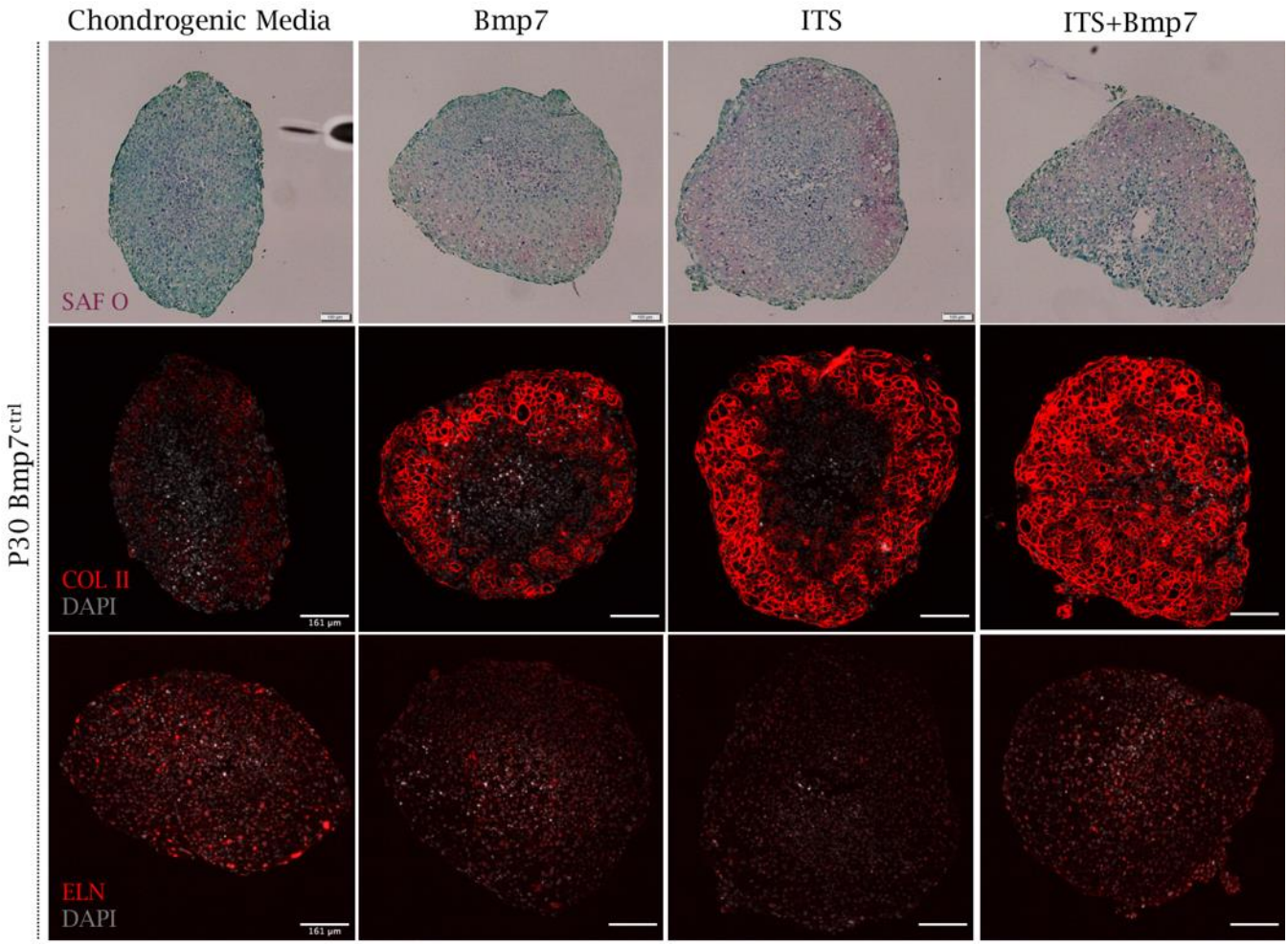

Figure 6. 2 P30 Bmp7^{ctrl} pellets demonstrate dynamic expression of SAF O and COL II.

SAF O staining was induced in the presence of Bmp7, ITS and ITS + Bmp7. COL II expression was similar to SAF O staining. No changes in ELN expression were observed when treated with Bmp7, ITS, and ITS + Bmp7. n = 3; SAF O: Safranin O; COL II: Collagen II; ELN: Elastin; P: postnatal, Bmp7: Bone Morphogenetic Protein 7; ITS: Insulin, Transferring, Selenium. Scale bar for SAF O stains is 100µm and for COL II and ELN is 161µm.

6.4.2 Addition of ITS + Bmp7 partially suppresses ELN expression in P30 Bmp7^{ncko} nasal chondrocytes

Assessment of P30 Bmp7^{ncko} pellets using SAF O demonstrated staining in all conditions (Figure 6.3). However, an increase in SAF O stain was observed in pellets treated with Bmp7. SAFO staining of pellets under the presence of ITS and ITS + Bmp7 were similar to that of pellets treated with Bmp7. COL II was expressed in the periphery of the pellets in all four treatment conditions. However, pellets treated with Bmp7 demonstrated COL II expression in the centre. Similar to Bmp7^{ctrl} pellets, expression of ELN was observed in all four treatment conditions in the Bmp7^{ncko} pellets. However, unlike control chondrocyte pellets, expression of ELN was slightly increased when Bmp7^{ncko} pellets were treated with ITS and decreased in the presence of ITS + Bmp7. This is suggestive that ITS + Bmp7 can partially suppress ELN expression. Since P30 Bmp7^{ncko} chondrocyte pellets demonstrate that it is challenging to alter cartilage characteristics once nasal septum deviation is established, we thus assessed nasal chondrocyte pellets from P7 Bmp7^{ctrl} and Bmp7^{ncko} mice to identify whether characteristics of chondrocytes can be altered before the establishment of septum deviation such that this pathology can be prevented.

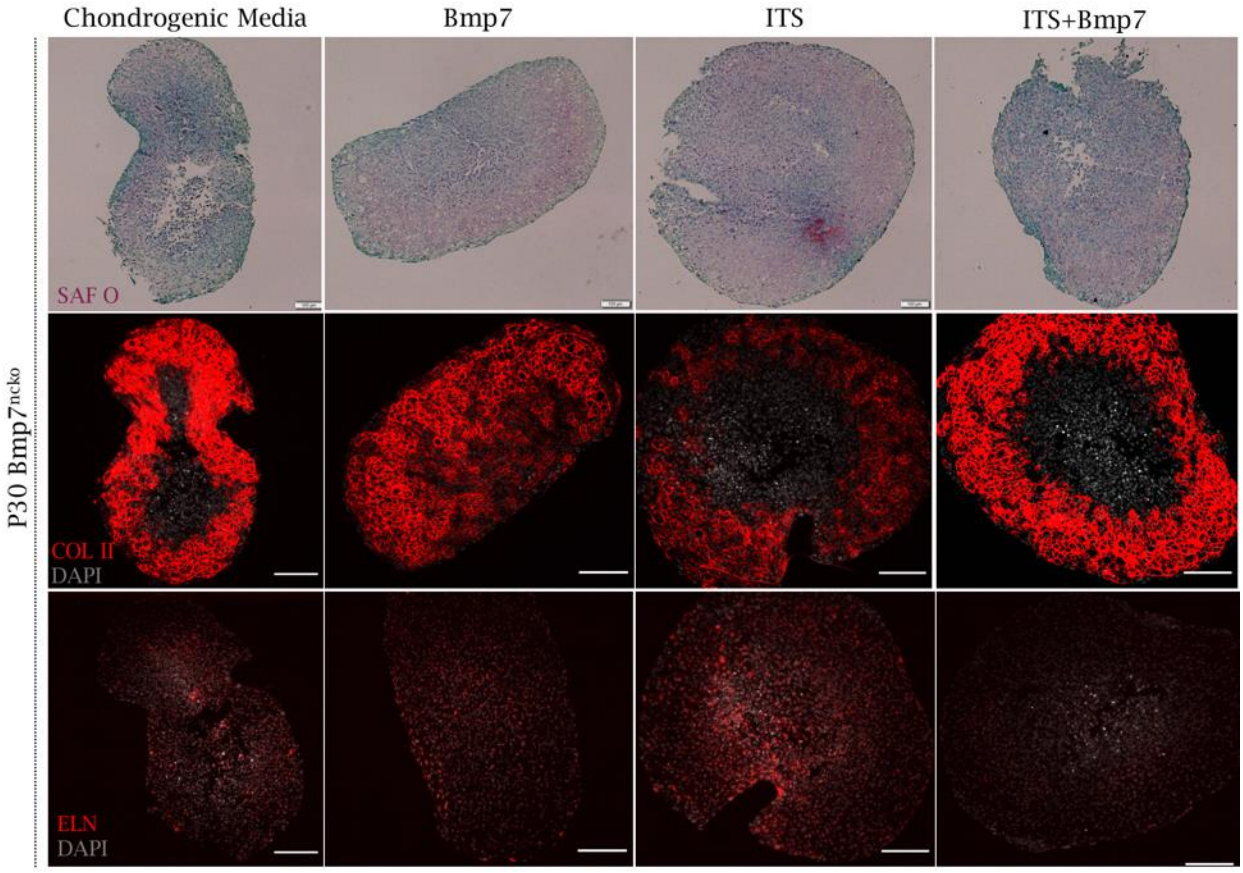

Figure 6. 3 P30 Bmp7^{ncko} pellets demonstrate partial reduction of ELN expression in the presence of ITS + Bmp7.

SAF O staining was induced in the presence of Bmp7, ITS and ITS + Bmp7. COL II expression was dynamic with an increase in expression when treated with Bmp7 and decrease in expression with treated with ITS. ELN expression was partially reduced when treated with ITS + Bmp7. n = 3; SAF O: Safranin O; COL II: Collagen II; ELN: Elastin; P: postnatal, Bmp7: Bone Morphogenetic Protein 7; ITS: Insulin, Transferring, Selenium. Scale bar for SAF O stains is 100µm and for COL II and ELN is 161µm.

6.4.3 Addition of ITS + Bmp7 suppresses COL II and ELN expression in P7 Bmp7^{ctrl} nasal chondrocytes

Bmp7^{ctrl} nasal chondrocyte pellets demonstrated similar characteristics as the P30 Bmp7^{ncko} pellets. SAF O staining in the Bmp7^{ctrl} pellets was highest when pellets were treated with just chondrogenic media (Figure 6.4). SAF O persisted in pellets treated with Bmp7; however, a loss of SAF O was observed in pellets exposed to ITS and ITS + Bmp7. COL II expression was observed in the periphery of the pellets in all four conditions. However, pellets in chondrogenic media alone and those treated with Bmp7 demonstrated COL II staining in the centre as well. Also, COL II expression was increased in the pellets treated with Bmp7 when compared to all the other conditions. Pellets treated with ITS suppressed COL II expression, and addition of Bmp7 to ITS is not able to rescue it. Expression of ELN was observed in the pellets treated with chondrogenic media, Bmp7 and ITS on its own. Pellets treated with ITS demonstrate a slight increase in ELN expression in comparison to the pellets treated with chondrogenic media and Bmp7. On the contrary, pellets treated with ITS + Bmp7 demonstrate suppression of ELN expression, suggesting that P7 Bmp7^{ctrl} nasal chondrocytes can maintain plasticity.

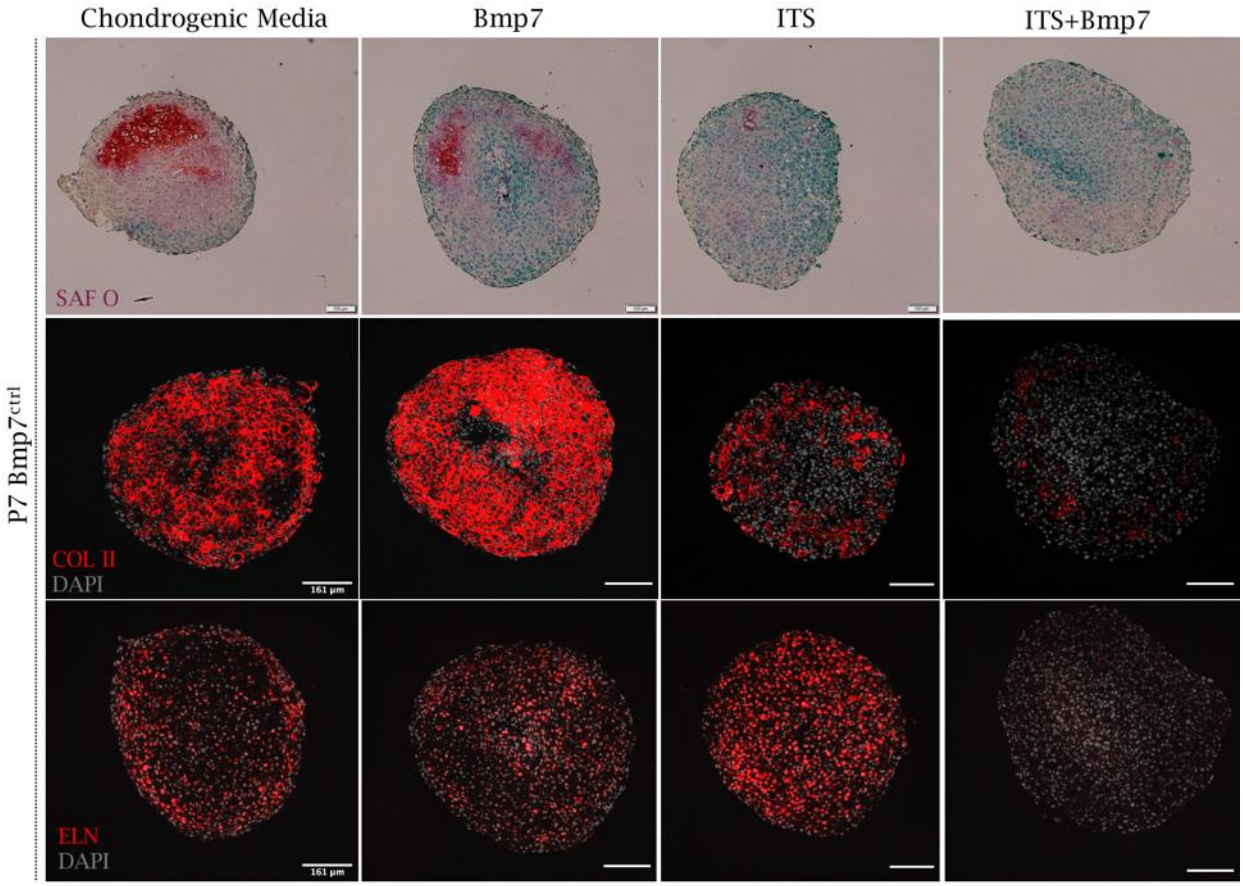

Figure 6. 4 P7 Bmp7^{ctrl} pellets demonstrate a decrease in COL II and ELN expression when treated with ITS+Bmp7.

SAF O staining was dynamic between treatment conditions. An increase in COL II expression was observed in the presence of Bmp7 and a decrease was observed when treated with ITS and ITS + Bmp7. ELN expression was increased when treated with ITS and was reduced in the presence of ITS + Bmp7. n = 3; SAF O: Safranin O; COL II: Collagen II; ELN: Elastin; P: postnatal, Bmp7: Bone Morphogenetic Protein 7; ITS: Insulin, Transferring, Selenium. Scale bar for SAF O stains is 100µm and for COL II and ELN is 161µm.

6.4.4 Addition of ITS + Bmp7 reduces expression of ELN and induces COL II expression in P7 Bmp7^{ncko} nasal chondrocytes

Assessment of P7 Bmp7^{ncko} pellets demonstrated no observable SAF O staining when pellets were treated with the four conditions (Figure 6.5). However, expression of COL II was present in the periphery of the pellets treated with chondrogenic media, Bmp7 and ITS + Bmp7. Interestingly, pellets treated only with ITS suppressed COL II expression and the concomitant addition of Bmp7 with ITS rescued the expression. COL II expression was only observed in the centre of the Bmp7 treated chondrocyte pellets. Dynamic expression of ELN was observed in the pellets during all treatment conditions. Addition of Bmp7 slightly reduces ELN expression when compared to expression of ELN in pellets treated with chondrogenic media alone. Moreover, pellets treated with ITS increase ELN expression and addition of Bmp7 and ITS together decrease the expression. Overall, this is indicative that P7 Bmp7^{ncko} nasal chondrocytes retain plasticity, although not to the same extent as P7 Bmp7^{ctrl} chondrocytes.

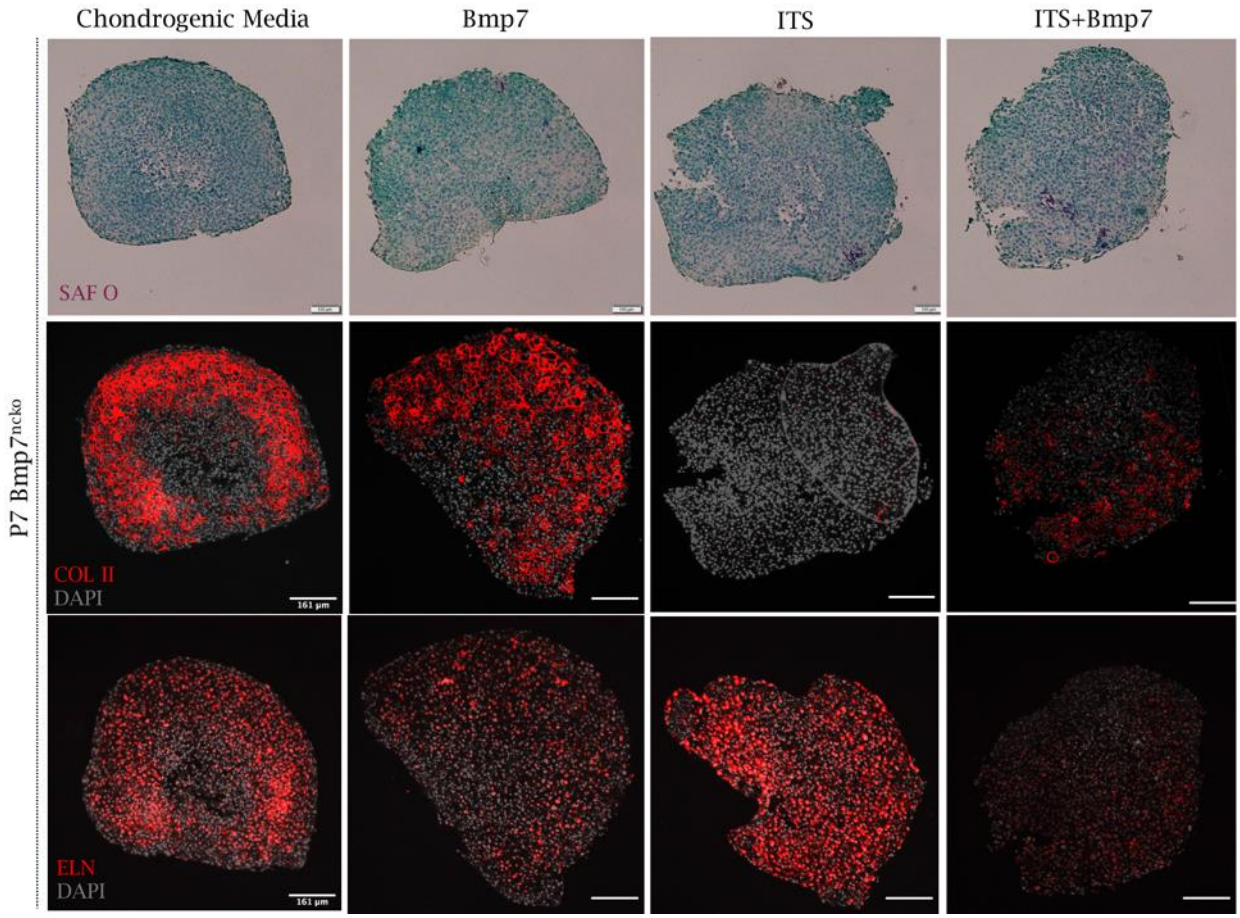

Figure 6. 5 P7 Bmp7^{ncko} pellets demonstrate reduction of COL II expression and increase of ELN expression in the presence of ITS.

SAF O staining was similar during all treatment conditions. COL II expression was dynamic with a decrease in expression when treated with ITS and a partial rescue in expression with treated with ITS + Bmp7. ELN expression was partially reduced when treated with Bmp7. Expression of ELN increased in the presence of ITS and was partially suppressed when treated with ITS + Bmp7. n = 3; SAF O: Safranin O; COL II: Collagen II; ELN: Elastin; P: postnatal, Bmp7: Bone Morphogenetic Protein 7; ITS: Insulin, Transferring, Selenium. Scale bar for SAF O stains is 100µm and for COL II and ELN is 161µm.

6.5 Discussion

This study strongly suggests that the cartilage type is determined at an early stage, potentially at the progenitor level, allowing chondrocytes to switch their properties based on exposure to different growth factors (Bmp7) and supplements (ITS). Our data also suggests that nasal chondrocytes from younger mice maintain chondrocyte plasticity, whereas chondrocytes from older mice don't retain this ability and are fixed in their developmental potential.

6.5.1 Plasticity of nasal chondrocytes

Both chondrocytes from P7 $Bmp7^{ctrl}$ and $Bmp7^{ncko}$ demonstrated noticeable plasticity evident by suppression of ELN when treated with concomitant Bmp7 and ITS. This suggests the existence of a lineage switch and highlights the ability of chondrocytes to differentiate into different cartilage lineages prior to chondrocytes maturation.

The P30 $Bmp7^{ctrl}$ pellet cultures demonstrated comparable SAF O, COL II and ELN expression, irrespective of the treatment conditions (Figure 6.2). P30 $Bmp7^{ncko}$ pellets did demonstrate limited plasticity, as ELN expression was partially suppressed when treated with Bmp7 and ITS. This minimal ability of P30 $Bmp7^{ncko}$ pellets to respond to the various treatment conditions, unlike P30 $Bmp7^{ctrl}$ pellets, suggests that adult nasal chondrocytes might be able to repair and remodel cartilage in response to pathology. However, there was a strong difference between P7 and P30 chondrocytes suggesting that chondrocytes lose the developmental plasticity with age. This inverse relationship between donor age and plasticity has already been demonstrated in articular chondrocytes from the knee[338] suggesting that the repair and regenerative capacity of the chondrocytes decrease with age. Moreover, our findings indicate that P7 $Bmp7^{ctrl}$ pellets are more plastic than P7 $Bmp7^{ncko}$ pellets as $Bmp7^{ctrl}$ pellets strongly respond to the treatment conditions, unlike the mutant pellets. This weakened response of $Bmp7^{ncko}$ pellets might indicate that the deletion of Bmp7 in neural crest cells preprogrammed the chondrocytes to change cartilage

characteristics at an earlier time-point, making it more challenging to completely rescue the phenotype. Overall, chondrocyte plasticity drives changes to cartilage characteristics when exposed to different growth factors and supplements. Thus, identifying the role of growth factors and supplements is critical for a better understanding of chondrocyte behaviour.

6.5.2 Role of Bmp7 and ITS in nasal chondrocytes

Addition of recombinant Bmp7 induces COL II expression to varying degrees. The variability in COL II induction within control pellets of the same treatment condition may be attributed to the age of the nasal septum chondrocytes whereas, variation between control and mutant pellets of the same treatment condition may be a result of both age and deletion of Bmp7 in neural crest cells. Moreover, it was observed that cartilage pellets from P7 nasal septum demonstrate stronger expression of COL II in the presence of Bmp7 when compared to P30 pellets. Thus, confirming findings from previous studies suggest expression of COL II is age-dependent and might not be a good indicator of cartilage type or cartilage quality [38,85].

Next, we assessed whether addition of Bmp7 is able to suppress ELN expression. Investigations in both $Bmp7^{ctrl}$ and $Bmp7^{ncko}$ pellets at P7 and P30 demonstrated that chondrocytes treated with only Bmp7 are not able to suppress ELN expression, suggesting that multiple factors contribute to the commitment of a cartilage type. Also, to our surprise, we observed that ELN expression was comparable between chondrogenic media and chondrogenic media + Bmp7 conditions at both ages and genotypes investigated. A role for Bmp7 in maintenance of progenitor cells has been previously described using colony-forming assays in kidney progenitor cells where Bmp7 inhibits differentiation of these progenitor cells[339]. Thus, no change in ELN expression could indicate that pellets in chondrogenic media are in a progenitor state expressing proteins abundant in various types of cartilage and that addition of Bmp7 maintains this progenitor state.

More detailed studies, in particular, the use of sequential rounds of differentiation, are required to establish this.

ITS has been commonly used in cell culture to promote growth[259]. Although a clear role of ITS in nasal chondrocyte pellet cultures has not been elucidated. Auricular [336] and articular cartilage pellet cultures[337], as well as monolayer cultures using nasal chondrocytes[337], demonstrate that ITS prevents dedifferentiation of chondrocytes and promotes chondrogenesis. Our findings contradict previous studies as we observe that nasal chondrocyte pellets exposed to ITS suppress COL II expression and increase ELN expression, suggestive that ITS might promote elastic cartilage-like characteristics rather than hyaline cartilage. This evidence is supported by the successful construction of elastic cartilage using ITS-treated hyaline cartilage-derived chondrocytes[340].

Interestingly, concomitant addition of Bmp7 and ITS suppresses ELN and promotes COL II expression in our pellet cultures, suggesting that addition of Bmp7 in ITS treated cells promotes hyaline cartilage characteristics rather than characteristics observed in elastic cartilage. Previous studies using a chondrogenic cell line, ATDC5, reported a similar role of Bmp7 in ITS treated chondrocytes where addition of Bmp7 promoted expression of COL II and suppressed genes expressed in hypertrophic chondrocytes [259]. Thus, suggesting that Bmp7 may play a role in lineage specification of chondrocytes. A similar function of Bmp7 in adipocytes has already been established where Bmp7 specifically induces adipocytes to differentiate into thermogenic, brown adipose tissue (BAT), whereas BMP2 promotes white adipose tissue (WAT) [314,341]. Overall, we observe that the chondrocytes respond to Bmp7 differently in the presence and absence of ITS. These changes may be a result of altered metabolic requirements of chondrocytes when exposed to Bmp7, ITS and Bmp7 + ITS. Since insulin in ITS promotes glucose uptake, this may alter

metabolism of chondrocytes and shift the characteristics of the chondrocytes. However, to confirm this interpretation, there is a need to investigate the role of metabolism in these chondrocyte pellets. Collectively, our data suggest that Bmp7 may have multiple roles during stages of cartilage development.

6.5.3 Implications for Tissue engineering

The 3D pellets cultures demonstrate that cells are preprogrammed to acquire a certain fate that may be determined at the progenitor stage. Efforts to alter cell fate are quite challenging and require careful consideration of donor age and underlying pathology when considering autologous cartilage transplantation. Since our findings, as well as previously established literature[342], demonstrate that chondrocytes have the ability to retain memory, careful characterization must be conducted while using chondrocytes that have undergone any genetic alterations as a result of pathology. The retention of cell memory may explain challenges associated with cartilage stability while using engineered cartilage from human donors. Additionally, the high recurrence rate and the need for revision surgery in patients with autologous chondrocyte implantation grafts might also be a consequence of memory retention in chondrocytes.

Collectively, our findings suggest that 1) careful considerations must be made on donor age of nasal chondrocytes for tissue engineering; 2) Bmp7 regulates ELN expression, and 3) ITS in cartilage tissue engineering should be used with caution as supplementation of ITS in nasal chondrocytes tends to promote characteristics similar to elastic cartilage.

Chapter 7: Discussion, Conclusions & Future Directions

7.1 Discussion

7.1.1 Summary of key findings

This thesis addresses aspects of how nasal cartilage develops, how its development is linked to midfacial physiology, and how alterations to cartilage development predispose to pathological conditions. Chapter 1 presents a scoping review aimed at painting an accurate, up-to-date picture of our understanding of nasal cartilage growth and development, biological and mechanical properties. It highlighted that the growth properties of the NSC are generally well described. It also demonstrated the need to conduct detailed species- and hyaline cartilage-specific investigations rather than inferring cartilage properties from other hyaline cartilages and different species. It also outlined the importance of understanding if and how cartilage properties are altered in nasal cartilage pathologies to prevent secondary pathologies such as sleep-disordered breathing, high recurrence rates and revision surgeries. Chapter 2 described approaches to characterize the NSD subjectively and objectively using CBCT scans. It additionally investigated whether the outlined approach could identify children at risk of SDB by correlating the presence and severity of NSD to post-sleep questionnaire scores. Correlating NSD with SDB based on CBCT scans alone is not possible, given the various aetiologies of airway obstruction and due to a lack of understanding of how NSC develops and why it deviates. Hence, in chapter 3, I present a detailed study on nasal cartilage development in wild-type mice. Mice rather than humans were used due to limited accessibility to healthy intact human nasal cartilage samples during all ages of development. Based on these findings, nasal cartilage is a heterogeneous structure that grows episodically both through initial proliferation and subsequent hypertrophy. This heterogeneous nature highlights the importance of considering age and location when working with NSC. To identify cartilage changes underlying NSD, we first established and characterized a mouse model

for NSD in chapter 4. Deletion of Bmp7 in neural crest cells ($Bmp7^{ncko}$) presented with midfacial hypoplasia, abnormalities to the cranial base along with NSD at a time when the mice undergo rapid midfacial growth. All the $Bmp7^{ncko}$ mice displayed septum deviation; however only 50% of the mice present with spontaneous apneas, recapitulating the clinical scenario where only a percentage of individuals with nasal septum deviation present with breathing disturbances. Having established a model for NSD, chapter 5 outlined the cartilage changes underlying NSD. An increase in proteins expressed in hypertrophic chondrocytes, acquisition of elastic cartilage characteristics, switch to glucose metabolism, and similarities to OA were some of the key characteristics of NSD. Chapter 5 also outlined that a balance of Bmp7 and Bmp2 signals can rescue septum deviation. However, it remained unclear whether Bmp7 directly regulated the acquisition of ELN expression in the nasal cartilage. Hence, chapter 6 used chondrocyte pellet cultures to demonstrate that Bmp7 regulates ELN expression. Treatment of chondrocyte pellets with ITS increased expression of ELN, whereas concomitant treatment of Bmp7 and ITS suppressed expression of ELN.

Collectively, the findings on physiological nasal septum growth contribute significantly to our understanding of nasal septum development and provide new insights into the role of NSC in midfacial growth. Whereas NSC behaviour under pathological conditions demonstrates the complexity of NSD leading to SDB. These findings also reiterate the multifactorial etiology of NSD and the challenges associated with it, which make it difficult to predict whether a child with NSD will develop secondary comorbidities (SDB) that may require surgical intervention. The cartilaginous changes observed in the $Bmp7^{ncko}$ mouse model may explain the etiology of NSD observed in children with pre-existing growth deficiencies. Moreover, these cartilage changes share similarities with changes observed in knee OA suggesting that both these hyaline cartilages,

irrespective of their different load-bearing requirements, may behave similarly. Since a majority of investigations about human knee OA are late stage, the identified cartilage changes preceding NSD in $Bmp7^{ncko}$ mice may be extrapolated to early-stage knee OA. The similarities between NSC and knee articular cartilage could explain the success observed in using nasal chondrocytes as a source to repair articular cartilage defects[129]. Although this interpretation may be an oversimplification of cartilage biology as these two hyaline cartilages have different growth rates, ECM characteristics and mechanical requirements [53,343].

7.1.2 Delineating cause and consequence of NSD

It has been recently demonstrated that SDB and midfacial hypoplasia both are associated with NSD [344]. However, isolating the cause and consequence of these malformations presents a complex challenge. Coordinated cartilage, bone and suture development forms the basis for the proportional growth of our face. There is controversy in the literature whether hypoplasia is the primary event leading to NSD and SDB or whether SDB can negatively affect cartilage growth leading to hypoplasia. It is difficult to investigate these pathologies in isolation in humans, thus negatively affecting choices with regards to the best type of surgical approach as well as the appropriate timing for surgical intervention. It also hampers optimal timing for non-surgical management, if possible. The $Bmp7^{ncko}$ mice studies investigated in this thesis demonstrate that reduced facial length and cell apoptosis might predispose mice to NSD. However, NSD alone may not result in breathing disturbances and the onset of secondary morbidities might be a cumulative effect caused by multiple craniofacial abnormalities. The inability to delineate cause and consequence of NSD stems largely from the unresolved controversy of whether nasal septum cartilage is required for midfacial growth. The varying growth rates of the nasal septum in comparison to its surrounding structures as established in Chapters 3 and 4 and the altered nasal

growth resulting in midfacial hypoplasia as demonstrated in Chapter 5 support Scott's theory which is suggestive that nasal septum significantly contributes to midfacial growth.

7.1.3 The influence of genetic background

It has been established that underlying genetics contribute significantly to bone development and, therefore, skull shape [345]. However, to what extent cartilage predetermines skull shape and predisposes individuals to craniofacial pathologies is largely unexplored. Cartilage induction and shape have been described to be contributing factors to the formation of facial bones and thus facial shape [346]. Specifically, a recent study has demonstrated a set of five genes (DCHS2, RUNX2, GLI3, PAX1 and EDAR) involved in determining the shape of the nose [347]. Mutations to these individual genes, although rare, have been associated with craniofacial syndromes and abnormalities. However, the mechanism elucidating the interactions of these five genes with each other as well as other genes under physiological and pathological conditions isn't clear. Two possibilities arise: either a concentration gradient of these genes drives nasal shape variation, or one specific gene acts as a master regulator influencing the expression of the rest of the genes to determine nasal shape. A better understanding of the genetic regulation underlying nasal shape may assist in predicting individuals at risk for nasal abnormalities and would greatly benefit the provision of personalized treatments.

While genetic regulation contributing to variation in nasal shape must be considered in humans, similarly careful attention must be given to the genetic background of the mouse models. A comparison of C3H/HeJ and C57BL/6J mice backgrounds described that the C3H/HeJ are more likely to present with NSD during development than C57BL/6J[24]. Thus, posing a challenge when attributing the etiology of NSD to the genetic deletion. However, this is not a limitation for our studies since $Bmp7^{ncko}$ mice were bred on the C57BL/6J background and wildtype mice, at the

timepoints investigated in the $Bmp7^{ctrl}$ and $Bmp7^{ncko}$, were assessed for NSD. C57BL/6J wildtype mice do not present with NSD at 4 weeks, the age when deletion of Bmp7 in neural crest cells presents with NSD.

For our mouse studies, we used the Wnt1-Cre driver. Over the last years, there has been ongoing controversy surrounding the use of this particular Wnt1-Cre driver. Specifically, it was demonstrated that this Cre-driver can cause ectopic expression of Wnt1. This was in particular demonstrated for midbrain development[234]. A new, improved Wnt1-Cre2 mouse was developed that supposedly overcomes this problem[234]. However, as is true for any genetically engineered mouse, a detailed study on fidelity is necessary to formally demonstrate that this new mouse line indeed overcomes the limitations of the original Wnt1-Cre driver. Such a detailed characterization is not only missing to date, but some literature indicates concerns regarding this improved Cre line as well[348]. From our side, we addressed this issue by testing whether the presence of the Wnt1-Cre allele in wildtype or heterozygous $Bmp7^{ncko}$ mice would lead to NSD at P30 using µCT analysis. NSD was not observed in any of those mice. Thus, the ectopic Wnt1 expression on its own cannot be attributed to the phenotype observed. Furthermore, the genetic reduction of Bmp2 in the Bmp7 mutant background rescues septum deviation, indicating an intricate regulation of nasal cartilage properties.

No measurable differences between male and female mice were observed when breathing was assessed using plethysmography. Hence, both sexes were considered together in most of the mouse studies conducted in this thesis. A minimum of n=3 biological replicates was used, to conduct statistical analysis. Due to the small n number, this thesis mostly reports findings that are explicit such that they can serve as markers to be assessed in human NSD samples in future.

7.2 Conclusions and Future Directions

This thesis addressed several gaps of knowledge surrounding NSC. It described growth and extracellular matrix composition of the NSC during development and established an in-depth understanding of the cartilage changes underlying NSD. It highlighted the importance of time windows for disease management and treatment of congenital disorders and provided new considerations for engineering cartilage with desired properties. Most importantly, as a result of these studies, we challenge the central dogma of cartilage biology that chondrocytes follow a linear differentiation pathway and pointed towards the possibility that different cartilage types are developmentally determined at an early stage of cartilage development. This realization opens new avenues to investigate how the cellular environment controls chondrocyte cell fate decision and cell differentiation that could have major ramifications for understanding cartilage degenerative diseases where a change in cartilage properties and type is observed as in OA. Although changes underlying NSD are reminiscent of knee OA, there are striking differences. During knee OA, the articular cartilage undergoes chondrocytes hypertrophy with chondrocytes becoming visibly large and expressing COL X, RUNX2 and IHH. However, in NSD, the chondrocytes do not grow in size but express the above-mentioned markers. This discrepancy establishes the need to clearly delineate whether when using the term 'chondrocyte hypertrophy' authors are referring to the size of chondrocytes, the underlying molecular regulation or both. Literally, the term 'hypertrophy' refers to size only and thus should not be associated with specific molecular changes. However, this distinction is not always observed when using terminology such as chondrocyte hypertrophy. Our observations hence highlight the need to revisit chondrocyte terminology. Future experiments should investigate the role of biomechanics on cartilage under physiological and pathological conditions. Also, identifying similar changes underlying mice and human NSD will greatly

contribute to better understanding and development of functional tissue-engineered nasal cartilage. Moreover, this thesis has outlined several novel considerations that are to be made to develop functional tissue-engineered nasal cartilage in future. Of significant importance is the initial molecular characterization of the chondrocytes being used as well as the growth factors and nutrients that they are supplemented with. We have demonstrated that these two aspects significantly drive the lineage specification of the chondrocytes in promoting a specific cartilage type. Additionally, we have demonstrated for the first time, using both *in vivo* and *in vitro* systems, that Bmp7 is one such factor that drives cartilage lineage specification. Although, an underlying mechanism of how Bmp7 regulates cartilage lineage specification is yet to be determined. A similar function of Bmp7 has already been established in adipocytes [314,341]. Thus, suggesting that Bmp7 may be utilized in repairing cartilage defects associated with pathologies such as OA since findings from this thesis as well as previous literature[261] has demonstrated that reduction of Bmp7 is detrimental to cartilage.

In summary, this thesis produced a detailed description of midfacial hypoplasia-driven NSD and provided insights into the key factors that are to be considered while engineering nasal septum cartilage to repair cartilage defects.

Bibliography

1. Hur M-S, Won H-S, Kwak D-S, Chung I-H, Kim I-B. Morphological Patterns and Variations of the Nasal Septum Components and Their Clinical Implications. *J Craniofac Surg*. 2016;27(8):2164-2167. doi:10.1097/SCS.0000000000002974

2. Dayeh AAA, Rafferty KL, Egbert M, Herring SW. Deformation of Nasal Septal Cartilage During Mastication. *J Morphol*. 2009;270(10):1209-1218. doi:10.1002/jmor.10750

3. Goergen MJ, Holton NE, Grunheid T. Morphological interaction between the nasal septum and nasofacial skeleton during human ontogeny. *Journal of anatomy*. 2017;230(5):689-700.

4. Evans HB, Ayad S, Abedin MZ, et al. Localization of Collagen Types and Fibronectin in Cartilage by Immuno Fluorescence. *Annals of the Rheumatic Diseases*. 1983;42(5):575-581.

5. Glant T, Levai G, Hadhazy C. The Localization of Proteo Glycans and Glyco Proteins in the Hyaline Cartilage. *Histochemistry*. 1977;53(4):291-300.

6. Bagher Z, Asgari N, Bozorgmehr P, Kamrava SK, Alizadeh R, Seifalian A. Will Tissue-Engineering Strategies Bring New Hope for the Reconstruction of Nasal Septal Cartilage? *Current Stem Cell Research & Therapy*. 2020;15(2):144-154.

7. Arksey H, O'Malley L. Scoping studies: towards a methodological framework. *International Journal of Social Research Methodology*. 2005;8(1):19-32. doi:10.1080/1364557032000119616

8. Kim J, Cho JH, Kim SW, Kim BG, Lee DC, Kim SW. Anatomical Variation of the Nasal Septum: Correlation Among Septal Components. *CLINICAL ANATOMY*. 2010;23(8):945-949.

9. Al Dayeh A, Herring SW. Cellular proliferation in the nasal septal cartilage of juvenile minipigs. *Journal of anatomy*. 2014;225(6):604-613.

10. Al Dayeh AA, Rafferty KL, Egbert M, Herring SW. Real-time monitoring of the growth of the nasal septal cartilage and the nasofrontal suture. *Am J Orthod Dentofacial Orthop*. 2013;143(6):773-783. doi:10.1016/j.ajodo.2013.01.012

11. Amano K, Okuzaki D, Aikawa T, Kogo M. Indian hedgehog in craniofacial neural crest cells links to skeletal malocclusion by regulating associated cartilage formation and gene expression. *FASEB Journal*. 2020;34(5).

12. Ashique AM, Fu K, Richman JM. Signalling via type IA and type IB bone morphogenetic protein receptors (BMPR) regulates intramembranous bone formation, chondrogenesis and feather formation in the chicken embryo. *International Journal of Developmental Biology*. 2002;46(2):243-253.

13. BABULA WJ, SMILEY GR, DIXON AD. ROLE OF CARTILAGINOUS NASAL SEPTUM IN MIDFACIAL GROWTH. *American Journal of Orthodontics*. 1970;58(3):250-.

14. Bruintjes TD, Van Olphen AF, Hillen B. Review of the functional anatomy of the cartilages and muscles of the nose. *Rhinology (Utrecht)*. 1996;34(2):66-74.

15. Burdi ALPHONSER. Sagittal growth of the nasomaxillary complex during the second trimester of human prenatal development. *J Dent Res*. 1965;44((1 Pt. 1)):112-125.

16. Carnevale GG, Tatum SA. Chondrocyte volume fraction distribution in porcine septal cartilage: An initial stereoscopic evaluation. *OTOLARYNGOLOGY-HEAD AND NECK SURGERY*. 1996;115(4):365-369.

17. CATALA AE, JOHNSTON LE. INTERSTITIAL GROWTH OF SEPTAL CARTILAGE IN THE YOUNG ALBINO-RAT. *Journal of dental research*. 1980;59(8):1453-1456.

18. COPRAY J. GROWTH OF THE NASAL SEPTAL CARTILAGE OF THE RAT INVITRO. *JOURNAL OF ANATOMY*. 1986;144:99-111.

19. Daultrey C, Hardman J, Anari S. The Caucasian Nasal Septum: An In Vivo Computed Tomography Study. *AESTHETIC SURGERY JOURNAL*. 2018;38(7):717-722. doi:10.1093/asj/sjx249

20. Delaire J, Precious D. Interaction of the Development of the Nasal Septum the Nasal Pyramid and the Face. *International journal of pediatric otorhinolaryngology*. 1987;12(3):311-326.

21. Diewert VM. Differential Changes in Cartilage Cell Proliferation and Cell Density in the Rat Cranio Facial Complex during Secondary Palate Development. *Anatomical Record*. 1980;198(2):219-228.

22. Elsaesser AF, Schwarz S, Joos H, Koerber L, Brenner RE, Rotter N. Characterization of a migrative subpopulation of adult human nasoseptal chondrocytes with progenitor cell features and their potential for in vivo cartilage regeneration strategies. *Cell Biosci*. 2016;6(101561195):11. doi:10.1186/s13578-016-0078-6

23. Adegani FJ, Langroudi L, Arefian E, Shafiee A, Dinarvand P, Soleimani M. A comparison of pluripotency and differentiation status of four mesenchymal adult stem cells. *Molecular biology reports*. 2013;40(5):3693-3703.

24. Foster A, Holton N. Variation in the Developmental and Morphological Interaction Between the Nasal Septum and Facial Skeleton. *Anat Rec (Hoboken)*. 2016;299(6):730-740. doi:10.1002/ar.23340

25. GRANSTROM G, MAGNUSSON BC. HISTOCHEMICAL ANALYSIS OF ENZYMES INVOLVED IN THE FORMATION AND METABOLISM OF THE NASAL SEPTAL CARTILAGE. *Acta Oto-Laryngologica*. Published online 1992:15-21.

26. Grymer LF, Bosch C. The nasal septum and the development of the midface. A longitudinal study of a pair of monozygotic twins. *Rhinology (Utrecht)*. 1997;35(1):6-10.

27. Hall BK, Precious DS. Cleft lip, nose, and palate: the nasal septum as the pacemaker for midfacial growth. *Oral Surg Oral Med Oral Pathol Oral Radiol*. 2013;115(4):442-447. doi:10.1016/j.oooo.2012.05.005

28. Holton NE, Franciscus RG, Marshall SD, Southard TE, Nieves MA. Nasal Septal and Premaxillary Developmental Integration: Implications for Facial Reduction in Homo. *Anatomical Record*. 2011;294(1):68-78. doi:10.1002/ar.21288

29. Holton NE, Yokley TR, Figueroa A. Nasal septal and craniofacial form in European- and African-derived populations. *Journal of anatomy*. 2012;221(3):263-274.

30. Howe A, Hawkins J, Webster W. The growth of the nasal septum in the 6-9 week period of foetal development - Warfarin embryopathy offers a new insight into prenatal facial development. *AUSTRALIAN DENTAL JOURNAL*. 2004;49(4):171-176. doi:10.1111/j.1834-7819.2004.tb00069.x

31. Hwang K, Huan F, Kim D. Mapping Thickness of Nasal Septal Cartilage. *JOURNAL OF CRANIOFACIAL SURGERY*. 2010;21(1):243-244. doi:10.1097/SCS.0b013e3181c5a203

32. Kaucka M, Petersen J, Tesarova M, et al. Signals from the brain and olfactory epithelium control shaping of the mammalian nasal capsule cartilage. *eLife*. 2018;7:e34465.

33. Kim IS, Lee MY, Lee KI, Kim HY, Chung YJ. Analysis of the Development of the Nasal Septum according to Age and Gender Using MRI. *CLINICAL AND EXPERIMENTAL OTORHINOLARYNGOLOGY*. 2008;1(1):29-34.

34. KVINNSLAND S. PARTIAL RESECTION OF CARTILAGINOUS NASAL-SEPTUM IN RATS - ITS INFLUENCE ON GROWTH. *ANGLE ORTHODONTIST*. 1974;44(2):135-140.

35. Long R, Greulich RC, Sarnat BG. Regional variations in chondrocyte proliferation in the cartilaginous nasal septum of the growing rabbit. *J Dent Res*. 1968;47(3):505. doi:10.1177/00220345680470033601

36. Marulanda J, Eimar H, McKee MD, et al. Matrix Gla protein deficiency impairs nasal septum growth, causing midface hypoplasia. *J Biol Chem*. 2017;292(27):11400-11412. doi:10.1074/jbc.M116.769802

37. Melsen B. Histological Analysis of the Post Natal Development of the Nasal Septum. *Journal of dental research*. 1976;55(SPEC ISSUE B):B296.

38. Pavlov MI, Sautier J-., Oboeuf M, Asselin A, Berdal A. Chondrogenic differentiation during midfacial development in the mouse: In vivo and in vitro studies. *Biology of the Cell (Paris)*. 2003;95(2):75-86.

39. Searles JC. A Radioautographic Study of Chondrocytic Proliferation in Nasal Septal Cartilage of the New Born Rat. *American Journal of Anatomy*. 1977;150(4):559-564.

40. Seltzer ALBERTP. The problem of the nasal septum. *Jour Albert Einstein Med Ctr*. 1963;11((4)):283-299.

41. Van Loosen J. The Nasal Septal Cartilage in the Newborn. *Rhinology (Utrecht)*. 1988;26(3):161-166.

42. vanLoosen J, Yiang J, Howard C, et al. Nasal cartilage maturation assessed by automated computer-assisted image analysis. In: *OTOLARYNGOLOGY IN ASEAN COUNTRIES*. Vol 51. ; 1997:51-60.

43. VETTER U, PIRSIG W, HEINZE E. GROWTH-ACTIVITY IN HUMAN SEPTAL CARTILAGE - AGE-DEPENDENT INCORPORATION OF LABELED SULFATE IN DIFFERENT ANATOMIC LOCATIONS. *PLASTIC AND RECONSTRUCTIVE SURGERY*. 1983;71(2):167-170. doi:10.1097/00006534-198302000-00001

44. VETTER U, PIRSIG W, HEINZE E. POSTNATAL-GROWTH OF THE HUMAN SEPTAL CARTILAGE - PRELIMINARY-REPORT. *ACTA OTO-LARYNGOLOGICA*. 1984;97(1-2):131-136. doi:10.3109/00016488409130973

45. Vidic B, Greditzer HG, Litchy WJ. The Structure and Pre Natal Morphogenesis of the Nasal Septum in the Rat. *Journal of Morphology*. 1972;137(2):131-148. doi:10.1002/jmor.1051370202

46. Aksoy F, Yildirim YS, Demirhan H, Ozturan O, Solakoglu S. Structural characteristics of septal cartilage and mucoperichondrium. *Journal of Laryngology and Otology*. 2012;126(1):38-42.

47. Ayad S, Weiss JB. A New Look at Vitreous Humor Collagen. *Biochemical Journal*. 1984;218(3):835-840.

48. Boukla A. Purification and Properties of Bovine Nasal Hyaline Cartilage Collagenase. *International Journal of Biochemistry*. 1990;22(11):1273-1282.

49. Holden PK, Liaw LH, Wong B. Human Nasal Cartilage Ultrastructure: Characteristics and Comparison Using Scanning Electron Microscopy. *LARYNGOSCOPE*. 2008;118(7):1153-1156.

50. Kim DH, Lim JY, Kim SW, et al. Characteristics of Nasal Septal Cartilage-Derived Progenitor Cells during Prolonged Cultivation. *OTOLARYNGOLOGY-HEAD AND NECK SURGERY*. 2018;159(4):774-782.

51. Lee JW, McHugh J, Kim JC, Baker SR, Moyer JS. Age-Related Histologic Changes in Human Nasal Cartilage. *JAMA FACIAL PLASTIC SURGERY*. 2013;15(4):256-262.

52. Neuman MK, Briggs KK, Masuda K, Sah RL, Watson D. A compositional analysis of cadaveric human nasal septal cartilage. *LARYNGOSCOPE*. 2013;123(9):2120-2124.

53. Pelttari K, Mumme M, Barbero A, Martin I. Nasal chondrocytes as a neural crest-derived cell source for regenerative medicine. *Curr Opin Biotechnol*. 2017;47:1-6. doi:10.1016/j.copbio.2017.05.007

54. Perin JP, Bonnet F, Jolles P. Comparative Studies on Human and Bovine Nasal Cartilage Proteo Glycan Complex Components. *Molecular and cellular biochemistry*. 1978;21(2):71-82.

55. Riedler KL, Shokrani A, Markarian A, Fisher LM, Pepper JP. Age-Related Histologic and Biochemical Changes in Auricular and Septal Cartilage. *LARYNGOSCOPE*. 2017;127(11):E399-E407.

56. Rotter N, Bonassar LJ, Tobias G, Lebl M, Roy AK, Vacanti CA. Age dependence of cellular properties of human septal cartilage - Implications for tissue engineering. *ARCHIVES OF OTOLARYNGOLOGY-HEAD & NECK SURGERY*. 2001;127(10):1248-1252.

57. Sasano Y, Mizoguchi I, Kagayama M, Shum L, Bringas. Jr Pablo, Slavkin HC. Distribution of type I collagen, type II collagen and PNA binding glycoconjugates during chondrogenesis of three distinct embryonic cartilages. *Anatomy and Embryology*. 1992;186(3):205-213.

58. Sasano Y, Takahashi I, Zhu J-X, Ohtani H, Mizoguchi I, Kagayama M. Gene and protein expressions of type I collagen are regulated tissue-specifically in rat hyaline cartilages in vivo. *European journal of morphology*. 2001;39(3):149-154.

59. Shafiee A, Kabiri M, Ahmadbeigi N, et al. Nasal Septum-Derived Multipotent Progenitors: A Potent Source for Stem Cell-Based Regenerative Medicine. *STEM CELLS AND DEVELOPMENT*. 2011;20(12):2077-2091.

60. Takahashi K, Kajii T, Tsukamoto Y, et al. Histological study of the nasal septal cartilage in BALB/c-bm/bm mouse which spontaneously induces malocclusion. *ORTHODONTICS & CRANIOFACIAL RESEARCH*. 2012;15(2):84-91. doi:10.1111/j.1601-6343.2011.01538.x

61. Theocharis AD, Karamanos NK, Papageorgakopoulou N, Tsiganos CP, Theocharis DA. Isolation and characterization of matrix proteoglycans from human nasal cartilage - Compositional and structural comparison between normal and scoliotic tissues. *BIOCHIMICA ET BIOPHYSICA ACTA-GENERAL SUBJECTS*. 2002;1569(1-3):117-126.

62. Ustunel I, Cayli S, Guney K, et al. Immunohistochemical distribution patterns of collagen type II, chondroitin 4-sulfate, laminin and fibronectin in human nasal septal cartilage. *Acta Histochem*. 2003;105(2):109-114.

63. Wan Y, Rogers MB, Szabo-Rogers HL. A six-gene expression toolbox for the glands, epithelium and chondrocytes in the mouse nasal cavity. *Gene Expression Patterns*. 2018;27:46-55.

64. Wiggenhauser PS, Schwarz S, Rotter N. The distribution patterns of COMP and matrilin-3 in septal, alar and triangular cartilages of the human nose. *Histochemistry and cell biology*. 2018;150(3):291-300. doi:10.1007/s00418-018-1672-y

65. Yu X, Kawakami H, Tahara N, et al. Expression of Noggin and Gremlin1 and its implications in fine-tuning BMP activities in mouse cartilage tissues. *Journal of Orthopaedic Research*. 2017;35(8):1671-1682. doi:10.1002/jor.23463

66. Zhang R, Chen F-M, Zhao S-L, Xiao M-Z, Smith AJ, Feng JQ. Expression of dentine sialophosphoprotein in mouse nasal cartilage. *Arch Oral Biol*. 2012;57(6):607-613. doi:10.1016/j.archoralbio.2011.10.012

67. Reuther MS, Briggs KK, Schumacher BL, Masuda K, Sah RL, Watson D. In vivo oxygen tension in human septal cartilage increases with age. *LARYNGOSCOPE*. 2012;122(11):2407-2410.

68. Alkan Z, Yigit O, Acioglu E, et al. Tensile Characteristics of Costal and Septal Cartilages Used as Graft Materials. *ARCHIVES OF FACIAL PLASTIC SURGERY*. 2011;13(5):322-326.

69. Al Dayeh AA, Herring SW. Compressive and tensile mechanical properties of the porcine nasal septum. *Journal of Biomechanics*. 2014;47(1):154-161.

70. Bos EJ, Pluemeekers M, Helder M, et al. Structural and Mechanical Comparison of Human Ear, Alar, and Septal Cartilage. *PLASTIC AND RECONSTRUCTIVE SURGERY-GLOBAL OPEN*. 2018;6(1).

71. Caffrey JP, Kushnaryov AM, Reuther MS, et al. Flexural Properties of Native and Tissue-Engineered Human Septal Cartilage. *OTOLARYNGOLOGY-HEAD AND NECK SURGERY*. 2013;148(4):576-581.

72. Colombo V, Cadova M, Gallo LM. Mechanical behavior of bovine nasal cartilage under static and dynamic loading. *Journal of Biomechanics*. 2013;46(13):2137-2144.

73. Correro-Shahgaldian M, Introvigne J, Ghayor C, Weber FE, Gallo LM, Colombo V. Properties and Mechanobiological Behavior of Bovine Nasal Septum Cartilage. *Annals of Biomedical Engineering*. 2016;44(5):1821-1831.

74. Flam E. The Tensile and Flexural Properties of Bovine Nasal Cartilage. *Journal of Biomedical Materials Research*. 1974;8(5):277-282.

75. Grellmann W, Berghaus A, Haberland E-., et al. Determination of strength and deformation behavior of human cartilage for the definition of significant parameters. *Journal of Biomedical Materials Research*. 2006;78A(1):168-174.

76. Iwanaga J, Watanabe K, Oskouian R, Tubbs R. Distribution of the internal nasal branch of the infraorbital nerve to the nasal septum: Application to rhinoplasty. *JOURNAL OF PLASTIC RECONSTRUCTIVE AND AESTHETIC SURGERY*. 2018;71(5):665-669. doi:10.1016/j.bjps.2017.12.004

77. Richmon JD, Sage A, Wong VW, Chen AC, Sah RL, Watson D. Compressive biomechanical properties of human nasal septal cartilage (vol 20, pg 496, 2006). *American Journal of Rhinology*. 2007;21(1):135-135.

78. Richmon JD, Sage AB, Wong VW, et al. Tensile biomechanical properties of human nasal septal cartilage. *American Journal of Rhinology*. 2005;19(6):617-622.

79. Rotter N, Tobias G, Lebl M, et al. Age-related changes in the composition and mechanical properties of human nasal cartilage. *Archives of Biochemistry and Biophysics*. 2002;403(1):132-140.

80. Tekke NS, Alkan Z, Yigit O, et al. Importance of nasal septal cartilage perichondrium for septum strength mechanics: a cadaveric study. *Rhinology*. 2014;52(2):167-171.

81. Tsao SW, Chuah MI. Development of Bone-Like Substance in Cartilaginous Rat Nasal Septum Under Experimental Conditions. *Anatomical Record*. 1988;221(4):834-840. doi:10.1002/ar.1092210407

82. Westreich RW, Courtland HW, Nasser P, Jepsen K, Lawson W. Defining nasal cartilage elasticity - Biomechanical testing of the tripod theory based on a cantilevered model. *ARCHIVES OF FACIAL PLASTIC SURGERY*. 2007;9(4):264-270.

83. Xia Y, Zheng S, Szarko M, Lee J. Anisotropic properties of bovine nasal cartilage. *MICROSCOPY RESEARCH AND TECHNIQUE*. 2012;75(3):300-306. doi:10.1002/jemt.21058

84. Youn JI, Telenkov SA, Kim E, et al. Optical and thermal properties of nasal septal cartilage. *Lasers in surgery and medicine*. 2000;27(2):119-128.

85. Baddam P, Kung T, Adesida AB, Graf D. Histological and molecular characterization of the growing nasal septum in mice. *J Anat*. 2021;238(3):751-764. doi:10.1111/joa.13332

86. Fertuzinhos A, Teixeira MA, Ferreira MG, et al. Thermo-Mechanical Behaviour of Human Nasal Cartilage. *POLYMERS*. 2020;12(1).

87. Naumann A, Dennis JE, Awadallah A, et al. Immunochemical and mechanical characterization of cartilage subtypes in rabbit. *Journal of Histochemistry and Cytochemistry*. 2002;50(8):1049-1058.

88. Richmon J, Sage A, Wong V, Chen A, Sah R, Watston D. Compressive biomechanical properties of human nasal septal cartilage. *AMERICAN JOURNAL OF RHINOLOGY*. 2006;20(5):496-501. doi:10.2500/ajr.2006.20.2932

89. Sriprakash V. Prevalence and clinical features of nasal septum deviation: a study in an urban centre. *International Journal of Otorhinolaryngology and Head and Neck Surgery*. 2017;3(4):842-844.

90. Georgalas C. The role of the nose in snoring and obstructive sleep apnoea: an update. *Eur Arch Otorhinolaryngol*. 2011;268(9):1365-1373. doi:10.1007/s00405-010-1469-7

91. Hsu DW, Suh JD. Anatomy and Physiology of Nasal Obstruction. *Otolaryngol Clin North Am*. 2018;51(5):853-865. doi:10.1016/j.otc.2018.05.001

92. Bixler EO, Vgontzas AN, Lin H-M, et al. Sleep Disordered Breathing in Children in a General Population Sample: Prevalence and Risk Factors. *Sleep*. 2009;32(6):731-736.

93. Kotagal S. Treatment of dyssomnias and parasomnias in childhood. *Curr Treat Options Neurol*. 2012;14(6):630-649. doi:10.1007/s11940-012-0199-0

94. Tarasiuk A, Reuveni H. The economic impact of obstructive sleep apnea. *Curr Opin Pulm Med*. 2013;19(6):639-644. doi:10.1097/MCP.0b013e3283659e1e

95. Silvoniemi P, Suonpää J, Sipilä J, Grénman R, Erkinjuntti M. Sleep disorders in patients with severe nasal obstruction due to septal deviation. *Acta Otolaryngol Suppl*. 1997;529:199-201. doi:10.3109/00016489709124121

96. Choi JH, Kim EJ, Kim YS, et al. Effectiveness of nasal surgery alone on sleep quality, architecture, position, and sleep-disordered breathing in obstructive sleep apnea syndrome with nasal obstruction. *Am J Rhinol Allergy*. 2011;25(5):338-341. doi:10.2500/ajra.2011.25.3654

97. Koutsourelakis I, Georgoulopoulos G, Perraki E, Vagiakis E, Roussos C, Zakynthinos SG. Randomised trial of nasal surgery for fixed nasal obstruction in obstructive sleep apnoea. *Eur Respir J*. 2008;31(1):110-117. doi:10.1183/09031936.00087607

98. Wu J, Zhao G, Li Y, et al. Apnea-hypopnea index decreased significantly after nasal surgery for obstructive sleep apnea: A meta-analysis. *Medicine (Baltimore)*. 2017;96(5):e6008. doi:10.1097/MD.0000000000006008

99. Lai C-C, Lin P-W, Lin H-C, et al. Clinical Predictors of Pediatric Obstructive Sleep Apnea Syndrome. *Ann Otol Rhinol Laryngol*. 2018;127(9):608-613. doi:10.1177/0003489418781961

100. Certal V, Catumbela E, Winck JC, Azevedo I, Teixeira-Pinto A, Costa-Pereira A. Clinical assessment of pediatric obstructive sleep apnea: a systematic review and meta-analysis. *Laryngoscope*. 2012;122(9):2105-2114. doi:10.1002/lary.23465

101. Certal V, Silva H, Carvalho C, et al. Model for prediction of pediatric OSA: Proposal for a clinical decision rule. *Laryngoscope*. 2015;125(12):2823-2827. doi:10.1002/lary.25438

102. Chervin null, Hedger null, Dillon null, Pituch null. Pediatric sleep questionnaire (PSQ): validity and reliability of scales for sleep-disordered breathing, snoring, sleepiness, and behavioral problems. *Sleep Med*. 2000;1(1):21-32. doi:10.1016/s1389-9457(99)00009-x

103. Ahn YM. Treatment of obstructive sleep apnea in children. *Korean J Pediatr*. 2010;53(10):872-879. doi:10.3345/kjp.2010.53.10.872

104. Eimar H, Al-Saleh M a. Q, Cortes ARG, Gozal D, Graf D, Flores-Mir C. Sleep-Disordered Breathing Is Associated with Reduced Mandibular Cortical Width in Children. *JDR Clin Trans Res*. 2019;4(1):58-67. doi:10.1177/2380084418776906

105. Chervin null, Hedger null, Dillon null, Pituch null. Pediatric sleep questionnaire (PSQ): validity and reliability of scales for sleep-disordered breathing, snoring, sleepiness, and behavioral problems. *Sleep Med*. 2000;1(1):21-32. doi:10.1016/s1389-9457(99)00009-x

106. El-Anwar MW, Hamed AA, Abdulmonaem G, Elnashar I, Elfiki IM. Computed Tomography Measurement of Inferior Turbinate in Asymptomatic Adult. *Int Arch Otorhinolaryngol*. 2017;21(4):366-370. doi:10.1055/s-0037-1598649

107. Kaditis AG, Alonso Alvarez ML, Boudewyns A, et al. Obstructive sleep disordered breathing in 2- to 18-year-old children: diagnosis and management. *Eur Respir J*. 2016;47(1):69-94. doi:10.1183/13993003.00385-2015

108. Gray LP. The development and significance of septal and dental deformity from birth to eight years. *Int J Pediatr Otorhinolaryngol*. 1983;6(3):265-277. doi:10.1016/s0165-5876(83)80128-1

109. Song SY, Kim IT, Chang KH, Lee KS, Kim HJ, Lim HJ. The Prevalence of Nasal Septal Deformities among Children in Kindergarten and First Grade in Anyang and Kunpo Cities. *Journal of Rhinology*. 2016;6(1):58-60.

110. Subarić M, Mladina R. Nasal septum deformities in children and adolescents: a cross sectional study of children from Zagreb, Croatia. *Int J Pediatr Otorhinolaryngol*. 2002;63(1):41-48. doi:10.1016/s0165-5876(01)00646-2

111. Aziz T, Biron VL, Ansari K, Flores-Mir C. Measurement tools for the diagnosis of nasal septal deviation: a systematic review. *J Otolaryngol Head Neck Surg*. 2014;43:11. doi:10.1186/1916-0216-43-11

112. Gozal D, Kheirandish-Gozal L. Sleep Disordered Breathing in Children - A Comprehensive Clinical Guide to Evaluation and Treatment | Leila Kheirandish-Gozal | Springer. Published 2012. Accessed June 17, 2021. https://www.springer.com/gp/book/9781607617242

113. Berger G, Hammel I, Berger R, Avraham S, Ophir D. Histopathology of the inferior turbinate with compensatory hypertrophy in patients with deviated nasal septum. *Laryngoscope*. 2000;110(12):2100-2105. doi:10.1097/00005537-200012000-00024

114. Egeli E, Demirci L, Yazýcý B, Harputluoglu U. Evaluation of the inferior turbinate in patients with deviated nasal septum by using computed tomography. *Laryngoscope*. 2004;114(1):113-117. doi:10.1097/00005537-200401000-00020

115. Kim I-S, Lee M-Y, Lee K-I, Kim H-Y, Chung Y-J. Analysis of the Development of the Nasal Septum according to Age and Gender Using MRI. *Clin Exp Otorhinolaryngol*. 2008;1(1):29-34. doi:10.3342/ceo.2008.1.1.29

116. Harkema J. Comparative Anatomy and Epithelial Cell Biology of the Nose. *Comparative Biology of the Normal Lung: Second Edition*. Published online December 31, 2015:7-19. doi:10.1016/B978-0-12-404577-4.00002-3

117. Al Dayeh AA, Herring SW. Cellular proliferation in the nasal septal cartilage of juvenile minipigs. *J Anat*. 2014;225(6):604-613. doi:10.1111/joa.12237

118. Grogan SP, Miyaki S, Asahara H, D'Lima DD, Lotz MK. Mesenchymal progenitor cell markers in human articular cartilage: normal distribution and changes in osteoarthritis. *Arthritis Res Ther*. 2009;11(3):R85. doi:10.1186/ar2719

119. Varela-Eirin M, Loureiro J, Fonseca E, et al. Cartilage regeneration and ageing: Targeting cellular plasticity in osteoarthritis. *Ageing Res Rev*. 2018;42:56-71. doi:10.1016/j.arr.2017.12.006

120. Cervantes-Diaz F, Contreras P, Marcellini S. Evolutionary origin of endochondral ossification: the transdifferentiation hypothesis. *Dev Genes Evol*. 2017;227(2):121-127. doi:10.1007/s00427-016-0567-y

121. Marconi A, Hancock-Ronemus A, Gillis JA. Adult chondrogenesis and spontaneous cartilage repair in the skate, Leucoraja erinacea. Rosen CJ, Sánchez Alvarado A, Debiais Thibaud M, eds. *eLife*. 2020;9:e53414. doi:10.7554/eLife.53414

122. Hall BK, Precious DS. Cleft lip, nose, and palate: the nasal septum as the pacemaker for midfacial growth. *Oral Surg Oral Med Oral Pathol Oral Radiol*. 2013;115(4):442-447. doi:10.1016/j.oooo.2012.05.005

123. Moss ML, Bromberg BE, Song IC, Eisenman G. The passive role of nasal septal cartilage in mid-facial growth. *Plast Reconstr Surg*. 1968;41(6):536-542. doi:10.1097/00006534-196806000-00004

124. Sarnat BG, Wexler MR. The snout after resection of nasal septum in adult rabbits. *Arch Otolaryngol*. 1967;86(4):463-466. doi:10.1001/archotol.1967.00760050465021

125. Stenström SJ, Thilander BL. Effects of nasal septal cartilage resections on young guinea pigs. *Plast Reconstr Surg*. 1970;45(2):160-170. doi:10.1097/00006534-197002000-00010

126. D'Ascanio L, Lancione C, Pompa G, Rebuffini E, Mansi N, Manzini M. Craniofacial growth in children with nasal septum deviation: a cephalometric comparative study. *Int J Pediatr Otorhinolaryngol*. 2010;74(10):1180-1183. doi:10.1016/j.ijporl.2010.07.010

127. Kemble JV. The importance of the nasal septum in facial development. *J Laryngol Otol*. 1973;87(4):379-386. doi:10.1017/s0022215100077021

128. Westreich RW, Burstein D, Fraser M. The effect of facial asymmetry on nasal deviation. *Facial Plast Surg*. 2011;27(5):397-412. doi:10.1055/s-0031-1288923

129. Mumme M, Barbero A, Miot S, et al. Nasal chondrocyte-based engineered autologous cartilage tissue for repair of articular cartilage defects: an observational first-in-human trial. *Lancet*. 2016;388(10055):1985-1994. doi:10.1016/S0140-6736(16)31658-0

130. Goergen MJ, Holton NE, Grünheid T. Morphological interaction between the nasal septum and nasofacial skeleton during human ontogeny. *J Anat*. 2017;230(5):689-700. doi:10.1111/joa.12596

131. Wealthall RJ, Herring SW. Endochondral ossification of the mouse nasal septum. *Anat Rec A Discov Mol Cell Evol Biol*. 2006;288(11):1163-1172. doi:10.1002/ar.a.20385

132. Gómez-Picos P, Eames BF. On the evolutionary relationship between chondrocytes and osteoblasts. *Front Genet*. 2015;6:297. doi:10.3389/fgene.2015.00297

133. Bi W, Deng JM, Zhang Z, Behringer RR, de Crombrugghe B. Sox9 is required for cartilage formation. *Nat Genet*. 1999;22(1):85-89. doi:10.1038/8792

134. Kozhemyakina E, Lassar AB, Zelzer E. A pathway to bone: signaling molecules and transcription factors involved in chondrocyte development and maturation. *Development*. 2015;142(5):817-831. doi:10.1242/dev.105536

135. Cattell M, Lai S, Cerny R, Medeiros DM. A new mechanistic scenario for the origin and evolution of vertebrate cartilage. *PLoS ONE*. 2011;6(7):e22474. doi:10.1371/journal.pone.0022474

136. Robins SP, Seibel MJ, Bilezikian JP. *Dynamics of Bone and Cartilage Metabolism*. 2nd ed. Elsevier; 2006. doi:10.1016/B978-0-12-088562-6.X5000-6

137. Hojo H, Ohba S, He X, Lai LP, McMahon AP. Sp7/Osterix Is Restricted to Bone-Forming Vertebrates where It Acts as a Dlx Co-factor in Osteoblast Specification. *Dev Cell*. 2016;37(3):238-253. doi:10.1016/j.devcel.2016.04.002

138. Zoch ML, Clemens TL, Riddle RC. New insights into the biology of osteocalcin. *Bone*. 2016;82:42-49. doi:10.1016/j.bone.2015.05.046

139. Enomoto H, Furuichi T, Zanma A, et al. Runx2 deficiency in chondrocytes causes adipogenic changes in vitro. *J Cell Sci*. 2004;117(Pt 3):417-425. doi:10.1242/jcs.00866

140. Vora SR, Camci ED, Cox TC. Postnatal Ontogeny of the Cranial Base and Craniofacial Skeleton in Male C57BL/6J Mice: A Reference Standard for Quantitative Analysis. *Front Physiol*. 2015;6:417. doi:10.3389/fphys.2015.00417

141. Las Heras F, Gahunia HK, Pritzker KPH. Articular cartilage development: a molecular perspective. *Orthop Clin North Am*. 2012;43(2):155-171, v. doi:10.1016/j.ocl.2012.01.003

142. Protocol Database - Histology, Immunohistochemistry, Molecular and Cell Biology. Accessed June 5, 2020. http://www.ihcworld.com/protocol_database.htm

143. Hu DP, Ferro F, Yang F, et al. Cartilage to bone transformation during fracture healing is coordinated by the invading vasculature and induction of the core pluripotency genes. *Development*. 2017;144(2):221-234. doi:10.1242/dev.130807

144. Hoyte DA. A critical analysis of the growth in length of the cranial base. *Birth Defects Orig Artic Ser*. 1975;11(7):255-282.

145. Yan B, Zhang Z, Jin D, et al. mTORC1 regulates PTHrP to coordinate chondrocyte growth, proliferation and differentiation. *Nat Commun*. 2016;7:11151. doi:10.1038/ncomms11151

146. Loparic M, Wirz D, Daniels AU, et al. Micro- and nanomechanical analysis of articular cartilage by indentation-type atomic force microscopy: validation with a gel-microfiber composite. *Biophys J*. 2010;98(11):2731-2740. doi:10.1016/j.bpj.2010.02.013

147. Prein C, Warmbold N, Farkas Z, Schieker M, Aszodi A, Clausen-Schaumann H. Structural and mechanical properties of the proliferative zone of the developing murine growth plate cartilage assessed by atomic force microscopy. *Matrix Biol*. 2016;50:1-15. doi:10.1016/j.matbio.2015.10.001

148. Chau M, Lui JC, Landman EBM, et al. Gene expression profiling reveals similarities between the spatial architectures of postnatal articular and growth plate cartilage. *PLoS ONE*. 2014;9(7):e103061. doi:10.1371/journal.pone.0103061

149. Farquharson C, Lester D, Seawright E, Jefferies D, Houston B. Microtubules are potential regulators of growth-plate chondrocyte differentiation and hypertrophy. *Bone*. 1999;25(4):405-412. doi:10.1016/s8756-3282(99)00187-8

150. Pockwinse SM, Rajgopal A, Young DW, et al. Microtubule-dependent nuclear-cytoplasmic shuttling of Runx2. *J Cell Physiol*. 2006;206(2):354-362. doi:10.1002/jcp.20469

151. Yang M, Arai A, Udagawa N, et al. Osteogenic Factor Runx2 Marks a Subset of Leptin Receptor-Positive Cells that Sit Atop the Bone Marrow Stromal Cell Hierarchy. *Sci Rep*. 2017;7(1):4928. doi:10.1038/s41598-017-05401-1

152. Henriet P, Eeckhout Y. Chapter 154 - Matrix Metallopeptidase-13/Collagenase 3. In: Rawlings ND, Salvesen G, eds. *Handbook of Proteolytic Enzymes (Third Edition)*. Academic Press; 2013:734-744. doi:10.1016/B978-0-12-382219-2.00154-X

153. Mitchell PG, Magna HA, Reeves LM, et al. Cloning, expression, and type II collagenolytic activity of matrix metalloproteinase-13 from human osteoarthritic cartilage. *J Clin Invest*. 1996;97(3):761-768. doi:10.1172/JCI118475

154. Inada M, Wang Y, Byrne MH, et al. Critical roles for collagenase-3 (Mmp13) in development of growth plate cartilage and in endochondral ossification. *Proc Natl Acad Sci USA*. 2004;101(49):17192-17197. doi:10.1073/pnas.0407788101

155. Sepulveda H, Aguilar R, Prieto CP, et al. Epigenetic Signatures at the RUNX2-P1 and Sp7 Gene Promoters Control Osteogenic Lineage Commitment of Umbilical Cord-Derived Mesenchymal Stem Cells. *J Cell Physiol*. 2017;232(9):2519-2527. doi:10.1002/jcp.25627

156. Wei J, Karsenty G. An overview of the metabolic functions of osteocalcin. *Curr Osteoporos Rep*. 2015;13(3):180-185. doi:10.1007/s11914-015-0267-y

157. Hallett SA, Ono W, Ono N. Growth Plate Chondrocytes: Skeletal Development, Growth and Beyond. *Int J Mol Sci*. 2019;20(23). doi:10.3390/ijms20236009

158. Hall BK, Miyake T. All for one and one for all: condensations and the initiation of skeletal development. *Bioessays*. 2000;22(2):138-147. doi:10.1002/(SICI)1521-1878(200002)22:2<138::AID-BIES5>3.0.CO;2-4

159. Kobayashi T, Soegiarto DW, Yang Y, et al. Indian hedgehog stimulates periarticular chondrocyte differentiation to regulate growth plate length independently of PTHrP. *J Clin Invest*. 2005;115(7):1734-1742. doi:10.1172/JCI24397

160. Kaucka M, Zikmund T, Tesarova M, et al. Oriented clonal cell dynamics enables accurate growth and shaping of vertebrate cartilage. *Elife*. 2017;6. doi:10.7554/eLife.25902

161. Claassen H, Schicht M, Fleiner B, et al. Different Patterns of Cartilage Mineralization Analyzed by Comparison of Human, Porcine, and Bovine Laryngeal Cartilages. *J Histochem Cytochem*. 2017;65(6):367-379. doi:10.1369/0022155417703025

162. Mizuhashi K, Ono W, Matsushita Y, et al. Resting zone of the growth plate houses a unique class of skeletal stem cells. *Nature*. 2018;563(7730):254-258. doi:10.1038/s41586-018-0662-5

163. Gibson G. Active role of chondrocyte apoptosis in endochondral ossification. *Microsc Res Tech*. 1998;43(2):191-204. doi:10.1002/(SICI)1097-0029(19981015)43:2<191::AID-JEMT10>3.0.CO;2-T

164. Ortega N, Behonick DJ, Werb Z. Matrix remodeling during endochondral ossification. *Trends Cell Biol*. 2004;14(2):86-93. doi:10.1016/j.tcb.2003.12.003

165. Aghajanian P, Mohan S. The art of building bone: emerging role of chondrocyte-to-osteoblast transdifferentiation in endochondral ossification. *Bone Res*. 2018;6:19. doi:10.1038/s41413-018-0021-z

166. Zhou X, von der Mark K, Henry S, Norton W, Adams H, de Crombrugghe B. Chondrocytes transdifferentiate into osteoblasts in endochondral bone during development, postnatal growth and fracture healing in mice. *PLoS Genet*. 2014;10(12):e1004820. doi:10.1371/journal.pgen.1004820

167. Morgenthaler TI, Kapen S, Lee-Chiong T, et al. Practice parameters for the medical therapy of obstructive sleep apnea. *Sleep*. 2006;29(8):1031-1035.

168. Gipson K, Lu M, Kinane TB. Sleep-Disordered Breathing in Children. *Pediatr Rev*. 2019;40(1):3-13. doi:10.1542/pir.2018-0142

169. Gozal D. Sleep-disordered breathing and school performance in children. *Pediatrics*. 1998;102(3 Pt 1):616-620. doi:10.1542/peds.102.3.616

170. Leger D, Bayon V, Laaban JP, Philip P. Impact of sleep apnea on economics. *Sleep Med Rev*. 2012;16(5):455-462. doi:10.1016/j.smrv.2011.10.001

171. Bozzini MFR, Di Francesco RC. Managing obstructive sleep apnoea in children: the role of craniofacial morphology. *Clinics (Sao Paulo)*. 2016;71(11):664-666. doi:10.6061/clinics/2016(11)08

172. Dewan NA, Nieto FJ, Somers VK. Intermittent Hypoxemia and OSA. *Chest*. 2015;147(1):266-274. doi:10.1378/chest.14-0500

173. Gabryelska A, Łukasik ZM, Makowska JS, Białasiewicz P. Obstructive Sleep Apnea: From Intermittent Hypoxia to Cardiovascular Complications via Blood Platelets. *Front Neurol*. 2018;9:635. doi:10.3389/fneur.2018.00635

174. Veasey S. Insight from animal models into the cognitive consequences of adult sleep-disordered breathing. *ILAR J*. 2009;50(3):307-311. doi:10.1093/ilar.50.3.307

175. Hoeve HL, Joosten KF, van den Berg S. Management of obstructive sleep apnea syndrome in children with craniofacial malformation. *Int J Pediatr Otorhinolaryngol*. 1999;49 Suppl 1:S59-61. doi:10.1016/s0165-5876(99)00134-2

176. Carithers JS, Gebhart DE, Williams JA. Postoperative risks of pediatric tonsilloadenoidectomy. *Laryngoscope*. 1987;97(4):422-429. doi:10.1288/00005537-198704000-00004

177. Tan A, Cheung YY, Yin J, Lim W-Y, Tan LWL, Lee C-H. Prevalence of sleep-disordered breathing in a multiethnic Asian population in Singapore: A community-based study. *Respirology*. 2016;21(5):943-950. doi:10.1111/resp.12747

178. Skotko BG, Macklin EA, Muselli M, et al. A predictive model for obstructive sleep apnea and Down syndrome. *Am J Med Genet A*. 2017;173(4):889-896. doi:10.1002/ajmg.a.38137

179. Cielo CM, Montalva FM, Taylor JA. Craniofacial disorders associated with airway obstruction in the neonate. *Semin Fetal Neonatal Med*. 2016;21(4):254-262. doi:10.1016/j.siny.2016.03.001

180. Hendricks JC, Kline LR, Kovalski RJ, O'Brien JA, Morrison AR, Pack AI. The English bulldog: a natural model of sleep-disordered breathing. *J Appl Physiol*. 1987;63(4):1344-1350. doi:10.1152/jappl.1987.63.4.1344

181. Strohl KP, Thomas AJ. Ventilatory behavior and metabolism in two strains of obese rats. *Respir Physiol*. 2001;124(2):85-93. doi:10.1016/s0034-5687(00)00190-0

182. Brennick MJ, Pack AI, Ko K, et al. Altered upper airway and soft tissue structures in the New Zealand Obese mouse. *Am J Respir Crit Care Med*. 2009;179(2):158-169. doi:10.1164/rccm.200809-1435OC

183. Polotsky M, Elsayed-Ahmed AS, Pichard L, et al. Effects of leptin and obesity on the upper airway function. *J Appl Physiol*. 2012;112(10):1637-1643. doi:10.1152/japplphysiol.01222.2011

184. Chopra S, Polotsky VY, Jun JC. Sleep Apnea Research in Animals. Past, Present, and Future. *Am J Respir Cell Mol Biol*. 2016;54(3):299-305. doi:10.1165/rcmb.2015-0218TR

185. Gangopadhyay N, Mendonca DA, Woo AS. Pierre Robin Sequence. *Semin Plast Surg*. 2012;26(2):76-82. doi:10.1055/s-0032-1320065

186. Kouskoura T, El Fersioui Y, Angelini M, Graf D, Katsaros C, Chiquet M. Dislocated Tongue Muscle Attachment and Cleft Palate Formation. *J Dent Res*. 2016;95(4):453-459. doi:10.1177/0022034515621869

187. Kouskoura T, Kozlova A, Alexiou M, et al. The etiology of cleft palate formation in BMP7-deficient mice. *PLoS ONE*. 2013;8(3):e59463. doi:10.1371/journal.pone.0059463

188. Zouvelou V, Luder H-U, Mitsiadis TA, Graf D. Deletion of BMP7 affects the development of bones, teeth, and other ectodermal appendages of the orofacial complex. *J Exp Zool B Mol Dev Evol*. 2009;312B(4):361-374. doi:10.1002/jez.b.21262

189. Seifert EL, Knowles J, Mortola JP. Continuous circadian measurements of ventilation in behaving adult rats. *Respir Physiol*. 2000;120(2):179-183. doi:10.1016/s0034-5687(00)00108-0

190. Lighton JRB. *Measuring Metabolic Rates: A Manual for Scientists*. Oxford University Press; 2008.

191. Drorbaugh JE, Fenn WO. A barometric method for measuring ventilation in newborn infants. *Pediatrics*. 1955;16(1):81-87.

192. Dejours P. *Principles of Comparative Respiratory Physiology*. Elsevier/North-Holland Biomedical Press; 1981.

193. Mortola JP. Breathing pattern in newborns. *J Appl Physiol Respir Environ Exerc Physiol*. 1984;56(6):1533-1540. doi:10.1152/jappl.1984.56.6.1533

194. Cummings KJ, Hewitt JC, Li A, Daubenspeck JA, Nattie EE. Postnatal loss of brainstem serotonin neurones compromises the ability of neonatal rats to survive episodic severe hypoxia. *J Physiol (Lond)*. 2011;589(Pt 21):5247-5256. doi:10.1113/jphysiol.2011.214445

195. Depocas F, Hart JS. Use of the Pauling oxygen analyzer for measurement of oxygen consumption of animals in open-circuit systems and in a short-lag, closed-circuit apparatus. *J Appl Physiol*. 1957;10(3):388-392. doi:10.1152/jappl.1957.10.3.388

196. Yamauchi M, Ocak H, Dostal J, Jacono FJ, Loparo KA, Strohl KP. Post-sigh breathing behavior and spontaneous pauses in the C57BL/6J (B6) mouse. *Respir Physiol Neurobiol*. 2008;162(2):117-125. doi:10.1016/j.resp.2008.05.003

197. Koonen DPY, Sung MMY, Kao CKC, et al. Alterations in skeletal muscle fatty acid handling predisposes middle-aged mice to diet-induced insulin resistance. *Diabetes*. 2010;59(6):1366-1375. doi:10.2337/db09-1142

198. Dougherty JP, Springer DA, Gershengorn MC. The Treadmill Fatigue Test: A Simple, High-throughput Assay of Fatigue-like Behavior for the Mouse. *J Vis Exp*. 2016;(111). doi:10.3791/54052

199. Wei X, Thomas N, Hatch NE, Hu M, Liu F. Postnatal Craniofacial Skeletal Development of Female C57BL/6NCrl Mice. *Front Physiol*. 2017;8. doi:10.3389/fphys.2017.00697

200. Milanesi J de M, Berwig LC, Schuch LH, Ritzel RA, Silva AMT da, Corrêa ECR. Nasal patency and otorhinolaryngologic-orofacial features in children. *Braz J Otorhinolaryngol*. 2019;85(1):83-91. doi:10.1016/j.bjorl.2017.10.014

201. Li P, Janczewski WA, Yackle K, et al. The peptidergic control circuit for sighing. *Nature*. 2016;530(7590):293-297. doi:10.1038/nature16964

202. Bastianini S, Alvente S, Berteotti C, et al. Post-sigh sleep apneas in mice: Systematic review and data-driven definition. *J Sleep Res*. 2019;28(6):e12845. doi:10.1111/jsr.12845

203. Fletcher EC, Lesske J, Behm R, Miller CC, Stauss H, Unger T. Carotid chemoreceptors, systemic blood pressure, and chronic episodic hypoxia mimicking sleep apnea. *J Appl Physiol*. 1992;72(5):1978-1984. doi:10.1152/jappl.1992.72.5.1978

204. Gozal D, Daniel JM, Dohanich GP. Behavioral and anatomical correlates of chronic episodic hypoxia during sleep in the rat. *J Neurosci*. 2001;21(7):2442-2450.

205. Farré R, Montserrat JM, Gozal D, Almendros I, Navajas D. Intermittent Hypoxia Severity in Animal Models of Sleep Apnea. *Front Physiol*. 2018;9. doi:10.3389/fphys.2018.01556

206. Almendros I, Farré R, Planas AM, et al. Tissue oxygenation in brain, muscle, and fat in a rat model of sleep apnea: differential effect of obstructive apneas and intermittent hypoxia. *Sleep*. 2011;34(8):1127-1133. doi:10.5665/SLEEP.1176

207. Tarasiuk A, Segev Y. Abnormal Growth and Feeding Behavior in Upper Airway Obstruction in Rats. *Front Endocrinol (Lausanne)*. 2018;9:298. doi:10.3389/fendo.2018.00298

208. Iida M, Murakami T, Ishida K, Mizuno A, Kuwajima M, Shima K. Substitution at codon 269 (glutamine --> proline) of the leptin receptor (OB-R) cDNA is the only mutation found in the Zucker fatty (fa/fa) rat. *Biochem Biophys Res Commun*. 1996;224(2):597-604. doi:10.1006/bbrc.1996.1070

209. Perlyn CA, DeLeon VB, Babbs C, et al. The craniofacial phenotype of the Crouzon mouse: analysis of a model for syndromic craniosynostosis using three-dimensional MicroCT. *Cleft Palate Craniofac J*. 2006;43(6):740-748. doi:10.1597/05-212

210. Hong M, Krauss RS. Cdon mutation and fetal ethanol exposure synergize to produce midline signaling defects and holoprosencephaly spectrum disorders in mice. *PLoS Genet*. 2012;8(10):e1002999. doi:10.1371/journal.pgen.1002999

211. Rosenberg P, Arlis HR, Haworth RD, Heier L, Hoffman L, LaTrenta G. The role of the cranial base in facial growth: experimental craniofacial synostosis in the rabbit. *Plast Reconstr Surg*. 1997;99(5):1396-1407. doi:10.1097/00006534-199704001-00030

212. Eimar H, Tamimi F, Retrouvey J-M, Rauch F, Aubin JE, McKee MD. Craniofacial and Dental Defects in the Col1a1Jrt/+ Mouse Model of Osteogenesis Imperfecta. *J Dent Res*. 2016;95(7):761-768. doi:10.1177/0022034516637045

213. Suzuki A, Sangani DR, Ansari A, Iwata J. Molecular Mechanisms of Midfacial Developmental Defects. *Dev Dyn*. 2016;245(3):276-293. doi:10.1002/dvdy.24368

214. Finkelstein Y, Wexler D, Berger G, Nachmany A, Shapiro-Feinberg M, Ophir D. Anatomical Basis of Sleep-Related Breathing Abnormalities in Children With Nasal Obstruction. *Arch Otolaryngol Head Neck Surg*. 2000;126(5):593-600. doi:10.1001/archotol.126.5.593

215. Lee RWW, Vasudavan S, Hui DS, et al. Differences in Craniofacial Structures and Obesity in Caucasian and Chinese Patients with Obstructive Sleep Apnea. *Sleep*. 2010;33(8):1075-1080.

216. Pacheco MCT, Fiorott BS, Finck NS, de Araújo MTM. Craniofacial changes and symptoms of sleep-disordered breathing in healthy children. *Dental Press J Orthod*. 2015;20(3):80-87. doi:10.1590/2176-9451.20.3.080-087.oar

217. Clark DW, Del Signore AG, Raithatha R, Senior BA. Nasal airway obstruction: Prevalence and anatomic contributors. *Ear Nose Throat J*. 2018;97(6):173-176. doi:10.1177/014556131809700615

218. Baddam P, Bussolaro C-T, Flores-Mir C, Graf D. Nasal cavity structural anomalies among children at high risk of sleep-disordered breathing: an exploratory cone-beam computed tomography study. *American Journal of Orthodontics & Dentofacial Orthopedics*. 2020;In Press.

219. Hsu DW, Suh JD. Anatomy and Physiology of Nasal Obstruction. *Otolaryngologic Clinics of North America*. 2018;51(5):853-865. doi:10.1016/j.otc.2018.05.001

220. Sanders MH, Moore SE. Inspiratory and expiratory partitioning of airway resistance during sleep in patients with sleep apnea. *Am Rev Respir Dis*. 1983;127(5):554-558. doi:10.1164/arrd.1983.127.5.554

221. Gleadhill IC, Schwartz AR, Schubert N, Wise RA, Permutt S, Smith PL. Upper airway collapsibility in snorers and in patients with obstructive hypopnea and apnea. *Am Rev Respir Dis*. 1991;143(6):1300-1303. doi:10.1164/ajrccm/143.6.1300

222. Yamauchi M, Tamaki S, Yoshikawa M, et al. Differences in Breathing Patterning During Wakefulness in Patients With Mixed Apnea-Dominant vs Obstructive-Dominant Sleep Apnea. *Chest*. 2011;140(1):54-61. doi:10.1378/chest.10-1082

223. Trosman I, Trosman SJ. Cognitive and Behavioral Consequences of Sleep Disordered Breathing in Children. *Med Sci (Basel)*. 2017;5(4). doi:10.3390/medsci5040030

224. Harkema JR, Morgan KT. Normal Morphology of the Nasal Passages in Laboratory Rodents. In: Jones TC, Dungworth DL, Mohr U, eds. *Respiratory System*. Monographs on Pathology of Laboratory Animals. Springer; 1996:3-17. doi:10.1007/978-3-642-61042-4_1

225. Agrawal A, Singh SK, Singh VP, Murphy E, Parikh I. Partitioning of nasal and pulmonary resistance changes during noninvasive plethysmography in mice. *J Appl Physiol*. 2008;105(6):1975-1979. doi:10.1152/japplphysiol.90700.2008

226. Niaki SEA, Shafaroodi H, Ghasemi M, Shakiba B, Fakhimi A, Dehpour AR. Mouth breathing increases the pentylenetetrazole-induced seizure threshold in mice: a role for ATP-sensitive potassium channels. *Epilepsy Behav*. 2008;13(2):284-289. doi:10.1016/j.yebeh.2008.04.013

227. Khurana A, Thach BT. Effects of upper airway stimulation on swallowing, gasping, and autoresuscitation in hypoxic mice. *Journal of Applied Physiology*. 1996;80(2):472-477. doi:10.1152/jappl.1996.80.2.472

228. Saito Y, Ezure K, Kobayashi M, Ito M, Saito K, Osawa M. A review of functional and structural components of the respiratory center involved in the arousal response. *Sleep Med*. 2002;3 Suppl 2:S71-74. doi:10.1016/s1389-9457(02)00170-3

229. Davis EM, O'Donnell CP. RODENT MODELS OF SLEEP APNEA. *Respir Physiol Neurobiol*. 2013;188(3):355-361. doi:10.1016/j.resp.2013.05.022

230. Pavan WJ, Raible DW. Specification of neural crest into sensory neuron and melanocyte lineages. *Dev Biol*. 2012;366(1):55-63. doi:10.1016/j.ydbio.2012.02.038

231. Annese V, Navarro-Guerrero E, Rodríguez-Prieto I, Pardal R. Physiological Plasticity of Neural-Crest-Derived Stem Cells in the Adult Mammalian Carotid Body. *Cell Rep*. 2017;19(3):471-478. doi:10.1016/j.celrep.2017.03.065

232. Segklia A, Seuntjens E, Elkouris M, et al. Bmp7 regulates the survival, proliferation, and neurogenic properties of neural progenitor cells during corticogenesis in the mouse. *PLoS ONE*. 2012;7(3):e34088. doi:10.1371/journal.pone.0034088

233. Choe Y, Kozlova A, Graf D, Pleasure SJ. Bone morphogenic protein signaling is a major determinant of dentate development. *J Neurosci*. 2013;33(16):6766-6775. doi:10.1523/JNEUROSCI.0128-13.2013

234. Lewis AE, Vasudevan HN, O'Neill AK, Soriano P, Bush JO. The widely used Wnt1-Cre transgene causes developmental phenotypes by ectopic activation of Wnt signaling. *Dev Biol*. 2013;379(2):229-234. doi:10.1016/j.ydbio.2013.04.026

235. Moss IR. Respiratory responses to single and episodic hypoxia during development: mechanisms of adaptation. *Respir Physiol*. 2000;121(2-3):185-197. doi:10.1016/s0034-5687(00)00127-4

236. Teppema LJ, Dahan A. The ventilatory response to hypoxia in mammals: mechanisms, measurement, and analysis. *Physiol Rev*. 2010;90(2):675-754. doi:10.1152/physrev.00012.2009

237. Peña F, Ramirez J-M. Hypoxia-induced changes in neuronal network properties. *Mol Neurobiol*. 2005;32(3):251-283. doi:10.1385/MN:32:3:251

238. Wellman A, Malhotra A, Jordan AS, Stevenson KE, Gautam S, White DP. Effect of oxygen in obstructive sleep apnea: role of loop gain. *Respir Physiol Neurobiol*. 2008;162(2):144-151. doi:10.1016/j.resp.2008.05.019

239. Mehta V, Vasu TS, Phillips B, Chung F. Obstructive sleep apnea and oxygen therapy: a systematic review of the literature and meta-analysis. *J Clin Sleep Med*. 2013;9(3):271-279. doi:10.5664/jcsm.2500

240. Xie A, Teodorescu M, Pegelow DF, et al. Effects of stabilizing or increasing respiratory motor outputs on obstructive sleep apnea. *J Appl Physiol*. 2013;115(1):22-33. doi:10.1152/japplphysiol.00064.2013

241. Hoffstein V, Viner S, Mateika S, Conway J. Treatment of obstructive sleep apnea with nasal continuous positive airway pressure. Patient compliance, perception of benefits, and side effects. The American review of respiratory disease. doi:10.1164/ajrccm/145.4_Pt_1.841

242. Gomes J, Finlay M, Ahmed AK, et al. Electrophysiological abnormalities precede overt structural changes in arrhythmogenic right ventricular cardiomyopathy due to mutations in desmoplakin-A combined murine and human study. *Eur Heart J*. 2012;33(15):1942-1953. doi:10.1093/eurheartj/ehr472

243. De Luca Canto G, Pachêco-Pereira C, Aydinoz S, Major PW, Flores-Mir C, Gozal D. Biomarkers associated with obstructive sleep apnea: A scoping review. *Sleep Med Rev*. 2015;23:28-45. doi:10.1016/j.smrv.2014.11.004

244. Krane SM, Kantrowitz FG, Byrne M, Pinnell SR, Singer FR. Urinary excretion of hydroxylysine and its glycosides as an index of collagen degradation. *J Clin Invest*. 1977;59(5):819-827. doi:10.1172/JCI108704

245. Tang L, Zeng J, Geng P, et al. Global Metabolic Profiling Identifies a Pivotal Role of Proline and Hydroxyproline Metabolism in Supporting Hypoxic Response in Hepatocellular Carcinoma. *Clin Cancer Res*. 2018;24(2):474-485. doi:10.1158/1078-0432.CCR-17-1707

246. Evans CA, Selvadurai H, Baur LA, Waters KA. Effects of Obstructive Sleep Apnea and Obesity on Exercise Function in Children. *Sleep*. 2014;37(6):1103-1110. doi:10.5665/sleep.3770

247. Serifoglu I, OZ İİ, Damar M, Buyukuysal MC, Tosun A, Tokgöz Ö. Relationship between the degree and direction of nasal septum deviation and nasal bone morphology. *Head Face Med*. 2017;13. doi:10.1186/s13005-017-0136-2

248. Wang J, Dou X, Liu D, et al. Assessment of the effect of deviated nasal septum on the structure of nasal cavity. *Eur Arch Otorhinolaryngol*. 2016;273(6):1477-1480. doi:10.1007/s00405-015-3770-y

249. Mandour YMH, Abo Youssef SM, Moussa HH. Polysomnographic and pulmonary function changes in patients with sleep problems after septoplasty with turbinectomy. *Am J Otolaryngol*. 2019;40(2):187-190. doi:10.1016/j.amjoto.2018.12.003

250. Alsufyani N, Isaac A, Witmans M, Major P, El-Hakim H. Predictors of failure of DISE-directed adenotonsillectomy in children with sleep disordered breathing. *J Otolaryngol Head Neck Surg*. 2017;46(1):37. doi:10.1186/s40463-017-0213-3

251. D'Ascanio L, Lancione C, Pompa G, Rebuffini E, Mansi N, Manzini M. Craniofacial growth in children with nasal septum deviation: a cephalometric comparative study. *Int J Pediatr Otorhinolaryngol*. 2010;74(10):1180-1183. doi:10.1016/j.ijporl.2010.07.010

252. Moghaddam MGh, Garcia GJM, Frank-Ito DO, Kimbell JS, Rhee JS. Virtual septoplasty: a method to predict surgical outcomes for patients with nasal airway obstruction. *Int J CARS*. 2020;15(4):725-735. doi:10.1007/s11548-020-02124-z

253. Lavernia L, Brown WE, Wong BJF, Hu JC, Athanasiou KA. Toward tissue-engineering of nasal cartilages. *Acta Biomater*. 2019;88:42-56. doi:10.1016/j.actbio.2019.02.025

254. Tchetina EV, Markova GA. Regulation of energy metabolism in the growth plate and osteoarthritic chondrocytes. *Rheumatol Int*. 2018;38(11):1963-1974. doi:10.1007/s00296-018-4103-4

255. Coles JM, Zhang L, Blum JJ, et al. Loss of cartilage structure, stiffness, and frictional properties in mice lacking PRG4. *Arthritis Rheum*. 2010;62(6):1666-1674. doi:10.1002/art.27436

256. Candela ME, Wang C, Gunawardena AT, et al. Alpha 5 Integrin Mediates Osteoarthritic Changes in Mouse Knee Joints. *PLoS One*. 2016;11(6):e0156783. doi:10.1371/journal.pone.0156783

257. Zhong L, Huang X, Rodrigues ED, et al. Endogenous DKK1 and FRZB Regulate Chondrogenesis and Hypertrophy in Three-Dimensional Cultures of Human Chondrocytes and Human Mesenchymal Stem Cells. *Stem Cells Dev*. 2016;25(23):1808-1817. doi:10.1089/scd.2016.0222

258. Liu S-S, Zhou P, Zhang Y. Abnormal expression of key genes and proteins in the canonical Wnt/β-catenin pathway of articular cartilage in a rat model of exercise-induced osteoarthritis. *Mol Med Rep*. 2016;13(3):1999-2006. doi:10.3892/mmr.2016.4798

259. Caron MMJ, Emans PJ, Cremers A, et al. Hypertrophic differentiation during chondrogenic differentiation of progenitor cells is stimulated by BMP-2 but suppressed by BMP-7. *Osteoarthritis Cartilage*. 2013;21(4):604-613. doi:10.1016/j.joca.2013.01.009

260. Huang X, Zhong L, Post JN, Karperien M. Co-treatment of TGF-β3 and BMP7 is superior in stimulating chondrocyte redifferentiation in both hypoxia and normoxia compared to single treatments. *Scientific Reports*. 2018;8(1):10251. doi:10.1038/s41598-018-27602-y

261. Merrihew C, Kumar B, Heretis K, Rueger DC, Kuettner KE, Chubinskaya S. Alterations in endogenous osteogenic protein-1 with degeneration of human articular cartilage. *J Orthop Res*. 2003;21(5):899-907. doi:10.1016/S0736-0266(03)00055-X

262. Baddam P, Biancardi V, Roth DM, et al. Neural crest-specific deletion of Bmp7 leads to midfacial hypoplasia, nasal airway obstruction, and disordered breathing modelling Obstructive Sleep Apnea. *Dis Model Mech*. Published online January 11, 2021. doi:10.1242/dmm.047738

263. Abula K, Muneta T, Miyatake K, et al. Elimination of BMP7 from the developing limb mesenchyme leads to articular cartilage degeneration and synovial inflammation with increased age. *FEBS Letters*. 2015;589(11):1240-1248. doi:10.1016/j.febslet.2015.04.004

264. Malik Z, Roth DM, Eaton F, Theodor JM, Graf D. Mesenchymal Bmp7 Controls Onset of Tooth Mineralization: A Novel Way to Regulate Molar Cusp Shape. *Front Physiol*. 2020;11. doi:10.3389/fphys.2020.00698

265. Malik Z, Alexiou M, Hallgrimsson B, Economides AN, Luder HU, Graf D. Bone Morphogenetic Protein 2 Coordinates Early Tooth Mineralization. *J Dent Res*. 2018;97(7):835-843. doi:10.1177/0022034518758044

266. Muzumdar MD, Tasic B, Miyamichi K, Li L, Luo L. A global double-fluorescent Cre reporter mouse. *Genesis*. 2007;45(9):593-605. doi:10.1002/dvg.20335

267. Bray NL, Pimentel H, Melsted P, Pachter L. Near-optimal probabilistic RNA-seq quantification. *Nat Biotechnol*. 2016;34(5):525-527. doi:10.1038/nbt.3519

268. Love MI, Huber W, Anders S. Moderated estimation of fold change and dispersion for RNA-seq data with DESeq2. *Genome Biol*. 2014;15(12):550. doi:10.1186/s13059-014-0550-8

269. Mi H, Muruganujan A, Ebert D, Huang X, Thomas PD. PANTHER version 14: more genomes, a new PANTHER GO-slim and improvements in enrichment analysis tools. *Nucleic Acids Res*. 2019;47(D1):D419-D426. doi:10.1093/nar/gky1038

270. Cox J, Neuhauser N, Michalski A, Scheltema RA, Olsen JV, Mann M. Andromeda: a peptide search engine integrated into the MaxQuant environment. *J Proteome Res*. 2011;10(4):1794-1805. doi:10.1021/pr101065j

271. Cox J, Mann M. MaxQuant enables high peptide identification rates, individualized p.p.b.-range mass accuracies and proteome-wide protein quantification. *Nat Biotechnol*. 2008;26(12):1367-1372. doi:10.1038/nbt.1511

272. Altman N, Krzywinski M. Analyzing outliers: influential or nuisance? *Nat Methods*. 2016;13(4):281-282. doi:10.1038/nmeth.3812

273. Kiernan JA. Sirius Red Staining Protocol for Collagen. IHC World. http://www.ihcworld.com/_protocols/special_stains/sirius_red.htm

274. T-Test Calculator for 2 Independent Means Calculator. Social Science Statistics. Accessed December 20, 2020. https://www.socscistatistics.com/tests/studentttest/default2.aspx

275. Yu JSL, Cui W. Proliferation, survival and metabolism: the role of PI3K/AKT/mTOR signalling in pluripotency and cell fate determination. *Development*. 2016;143(17):3050-3060. doi:10.1242/dev.137075

276. Zelenski NA, Leddy HA, Sanchez-Adams J, et al. Collagen VI regulates pericellular matrix properties, chondrocyte swelling, and mechanotransduction in articular cartilage. *Arthritis Rheumatol*. 2015;67(5):1286-1294. doi:10.1002/art.39034

277. Gerstenfeld LC, Shapiro FD. Expression of bone-specific genes by hypertrophic chondrocytes: implication of the complex functions of the hypertrophic chondrocyte during endochondral bone development. *J Cell Biochem*. 1996;62(1):1-9. doi:10.1002/(SICI)1097-4644(199607)62:1%3C1::AID-JCB1%3E3.0.CO;2-X

278. Sanchez C, Bay-Jensen A-C, Pap T, et al. Chondrocyte secretome: a source of novel insights and exploratory biomarkers of osteoarthritis. *Osteoarthritis and Cartilage*. 2017;25(8):1199-1209. doi:10.1016/j.joca.2017.02.797

279. Caron MMJ, Emans PJ, Surtel DAM, van der Kraan PM, van Rhijn LW, Welting TJM. BAPX-1/NKX-3.2 acts as a chondrocyte hypertrophy molecular switch in osteoarthritis. *Arthritis Rheumatol*. 2015;67(11):2944-2956. doi:10.1002/art.39293

280. Lian JB, McKee MD, Todd AM, Gerstenfeld LC. Induction of bone-related proteins, osteocalcin and osteopontin, and their matrix ultrastructural localization with development of chondrocyte hypertrophy in vitro. *J Cell Biochem*. 1993;52(2):206-219. doi:10.1002/jcb.240520212

281. Schiavinato A, Becker A-KA, Zanetti M, et al. EMILIN-3, Peculiar Member of Elastin Microfibril Interface-located Protein (EMILIN) Family, Has Distinct Expression Pattern, Forms Oligomeric Assemblies, and Serves as Transforming Growth Factor β (TGF-β) Antagonist. *J Biol Chem*. 2012;287(14):11498-11515. doi:10.1074/jbc.M111.303578

282. Ishikawa Y, Rubin K, Bächinger HP, Kalamajski S. The endoplasmic reticulum-resident collagen chaperone Hsp47 interacts with and promotes the secretion of decorin, fibromodulin, and lumican. *J Biol Chem*. 2018;293(35):13707-13716. doi:10.1074/jbc.RA117.000758

283. Lee S-Y, Abel ED, Long F. Glucose metabolism induced by Bmp signaling is essential for murine skeletal development. *Nature Communications*. 2018;9(1):4831. doi:10.1038/s41467-018-07316-5

284. Méndez-Maldonado K, Vega-López G, Caballero-Chacón S, Aybar MJ, Velasco I. Activation of Hes1 and Msx1 in Transgenic Mouse Embryonic Stem Cells Increases Differentiation into Neural Crest Derivatives. *Int J Mol Sci*. 2018;19(12). doi:10.3390/ijms19124025

285. Zhong L, Huang X, Karperien M, Post JN. Correlation between Gene Expression and Osteoarthritis Progression in Human. *Int J Mol Sci*. 2016;17(7). doi:10.3390/ijms17071126

286. Cheung HC, Hai T, Zhu W, et al. Splicing factors PTBP1 and PTBP2 promote proliferation and migration of glioma cell lines. *Brain*. 2009;132(Pt 8):2277-2288. doi:10.1093/brain/awp153

287. Cornella N, Tebaldi T, Gasperini L, et al. The hnRNP RALY regulates transcription and cell proliferation by modulating the expression of specific factors including the proliferation marker E2F1. *J Biol Chem*. 2017;292(48):19674-19692. doi:10.1074/jbc.M117.795591

288. Nishimura K, Murozumi K, Shirahata A, Park MH, Kashiwagi K, Igarashi K. Independent roles of eIF5A and polyamines in cell proliferation. *Biochem J*. 2005;385(Pt 3):779-785. doi:10.1042/BJ20041477

289. Culley KL, Lessard SG, Green JD, et al. Inducible knockout of CHUK/IKKα in adult chondrocytes reduces progression of cartilage degradation in a surgical model of osteoarthritis. *Sci Rep*. 2019;9(1):8905. doi:10.1038/s41598-019-45334-5

290. Xu D, Jin T, Zhu H, et al. TBK1 Suppresses RIPK1-Driven Apoptosis and Inflammation during Development and in Aging. *Cell*. 2018;174(6):1477-1491.e19. doi:10.1016/j.cell.2018.07.041

291. Guo J, Fang W, Chen X, et al. Upstream stimulating factor 1 suppresses autophagy and hepatic lipid droplet catabolism by activating mTOR. *FEBS Lett*. 2018;592(16):2725-2738. doi:10.1002/1873-3468.13203

292. vanLieshout TL, Ljubicic V. The emergence of protein arginine methyltransferases in skeletal muscle and metabolic disease. *American Journal of Physiology-Endocrinology and Metabolism*. 2019;317(6):E1070-E1080. doi:10.1152/ajpendo.00251.2019

293. Iwasaki H, Yada T. Protein arginine methylation regulates insulin signaling in L6 skeletal muscle cells. *Biochem Biophys Res Commun*. 2007;364(4):1015-1021. doi:10.1016/j.bbrc.2007.10.113

294. Jiang P, Xia L, Jin Z, et al. New function of the CD44 gene: Lipid metabolism regulation in bovine mammary epithelial cells. *J Dairy Sci*. 2020;103(7):6661-6671. doi:10.3168/jds.2019-17415

295. Gu H-Y, Yang M, Guo J, et al. Identification of the Biomarkers and Pathological Process of Osteoarthritis: Weighted Gene Co-expression Network Analysis. *Front Physiol*. 2019;10. doi:10.3389/fphys.2019.00275

296. Mráček T, Drahota Z, Houštěk J. The function and the role of the mitochondrial glycerol-3-phosphate dehydrogenase in mammalian tissues. *Biochimica et Biophysica Acta (BBA) - Bioenergetics*. 2013;1827(3):401-410. doi:10.1016/j.bbabio.2012.11.014

297. Gibson JS, Milner PI, White R, Fairfax TPA, Wilkins RJ. Oxygen and reactive oxygen species in articular cartilage: modulators of ionic homeostasis. *Pflugers Arch*. 2008;455(4):563-573. doi:10.1007/s00424-007-0310-7

298. Kumar Y, Biswas T, Thacker G, et al. BMP signaling-driven osteogenesis is critically dependent on Prdx-1 expression-mediated maintenance of chondrocyte prehypetrophy. *Free Radic Biol Med*. 2018;118:1-12. doi:10.1016/j.freeradbiomed.2018.02.016

299. Morita K, Miyamoto T, Fujita N, et al. Reactive oxygen species induce chondrocyte hypertrophy in endochondral ossification. *J Exp Med*. 2007;204(7):1613-1623. doi:10.1084/jem.20062525

300. Gamer LW, Pregizer S, Gamer J, et al. The Role of Bmp2 in the Maturation and Maintenance of the Murine Knee Joint. *J Bone Miner Res*. 2018;33(9):1708-1717. doi:10.1002/jbmr.3441

301. Teixeira J, Certal V, Chang ET, Camacho M. Nasal Septal Deviations: A Systematic Review of Classification Systems. *Plast Surg Int*. 2016;2016:7089123. doi:10.1155/2016/7089123

302. Taghiloo H, Halimi Z. The frequencies of different types of nasal septum deviation and their effect on increasing the thickness of maxillary sinus mucosa. *J Dent Res Dent Clin Dent Prospects*. 2019;13(3):208-214. doi:10.15171/joddd.2019.032

303. Harugop AS, Mudhol RS, Hajare PS, Nargund AI, Metgudmath VV, Chakrabarti S. Prevalence of Nasal Septal Deviation in New-borns and Its Precipitating Factors: A Cross-Sectional Study. *Indian J Otolaryngol Head Neck Surg*. 2012;64(3):248-251. doi:10.1007/s12070-011-0247-1

304. Albert AM, Payne AL, Brady SM, Wrighte C. Craniofacial Changes in Children-Birth to Late Adolescence. *ARC Journal of Forensic Science*. 2019;4(1):1-19.

305. Gómez-Picos P, Eames BF. On the evolutionary relationship between chondrocytes and osteoblasts. *Front Genet*. 2015;6:297. doi:10.3389/fgene.2015.00297

306. Wong MK, Shawky SA, Aryasomayajula A, et al. Extracellular matrix surface regulates self-assembly of three-dimensional placental trophoblast spheroids. *PLoS One*. 2018;13(6). doi:10.1371/journal.pone.0199632

307. Yu X, Kawakami H, Tahara N, et al. Expression of Noggin and Gremlin1 and its implications in fine-tuning BMP activities in mouse cartilage tissues. *J Orthop Res*. 2017;35(8):1671-1682. doi:10.1002/jor.23463

308. Kaucka M, Zikmund T, Tesarova M, et al. Oriented clonal cell dynamics enables accurate growth and shaping of vertebrate cartilage. *Elife*. 2017;6. doi:10.7554/eLife.25902

309. Seol D, McCabe DJ, Choe H, et al. Chondrogenic Progenitor Cells Respond to Cartilage Injury. *Arthritis Rheum*. 2012;64(11):3626-3637. doi:10.1002/art.34613

310. Asnaghi MA, Power L, Barbero A, et al. Biomarker Signatures of Quality for Engineering Nasal Chondrocyte-Derived Cartilage. *Front bioeng biotechnol*. 2020;8(101632513):283. doi:10.3389/fbioe.2020.00283

311. Chen J, Long F. mTOR signaling in skeletal development and disease. *Bone Res*. 2018;6. doi:10.1038/s41413-017-0004-5

312. Mao Z, Zhang W. Role of mTOR in Glucose and Lipid Metabolism. *Int J Mol Sci*. 2018;19(7). doi:10.3390/ijms19072043

313. Yoshinari K, Sato T, Okino N, Sugatani J, Miwa M. Expression and induction of cytochromes p450 in rat white adipose tissue. *J Pharmacol Exp Ther*. 2004;311(1):147-154. doi:10.1124/jpet.104.067066

314. Schulz TJ, Tseng Y-H. Emerging role of bone morphogenetic proteins in adipogenesis and energy metabolism. *Cytokine Growth Factor Rev*. 2009;20(5-6):523-531. doi:10.1016/j.cytogfr.2009.10.019

315. Luo P, Gao F, Niu D, et al. The Role of Autophagy in Chondrocyte Metabolism and Osteoarthritis: A Comprehensive Research Review. *Biomed Res Int*. 2019;2019. doi:10.1155/2019/5171602

316. Hollander JM, Zeng L. The Emerging Role of Glucose Metabolism in Cartilage Development. *Curr Osteoporos Rep*. 2019;17(2):59-69. doi:10.1007/s11914-019-00506-0

317. Blázquez-Medela AM, Jumabay M, Boström KI. Beyond the Bone: Bone Morphogenetic Protein (BMP) Signaling in Adipose Tissue. *Obes Rev*. 2019;20(5):648-658. doi:10.1111/obr.12822

318. Mariani E, Pulsatelli L, Facchini A. Signaling Pathways in Cartilage Repair. *Int J Mol Sci*. 2014;15(5):8667-8698. doi:10.3390/ijms15058667

319. van der Kraan PM, van den Berg WB. Chondrocyte hypertrophy and osteoarthritis: role in initiation and progression of cartilage degeneration? *Osteoarthritis Cartilage*. 2012;20(3):223-232. doi:10.1016/j.joca.2011.12.003

320. Tsolis KC, Bei ES, Papathanasiou I, et al. Comparative proteomic analysis of hypertrophic chondrocytes in osteoarthritis. *Clin Proteomics*. 2015;12(1). doi:10.1186/s12014-015-9085-6

321. Liu Q, Zeng H, Yuan Y, Wang Z, Wu Z, Luo W. Osteopontin inhibits osteoarthritis progression via the OPN/CD44/PI3K signal axis. *Genes & Diseases*. Published online June 27, 2020. doi:10.1016/j.gendis.2020.06.006

322. Alexopoulos LG, Youn I, Bonaldo P, Guilak F. DEVELOPMENTAL AND OSTEOARTHRITIC CHANGES IN Col6a1 KNOCKOUT MICE: THE BIOMECHANICS OF COLLAGEN VI IN THE CARTILAGE PERICELLULAR MATRIX. *Arthritis Rheum*. 2009;60(3):771-779. doi:10.1002/art.24293

323. Houben A, Kostanova-Poliakova D, Weissenböck M, et al. β-catenin activity in late hypertrophic chondrocytes locally orchestrates osteoblastogenesis and osteoclastogenesis. *Development*. 2016;143(20):3826-3838. doi:10.1242/dev.137489

324. Brunt LH, Begg K, Kague E, Cross S, Hammond CL. Wnt signalling controls the response to mechanical loading during zebrafish joint development. *Development*. 2017;144(15):2798-2809. doi:10.1242/dev.153528

325. Armiento AR, Alini M, Stoddart MJ. Articular fibrocartilage - Why does hyaline cartilage fail to repair? *Advanced Drug Delivery Reviews*. 2019;146:289-305. doi:10.1016/j.addr.2018.12.015

326. Brittberg M, Lindahl A, Nilsson A, Ohlsson C, Isaksson O, Peterson L. Treatment of deep cartilage defects in the knee with autologous chondrocyte transplantation. *N Engl J Med*. 1994;331(14):889-895. doi:10.1056/NEJM199410063311401

327. Behrens P, Bitter T, Kurz B, Russlies M. Matrix-associated autologous chondrocyte transplantation/implantation (MACT/MACI)--5-year follow-up. *Knee*. 2006;13(3):194-202. doi:10.1016/j.knee.2006.02.012

328. Knutsen G, Drogset JO, Engebretsen L, et al. A randomized trial comparing autologous chondrocyte implantation with microfracture. Findings at five years. *J Bone Joint Surg Am*. 2007;89(10):2105-2112. doi:10.2106/JBJS.G.00003

329. Zheng M-H, Willers C, Kirilak L, et al. Matrix-induced autologous chondrocyte implantation (MACI): biological and histological assessment. *Tissue Eng*. 2007;13(4):737-746. doi:10.1089/ten.2006.0246

330. Kim B-S, Shin H-R, Kim H-J, et al. Septal chondrocyte hypertrophy contributes to midface deformity in a mouse model of Apert syndrome. *Sci Rep*. 2021;11(1):7979. doi:10.1038/s41598-021-87260-5

331. Baddam P, Young D, Dunsmore G, et al. Nasal Septum Deviation as the Consequence of BMP-Controlled Changes to Cartilage Properties. *Front Cell Dev Biol*. 2021;9. doi:10.3389/fcell.2021.696545

332. Nishimura R, Hata K, Nakamura E, Murakami T, Takahata Y. Transcriptional network systems in cartilage development and disease. *Histochem Cell Biol*. 2018;149(4):353-363. doi:10.1007/s00418-017-1628-7

333. Anderson-Baron M, Liang Y, Kunze M, et al. Suppression of Hypertrophy During in vitro Chondrogenesis of Cocultures of Human Mesenchymal Stem Cells and Nasal Chondrocytes Correlates With Lack of in vivo Calcification and Vascular Invasion. *Front bioeng biotechnol*. 2020;8(101632513):572356. doi:10.3389/fbioe.2020.572356

334. van Osch GJ, Marijnissen WJ, van der Veen SW, Verwoerd-Verhoef HL. The potency of culture-expanded nasal septum chondrocytes for tissue engineering of cartilage. *Am J Rhinol*. 2001;15(3):187-192.

335. Mandl EW, van der Veen SW, Verhaar JAN, van Osch GJVM. Serum-free medium supplemented with high-concentration FGF2 for cell expansion culture of human ear chondrocytes promotes redifferentiation capacity. *Tissue Eng*. 2002;8(4):573-580. doi:10.1089/107632702760240490

336. Liu X, Liu J, Kang N, et al. Role of insulin-transferrin-selenium in auricular chondrocyte proliferation and engineered cartilage formation in vitro. *Int J Mol Sci*. 2014;15(1):1525-1537. doi:10.3390/ijms15011525

337. Chua KH, Aminuddin BS, Fuzina NH, Ruszymah BHI. Insulin-transferrin-selenium prevent human chondrocyte dedifferentiation and promote the formation of high quality tissue engineered human hyaline cartilage. *Eur Cell Mater*. 2005;9(100973416):58-67.

338. Walsh SK, Schneider SE, Amundson LA, Neu CP, Henak CR. Maturity-dependent cartilage cell plasticity and sensitivity to external perturbation. *J Mech Behav Biomed Mater*. 2020;106:103732. doi:10.1016/j.jmbbm.2020.103732

339. Tomita M, Asada M, Asada N, et al. Bmp7 Maintains Undifferentiated Kidney Progenitor Population and Determines Nephron Numbers at Birth. *PLOS ONE*. 2013;8(8):e73554. doi:10.1371/journal.pone.0073554

340. Mizuno M, Takebe T, Kobayashi S, et al. Elastic Cartilage Reconstruction by Transplantation of Cultured Hyaline Cartilage–Derived Chondrocytes. *Transplantation Proceedings*. 2014;46(4):1217-1221. doi:10.1016/j.transproceed.2013.12.006

341. Li T, Chen S, Pei M. Contribution of neural crest-derived stem cells and nasal chondrocytes to articular cartilage regeneration. *Cell Mol Life Sci*. 2020;77(23):4847-4859. doi:10.1007/s00018-020-03567-y

342. Driessen BJH, Logie C, Vonk LA. Cellular reprogramming for clinical cartilage repair. *Cell Biol Toxicol*. 2017;33(4):329-349. doi:10.1007/s10565-017-9382-0

343. Richmon JD, Sage AB, Shelton E, Schumacher BL, Sah RL, Watson D. Effect of growth factors on cell proliferation, matrix deposition, and morphology of human nasal septal chondrocytes cultured in monolayer. *Laryngoscope*. 2005;115(9):1553-1560.

344. Rodrigues MM, Gabrielli MFR, Garcia Junior OA, Pereira Filho VA, Passeri LA. Nasal airway evaluation in obstructive sleep apnoea patients: volumetric tomography and endoscopic findings. *Int J Oral Maxillofac Surg*. 2017;46(10):1284-1290. doi:10.1016/j.ijom.2017.05.009

345. Unger CM, Devine J, Hallgrímsson B, Rolian C. Selection for increased tibia length in mice alters skull shape through parallel changes in developmental mechanisms. Perry GH, Grabowski M, eds. *eLife*. 2021;10:e67612. doi:10.7554/eLife.67612

346. Kaucka M, Adameyko I. Evolution and development of the cartilaginous skull: From a lancelet towards a human face. *Seminars in Cell & Developmental Biology*. 2019;91:2-12. doi:10.1016/j.semcdb.2017.12.007

347. Adhikari K, Fuentes-Guajardo M, Quinto-Sánchez M, et al. A genome-wide association scan implicates DCHS2 , RUNX2 , GLI3 , PAX1 and EDAR in human facial variation. *Nat Commun*. 2016;7(1):11616. doi:10.1038/ncomms11616

348. Debbache J, Parfejevs V, Sommer L. Cre-driver lines used for genetic fate mapping of neural crest cells in the mouse: An overview. *Genesis*. 2018;56(6-7):e23105. doi:10.1002/dvg.23105